The Role of Multidrug Resistance Protein 1 in the Biology of Glioblastoma

by

Mohammed Ahmed Alnakhli

Thesis Submitted to Flinders University
for the degree of

Doctor of Philosophy

Molecular Medicine and Pathology, School of Medicine,

June 2020

CONTENTS:

Figures:

TABLES:

DECLARATION:

I certify that this thesis does not incorporate without acknowledgement any material previously submitted for a degree or diploma in any university; and that to the best of my knowledge and belief it does not contain any material previously published or written by another person except where due reference is made in the text.

Mohammed Ahmed Alnakhli

ACKNOWLEDGEMENTS:

In the name of God, the Merciful, the Compassionate. Finally, the day comes to thank people who inspired and supported me throughout my journey of my PhD. There are lots of people who had an impact on me during thesis experimentation and writing. I have been through a lot in terms of learning scientifically and also life lessons.

I am greatly indebted to Associate Professor Bryone Kuss, who is one of the most generous people. She has been the shining light that led me to the right direction in my whole research.

Secondly, I wish to express my gratitude to Dr. Sinoula Apostolou, who was the motor that pushed me hard through my PhD. She was the first person I turned to every time I had issues and has been the light in the dark.

I am grateful to Professor Nicolas Voelcker and his team at the Mawson Institute, University of South Australia. They accepted me as visitor researcher in their lab. Also, we established great collaborative work in the Nanoparticles field.

I am thankful to all members of the Molecular Medicine and Pathology department. They were my second family.

My father and mother have been through a lot during my study; praying, worrying, and I could not be helpful when they required me close to them. They pushed me hard to finalise this work and are proud of me. My parents, I am so lucky to have you in my life with your blessing and love.

My wife Fatimah and my daughters are angels in the dark sky. I have been stressed and annoyed however, they were supportive and stand all the time by my side. They suffered a bad time with my unstable mood.

I thank my brothers and sisters for all the emotional support. They never give up on me.

Also, I would like to express my great thank to my government for giving me the chance to study and supported me financially. In addition, they gave me all the assistance required during my study.

Finally, I would like to dedicate my work to those whom have suffered or died in the journey of cancer. To those I lost during my journey.

ABBREVIATIONS:

%	Percent
˚C	Degrees Celsius
ABC	ATP-binding cassette
ATCC	American Type Culture Collection
ATP	Adenosine Triphosphate
BBB	Blood-brain barrier
cDNA	Complementary DNA
cm^2	$Centimeter^2$
CNS	central nervous system
CO_2	Carbon Dioxide
Ct	Threshold cycle
DAPI	4’-6’-Diamidino-2-phenylindole
ddH_2O	Double deionised water
DEPC	Diethylpyrocarbonate
DLS	dynamic light scattering

DMEM	Dulbecco's modified eagle's medium
DMSO	Dimethyl sulfoxide
DNA	Deoxyribonucleic acid
dNTP	Deoxy-A/C/G/T- trisphosphate
DOX	Doxorubicin
EDTA	Ethylenediaminetetraacetic acid
EtOH	Ethanol
FACS	Fluorescence activated cell sorting
FBS	Fetal bovine serum
FCS	Fetal Calf Serum
FDA	The U.S. Food and Drug Administration
FITC	Fluorescein isothiocyanate
GBM	Glioblastoma multiforme
Gli1-3	Gli zinc finger transcription factor 1-3
GSH	Glutathione
h	Hour

H_2O	Water
MDR	Multidrug resistance
mg	Milligram
mg /mL^{-1}	Milligram per millilitre
MgCl	Magnesium Chloride
Min	Minute
MK-571	(E)-3-((3-(2-(7-chloroquinolin-2-yl)vinyl)phenyl)(3-(dimethylamino)-3-oxopropylthio)methylthio) propanoic acid
mL	Millilitre
mM	Millimolar
MRI	Magnetic resonance imaging
mRNA	Messenger RNA
MRP	Multidrug resistance protein
NaCl	Sodium Chloride
NaOH	Sodium Hydroxide
NCBI	National Centre for Biotechnology Information
ng	Nanogram

nM	Nanomolar
nmol	Nanomole
OD	Optical density
P-gp	P-glycoprotein
PBS	Phosphate buffered saline
PCR	Polymerase chain reaction
PEI	Polyethyleneimine
PI	Propidium Iodide
Ptch	Patched
PTEN	Phosphatase and tensin homology
PTX	Paclitaxel
qPCR	Quantitative polymerase chain reaction
RNA	Ribonucleic acid
RNAi	RNA interference
RNase	Ribonuclease
rpm	Revolutions per minute

RT-qPCR	Real-time quantitative polymerase chain reaction
SD	Standard deviation
SEM	Standard Error of Mean
Shh	Sonic hedgehog
siRNA	Small interfering RNA
Smo	Smoothened
SuFu	Suppressor of Fused
TEM	Transmission electron microscopy
TP53	Tumor protein 53
V	Volts
v/v	Volume/volume
WHO	World Health Organization
µL	Microlitre
µm	Micrometer
bp	Base pair
kg	Kilogram

L	Litre
pmol	Picomole
QC	Quality Control
RPKM	Reads Per Kilobase of Transcript per Million Mapped

ABSTRACT:

Glioblastoma multiforme (GBM) is an aggressive, malignant and incurable brain tumour. The median survival after diagnosis is 15 months. The poor prognosis of GBM tumours is due to multiple factors including intrinsic tumour cell chemo-resistance. The expression of ABC transporter multidrug resistance (MDR) proteins including MRP1 on tumour cells and the endothelium of the BBB critically contributes to drug resistance of this tumour. Therefore, MRP1 is a potential target for molecular therapy of GBM tumours which, if successfully targeted may impact drug resistance of the tumour and therapeutic outcome for the patient. Other signalling pathways such as the Sonic Hedgehog (SHH) pathway are critical for GBM development however their link to the MDR phenotype is incompletely understood.

In this thesis, it was hypothesised that MRP1 expression is a critical determinant of the malignant and drug resistance phenotype of glioblastoma tumour cells, in association with other key cellular pathways including the Sonic Hedgehog signalling pathway. It was further hypothesised that RNA interference technology could be used to target and knock down MRP1 gene expression in glioblastoma cell lines to assess the contribution of this drug transporter to the biological behaviour of the tumour cells. Specific siRNAs were synthesised and delivered with lipofectamine in vitro to the T98G GBM cell line and demonstrated to be effective in downregulating MRP1 mRNA and protein. A nanoparticle delivery system was then developed and investigated in tissue culture. Optimisation of this delivery system led to the use of PEI (polyethyleneimine) coated nanoparticles preloaded with MRP1 targeting siRNAs that proved effective in a slow sustained release of the siRNA. Down regulation of MRP1 in the T98G GBM cell line was achieved using

this delivery system and was found to be associated with reduction in proliferation rate of GBM cells associated with cellular G2 arrest and morphological changes including the accumulation of lipid droplets within the GBM cells. No sustained apoptosis was evident following this treatment. The nanoparticle delivery system was applied in a proof of principle *in vivo* experiment which demonstrated effective downregulation of MRP1 in xenografted tumour tissues of U87MG cells (82% at 48 hrs and 65% at 72 hrs) and also downregulation of MRP1 in non-tumour organ systems (duodenum and kidney). However, there was no evidence of end organ damage associated with MRP1 downregulation in the examined tissues. To further investigate the observed G2 arrest, a functional inhibitor of MRP1 (MK571) was investigated and found to cause identical results in T98G cells. The expression of SHH pathway members were simultaneously explored using a qRT-PCR approach and it was discovered that key members of this pathway (Gli1, Gli2, Gli3, PATCH 1 and 2, and SUFU) were reduced in their expression following both siRNA inhibition of MRP1 expression and functional inhibition. To further investigate these findings, global expression of mRNA of the siRNA treated cells was explored using an RNAseq approach. This approach failed to corroborate the qRT-PCR data and further experiments will need to be re-performed to assist interpretation of this final piece of data. This thesis has demonstrated that downregulation of MRP1 can be achieved in T98G and U87MG glioblastoma cell lines through RNA interference delivered in a sustained release nanoparticle system and that this is associated with G2 arrest and alteration of the SHH signalling pathway, which is not previously demonstrated.

PUBLICATIONS DURING CANDIDATURE:

Published:

Kafshgari, **M.H., Alnakhli**, M., Delalat, B., Apostolou, S., Harding, F.J., Mäkilä, E., Salonen, J.J., Kuss, B.J. and Voelcker, N.H., 2015. *Small interfering RNA delivery by polyethylenimine-functionalised porous silicon nanoparticles.* Biomaterials science, 3(12), pp.1555-1565. (Equal first author)

Tong, WY, **Alnakhli, M**, Bhardwaj, R, Apostolou, S, Sinha, S, Fraser, C, Kuchel, T, Kuss, B & Voelcker, NH 2018, *Delivery of siRNA in vitro and in vivo using PEI-capped porous silicon nanoparticles to silence MRP1 and inhibit proliferation in glioblastoma*. Journal of nanobiotechnology, 16(Węglarz et al.), p. 38. (Equal first author)

Poster Presentation:

Mohammed A. Alnakhli, Sinoula Apostolou, Bryone Kuss. *Multidrug Resistance Modulation in Glioblastoma: Role of MRP1 and SHH.* SA Australian Science and Medical Research Annual Meeting, the National Wine Centre, Adelaide, South Australia, Australia, 3rd June 2015

1 INTRODUCTION AND LITERATURE REVIEW

1.1 Cancer

Cancer continues to be a leading cause of morbidity and mortality in the 21st century. The clinical phenotype of cancer is due to an inherent abnormality in the growth and death regulation of somatic cells which is frequently associated with gene mutation or abnormal expression, and often results in the invasion of distant organs, through metastasis via the lymphatic and blood systems. Exposure to risk factors such as smoking and dietary habits may result in the development of cancer by altering the genetic material of somatic cells (de Robles et al., 2015). Cancer genetics clearly plays an important role in development and the biological behaviour of a malignant tumour (Vital et al., 2010, Agnihotri et al., 2013).

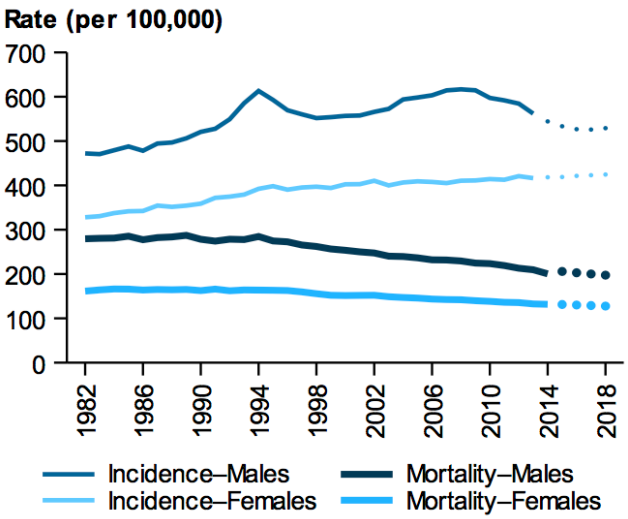

Figure 1-1 Age-standardised mortality and incidence rates for all cancers, by sex, between 1982–2018 in Australia.
Adapted from (AIHW, 2017)

The malignant phenotype may be defined as an abnormal and invasive proliferation of cells, with the capacity to metastasise to distant sites, causing organ dysfunction. However, it may also be defined as malignant due to locally aggressive behaviour as is evident in brain tumours (Becker and Baehring, 2017). Cancer can develop at any age. Although, some cancers are more common in children; in general, the elderly are more likely to develop cancer. The ability to survive cancer among other things, is affected by the tumour type, its location, the stage at diagnosis, the available therapies and the biological fitness of the patient.

Worldwide, cancer is a leading cause of death (Siegel et al., 2016, Siegel et al., 2018). Currently in Australia, around 140 cancer deaths are reported every day, representing 47,753 deaths annually (Figure 1-1). In 2018, 138,321 Australians were expected to be diagnosed with cancer (https://goo.gl/AfWWEy). While some cancers have shown improvement in the rate of five-year survival, such as prostate cancer, non-Hodgkin's lymphoma, kidney cancer, breast cancer and multiple myeloma, the survival from brain tumours remains dismal (Keegan et al., 2016).

1.2 Brain Tumours

Brain tumours are the most common solid tumour in childhood, and are a leading cause of death compared to other cancers in children and adults. The morbidity and mortality are high and risks of therapy include generalised loss of brain function or dementia. Worldwide, every year a quarter of a million cases of primary malignant brain tumours are diagnosed. The lack of successful therapeutics and the critical location contribute to the poor outcomes (Ostrom et al., 2015). Based on the 2004–2013 incidence data in

Australia, it was estimated that 1891 brain tumour cases would be diagnosed in 2017, encompassing 1,109 males and 782 females. Approximately, 1400 people were expected to die as a result (AIHW, 2017).

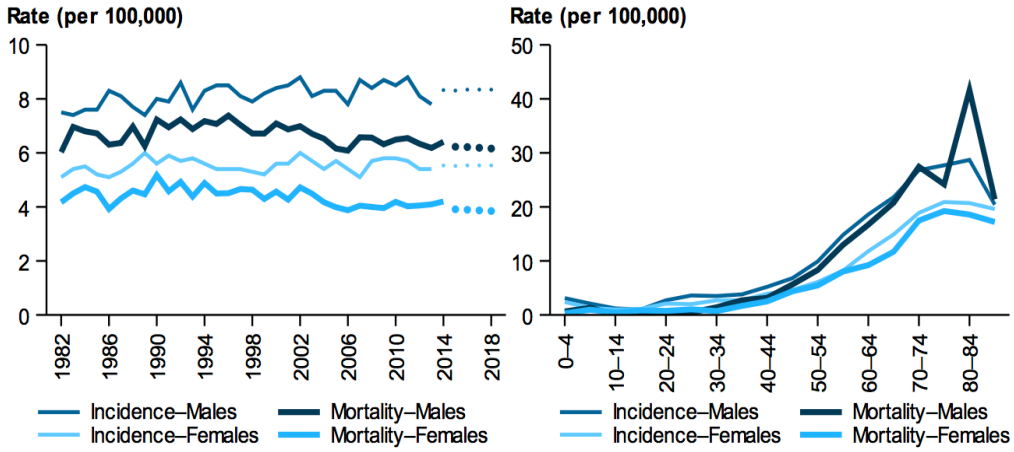

Figure 1-2 Mortality and incidence rates of brain cancer by (A) sex and by (B) age between 1982–2018 in Australia. Adapted from (AIHW, 2017).

Glioma is the most common primary brain tumour, arising from glial cells, comprising approximately 77% of primary malignant brain tumours and 30% of all CNS tumours. Glial cells are specialised cells that support neuronal function, and are responsible for providing nutrition to the neuron. The incidence of gliomas has increased significantly over the last two decades. However, this may in part be driven by improved diagnostic procedures (Sonali et al., 2018, Evans and Evans, 2016, Li et al., 2014). The annual incidence of glioma in Australia is 7 per 100,000 people. (AIHW, 2017, Ostrom et al., 2014, Ostrom et al., 2018). To date, there is no conclusive evidence that identifies the risk factors for glioblastoma occurrence despite some reports claiming that mobile phone radiation can increase the incidence of brain cancer (Morgan et al., 2016, Swerdlow et al., 2011, Sadetzki et al., 2005), and other electronic devices that have high signal

strengths (Mrugala, 2013, Swerdlow et al., 2011). GBM tumours have been found in all cortical areas, the cerebellum, the brainstem, and the spinal cord (Ostrom et al., 2015, Oslobanu and Florian, 2015).

The World Health Organisation (Yao et al.) categorises gliomas as either low grade or high grade based on the histopathology of the tumour (

Figure 1-3). Grading is based on a comparison between the tumour cells and normal brain cells and includes an estimate of growth, tissue necrosis, and changes in blood vessels. In addition, the location of the tumour, either above the tentorium (precentorial) or below the tentorium (infratemporal), is also used to classify gliomas.

Low grade (Grade I and II) have improved prognosis, whereas high grade tumours (Grade III and IV) are clinically aggressive with poor prognosis. Glioblastoma multiforme is grade IV and accounts for approximately 75% of gliomas and has an exceedingly poor prognosis.

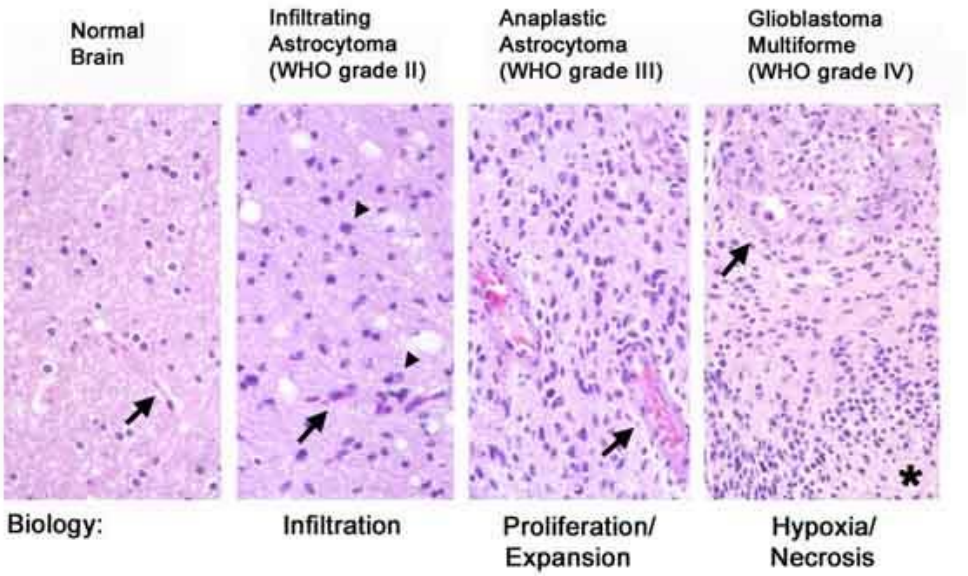

Figure 1-3 Histopathological progression of infiltrating astrocytomas (WHO grade II, left) to glioblastoma multiforme (GBM; WHO grade IV, right).
Blood vessel architecture (arrows) and density are similar in the infiltrating astrocytoma and normal brain. Moreover, tumour cells are dispersed within the neuropil. In anaplastic astrocytoma, the blood vessels (arrows) are dilated and tumour cell number is increased. GBM (*) is characterised by the presence of necrotic cells and microvascular hyperplasia. Adapted from (Brat et al., 2003, Louis et al., 2016, Wesseling and Capper, 2018, Ceccarelli et al., 2016).

1.3 Overview of Glioblastomas

Glioblastoma multiforme (GBMs) is an incurable aggressive cancer that affects the central nervous system. The tumours are heterogeneous, intraparenchymal and characterised with haemorrhage and necrosis. They consist of a number of different cell types including hyper-proliferative endothelial cells, glioma cells, as well as normal brain cells trapped by the invading glioma and macrophages (Jain et al., 2007, Holland, 2001). Difficulties in diagnosis, coupled with the chemo-resistance of these tumours, results in poor patient survival. GBMs affect children and adults in similar ways. Symptoms include nausea, vomiting, headache, cranial nerve palsies, gait imbalance, and paralysis. Magnetic

resonance imaging is used to guide biopsies of the tumours to identify the histological features of the GBM tumour (

Figure 1-3).

Patients are usually treated by micro-neurosurgery in combination with radio-, chemo-, and immunotherapies, but these only slightly improve survival time (Bredel, 2001). In the case of grade IV glioblastoma, individuals treated with these therapies typically survive between six months to one year. Less than 4% of glioblastoma patients survive for five years. Glioblastoma is the second leading cause of death amongst children with cancer, and the most prevalent cause of death among 20 to 39-year old adults with cancer (Ernest and Sontheimer, 2009).

1.4 Glioblastoma Standard Treatments

Currently, there is no cure for GBM. Standard treatment of GBM in newly diagnosed patients starts with maximal surgical resection, followed by radiotherapy and adjuvant chemotherapy with temozolomide (TMZ) (Saran et al., 2016). Surgery is the most effective method for the treatment of GBM. However, the tumour limits of glioblastomas, are difficult to detect, and residual tumour tissue may extend into healthy brain tissues, even after surgery, leading to an increased risk of recurrence. (De Bonis et al., 2013, Stummer et al., 2000, Lacroix et al., 2001, Castro et al., 2003, Wallner et al., 1989).

Radiation and chemotherapy are used to reduce growth of any tumour that remains after surgery. Brain tumours are generally treated with radiation 4–6 weeks after tumour resection. In some cases, where the tumour is in a region that is difficult to access and

therefore cannot be resected, radiation is the only available solution. Radiation is administered at 1.8–2.0 Gy per fraction, five days a week. The most common adverse effect of using radiotherapy is damage to healthy and normal cells (Jelsma and Bucy, 1967, Castro et al., 2003, Keime-Guibert et al., 2007).

Due to the chemo-resistance of brain tumour cells, new approaches are required to control and minimise tumour growth. Nitrosoureas (BCNU and CCNU), platinum-based drugs (cisplatin, cisplatinum, and carboplatin), temozolomide (TMZ), procarbazine, and naturally occurring compounds (Taxol) are the drugs most commonly used to treat glioblastoma patients. These drugs can be utilised alone, or in combination with surgery or radiotherapy. A combination of BCNU, procarbazine, and vincristine has been shown to be only minimally effective in patients and resulted in an increased survival of only a few months. TMZ is an imidazotetrazine derivative whose mechanism of action is through methylation of specific DNA sites. It is currently used as first-line treatment for GBMs, (Minniti et al., 2009, Perazzoli et al., 2015).

The side effects of chemotherapy are significant and can adversely affect the patient's quality-of-life. To date, it has not been possible to cure recurrent GBM with improved chemotherapeutics (Kemper et al., 2004). Intra-tumoral chemotherapy levels are reduced by drug efflux through multidrug resistance proteins expressed in the endothelial and other cells including the blood brain barrier. Chemotherapeutic drugs also induce MDR in cancer cells (Castro et al., 2003, Wu et al., 2017, Minniti et al., 2009).

Molecular therapies have also been used in conjunction with chemotherapies in some instances with variable success (Guo et al., 2013). However, despite best efforts, the

quality of life of the patients is severely affected and the outcome remains dismal (Stupp et al., 2005, Chinot et al., 2014, Zhang et al., 2016).

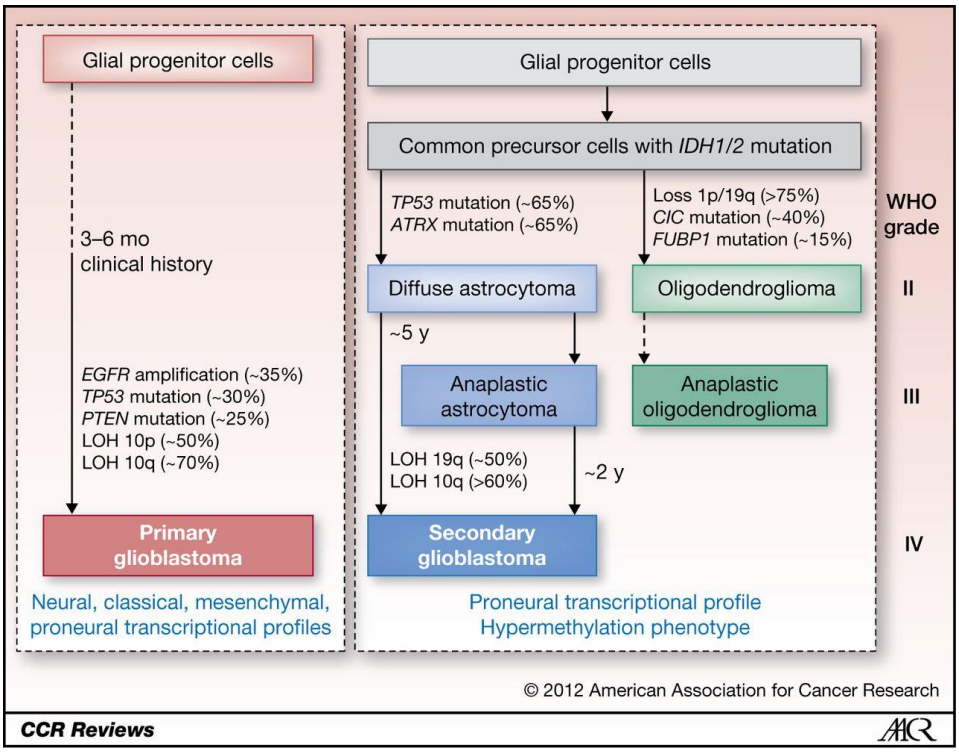

Figure 1-4 Summary of the genetic pathways leading to primary and secondary glioblastomas. Adapted from (Ohgaki and Kleihues, 2013b). (AACR, License Number: 4132221047825).

1.5 Molecular Alteration and Pathology of GBM

The use of advanced molecular techniques has recently provided a clearer understanding of the mechanism of gliomagenesis. Like other cancers, the malignant process is linked to abnormalities in genes which control the cell cycle, signal transduction, cell proliferation, differentiation, and apoptosis (Appin and Brat, 2015, Stratton et al., 2009).

Distinction can be made between primary and secondary glioblastomas. Primary glioblastomas present at diagnosis as completed tumours, without clinical, radiological, or histopathological evidence of a precursor lesion or in-situ cancer. They already

however have complex genetic alterations. Secondary glioblastomas develop gradually through de-differentiation from low-grade diffuse astrocytoma (WHO grade II) or anaplastic astrocytoma (WHO grade III). The diagnosis of secondary glioblastoma requires evidence of evolution from a less malignant astrocytoma to make the diagnosis.

The Cancer Genome Atlas Research Network (Brennan et al.) performed a large-scale study involving a 209 GBM patient cohort to categorise genomic abnormalities that drive tumorigenesis (Cancer Genome Atlas Research, 2008). Six hundred-and-one genes from ninety-one patients were sequenced and analysed. In addition, an interim integrative analysis of DNA copy number, gene expression, and DNA methylation aberrations was reported. This report described the mutational spectrum of GBM identifying PIK3R1, NF1, and ERBB2, receptor tyrosine kinase pathways as containing recurrent mutational events and confirmed the presence of TP53 gene mutations (Cancer Genome Atlas Research, 2008).

Understanding and classification of GBM transcriptomic and genomic features have begun to impact anti-GBM therapeutic development. GBM can be divided into pro-neural, classical, neural, and mesenchymal subtypes, based on gene expression (Ohgaki and Kleihues, 2013). Specifically, this molecular classification is based on aberrations in the gene expression of EGFR, NF1, and PDGFRA/IDH1. For example, aberrant EGFR amplification, an astrocytic cell expression pattern, and loss of chromosome 10 are found in classical GBMs. However, mutations in IDH1, TP53, or NF1 are not commonly found. In contrast, mutations in NF1 and PTEN are a feature of mesenchymal GBMs, which have less EGFR amplification. Pro-neural GBM is characterized as containing mutations in TP53, IDH1, along with PDGFRA focal amplification. Neural GBM is defined as having the

expression profile of normal brain tissue and the presence of astrocytic/oligodendrocytic cell markers (Figure 1-4) (Verhaak et al., 2010). Clinically, the best therapeutic outcome is seen in classical GBM, and the poorest prognosis seen in pro-neural GBM (Verhaak et al., 2010). IDH, TP53, and ATRX mutations are frequently found in secondary GBMs, whereas primary GBMs lack IDH mutations. In addition, primary GBMs have mutations in the EGFR, TP53, PDGFRA, PTEN, CDKN2A/B, NF1 and TERT promoters (Appin and Brat, 2015, Holland, 2001, Brennan et al., 2009, Verhaak et al., 2010).

As a consequence of the clinicopathological correlation the current classification of GBMs divides those into IDH-wildtype containing and those containing an IDH-mutation (Louis et al., 2016, Wesseling and Capper, 2018, Ceccarelli et al., 2016). The IDH-wildtype containing GBMs accounts for about 90% of cases, is frequently found in patients over 55 years of age and is found clinically in both primary and secondary GBMs. The GBMs containing an IDH-mutation are generally associated with secondary GBMs in younger patients and accounts for about 10% of cases. A third category is NOS (Not Otherwise Specified) GBMs for which there is no full evaluation of the IDH status available (Ohgaki and Kleihues, 2013, Louis et al., 2016, Brennan et al., 2009). While there are no histopathological differences between primary and secondary glioblastomas, genetic and epigenetic makers, as well as their expression levels, are distinct. For example, in primary GBMs, the frequency of EGFR alterations, PTEN mutations, MDM2 duplications, and homozygous CDKN2A deletions are higher than in secondary GBMs. In contrast, mutations in IDH1 and TP53, MET amplification, and overexpression of PDGFRA are lower in primary GBMs compared to secondary GBMs (Figure 1-4) (Ohgaki and Kleihues, 2013, Parsons et al., 2008, Nobusawa et al., 2009, Tso et al., 2006).

1.6 The multidrug resistance phenotype in GBM

Apart from individual mutation events which lead to drug resistance, particularly mutations in TP53, drug resistance proteins and signalling pathways that control the development of the normal brain and also protect neuronal cells from damage, have an impact on GBM prognosis (Hombach-Klonisch et al., 2018, Jha et al., 2015). GBM relapsed patients are largely unresponsive to chemo- and radio-therapy. This phenomenon is associated with increased multidrug resistance protein expression both on the tumour cells but also the endothelium and blood-brain. However, multidrug resistance is likely to be more complex than the expression of membrane associate drug pumps. Members of the Sonic Hedgehog signalling pathway: glioma-associated oncogene-1 (Gli1), an oncogene that is involved in GBM pathogenesis (Clement et al., 2007) has its expression linked with SHH expression and also therapeutic resistance in glioblastomas. Studies have shown that the MDR phenotype can be induced when the SHH pathway is activated, and importantly SHH signalling appears to promote MDR by increasing the transcription of a subset of ABC transporter proteins (Xu et al., 2013, Das et al., 2013, Sims-Mourtada et al., 2007, Bidet et al., 2012). This thesis intends to explore this link between the MDR phenotype and the SHH pathway as well as exploring mechanisms of MDR reversal. The remainder of this literature review focusses on these two pathways for drug resistance in GBM.

1.7 Drug resistance in Brain Tumours

Cellular events such as alterations in cell cycle checkpoints, loss of TP53 expression, modulation of apoptotic pathways, and repair of damaged cellular targets, all make significant contributions to the MDR phenotype. However, a primary mechanism of

resistance to chemotherapeutic agents is affected through the expression of ATP dependent cell membrane pumps that expel the drug from the intracellular compartment of the cell. Examples of these ATP pumps include MDR1 and MRP1.

1.8 Multidrug Resistance Protein 1

The mechanism of MDR has been widely studied using cytotoxic agents (including hydrophobic and amphipathic natural products) in cultures of cancer cells (Gottesman et al., 2002, Ozben, 2006, Kartal-Yandim et al., 2016). There are two different cellular resistance mechanisms. The first is a transport-based classical MDR mechanism that involves the ATP-binding transport cassette family (ABC). The second mechanism is a non-classical MDR mechanism which involve enzymes such as topoisomerase and glutathione S-transferase (GST) (Stavrovskaya, 2000, Kartal-Yandim et al., 2016). Gyorffy et al. studied thirty different cancer cell lines treated with eleven different anticancer therapies. In total, 1481 genes were found to be associated with drug resistance. From those genes, 1,033 genes were linked to one therapy. In addition, they identified sixty-seven multidrug resistance candidate genes associated with resistance to four or five anticancer therapies (Gyorffy et al., 2006).

The ATP-binding cassette (ABC) protein family is the major family related to drug resistance. Forty-eight human ABC genes have been identified, and these can be divided into seven subfamilies (ABC-A to G) that are expressed in normal tissues, as well as tumours. Of these 48 human ABCs only 3 have substantiated evidence of principle drug resistance mechanisms: Pgp, ABCG2/BCRP and MRP1. Hence the gene principally responsible for multidrug resistance is MDR1/P-glycoprotein (ABCB1), which is highly

expressed on the cell plasma membrane, where it acts to protect the cell from toxic agents (Ozben, 2006, Kathawala et al., 2015). In addition, there are twelve multidrug resistance-associated proteins (MRP) that are involved in drug transport (MRP1-12) and a pseudogene originally named ARA. These genes are expressed in a range of different tissues. However, multidrug resistance protein 1 (MRP1) is expressed in the absence of MDR1/P-glycoprotein, and has a significant overlap in activity with MDR1. Clinically, MRP1 is responsible for drug resistance in a range of tumour types (Kathawala et al., 2015, Leschziner et al., 2006, Słomka et al., 2015).

MRP1 is a member of the adenosine triphosphate (ATP-binding cassette) transporter protein, sub-family C (CFTR/MRP), member 1 (ABCC1), and is 190 kDa in size (Cole 2014). It can be found within the plasma membrane, intracellular membranes of brain capillary endothelial cells, but it remains controversial whether it is found at the BBB (Boumendjel et al., 2005, Zhang et al., 2004). It was first discovered in the H69AR human small cell lung cancer cell line in 1992, and in the CNS in 1998 (Cole et al., 1992, Regina et al., 1998).

The MRP1 protein is highly expressed in a range of animal and human tissues, with the exception of the liver, neuronal, intestine, colon, and peripheral blood mononuclear cells where it is expressed at lower levels. Importantly, MRP1 protein is expressed in a variety of different tumour types including neuroblastoma, glioblastoma, breast, lung, colon, prostate, and in leukaemia (Leslie et al., 2005). In the brain, MRP1 is expressed in polarised epithelial cells and localised to the basolateral membrane (Sharom, 2008). In addition, brain capillaries and brain capillary endothelial cell cultures have been examined for MRP1 mRNA and protein expression (Hartz and Bauer, 2011). The expression of MRP1 has been extensively studied in lymphoblastic leukaemia, astrocytes,

the choroid plexus, and microglia (Winter et al., 2013, Gennuso et al., 2004, Stein et al., 2002).

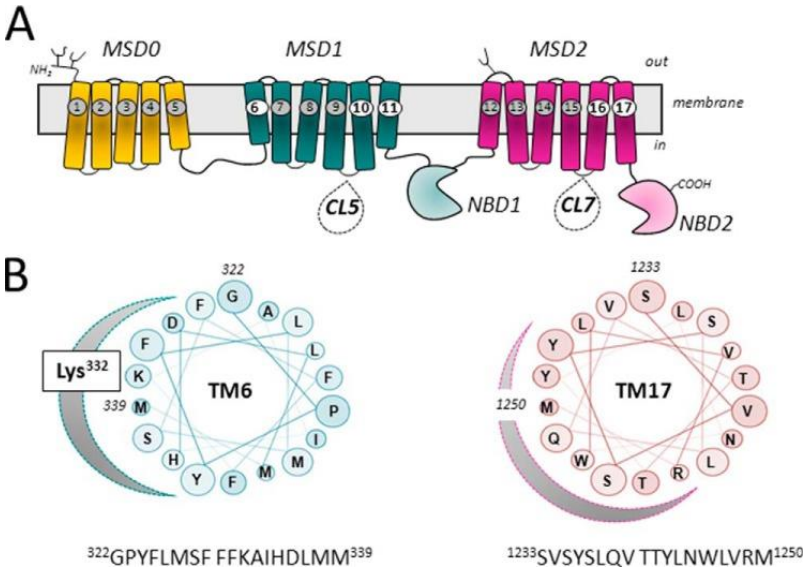

Figure 1-5 Topology of MRP1 and projections of amphipathic TM α-helices 6 and 17.
A, shown is a schematic diagram of a predicted secondary structure of MRP1/ABCC1. The positions of TMs 6, 10, 11, 16, and 17, which have been identified as containing key determinants of MRP1 substrate specificity, are highlighted. Also indicated are CL5 and CL7, which contain amino acids involved in substrate specificity, proper folding, and plasma membrane trafficking, as well as the transport mechanism of MRP1. B, shown are helical wheel projections of 18 amino acids of the amphipathic TM6 (in MSD1) and TM17 (in MSD2) of MRP1. The clustering on one side of each TM helix of polar residues with side chains capable of H-bonding is indicated by the shaded curve. Highlighted on the projection of TM6 is Lys, which is particularly critical for LTC4 and GSH transport. Figure taken directly from Cole et al 2014

The mechanism of MRP-mediated transport is unclear and complex in normal brain and tumours at the sites of the BBB blood–CSF barrier and intracellular localisation (Golden and Pollack, 2003). Its main function is in cellular defence as it protects healthy or cancerous cells from toxic or harmful agents. It can work either independently or in combination with MDR1 to cause the cellular efflux of drugs (Calatozzolo et al., 2005). MRP1 transport relies on the presence of intracellular glutathione (Loe et al., 1996, Renes et al., 1999) and can transport natural product drugs such as doxorubicin, vincristine, and VP-16 (Karvar, 2014).

MRP1 structure (Cole, 2014, Gelbmann and Kalejta, 2019) is shown in Figure 1-5. In addition, it does not play a role in phase II metabolism. However, due to its Phase III (distribution) and Phase Iv elimination through transport of GSH-, glucuronate-, and sulphate- conjugated organic anions are transported by MRP1. MRP1, and other members of its family, have been found to be highly expressed in GBMs, the parenchymal tissue surrounding the tumour, and the tumour vasculature, which can therefore affect the efficacy of a chemotherapeutic agent, manifesting itself as chemoresistance. Consequently, this allows an aggressive tumour to increase in size. Thus, a poor response to anticancer drugs in patients is frequently due to expression of the MRP1 protein, as well as other family members. Based on this, it has been suggested that ABC transporter inhibitors, and/or ABC transporter modulation, may be a useful strategy to increase the efficacy of chemotherapeutic reagents (Tong et al., 2012, Spiegl-Kreinecker et al., 2002, Abe et al., 1998, Calatozzolo et al., 2005, Hartz and Bauer, 2011, Holland, 2011). However, this role of drug transportation is not a universal feature of ABC transporters as only a small subset is actually involved in this directly and only 3 involved in drug resistance.

Tivnan et al. examined the role of MRP1 in the transport of chemotherapeutic agents temozolomide (TMZ), vincristine, and etoposide, used for the treatment of GBM, in both primary and recurrent patient-derived GBM cell lines (Tivnan et al., 2015). In this study, they used a small-molecule inhibitors of MRP1 (MK-571and Reversan), along with gene silencing of MRP1 using siRNA. The use of these MRP1 inhibitors in both cells lines improved chemosensitisation to vincristine and etoposide, resulting in increased cell death and reduced cell viability. TMZ did not induce cell death in these GBM cell lines when treated with the MRP1 siRNA or MK-571, whereas in the presence of Reversan

there was enhanced cell death (Tivnan et al., 2015). Additionally, an MRP homolog also found in GBM is MRP3. GBMs overexpress MRP3 at both mRNA and protein levels. Multidrug-resistance protein 3 has potential correlation with survival and is thought to be a potential target for immunotherapy as a cancer immunogen. (Kuan et al 2010). These findings suggest the ABC transporters may have a significant role in GBM biology.

1.9 Sonic Hedgehog Signalling Pathway

Sonic hedgehog (Nachmias et al.) is one of a group of three proteins in the mammalian hedgehog signalling pathway family, with the others being Indian hedgehog homolog (IHH) and Desert hedgehog homolog (DHH) (Nachmias et al., 2004). In 1980, Christiane Nusslein-Volhard and Eric F. Weischaus discovered the Hh genes unexpectedly when they were looking for mutations that disrupt the Drosophila larval body plan (Nüsslein-Volhard and Wieschaus, 1980, Elamin et al., 2010). IHH and DHH have significant roles in the development of normal tissues and bone formation. (Hebrok et al., 2000, Kawahira et al., 2003, St-Jacques et al., 1999, Yao et al., 2002). SHH is the most potent and extensively expressed in adult neuronal tissue compared with IHH and DHH (Pathi et al., 2001, Ingham and McMahon, 2001, Wu et al., 2017, St-Jacques et al., 1999). However, within the primary cilia of mammalian cells, all three HH orthologues mediate HH signalling (Zhang et al., 2017).

Sonic hedgehog (Nachmias et al.) signalling is involved in several different molecular and cellular mechanisms including protein-protein interactions, positive and negative feedback loops and protein trafficking. It is also involved in post-translational modifications including lipidation, phosphorylation, and proteolytic cleavage. This

enables tightly controlled regulation of HH signalling in a spatially and temporally specific manner, a necessary key factor for cell fate determination, self-renewal and tissue patterning (Cochrane et al., 2015).

The SHH signalling pathway is an important mediator that is key in embryonic development and differentiation of the brain, as well as other organs. It has an essential role in the formation of embryonic structures in vertebrates, including the cerebellum, neural crest, gut, heart, lung, gonads, eye, bone, cartilage, muscle, limbs, prostate, pancreas, blood cells, tongue and teeth. In addition, it plays a role in the repair and renewal of adult tissues, as well as adult tissue homeostasis regulation and gastrointestinal tract stem cells, blood and brain maintenance (Ingham and McMahon, 2001, Jiang and Hui, 2008, Varjosalo and Taipale, 2008, Scales and de Sauvage, 2009, Wu et al., 2017, Patel et al., 2017, Sun et al., 2016). HH signalling has various effects on cell and microenvironment interactions including motility and adhesion changes, directing cell fate determination, cell proliferation, epithelial-to-mesenchymal transitions and the receiving cell type. Defects in the activation of the Hh signalling pathway during human fetal development can result in children being born with congenital defects in the face and the brain. Cyclopia, microencephaly, holoprosencephaly, the absence of a nose, and cleft palate are examples of symptoms that can arise in humans in the absence of HH signalling (Petryk et al., 2015, Muenke and Beachy, 2000, Hu and Marcucio, 2009). SHH hyperactivation in the CNS is linked with different brain tumours such as medulloblastoma, gliomas, glioblastoma multiforme, primitive neuroectodermal tumours, and pituitary adenomas (Varjosalo and Taipale, 2008).

The HH pathway is activated through the interactions of hedgehog, patched, and smoothened genes. In the presence of the hedgehog ligand, three GLI transcription factors that lie downstream in the pathway are activated. GLI1 and GLI2 function as activators (under some circumstances, GLI2 can function as a repressor), and GLI3 is a repressor. These three transcription factors are homologs of the Ci (Cubitus interruptus) gene in Drosophila.

In the target cell, the HH signalling cascade is induced by the binding of HH ligand to the Patched 1 protein (PTCH). PTCH catalytically represses the activity of SMO in the absence of the HH ligand, by affecting its localisation at the cell surface. PTCH is a twelve-transmembrane domain protein with its intracellular loop localised at the primary cilium base (**Error! Reference source not found.**). Also, PTCH transports an endogenous i ntracellular small molecule outside the cell (by preventing SMO translocation to primary cilia) that can prevent its binding to SMO. In the absence of active SMO in the ciliary membrane, GLI1, GLI2 and GLI3 remain in complex with SUFU (suppressor of the fused and negative regulator). PTCH loses its activity upon binding to Hh resulting in activation of SMO, and thus transduction of the SHH signal (Ming et al., 1998, Marti and Bovolenta, 2002, Pak and Segal, 2016). Also, in the absence of SHH, protein kinase A (PKA) has an inhibitory role in hedgehog gene transcription. It phosphorylates GLI proteins directly by translocating them out and into the cilia (Figure 1-). GLI protein phosphorylation results in their alteration into transcriptional repressors leading to abrogation of SHH gene expression target (Niewiadomski et al., 2013, Wang et al., 2000, Tempé et al., 2006, Tuson et al., 2011).

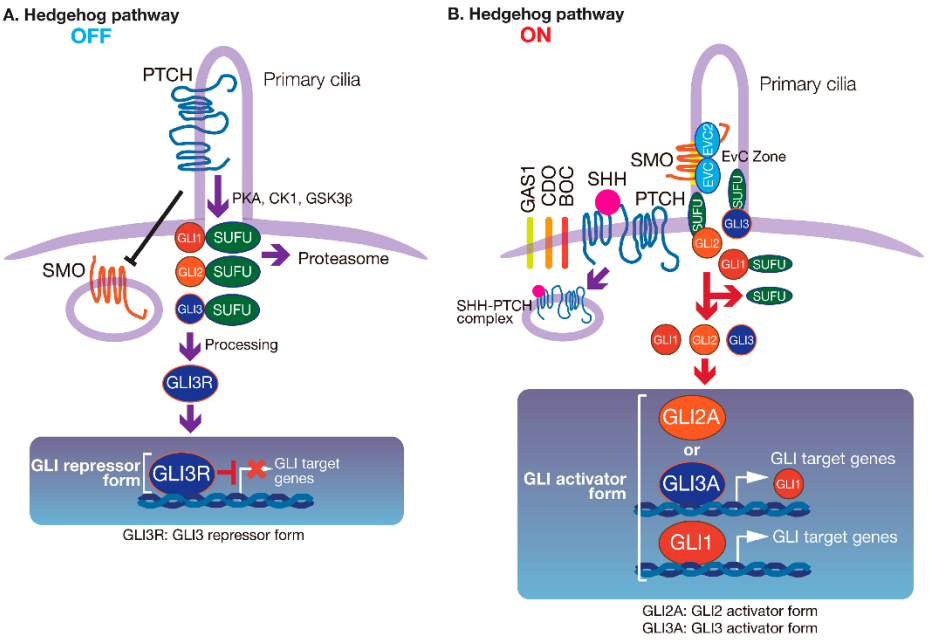

Figure 1-6 Hedgehog Signalling Pathway. A) Deactivated pathway. SMO primary cilium localisation blocked by PTCH in the absence of HH B) Activated pathway, in the presence of HH, SMO released and activated while PATCH degraded. Activation of SMO result in translocation of GLI into nucleus. HH target genes transcription induce. Adapted from (doi:10.3390/jdb5040012)

Cytoplasmic protein suppressor of Fused (Deli et al.) negatively regulates HH signalling through the GLI protein in the cytoplasm which results in suppression of the activation of GLI transcription (Tostar et al., 2012, Zhang et al., 2017). It protects GLI2, and GLI3 proteins from being degraded by the proteasome and from SPOP-CUL3 mediated ubiquitination. This function of protection a pool of GLI2 and GLI3 from being converted into GLI repressor and activator. This feature of the hedgehog pathway is evolutionarily conserved and independent of the cilium (Tostar et al., 2012, Chen et al., 2009, Cheng and Yue, 2008, Hoelzl et al., 2017).

As a result, there is an alteration in the balance between the activator and repressor forms of the Ci /GLI family to transmit the HH signal. Additionally, the atypical kinesin-

like protein, Fused (Fu), Costal 2 (Cos2), SUFU, and the transcription factor Ci form a protein complex that serves to transmit the HH signal. Gli and SUFU form a complex in the cytosol, which is proteolysed to the short repressor. When the pathway is activated, this complex is disrupted leading to inhibition of proteolysis and the release of active GLI. GLI is then able to translocate to the nucleus and transcribe Hedgehog target genes (Wetmore, 2003, Rimkus et al., 2016, Ruiz i Altaba et al., 2002, Ingham and McMahon, 2001, Tukachinsky et al., 2010, Cooper et al., 2005, Jia et al., 2009).

1.10 SHH Signalling in Cancer

In adults, the HH signalling pathway normally regulates epithelial cells of human organs and has significant roles in controlling the communication between tissues and cells. Through the alteration of these functions, aberrant HH signalling activation in adults contributes to the origin, growth and maintenance of cancer and can increase treatment failure in cancer patients by increasing cancer aggressiveness, chemotherapeutic response limitation and drug resistance (Cochrane et al., 2015).

Over-expression of genes in the HH pathway have been studied in many different cancers including basal cell carcinoma (Atwood et al., 2015, Hahn et al., 1996), medulloblastoma, leukaemia (Zeng et al., 2015), as well as gastrointestinal (Sukegawa et al., 2000), breast (Im et al., 2013), prostate, hepatocellular carcinoma,(Li et al., 2016, Ertao et al., 2016), lung, bladder, oral and pancreatic cancers (Drenkhahn et al., 2013, Tang et al., 2012, Kelleher, 2011, Ishikawa et al., 2014, Thayer et al., 2003, Sukegawa et al., 2000, Gupta et al., 2010, Ertao et al., 2016).

In cancer, the HH signalling pathway critically affects the therapeutic response, tumorigenesis, increases tumour invasiveness, and tumour progression. Recently, the HH signalling pathway has been studied as a novel therapeutic target, as an important signalling pathway in cancer. Glioma-associated oncogene homolog (GLI) and Smoothened (SMO), which are downstream effectors of the Shh pathway have been targeted as potential therapeutic genes (Shahi et al., 2008).

The mechanisms of HH signalling activation in cancer can be divided into four types: mutation (Type I; ligand-independent), autocrine (Type II; ligand-dependent), and two different types of paracrine signalling (Type IIIa and Type IIb). See figure 1.6.

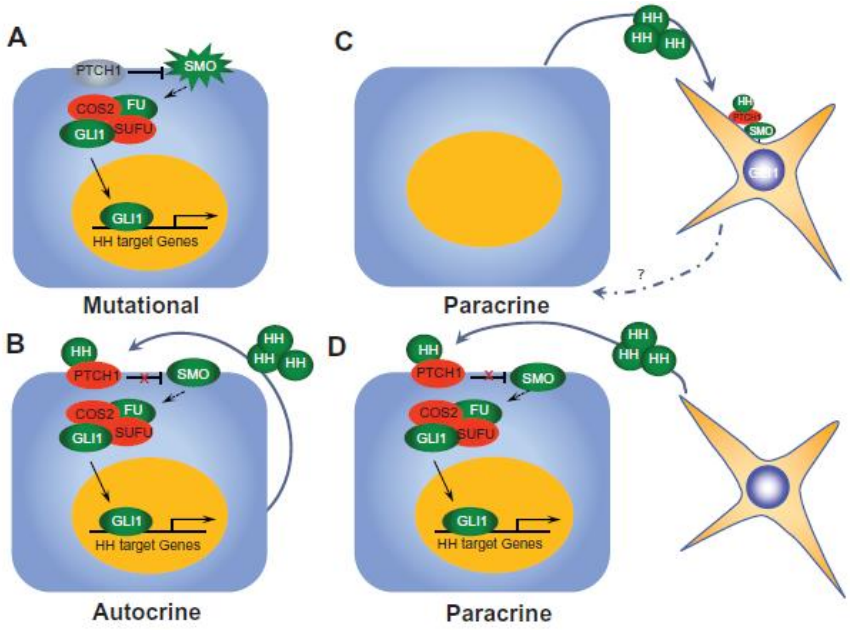

Figure 1-7 Mechanisms of HH signalling activation in cancer. Activation by mutation of specific HH genes which result in promotion of cell growth and survival. (B) HH is secreted and acts on the same cell in an autocrine fashion (self-secretion of Hh). (C) Paracrine HH from a tumour acting on the adjacent stroma (creates microenvironment suitable for tumour growth). (D) Reverse paracrine signalling: the tumour stroma secretes HH, which then acts on the tumour cell. Adapted from (Lin and Matsui, 2012).

Type I SHH signalling is activated by mutation of specific genes in the pathway within a tumour cell, leading to ligand-independent constitutive signalling. For example, most HH signalling activation in basal cell carcinoma (BCCs) is achieved as a result of an inactivate mutation in PTCH (85-90%), or an activate mutation in SMO (10-20%), GLI1 and GLI2 gene amplification and translocation may occur, and in a few cases -a mutation in SUFU (**Error! R eference source not found.**7 A). These changes are also found in patients with medulloblastoma, a paediatric cancer of the cerebellum, rhabdomyosarcoma and skin tumours of keratinocytes. The SHH pathway therefore appears critical in a range of aggressive tumours and is affected by a number of molecular mechanisms disturbing its regulation. Understanding the downstream activation effects of these events, including SMO mutations, may indicate potential targets for specific inhibitors as anticancer agents. Tumours utilising HH pathway activation are less sensitive to direct inhibitors of Hh currently in development, requiring different therapeutic approaches to be formulated (Xie et al., 1998, Taylor et al., 2002, Tostar et al., 2006, Cochrane et al., 2015, Bonilla et al., 2015, Sekulic and Von Hoff, 2016).

1.11 SHH in Glioblastoma

GLI1, PTCH1, SMO, and SHH are all expressed in glioblastomas, which appear to be HH signalling active. These genes are found to be active in glioma stem cell cultures (gliomaspheres) and glioblastoma multiforme (GBM)-derived neurospheres (Bar et al., 2007, Ehtesham et al., 2007). Tumour progression and tumorigenesis in the brain appears to be influenced by the activation of SHH signalling pathway (Carpenter and Lo, 2012).

GLI 1 was reported as highly expressed in glioma cells: approximately 50-fold increased over normal cells (Kinzler et al., 1987). GLI1 has also been found to be expressed 10-fold in conditioned media obtained from GBM-derived neurosphere cultures. Bar et al. found that GLI1, SMO, and PATCH were activated in eight primary GBM cells, and were subsequently able to establish six GBM cell lines from independent primary tumours. In GBM, SHH-GLI pathway signalling is also directly linked with the reduction of patient survival. About 75% of GBM sections obtained from 106 patients were found to express GLI1 highly, and this was associated with a poor prognosis. Thus, overexpression of GLI1 has been proposed to be a predictive marker for clinical outcome and fundamental to the malignant process (Rossi et al., 2011).

The impact of GLI1 on patient outcome likely arises due to activation of the SHH pathway leading to enhanced growth and invasiveness of the tumour, associated with alteration of the phosphoinositide-3 kinase/AKT pathway, through the induction of matrix metalloproteinase-2 and-9 production (Chang et al., 2015). Additionally, neurospheres treated with a siRNA targeting SMO, or cycoplamine, an SMO inhibitor, resulted in the downregulation of the mRNA expression of GLI1, the stem cell genes SOX2, OCT4, NANOG, NESTIN and BMI1, as well as reducing cell growth (Ehtesham et al., 2007, Bar et al., 2007, Clement et al., 2007) thus confirming SHH dependence.

GLI1 was first isolated from a human GBM, however its role in GBM biology is still incompletely understood. GLI1 is required in many cellular signalling pathways, including Hedgehog, K-RAS, transforming growth factor-beta, protein kinase A, and epidermal growth factor receptor signalling, all of which facilitate cellular processes involved in oncogenesis, tumour progression, and proliferation (Shevde and Samant, 2014, Stecca et

al., 2007, Schnidar et al., 2009, Filbin et al., 2013). Activation of GLI1, and mutation of SMO, have been reported to correlate with therapeutic resistance in different tumours, and are also thought to be associated with poor outcomes due to an increase in cell proliferation, invasiveness, cell mobility, and differentiation (Li et al., 2016, Chen et al., 2011, Long, 2015, Mozzetti et al., 2012, Ferruzzi et al., 2012). SHH signalling was downregulated in Glioblastoma cell lines T98G and U87MG using curcumin (is an indian traditional medicine and the main active ingredient in turmeric, which give it the yellow colour. Its belong to family Zingi-beraceae)(Shanmugam et al., 2019). Protein and mRNA expression were studied and each showed a reduction. Additionally, U87-implanted nude mice injected with intraperitoneal curcumin demonstrated reduction of tumour GLI expression and tumour size, as well prolonged survival. In addition, curcumin has been used in ayurvedic medicine and been studied well in glioma cell lines. However, many molecular pathways demonstrated response to curcumins such as celluar proliferation, autophagy, apoptosis, angiogenesis, invasion, immunomodulation, metastasis, and multidrug resistance implying the effects may not be specific to HH inhibition (Klinger and Mittal, 2016, Du et al., 2013, Lian et al., 2015, Zanotto-Filho et al., 2015, Meng et al., 2017, Zanotto-Filho et al., 2011).

In addition there also appears to be interaction with this pathway between the tumour and its stroma. In glioblastoma cells, HH ligand secreted from the tumor stroma enhanced the SHH pathway maintenance activity. Bruan et al. developed a reporter gene that was able to indicate whether the HH ligand was extracellular or intracellular. Using this reporter, they observed a negative effect of cycoplamine on GBM cells, indicating that HH acts in an autocrine manner in GBM (Braun et al., 2012, Ferruzzi et al., 2012).

Therefore, specific inhibition of the HH pathway may be associated with improved effectiveness of therapy of glioblastoma by limiting tumour growth, tumour microenvironment interaction and improving clinical outcome by overcoming the intrinsic resistance of the tumour to standard treatments.

The relationship between the SHH signalling pathway and chemoresistance has been previously explored in a number of studies. Inhibition of GLI transcription factor activity demonstrated impaired DNA repair response and reduced drug transfer by ABC transporters in different tumour cell lines including glioblastoma (Chen et al., 2014, Cui et al., 2010, Queiroz et al., 2010, Cherepanov et al., 2016). Cui studied the effect of HH pathway inhibition on U251MG, U87MG and SHG44 Glioma and GBM cell lines and found inhibition of the HH pathway resulted in down-regulation of MDR1, MRP1, LRP, MGMT, Bcl-2 and Survivin mRNA expression (Cui et al., 2010). In another study by Sims-Mourtada et al, different tumour cells including SEG-1 (oesophageal adenocarcinoma); LnCaP (androgen-receptor-positive prostate carcinoma); PC3 (androgen-receptor-negative prostate carcinoma) and DM14 (metastatic squamous cell carcinoma) were treated with exogenous Shh ligand and GLI1-siRNA to investigate chemo-resistance associated with HH signalling. Their results showed Shh ligand binding resulted in a significant decrease in drug uptake as well as increased expression of Gli-1, MDR1 and BCRP. While GLI1-siRNA treated cells demonstrated decreased the expression of these molecules (Sims-Mourtada et al., 2007). He mechanisms underlying these relationships are not currently understood.

1.12 Reversal of Drug Resistance

Reversal of the drug resistant phenotype in cancer is a holy grail. Innovative approaches are required to target drug resistance mechanisms. Antisense oligonucleotides (ASOs), which can enhance cell apoptosis, are short single-stranded DNA molecules of approximately 20 nucleotides that target specific mRNAs and have potential in targeting multidrug resistance proteins (Chan et al., 2006). ASOs require a delivery system to allow for effective targeting of the tumour *in vivo* (Astriab-Fisher et al., 2000, Brigui et al., 2003). Studies using a specific MRP1 ASO, followed by chemo-sensitisation to single-agent chemotherapy using VP16 (etoposide) (Kuss et al., 2002), demonstrated that a lower dose of VP16 was required to kill neuroblastoma cells, compared to cells treated with VP16 alone.

1.13 siRNA: A More Recent Advance in Cancer Therapy

In 1997, Fire and Mello discovered RNA interference, and in the process invented a new mechanism for studying eukaryotic gene function, for which they were awarded a Nobel Prize in 2006. The injection of a specific double-stranded RNA (dsRNA) into cells was able to target a specific mRNA in Caenorhabditis elegans (Fire et al., 1998). As a result, scientists have studied the pathways induced by the exogenous dsRNA and its effect on nuclease activities in cells and have termed this process RNAi interference. RNAi interference can be used to specifically target genes in eukaryotes. MicroRNAs (miRNAs), and small interfering RNAs (siRNAs) are the major small non-coding RNAs that are involved in direct gene regulation (Manjunath and Dykxhoorn, 2010, Brantl, 2002, Bobbin and Rossi, 2016).

siRNAs are 20–25-nucleotide double-stranded RNA molecules that turn off gene expression by directing the degradation of specific mRNAs and changing chromatin structure in combination with the RNA-induced silencing complex (RISC) (Alberts et al., 2008). siRNAs have been developed over the last decade and are a powerful tool that can target and knock-down genes, owing to their specificity, and their ability to target specific mRNA sequences without affecting other untargeted genes. This feature of RNAi can be used to target different disease-causing proteins (Ge, 2010, O'Keeffe and Campbell, 2016).

However, siRNAs rapidly degrade in serum, they are inherently immunogenic, have poor bioavailability, and potential off-target effects (Hu and Zhang, 2012, Selvam et al., 2017). All of these reduce the ability of siRNA to be an optimal drug-like molecule. In order to overcome the challenges associated with siRNA therapeutics, the identification of appropriate chemical modifications that improve the stability, specificity, and potency of siRNA is essential (Selvam et al., 2017). Several modifications of siRNA such as of the sugar residues, the phosphate linkage, the base, the overhangs and the termini, can modify the architecture of the duplex (Figure 1-). Modification on the sugar moiety at the 2'-OH position is the most common and widely used, and includes 2'-O-methoxyethyl (2'-MOE), 2'-fluoro (2'-F), 2'-O-methyl, 2',4'-constrained 2'-O-ethyl (cEt), and locked nucleic acid (LNA) modifications (Bennett and Swayze, 2010). Modification of the 2'-OH does not affect the targeting ability of the siRNA. Methylation of the 2'-OH has however been found to increase nuclease stability and binding affinity. However, it has been argued that 2'-O-methylation can reduce the function and activity of the siRNA (Chiu and Rana, 2003, Braasch et al., 2003, Czauderna et al., 2003, Choung et al., 2006). On the other

hand, modifying the 2'-position of a functional siRNA by adding fluorine instead of a hydroxyl, alkoxy, or aryloxy substituent has been shown to increase serum stability, binding affinity, and nuclease stability, and therefore this represents the most useful modification (Chiu and Rana, 2003, Shen et al., 2015, Bumcrot et al., 2006). Using siRNA as a therapeutic target in different diseases has had some significant success. There are several clinical trials that are progressing well in Phase III (Bobbin and Rossi, 2016). Therefore, siRNA may represent the future of disease therapy.

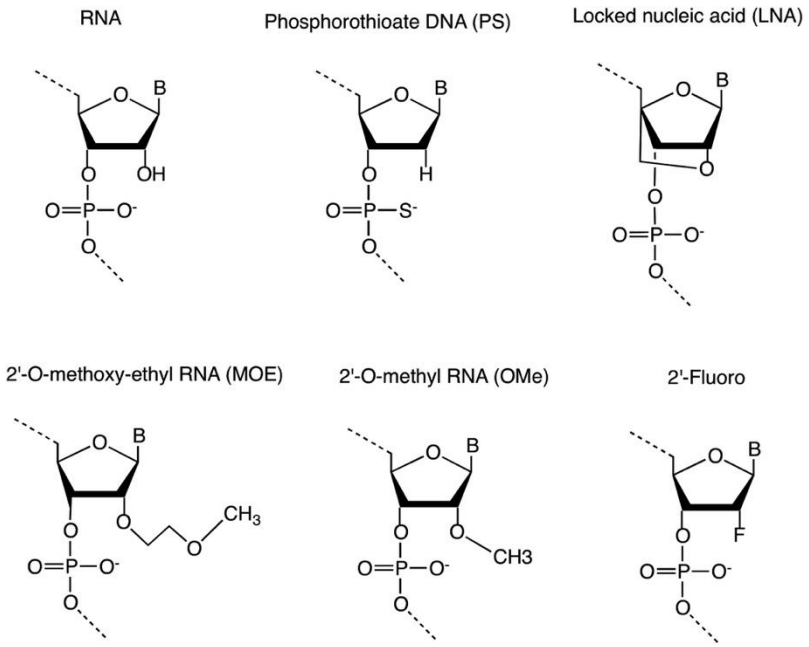

Figure 1-8 Examples of therapeutic nucleic acid chemical modifications (Indicated in figure). Adapted from (Burnett and Rossi, 2012). Permission obtained from Elsevier Publishing Group, License Number: 4095530909485

siRNA helps the RISC complex cleave the target gene mRNA (Kurreck, 2008) by binding to mRNA then allowing the endonuclease to cleave the target mRNA into small pieces

(Figure 1-). As a result, this process blocks and inhibits mRNA transcription and translation, thus prevents protein production (Alberts, 2008, Bruno, 2011).

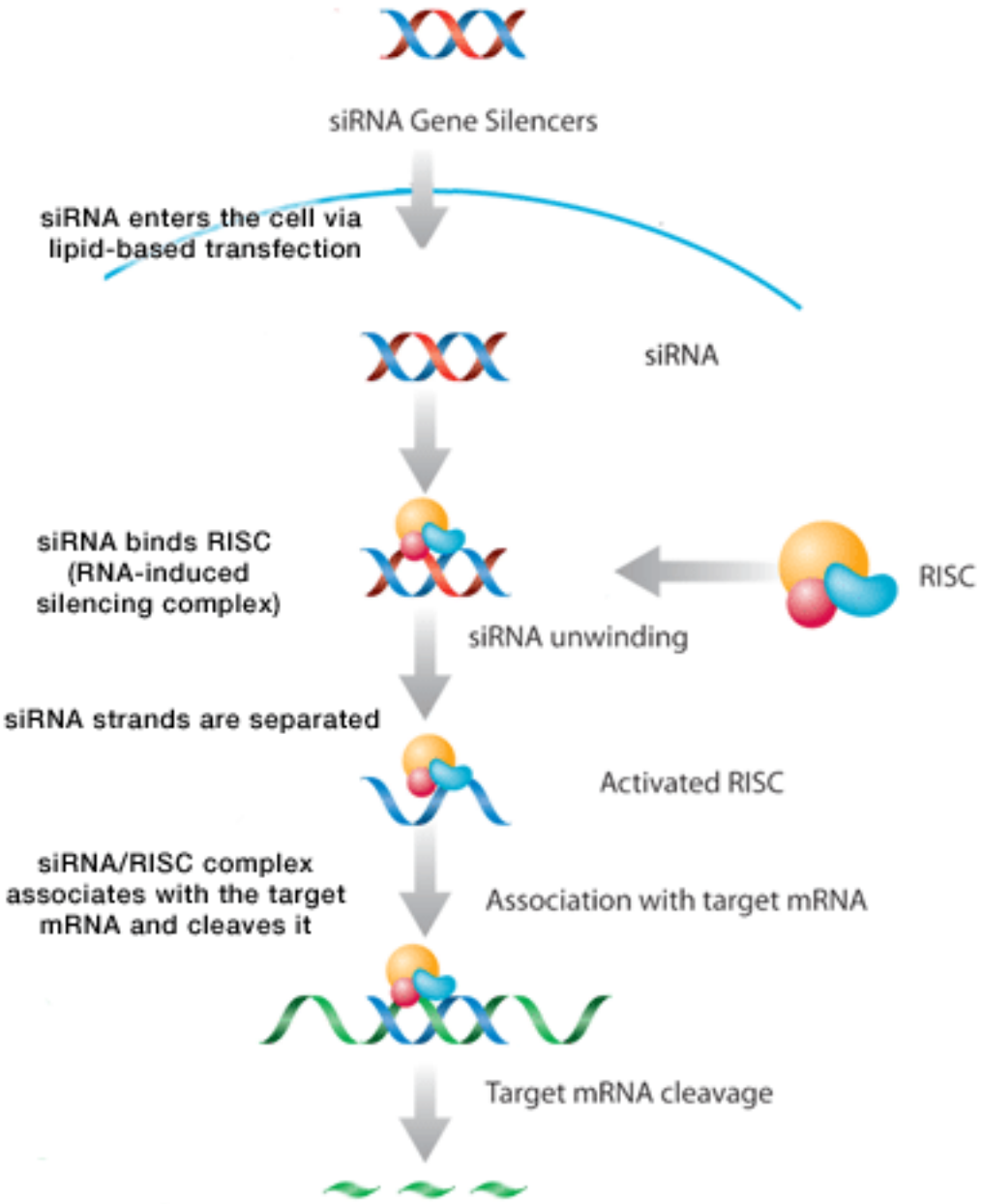

Figure 1-9 Schematic illustration of the gene silencing mechanism of siRNA in eukaryotic cells. The successful entrance of siRNA into the cell is followed by incorporation into the RNA-induced silencing complex (RISC). Following this, the siRNA unwinds to form a single strand. The resultant activated RISC containing the siRNA can then bind to its target site on the target mRNA. Following binding of the siRNA to its site, it induces mRNA cleavage that results in gene silencing. This diagram is adapted from http://www.scbt.com/images/en/gene_silencers/sirna_gene_silencers

1.14 Drug Delivery for the Treatment of Glioblastoma

It is important to stress that MRP1 expression is intrinsic to the chemoresistance of tumours in the central nervous system (CNS). (Mohri et al., 2000) MRP1 has been found to be expressed in nine out of eleven glioblastomas, and three out of six anaplastic astrocytomas. The mRNA and protein levels of MRP1 have been reported to be 4.5-fold higher in T98G glioblastoma cells compared to glioma cells (Mohri et al., 2000). MRP1 protein expression was reduced to 25% by treating cells with antisense oligonucleotides, and increasing the sensitivity of glioblastoma cells to chemotherapeutics, compared to control oligonucleotide-treated cells. This result confirms that human glioblastomas express functional MRP1, and that blocking its expression enhances chemosensitivity (Mohri et al., 2000). Targeting MRP1 may also have unique effects on tumour biology since an antisense oligonucleotide (ASO) molecule targeting MRP1 has been shown to cause significant apoptosis with reduced MRP1 expression in neuroblastoma, another tumour of the nervous system, without the addition of chemotherapeutic agents (Kuss et al., 2002, Kuss et al., 2011).

The effect of chemotherapeutic agents on apoptosis in human brain tumours can be increased with localised drug delivery. The combination of paclitaxel and curcumin has been shown to enhance apoptosis in glioblastomas using a nanoemulsion delivery system (Ganga, 2008). The idea of using localised therapy in glioblastoma cases can potentially overcome the side-effects experienced with the administration of high-dose systemic chemotherapy. Recently, the concept of inserting wafers loaded with chemotherapy drugs into tumour cavities was developed for use in cases of malignant glioma (Bota et al., 2007). The GLIADEL Wafer was developed by Guilford Pharmaceuticals and was

designed to release drugs over a two-to-three-week period. The GLIADEL Wafer is biodegradable and has been approved by the FDA since 2002. It increases the survival period in newly diagnosed patients up to several weeks (Kemper et al., 2004, Bota et al., 2007, Brem et al., 1995). However, it is limited with regard to the drugs that it can be loaded with, the amount of drug that can be released, and its release kinetics. Another potential method is siRNA delivery with liposomes and, more recently, with nanoparticles (Sawyer et al., 2006), which serve to protect the siRNA from rapid degradation, and localise it to specific sites (Ge, 2010).

1.15 The Difficulty of Drug Delivery

The current methods of delivering therapeutics to human brain tumours include both invasive and non-invasive strategies. The non-invasive strategies are systemic administrations through intravenous and oral routes, which have limited success due to chemoresistance. Administering high doses of drug to overcome chemoresistance has not improved the success of the treatment, and shows increased toxicity. The invasive strategy involves the administration of therapeutics by intra-arterial (IA) methods, using hydrostatic pressure via a catheter located within or around a tumour, or the intracerebral implantation of chemotherapeutic agents (Laquintana et al., 2009). This has also failed due to the BBB which is the connection that is formed between cerebral endothelial cells, and other neighbouring cells as pericytes, astroglia, neurons, perivascular cells, and microglia. The BBB constitutes a barrier of inter-endothelial tight junctions (TJ), uptake and efflux transport systems, as well as metabolic and enzymatic barriers (Deli et al., 2005, Abbott, 2005). TJ function controls the paracellular movement of micro- and macro-molecules, whereas the endothelial cells are responsible for the

movement of large solutes and trans-endothelial vesicular trafficking. In addition, these cells facilitate the CNS requirements such as ions, nutrients, potentially toxic metabolites, and metabolites that are expressed by plasma membrane transporters (Miller, 2015).

The BBB and the blood–cerebrospinal fluid barrier (BCSFB) control circulation in the microvasculature and cerebrospinal fluid (CSF), respectively, which are the most important gateways to enter the brain parenchyma. Thus, the majority of small molecule drugs and macromolecule agents, such as proteins, peptides, and antibodies do not permeate into the brain parenchyma, which is one of the most significant challenges for developing an effective CNS drug delivery.

The BBB creates a privileged microenvironment (Blecharz et al., 2015). The main problem associated with therapeutic approaches is the reduction in the response of brain cells to pharmacotherapy in general. About 30–40% of patients do not respond to psychoactive drugs, although they do readily penetrate the BBB (Su et al., 2009). Many factors play a role in this situation, the most important of which is genetics. However, researchers have found that MDR1 also plays a key role as the majority of drugs are MDR1 substrates, meaning that MDR1 affects their pharmacokinetics, interactions, and efficacy (Su et al., 2009). Su found that the concentration of a metabolite of amitriptyline in brains lacking MDR1 at the BBB, is up to 10-fold higher than in brains expressing MDR1. In addition, the short half-lives of some therapeutic agents in blood plays a role in limiting their concentration in glioblastoma cells. Hence a delivery system that either penetrates the BBB or be able to be delivered locally with high cellular penetration and longevity within the cell is required.

As described in previous studies, many kinds of delivery systems can be used to deliver oligonucleotides such as cationic lipid complexes, polypeptides, surfactants, liposomes, and polycationic dendrimers. However, it is difficult to use these materials in human brain tumours for several reasons. For example, (Yoo and Juliano, 2000) found that polycationic dendrimers are toxic when not in serum. Furthermore, the behaviour of most of these materials within the body is not entirely understood (Yoo and Juliano, 2000).

Exogenously delivered siRNA can silence the MRP1 gene, and facilitate the diffusion of hydrophobic chemotherapeutic molecules (e.g. camptothecin and doxorubicin) across the lipid bilayer of the cell membrane (Munoz et al., 2007, Cole, 2014). The administration of naked siRNA has been shown to increase the efficacy of some chemotherapeutics in some cancers (Devi, 2006, Guo et al., 2013). However, negatively charged naked siRNA is subject to poor cellular uptake, as well as intracellular degradation, because of endogenous enzymes in the cytoplasm (Zeng and Cullen, 2002). Therefore, to facilitate the transfection of siRNA in a clinical setting, non-viral vectors have been used to treat cancer cells.

Recently, researchers have attempted to use a new methodology that uses nanostructured porous silicon to deliver oligonucleotides into tumour tissue (Laquintana et al., 2009). The delivery of siRNAs to GBM tumour cells using nanoparticles (NPs) has been shown to protect siRNAs from nucleases and promote sustained release of the siRNA (Deeken and Löscher, 2007, Ballarin-Gonzalez et al., 2013, Shi et al., 2014).

1.16 Nanomedicine:

Nanoparticles are an attractive biomaterial whose use has increased dramatically in the biomedical field, especially in the therapy of cancer. They can be used as highly specific materials for the delivery of drugs or genes to organs and tissue sites (Gutkin et al., 2016). Different types of nanomaterials have been used in cancer therapy, such as polymers, spheres, and capsules (Gaitzsch et al., 2015), semiconductor quantum dots (Das et al., 2015), iron oxide (Kievit et al., 2011), gold (Cheng et al., 2015), silver (Hernandez et al., 2012), metal-organic frameworks (Furukawa et al., 2013), carbon nanotubes (Kostarelos, 2007), liposomes (Yang et al., 2014), and mesoporous silica (Shen et al., 2014).

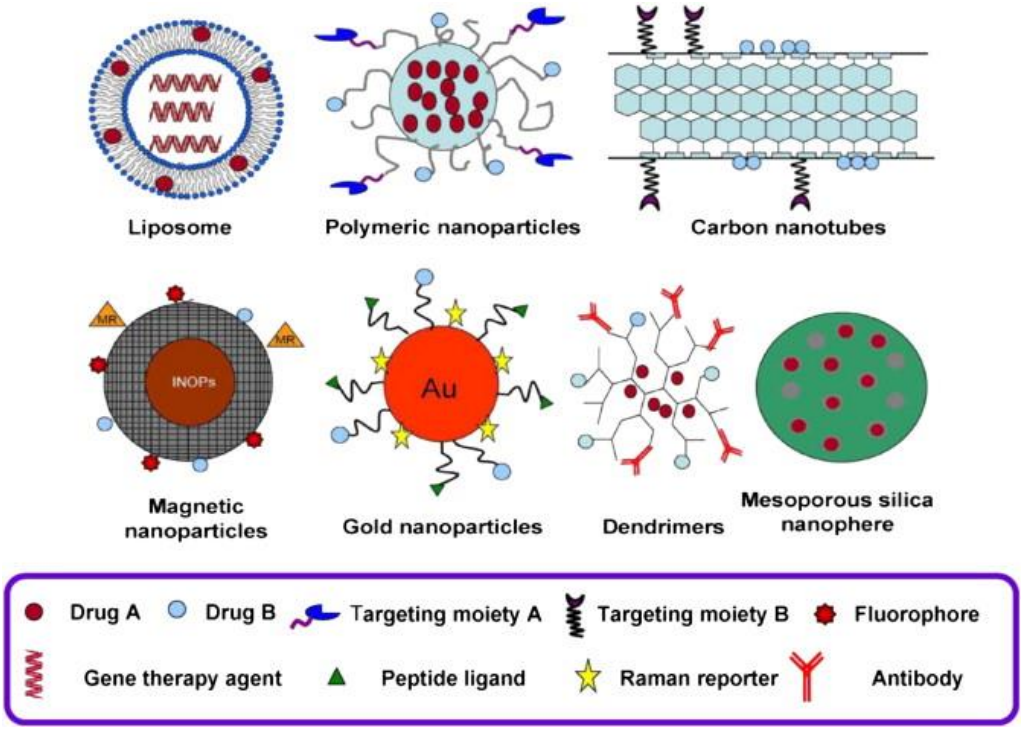

Figure 1-10 Schematic illustration of the different types of nanoparticles commonly used for biomedical applications and drug delivery. Adapted from (Gao et al., 2014).

Some nanoparticles can function to co-deliver two or more drugs for combination therapy, are able to deliver poorly water-soluble drugs (such as paclitaxel) as well as macromolecular drugs to intracellular sites; and can be used for drug delivery site visualisation by incorporating imaging capability. An important property of nanoparticles is their size. In addition, nanoparticles can penetrate up to ten-fold more in tumour tissues than in normal tissues (Meng et al., 2013, Barreto et al., 2011, Kamaly et al., 2012). This increased accumulation of nanoparticles is due to a phenomenon referred to as enhanced permeability and retention (EPR). Blood plasma circulation time is an important parameter in the delivery of nanoparticles. In tumour tissue, abnormalities in the space between endothelial cells, and dilation of tumour blood vessels cause hyperpermeability of the blood vessels, leading to leakage of blood plasma into the

interstitial tumour tissue spaces. This enlargement in the size (of the order of hundreds of nm, compared to normal tissue which is of the order of tens of nm) leads to an increased penetration of nanoparticles into tumour tissues (Torchilin, 2011, Nichols and Bae, 2014, Stylianopoulos, 2013, Hobbs et al., 1998).

1.17 Porous Silicon Nanoparticles (pSiNPs)

Porous silicon nanoparticles (pSiNPs) are a nanoparticle-based drug delivery vehicle that is a new addition to the field of nanomedicine. Recent research into glioblastomas has shown that it is possible to use biocompatible, biodegradable, synthetic materials with high porosity as drug vehicles for delivering oligonucleotides into tumours (Steiniger et al., 2004, Fang et al., 2015, Lee et al., 2015). Canham was the first to use porous silicon (pSiNPs), a high surface-area form of the semiconductor silicon in vivo, and optimise absorbability and biocompatibility of this material (Canham, 1995, Anglin et al., 2008). pSiNPs can be used as a device to deliver many drugs, including the steroid dexamethasone, ibuprofen, cisplatin, doxorubicin, insulin, and anticancer drugs. Its principal use is to minimise the risk and side effects of drugs, while simultaneously increasing their potency. Numerous studies have shown the successful use of pSiNPs as a drug delivery method (Anglin et al., 2008, Yalçın et al., 2016, Tosi et al., 2016). The size of the pores in pSiNPs can be controlled by the fabrication conditions using electrochemical anodization. Using this, it is possible to generate micropores (<5 nm), mesopores (5–50 nm), and macropores (>50 nm) (Canham, 1997, Anglin et al., 2008, Kopermsub et al., 2011, Pastorino et al., 2016). These materials can be loaded with a variety of bioactive materials, such as proteins, nutrients, drugs, peptides, and oligonucleotides, owing to their large surface area of about 400–1000 m2/g (Cheng et al.,

2008, Vasani et al., 2011). Approximately 1.95–2.02 µg of siRNA could be successfully loaded onto 1 mg of oxidised and amine-functionalised pSiNPs nanoparticles (Kopermsub et al., 2011). There are additional properties that encourage the use of pSiNPs nanoparticles as vehicles. Non-toxicity and degradation within the body increase their usability compared to other nanomaterials such as carbon nanotubes or quantum dots. Under conditions of chronic dosing, pSiNPs are preferred because they do not need to be removed, whereas carbon nanotubes remain in the body, and can induce toxicity. Degradation of the pSiNPs in aqueous solution over time results in a complete conversion into the non-toxic silicic acid, the major bioavailable silicon form, which is physiological and well tolerated. The dissolution of pSiNPs materials is expected to occur over a period of eight-nine weeks (Kashanian et al., 2010). Another advantage of Si-based nanoparticles is that they can be easily sterilised due to their inorganic nature (Anglin et al., 2008, Jane et al., 2009, Low et al., 2009, McInnes and Voelcker, 2009, Vasani et al., 2011). The surface of pSiNPs can also be easily chemically modified compared to other polymeric biomaterials, without affecting the material's properties. Furthermore, pSiNPs can be assembled into membranes, films, pellets, and particles, and their degradation kinetics can be finely controlled via chemical alteration of the silicon material base, fabrication conditions, and the type of surface functionalization used (Low et al., 2009). The structural integrity of the material can be improved by ozone oxidation, and subsequent surface treatments with silanes and biological materials, such as rat collagen or foetal calf serum. Once synthesised, the surfaces can be characterised using a variety of commonly used methods, including atomic force microscopy for topography, water contact angle measurement for wettability, interferometric reflectance spectroscopy for stability in aqueous solution, and Fourier-transform infrared spectroscopy for surface

chemistry (Anglin et al., 2008, Low et al., 2009, Vasani et al., 2011, Worsfold et al., 2006). Compared to other polymeric materials, the surface chemistry of pSiNPs can be modified with a simple one-step chemical treatment without changing properties (Voelcker, 2014, Sweetman et al., 2011). The degradation kinetics and structural integrity of the material can be preserved by stabilising the pSiNP surface in contact with physiological fluids. Controlling these parameters can change the half-life *in vivo* from hours to months. Optimisation can be achieved by changing the chemistry of the silicon material base, surface functionalisation, as well as the conditions used for synthesis (McInnes and Voelcker, 2009, Yildirimer et al., 2015, Kamaly et al., 2016).

Currently, pSiNPs are being adopted for a range of different uses. In the optical biosensor industry, silanized pSiNPs have been used for the capture and cross-linking of peptides, oligonucleotides, and antibodies (Jane et al., 2009). Nanostructured pSiNPs have also been used as a scaffold for orthopaedic (Coffer et al., 2005) and ophthalmic implants (Kashanian et al., 2010), including implants into the vitreous of rabbit eyes (Cheng et al., 2008). Nanostructured pSiNPs attached to both human and rat optical tissues (Cheng et al., 2008, Kashanian et al., 2010), and their derivative materials, were shown to support the attachment and growth of these different mammalian cells (Low et al., 2006, Khung et al., 2006, Khung et al., 2008). Previous studies have shown that epithelial cells could not be easily attached to ozone-oxidised or polyethylene glycol-silanized surfaces, due to the inclusion of collagen-coated and amino-silicone surfaces on the pSiNP. However, increased degradation of the pSiNPs occurred over a time period of 24 hours, despite the success in the attachment of a wide range of mammalian cells in morphology studies (Kashanian et al., 2010, Low et al., 2006, Khung et al., 2008).

Taken together, these previous reports suggest that pSiNPs are a suitable choice of material to be placed in the brain tissue cavity after tumour resection, in order to increase the apoptosis of glioblastoma cells induced by the controlled delivery of therapeutic oligonucleotides. There are several examples of the use of pSiNPs in GBM. Intratumoral hypoxia in GBM could be treated using an NP-siRNA targeting hypoxia-inducible factor-1α (HIF-1α) (Aldea et al., 2016, Liu et al., 2012). In addition, other researchers (Ebrahimi Shahmabadi et al., 2014), have demonstrated an effect of cisplatin loaded polybutylcyanoacrylate (PBCA) nanoparticles (NPs) in GBM. As a similar approach, the most widely used chemotherapeutic for the treatment of GBM, TMZ, has been successfully loaded onto pSiNPs, and successfully delivered to GBM cells. Compared to TMZ treatment alone, this resulted in an increase in uptake of 2–6 fold, and shift of 50–90% in the IC50 72 h post-treatment (Fang et al., 2015).

Further modifications to the surface, and the porous properties of the material may, however, be required, including the use of 150-µm thick n-type silicon, which has a slower degradation in aqueous solution; changing the thickness of the porous material increases the degradation period by up to eight weeks. There are several procedures used to prepare pSiNPs, including low-pressure plasma using Low Pressure Microwave Reactor (Knipping et al., 2004), solution phase synthesis (Zou et al., 2004), and the use of reverse micelles (Eastoe et al., 2006, Takemi Tanaka et al., 2010). However, these methods produce non-porous particles, which means that they are not useful for developing a drug delivery system. In contrast, an alternate method has been described that can be used to prepare particles with a size of 100–200 nm that demonstrates luminescence after incubation in water, due to the quantum confinement effect and the

presence of oxide defects at the silicon oxide-silicon interface. This approach uses electrochemical etching of the single-crystal wafers, followed by lifting of the porous film, ultrasonication, and filtration (Secret et al., 2013). Furthermore, the synthetic process and the subsequent complexing of the pSiNPs with therapy affect the pSiNPs surface charge which may then be either positive, negative or neutral depending on what is bound.

1.18 Delivery of siRNA Loaded into pSiNPs

As previously described, siRNAs loaded into pSiNPs are required in order for the siRNA not to be rapidly degraded in solution. In addition, loading into the pSiNP allows for slow release, increasing its targeting effectiveness.

In contrast to the rapid degradation of freshly prepared pSiNPs in aqueous solutions (which occurs within minutes), which accelerates the release of loaded oligonucleotides, thermal hydro-carbonisation (THC) of pSiNPs post-fabrication produces a stable Si–C layer on the pSi surface (Kafshgari et al., 2015a). As a result, the release of peptides, oligonucleotides, and hydrophobic model drugs, from THC-pSiNPs is sustained *in vitro* and *in vivo* (Liu et al., 2013, Kovalainen et al., 2012). Capping the pSiNP pores after loading with positively charged polymers such as polyethyleneimine (PEI) can further extend release and also promotes the cellular uptake of the negatively charged siRNA (Li et al., 2011, Takemi Tanaka et al., 2010). Endosomal escape of siRNA from the siRNA-loaded nanocarriers is crucial for silencing of the target gene to occur (Figure 1-) (Ma, 2014, Gilleron et al., 2013).

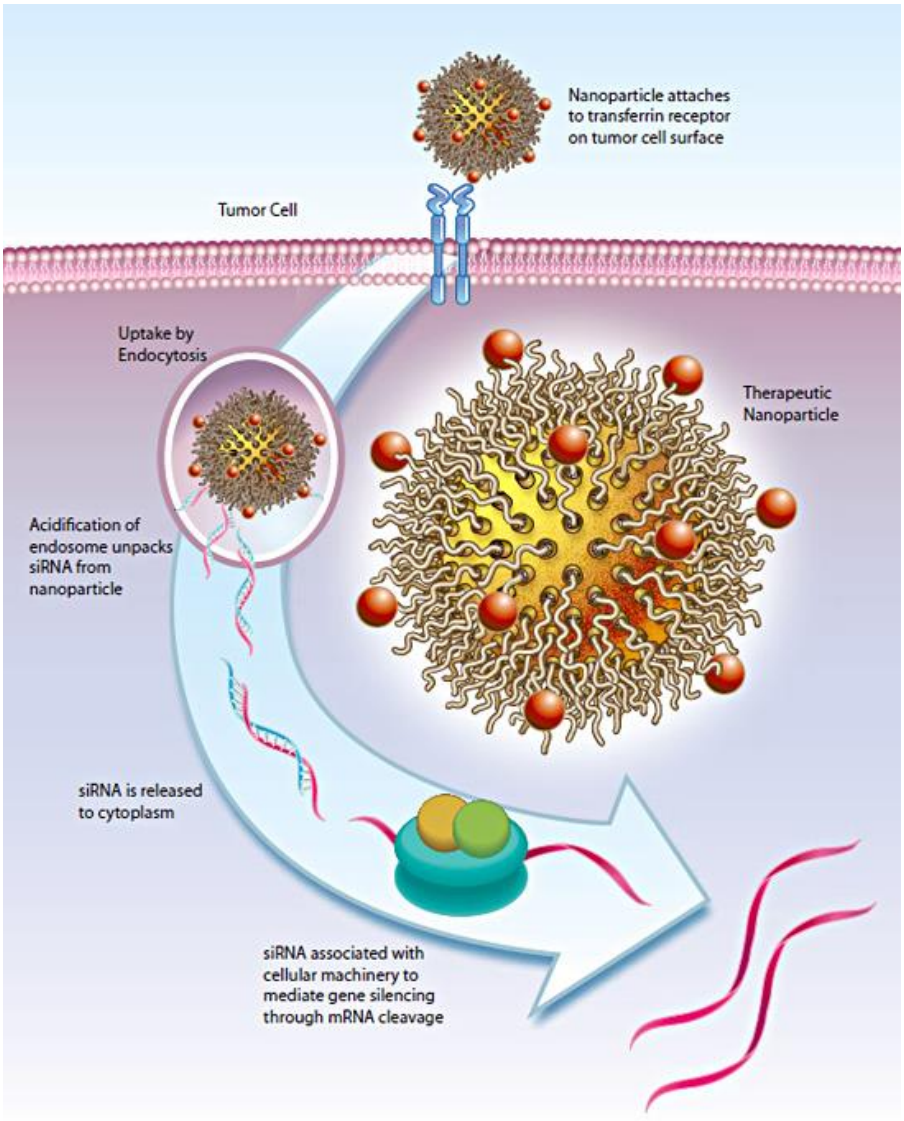

Figure 1-11 Schematic illustration of the delivery of nanoparticles followed by siRNA release into the cytoplasm and cleavage of the target mRNA. Adapted from http://arrowheadnew.designlogic.us/technology/rondel

The pH-responsiveness of PEI also aids in the endosomal escape of pSiNPs via the 'proton sponge effect' allowing the oligonucleotide payload to reach its cytoplasmic target. The proton sponge effect states that after endocytosis the endosome may burst resulting in a rapid release of its contents into the cytoplasm. This effect is utilized as a drug delivery method for example to release contents packaged in micelles (usually coated in PEG or

another protective polymer) into the cytoplasm of a cell after being endocytosed. pSiNps can also utilise this effect. Recently, an siRNA delivery model, using mesoporous silica NPs (MSNs) coated with PEI, demonstrated the downregulation of green fluorescent protein gene expression (Li et al., 2011). However, the well-documented cytotoxicity of MSNs, due to their disruption of mitochondrial membranes and the generation of reactive oxygen species (ROS), is a major limitation for their use (Lee et al., 2013, Jambhrunkar et al., 2014, Di Pasqua et al., 2008, Dunnick et al., 2014). pSiNPs do not show this level of toxicity either *in vitro* or *in vivo* and should therefore be of greater utility (Park et al., 2009). In this regard, PEI-facilitated cellular accumulation and internalisation of pSiNPs has been shown to accelerate apoptosis in solid tumours (Shen et al., 2013). Although post-fabrications such as amine and oxidised modifications on the surface of pSiNPs may induce inflammation, such toxicity can be eliminated through the use of a final polymeric coating (Bax et al., 2014, Licciardi et al., 2013, Kafshgari et al., 2015).

AIMS AND HYPOTHESIS

Hypothesis

It was hypothesised that MRP1 expression is a critical determinant of the multidrug resistance phenotype in glioblastoma tumours and that down regulation of MRP1 would result in alteration of the malignant phenotype. It was also hypothesised that by downregulation of MRP1 other key cellular pathways may be affected which contribute to the multidrug resistance phenotype in glioblastoma due to its known transporter functions within the cell membrane. It was the original intention of this thesis to explore Sonic Hedgehog Expression in GBM and to modulate its expression using porous silicon particles as a delivery system. However, upon discovery of a relationship in expression in GBM of MRP1 and members of the sonic hedgehog pathway, this latter aim was modified.

1. Reducing the expression of MRP1 is predicted to change the biology of GBM including the MDR phenotype.
2. That the multidrug resistance phenotype of glioblastoma cells is enhanced by a relationship between the SHH pathway and MRP1 expression.

Aims

To develop a nanoparticle system capable of delivering siRNA or small molecules to Glioblastoma cell lines both *in vitro* and *in vivo*.

To establish whether a relationship exists between MRP1 and the SHH pathway as a driver of the MDR phenotype.

To explore the change in the gene expression profile of GBM cell lines in response to downregulation or functional inhibition of the MRP1 protein.

2 MATERIALS AND METHODS:

2.1 Cell Culture Materials

All cell culture methods were published and in current use in Molecular Medicine and Pathology, Flinders University. All cell culture was performed under sterile conditions in laminar flow hoods. Millipore Milli-Q water with a resistivity of 18 MΩ cm was used for all the experiments.

2.2 Cell Culture Medium:

Roswell Park Memorial Institute Medium (RPMI) Media 1640 and Dulbecco's Modified Eagle Medium (DMEM) were purchased from Sigma-Aldrich (St. Louis, MO, USA).

Opti-MEM reduced serum medium, Fetal Bovine Serum (FBS), L-glutamine, and penicillin/streptomycin were purchased from Invitrogen (Carlsbad, CA, USA).

The medium was supplemented with 10% Fetal Bovine Serum (FBS), L-Glutamine-200 mM at 10 uL/mL of media, sodium bicarbonate, 100 units/mL of Penicillin and 100 µg/mL of streptomycin.

RPMI 1640 and DMEM were used to maintain cell line growth. Opti-MEM reduced serum medium was used in siRNA transient transfection, THCpSiNPs and MK-571 treatments.

2.3 Cell Culture Methods:

2.3.1 Thawing Cells:

Cell lines stored in liquid nitrogen in liquid phase were removed from liquid nitrogen storage as required. Upon removal, cell vials were rapidly thawed in a 37°C water bath.

This process was performed as rapidly as possible to avoid cell toxicity from Dimethyl sulfoxide (DMSO). 1 mL of appropriately warmed (37°C) media was immediately added to each vial drop by drop over 5 min. The cell suspensions were then transferred to sterile 10 mL tubes, and an additional 8 mL of media was added to a total volume of 10 mL. 50 µL samples were then removed from each tube for counting and remaining cells pelleted by centrifugation at 500 g for 5 min. The supernatant was then removed, and cells resuspended in 1 mL of media for viable cell counting using Trypan Blue exclusion (Section 2.3.2).

2.3.2 Freezing Cells:

Cell lines were frozen and stored in liquid nitrogen to maintain stocks. Confluent cells were trypsinised, centrifuged and resuspended in freezing medium. The freezing mix prepared prior to use contains 2.5 mL media, 1 mL FBS and 1.5 mL DMSO which is filtered through a 0.2 µm filter in a cryogenic vial. Cells were transferred immediately to liquid nitrogen storage.

2.3.3 Cell Lines:

The experiments in this thesis were performed with two human high-grade glioblastoma cell lines, T98G and U87MG, which express MRP1 (Mohri et al., 2000; Bähr et al., 2003, Peigñan et al., 2011). The T98G GBM cell line has been shown to possess the highest drug and radiation resistance while U87MG has lower resistance (Kundu et al., 2012). U87MG and T98G are kind gifts from Dr Kerrie McDonald, Cancer Institute NSW (Fowler et al., 2011). The T98G glioblastoma cell line was derived from a 61-year-old Caucasian male diagnosed with GBM tumour. A characteristic of the T98G GBM cell line is that it enters a viable G1 arrested state if overgrown (confluent) or deprived of serum. In culture, T98G

cells grow as anchorage independent cells (Stein, 1979). The chromosome count of the T98G cell line is hyper pentaploid with 128 to 132 as the standard number of chromosomes (American Type Culture Collection (ATCC)). However, only 1.39% of cells have been demonstrated to possess the hyper pentaploid karyotype (Stein, 1979, Rostomily et al., 1997).

In these studies, 10% FBS supplemented media was pre-warmed to 37°C in a water bath prior to use. T98G and U87MG cell lines were incubated at 37°C, in a humidified 5% carbon dioxide (CO_2) atmosphere in 20 mL of appropriate media in T75 (75 cm^2) flasks. Cells were split twice a week when they reached 80% confluence and passaged at a ratio of 1:3.

2.3.4 Maintenance of Cell Lines:

2.3.5 Cell Trypsinisation:

Trypsin was used to harvest cells. Cells were washed with 3 ml of PBS in T75 flasks following aspiration of the medium. 1ml of 0.25% Trypsin/EDTA was then added to each flask and incubated until cells detached from the surface at room temperature. 9 mL of medium was added to each flask to deactivate and neutralise the trypsin then cells were transferred into a fresh 10 mL tube. 50 µL of cells were removed to determine cell viability. Cells were spun at 1200 g for 5 min, then resuspended in 1mL fresh media prior to cell counting and further experimental procedures.

2.3.6 Cell Counting and Viability Assay with Trypan Blue

Prior to each experiment, the viable cell number was ascertained. Cells were counted using a haemocytometer under a light microscope with 10 times magnification. 50 µL of cells were taken from harvested cell lines and mixed with an equal volume of Trypan Blue.

The viable cell count was established by Trypan Blue exclusion, bright cells are viable and blue cells non-viable, using the following equation, where the result is cells/mL

$$\frac{\textbf{Total number of cells in 2 squares}}{\textbf{Number of Haemocytometer squares counted}} \times 2(Dilution\ factor) \times 10x^4$$

2.3.7 Mycoplasma Detection Methods

All cell lines were screened for mycoplasma contamination upon establishment in culture. All cell cultures used in this project tested negative for mycoplasma infection. Three methods were used to clarify mycoplasma negativity in cell lines; Polymerase Chain Reaction (PCR), 4'-6'-Diamidino-2-phenylindole (DAPI), and Mycoplasma Detection Kit – QuickTest (Bio-tool).

2.3.8 Mycoplasma Detection by PCR:

A 200 µL cell suspension was taken from each flask and 1 mL of sterile saline added before cells were pelleted by centrifugation at 6500x g for 5 min, and the supernatant removed. The pellet was then resuspended in 90 µL 0.05M NaOH then the solution incubated for 10 min at 98°C to simultaneously lye cells and extract DNA. The solution was then neutralised with 10 µL 1M Tris-HCl, pH7.5 and allowed to cool. DNA was then diluted 1:10 with sterile water for injection BP in preparation for PCR.

Primers MGSO 5'-TGCACCATCTGTCACTCTGTTAACCTC-3' (mycoplasma genus-specific oligonucleotide) and GPO-1 5'-ACTCCTACGGGAGGCAGCAGTA-3' (a primer complementary to mycoplasma 16S rRNA) were used to amplify a mycoplasma genus-specific sequence of 715 bp that is routinely used for the detection of mycoplasma

contamination in cell cultures. An internal control gene was also amplified using primer specific to HRAG1 (see Table 1 for primer sequences).

Table 2-1 Primers used for mycoplasma testing of cell lines

Primer	Sequence	Product Length
Mycoplasma specific		715bp
GPO-1 (forward)	5' ACTCCTACGGGAGGCAGCAGTA 3'	
MGSO (reverse)	5' TGCACCATCTGTCACTCTGTTACCCTC 3'	
Internal Control		573bp
HRAG1 (forward)	5' GCCATGAAGAGCAGTGAATTA 3'	
HRAG1 (reverse)	5' AGGAATTAACTCACAAACTGC 3'	

For PCR reactions, each tube contained the following: 2.5 µL 10x AmpliTaq Gold buffer, 1 µL 50 mM MgCl2, 10 mM dNTPs, 100 ng GPO-1 primer, 100 ng MGSO primer, 50 ng HRAG1-forward primer, 50 ng HRAG1-reverse primer, 0.2 µL AmpliTaq Gold, 15.8 µL sterile water for injection, and 2 µL DNA for a final volume of 25 µL. (van Kupperveld 1992) Two additional cell lines were also used as controls; one a known positive for mycoplasma contamination and another known negative for mycoplasma.

PCR products were run in an iCycler thermocycler. PCR cycling conditions were as per Table 2.

Table 2-2 Mycoplasma PCR cycling conditions

Number of Cycles	Cycle duration	Temperature
1 cycle	10 min	94°C
50 cycles	30 seconds denaturation	94°C
	1 min annealing	53°C
	1 min elongation	72°C
1 cycle	5 min last extension cycle	72°C

The absence of the mycoplasma specific 715 bp band indicated the mycoplasma result is negative.

2.3.8.1 Agarose Gel Electrophoresis

Agarose gel electrophoresis was routinely used to visualise PCR products throughout this thesis. 1X TBE buffer (10.8 g Tris and 5.5 g, Boric acid in 900 ml distilled water and 4 ml 0.5 M Na2EDTA (pH 8.0)) was used to make and run gels. PCR products were analysed in 2% agarose (LE, analytical grade) gels containing 5% ethidium bromide. Gels were run at 180 volts for approximately 1.5 hrs. Products were subsequently visualised with UV trans-illumination.

2.3.9 Mycoplasma Detection Kit – QuickTest

The principle of this kit is to detect the degradation of culture medium components by the metabolic enzyme produced by mycoplasma. These metabolites are highly specific to mycoplasma and are not produced by bacteria or eukaryotic cells. The QuickTest kit contains test strips, reaction A, reaction B, stop solution and positive control. The mixture changes colour according to the concentration of the metabolites produced by

mycoplasma. If the sample is infected with mycoplasma, the colour will turn greenish-blue. The OD value of the examined samples was measured and compared to negative and positive controls. All materials and samples were stored at room temperature. 100 µL of reaction A was added to all wells. The first well was left blank and 10 µL of media was added to the second well as a negative control. This media was incubated under the same conditions as cells in culture for 48 hours. Then, 10 µL of the sample supernatants was added to all wells. 100µL of reaction buffer B was added to all wells and shaken gently. Samples were incubated at room temperature for 7 minutes, then 10 µL of stop solution was added. Samples were measured at Em630 nm using a fluorescent microplate reader.

The OD value of the blank well was set as zero, and OD of samples were measured. The equation for calculating the value of OD was as follows:

$$OD_{sample}\ (ODs) - OD_{negative\ control}\ (ODc).$$

If the ODs – ODc is ≥ 0.105, the sample is defined to be contaminated by mycoplasma. In contrast, if ODs – ODc is < 0.105, the sample is free of mycoplasma.

2.3.9.1 Mycoplasma Detection by DNA fluorescence staining (DAPI):

Cells were grown in 6 well plates. After medium was aspirated, cells were incubated with 4% paraformaldehyde at room temperature for 15 minutes, followed by two washes with 1xPBS and incubated for one minute with DAPI solution. Cells were washed three times with 1xPBS and resuspended in 500uL of 1xPBS then visualised using an Olympus FV1000 confocal microscope. Also, 50uL of fixed cells were mounted on a slide and one drop of DAPI was added and visualised using immunofluorescence microscope. If the sample is negative for mycoplasma contamination, the nuclei have a clear appearance without any

polymorphic bodies surrounding the cells. In contrast, if clusters surround the nuclei, the sample is positive for mycoplasma.

2.4 MRP1 Targeted in T98G Glioblastoma Cell Line:

2.4.1 Plating/Preparation:

Cells were seeded at a density of $3x10^5$ per well in 6 well plates with 2 mL Opti-MEM® I Reduced Serum Medium 24hrs prior to treatment with siRNA to allow cell adherence to the well surface. The experiment contained controls, untreated cells, negative control siRNA, and two different siRNAs targeted to MRP1. Each sample was plated in triplicate for two-time points, 48 and 72 hours (based on the half-life of the MRP1 protein 48, 72 hr) (Stewart, 1996), post-treatment. Cells were incubated under standard incubation conditions (37°C, 5% CO_2).

2.4.2 DMEM without Antibiotic:

DMEM (Sigma-Aldrich) with supplement no antibiotic or FBS was used to grow cells before and after siRNA transfection. Media with 10% FBS was used 24 hours after the second treatment

2.4.3 Opti-MEM® Reduced-Serum Medium:

Opti-MEM® Reduced-Serum Medium (Invitrogen) was used to prepare siRNA and Lipofectamine prior to transfection. Reduced serum reduces siRNA degradation (Hu and Zhang, 2012). Transfected cells were grown in Opti-MEM® reduced serum media after transfection for 24 hours.

2.4.4 Cell Viability:

50 µL of treated and untreated harvested cells were taken at 24, 48, 72 and 96 hour time-points following the treatment. These samples were analysed for cell viability using Trypan blue exclusion (Trypan Blue purchased from BDH Chemical Ltd, Poole, England and prepared as 0.2% w/v solution in 0.9% w/v sodium chloride solution).

2.4.5 Harvesting/ Time (post-treatment time points):

Media was aspirated from the wells and retained. Cells were then washed with 1xPBS followed by the addition of trypsin. This wash was added to the retained media. Trypsinised cells were washed twice with 1xPBS and centrifuged at 1200 g for 5 min for RNA extraction, Annexin V analysis (2.7.2), protein level analysis (2.7.1), Calcein-AM uptake (2.7.3) and cell cycle analysis (2.7.4).

2.4.6 siRNA Treatment:

2.4.6.1 Lipofectamine:

Lipofectamine 2000 (Invitrogen) and siRNA complex diluted in Opti-MEM reduced serum media were freshly prepared according to the manufacturer's recommendations. In summary, on the day of transfection, 9uL of Lipofectamine reagent was diluted with 150uL of Opti-MEM® Reduced-Serum Medium for 5 min at room temperature. At the same time, 9uL of 20uM siRNA duplex stock was diluted in 150uL of Opti-MEM® Reduced-Serum Medium. The siRNA duplex, and Lipofectamine reagent solutions were gently mixed together followed by incubation for 20 mins at room temperature. After that, siRNA-Lipofectamine solution was added to cells in each well as per treatment requirement.

2.4.7 Transient Transfection of MRP1-siRNA in T98G Cells:

Cells were exposed to siRNAs to accomplish transient transfection using 150nM of two species of siRNA against MRP1 and a third representing a negative control (NC-siRNA) (see details in section 2.4.2). In brief, cells were plated at $3x10^5$ per well in Opti-MEM® Reduced-Serum media using a 6 well plate and grown overnight to allow adherence. Transfections were carried out using 9µL of lipofectamine and were performed at 0 and 24 hours.

2.4.8 siRNA:

siRNA was designed and synthesised by Shanghai GenePharma (Shanghai, China) by contractual arrangement with the department of Haematology using design principles as outlined on their website. siRNA duplexes, negative control siRNA and fluorescent-labelled siRNA were also designed by Shanghai GenePharma (Shanghai, China). The effectiveness and specificity of all agents were tested in the Flinders laboratory to confirm efficacy. Fluorescence-labelled siRNA sequence is identical to the siRNA for the MRP1 sequence. The BLOCK-iT™ Fluorescent Oligo, a fluorescein-labelled double-stranded RNA duplex (16.1 kDa), was designed as a detection tool for uptake of siRNA into cells (Invitrogen, Mulgrave, VIC, Australia. Exon 7 encoded for the protein membrane-spanning polymorphism domains while exon 17 encoded for the intracellular region of the protein hydrophilic nucleotide binding domains (NBDs) (Słomka et al., 2015).

Table 2-3 Oligonucleotide Sequences

		Sequence	(MRP1) Exon number
2'-Fluoro modified MRP1 siRNA (siRNA_A)	Sense	5'GAGGCUUUGAUCGUCAAGUTT3'	7
	Antisense	5'ACUUGACGAUCAAAGCCUCTT3'	
2'-Fluoro modified MRP1 siRNA (siRNA_B)	Sense	5'GGCCUGGAUUCAGAAUGAUTT3'	17
	Antisense	5'AUCAUUCUGAAUCCAGGCCTT3'	
Negative control siRNA (NC-siRNA)	Sense	5'UUCUCCGAACGUGUCACGUTT3'	
	Antisense	5'ACGUGACACGUUCGGAGAATT3'	
Block-iT™	---	FITC labelled oligonucleotide	

2.5 Porous Silicon Membrane:

2.5.1 Porous Silicon Membrane Synthesis:

The pSi membrane was synthesised by Morteza Hasanzadeh Kafshgari, Mawson Institute, UniSA. The fabrication of THCpSiNPs, Nitrogen sorption measurements, Dynamic light scattering and zeta potential, scanning electron microscopy (SEM), and TEM of cells were performed by MH Kafshgari. siRNA loading and release, PEI coating on siRNA/THCpSiNPs and Confocal microscopy experiments were performed by MH Kafshgari and Mohammed Alnakhli. Experiments for cell viability and proliferation, annexin V, qRT-PCR and protein level were performed by M Alnakhli. Additionally, mouse experiments were handled by WingYin Tong, Mawson Institute, UniSA, while RNA extraction and qRT-PCR were accomplished by M Alnakhli.

2.5.2 Fabrication of THCpSiNPs:

p+ type (0.01–0.02 Ωcm) silicon wafers were used to fabricate pSiNPs by periodically etching at 50 mA/cm2 (2.2 s period) and 200 mA/cm2 (0.35 s period) in an aqueous 1:1 HF(38%):EtOH electrolyte for a total etching time of 20 min. The pSi films were detached from the silicon substrate by increasing the current density to electropolishing conditions

(250 mA/cm2, 3 s period). In order to stabilise freshly etched hydride terminated pSi membranes, the detached multilayer films were thermally hydrocarbonised under N2/acetylene (1:1) flow at 500 °C for 15 min, and then cooled down to room temperature under a stream of N2 gas. Films were subsequently converted to THCpSiNPs using wet ball-milling with a ZrO2 grinding jar (Pulverisette 7, Fritsch GmbH, Idar-Oberstein, Germany) in 1-decene. THCpSiNPs were harvested by centrifugation (1500 × g, 5 min).

2.5.3 siRNA Loading

To load Block-iTTM (40 µL of 322 µg/mL in water) and siRNA (25 µL of 500 µg/mL in water) into the THCpSiNPs (0.1 mg/mL, 250 µL, suspended in EtOH) for the cellular uptake and reverse transcription polymerase chain reaction (RT-PCR) experiments, the particles were dispersed by sonication for 1 min, then incubated at 5 °C overnight. Following incubation, the supernatant was separated from NP by centrifugation (5000 rpm, 5 min) and the THCpSiNPs with the loaded siRNA (siRNA/THCpSiNPs) or the loaded Block-iTTM (Block-iTTM/THCpSiNPs) were collected. The amount of the absorbed oligonucleotides was measured by UV-Vis spectrophotometry (HP8453, Agilent Technologies, Santa Clara, CA, USA) at 260 nm from three replicates. The concentration of oligonucleotide in the supernatant was subtracted from the initial concentration of oligonucleotide in the loading solution. The amount of oligonucleotides absorbed onto the pSiNPs, P (mg/mg) was calculated using the following equation:

$$P = \frac{V(C_0 - C)}{W_D}$$

Where V (mL) is the volume of the oligonucleotide solution. C0 and C (μg/mL) are the initial oligonucleotide concentration and the oligonucleotide concentration at the measurement time, respectively. WD (Kim et al.) is the weight of the pSiNPs.

The total amount of siRNA loaded was 0.4 nmol/sample and found to be constant for the different loading times

All siRNA loading processes were performed in a biosafety cabinet (Aura 2000, Microprocessor Automatic Control, Firenze, Italy) to keep the NPs sterile for subsequent cell uptake studies.

2.5.4 PEI Coating on siRNA/THCpSiNPs:

To coat siRNA/THCpSiNPs with PEI (PEI/siRNA/THCpSiNPs), the sterile siRNA/THCpSiNPs (0.1 mg/mL) were dispersed by 1 min sonication into PEI solution (250 μL) at concentrations of 0.05 and 0.1 and 0.2% w/v. The coating was performed at pH 5.7, above the IEP (= 5.2) of siRNA/THCpSiNPs but below the pKa of PEI (= 9.08 42). The pSiNP suspension was incubated at 5 °C for 20 min, and then centrifuged at 5000 rpm at 5 °C for 5 min to collect the coated NPs. After removing the supernatant containing the unconjugated PEI, the amount of siRNA released during the coating process was measured using UV-Vis spectrophotometry at 260 nm to determine the final amount of loaded siRNA into the NPs. The sterile PEI/siRNA/THCpSiNPs were kept at 5 °C until use in siRNA release and cell uptake studies. The mean particle size and size distribution of the prepared PEI/siRNA/THCpSiNPs were determined by DLS and scanning electron microscopy (SEM). The surface charge after PEI coating was determined from zeta potential measurements. The same procedure was carried out for the PEI coating of the

Block-iTTM/THCpSiNPs (PEI/block-iTTM/THCpSiNPs). All PEI coating processes were carried out in the biosafety cabinet to keep the NPs sterile for future cell uptake studies.

2.5.5 Nitrogen Sorption Measurements

The pore volume, average pore diameter, and specific surface area of THCpSiNPs were calculated from nitrogen sorption measurements performed using a Tristar 3000 porosimeter (Micromeritics Inc., Norcross, GA, USA).

2.5.6 Dynamic Light Scattering and Zeta Potential

The mean hydrodynamic diameter of NPs, size distribution along with the polydispersity index (PDI) and surface zeta (ζ)-potential of NPs were determined by dynamic light scattering (DLS) using a Zetasizer Nano ZS (Malvern, Worcestershire, UK). A scattering angle of 90° and a temperature of 25 °C was used with NPs dispersed in Milli-Q water.

2.5.7 Scanning Electron Microscopy (SEM)

Images of THCpSiNPs and PEI-coated siRNA/THCpSiNPs (PEI/siRNA/THCpSiNPs) were acquired by a SEM (Crossbeam 540, Carl Zeiss AG, Oberkochen, Germany) by collecting the back-scattered electrons (0.7 kV beam energy under high vacuum 2×10^{-4} Pa). The samples were prepared by allowing a single drop of nanoparticle suspension to dry overnight at room temperature on a thin layer graphite attached to a standard SEM holder by double-sided carbon tape.

2.5.8 siRNA Release Experiment:

To study release kinetics, the prepared siRNA/THCpSiNPs and PEI/siRNA/THCpSiNPs (coated with PEI solution at concentrations 0.05, 0.1 and 0.2%w/v) were suspended at 0.1 mg/mL in PBS (100 µL). The solution was transferred into a cellulose membrane dialysis “bag” (to avoid NP interference in UV absorbance measurements) fitted inside of

a quartz cuvette (3 mL) filled with PBS and maintained at 37 ± 0.5 °C. The amount of oligonucleotide released was measured using the UV/Vis spectrophotometry every 5 min for 35 h. All release experiments were conducted in triplicate.

2.5.9 Confocal Microscopy:

T98G cells were seeded onto flat-bottomed 24-well tissue culture plates (Thermo Fisher Scientific Inc., SA, Australia) at a density of 3×10^4 cells/cm^2 in DMEM supplemented with 10% v/v FBS, 2 mM L-glutamine, 100 U/mL penicillin, 100 µg/mL streptomycin and cultured in a 37 °C, 5% CO_2 humidified atmosphere for 24 hours prior to incubation with NPs. Cells were grown to 80% confluence before exposure to NPs. After 24 hours, the medium was removed and cells were exposed to Opti-MEM culture medium supplemented with 5% (v/v) FBS containing 0.1 mg/mL of PEI/block-iTTM/THCpSiNPs or PEI/FAM-siRNA_A/THCpSiNPs at 37 °C, 5% CO_2 as specified above. The cell culture medium did not contain antibiotics. Controls (untreated cells) were generated by incubating T98G GBM cells in Opti-MEM without NPs for an identical time period. Following incubation (24 hours), the cells were washed with PBS to remove the non-internalised NPs. Subsequently, the cells were fixed in 4% paraformaldehyde solution for 30 min, then permeabilised with 0.25% Triton X100 for 5 min at room temperature. The nuclei of cells were stained with 2 µg/mL Hoechst 33342 for 15 min at room temperature. Cells were also stained with 100 µM phalloidin-TRITC for 45 min. After washing with PBS, cells were mounted with the Fluoro-gel mounting reagent. Cells were imaged using a Nikon A1 laser scanning confocal microscope (Nikon Inc., Rhodes, NSW, Australia) equipped with the appropriate filters. The efficiency of cellular uptake of NPs was assessed by counting the number of cells that exhibited green fluorescence (from the Block-iTTM or FAM-siRNA), together with the total number of cells present.

2.5.10 TEM of Cells:

Cellular uptake was illustrated using TEM imaging. Briefly, cellulose membrane dialysis tubes were placed in a 24-well plate, then T98G cells were seeded at a density of 3×10^4 cells/cm^2 for 24 hours in DMEM supplemented (see section confocal microscopy 2.5.9). After incubation, the medium was removed and cells were exposed to Opti-MEM culture medium supplemented with 5% v/v FBS containing 0.1 mg/mL of PEI/siRNA/THCpSiNPs for 24 hours at 37 °C, 5% CO_2. For control experiments, medium without the NPs was used. After incubation, T98G cells cultured on the cellulose membrane were fixed using 4% paraformaldehyde with 4% sucrose in 0.1 M PBS (pH 7.2) overnight. Aqueous osmium tetroxide solution (2.0% w/v) was added to the fixed cells before dehydrating cells by exposure to a series of ethanol/water mixtures (70% to 100% ethanol with 5% step increases). The dehydrated cells were embedded in absolute ethanol, and resin mixture (Araldite 502, procure 812, D.D.S.A., DMP-30) (1:1) then incubated in pure resin mixture. The cells were transferred to embedding moulds containing fresh pure resin mixture, which was then polymerised for 24 hours at 70 °C. Samples were cut with a diamond knife (sections of 60-100 nm thickness) and placed on a 200-mesh copper grid ProSciTech Co., Thuringowa, Qld, Australia). The cells placed on the grids were stained with uranyl acetate for 15 min, and rinsed with de-ionised water, subsequently stained with lead citrate for 3-5 min, and then rinsed with de-ionised water. The samples were imaged on a Tecnai™ Spirit Philips TEM (Hillsboro, OR, USA) at 20–120 kV beam energy under high vacuum (1×10^{-5} Pa).

2.5.11 Mouse Tumour Model:

To assess the siRNA delivery, MRP1 knockdown and its subsequent influence on the proliferative state, and the effect of knockdown on distal organs, a subcutaneous

xenograft tumour model was established using CD-1 nude mice (nu/nu) of mixed gender (total of 20 mice). Animal procedures were performed according to a protocol approved by the South Australian Health & Medical Research Institute Animal Ethics Committee (Approval number, SAM#98). U87MG cells were trypsinised, washed with warm PBS and counted. $5x10^6$ cells in chilled PBS were then mixed 1:1 with Matrigel (E1270, Sigma) to a total volume of 100 µl. CD-1 nude mice between 6 to 8 weeks of age were then subcutaneously inoculated with the prepared cells on both flanks. Unlimited food and water were provided ad libitum, and since CD-1 nudes are immunocompromised, they were housed in individually ventilated cages (IVC). On week 4 post-inoculation, mice baring tumours reaching 250 mm^3 were paired into groups receiving either pSiNP/ Saline, pSiNP/ ctrl siRNA, or pSiNP/ siRNA. Each group and time point contained two mice bearing four tumours. Each group of mice then intravenously received 2 doses of prescribed treatment separated by 24 hours. Each mouse received 31.25mg/ kg of pSiNP carrying the respective siRNA including control siRNA, or equivalent saline per dose. Mice were humanely killed at 24, 48 and72 hours post-treatment. Tumours, kidneys and duodenums were harvested. For mRNA level analysis (2.8), tissues were immersed into RNAlater (AM7023, ThermoFisher).

2.6 MK-571 Functional Inhibitor for MRP1:

MK-571 (Santa Cruz Bio- technology, Inc., Dallas, TX, USA) is an effective MRP1 inhibitor as well as several ATP transporters (Vellenga et al., 1999, Zhang et al., 2006, Robbiani et al., 2000) and a CysLT receptor antagonist (formerly known as LTD4 Receptor). When MRP1 is functionally active in the cell, Calcein AM is exported by MRP1 and therefore can be used as an indicator of its transporter function. Calcein-AM is a cell permeable, non-

fluorescent compound which converts into a highly fluorescent molecule when cellular esterases cleave the acetoxymethyl ester (AM) moiety. In cells with low or no endogenous expression of MRP1, Calcein fluorescence will accumulate and be detectable by flow cytometry or fluorescence microscopy. In contrast, there will no or low fluorescence of Calcein-AM in cells with high expression of MRP1.

In this project, we used MK-571 to demonstrate the inhibition of MRP1 and compared this result with the effect of MRP1-siRNA on MRP1 in the GBM cell line. Cells were seeded at 3×10^5 cells/well in a 6 well plate and allowed to adhere overnight. Subsequently, a total of 25uM MK-571 was added and cells were allowed to grow for up to 72 hours in media containing MK-571. Only one dose was required to inhibit MRP1 function for 72 hrs as tested by Calcein-AM transport experiments. Cells were then washed twice with PBS at room temperature and analysed by flow cytometry with the FL1 detector channel. The cells were analysed (Annexin V analysis (2.7.2), protein level analysis (2.7.1), Calcein-AM uptake (2.7.3) and cell cycle (2.7.4)) for the downstream effects of MRP1 inhibition at 24, 48, 72 hours.

2.7 Flow Cytometry Analysis:

2.7.1 Determining Protein Level by Flow Cytometry:

Flow cytometry of MRP1 protein levels was performed as follows. Cells treated with MRP1-siRNA were trypsinised and washed twice with 1xPBS then centrifuged (1200 g) for 5 min (as described previously (2.4)). Subsequently, 300 µL of BD Cytofix/Cytoperm solution was added to each tube containing the trypsinised cells (3×10^5 per tube). The cells were incubated in the dark at -20 °C for 30 min, washed twice with the BD Perm/Wash buffer (1 mL) then centrifuged at 1200 g (3 min). Afterwards, treated cells

were incubated with 10 µL of MRP1 antibody (QCRL-1; 200 µg/mL) for 90 min (-20 °C in the dark), then washed twice with the BD Perm/Wash buffer. 50 µL of the 1/50 Sheep anti-Mouse Ig, PE Conjugated Affinity Purified F (ab') secondary antibody was then added to the cells and kept for 30 min at room temperature. Prior to protein level analysis using flow cytometry, cells were rinsed twice with PBS. The same procedure was performed for all samples. A sample without antibodies and sample with secondary antibody were included in each analysis to address cell auto-fluorescence and non-specific binding respectively. Dead cells were excluded from analysis. For each sample, a total of 10,000 events were counted. The results were displayed in overlay histograms. All experiments were carried out in triplicate as technical replicates for each analysis conducted.

2.7.2 Annexin V Analysis:

Treated cells were trypsinised then (1×10^6 cells/tube) resuspended in 500 µL of the Annexin V binding buffer (10 mM HEPES/NaOH, PH 7.4, 140 mM NaCl, and 2.5 mM $CaCl_2$) (final concentration 3×10^5 cells/100 µL). The suspension was then divided into four FACS tubes (Falcon™ round-bottom tube, Thermo Fisher Scientific Inc., Waltham, MA, USA). Samples included cells without Annexin V- FITC or PI, cells with 10 µL of PI (2.5 mg/mL), cells with 5 µL of Annexin V- FITC (1 mg/mL), and cells with both PI and Annexin V-FTIC. Subsequently, the tubes were incubated for 30 minutes at ambient temperature and protected from light before analysis with the Accuri-C6 flow cytometer (BD Accuri Cytometers Inc., USA). The same treatment was repeated for control agents. The tests were performed in triplicate. For each sample, a total of 10,000 events were counted. FSC-A vs SSC-A plots were used for gating cells and to identify changing scatter properties of the cells. Ungated events showed all debris came from the remains of dead cells and crystals from washing and agents. Various Annexin V FITC / Propidium Iodide populations

of gated cells were assessed: viable (Annexin V^- PI^-), early apoptotic (Annexin V^+PI^-), and late apoptotic (Annexin V^+PI^+) cells. Both early and late apoptotic populations were added to present a final quantification of apoptosis in all cell samples after treatments. All experiments were carried in triplicate.

2.7.3 MRP1 Transport Activities (Calcein AM Uptake):

Calcein acetoxymethyl ester (Calcein AM) is a commonly used model substrate for multidrug resistance proteins. It is a fluorescent dye originally developed for intracellular calcium ion quantification. Although Calcein uptake is not specific for MRP1 and is also transported by Pgp, and other related transporters, its use as a tool for the measurement of change in MRP1 function is recognised particularly where functional or translational blockade of MRP1 is used within the one cell line. (Feller 1995) Cells were trypsinised and washed as previously described (2.4.5) at the 48 and 72 hours-time points followed by incubation with a total of 0.02uM of Calcein AM solution in 500uL DMEM medium for 30 minutes in a CO_2 incubator at 37°C. Cells were then washed twice and resuspended in cold PBS. Intracellular fluorescence was quantified using Accuri-C6 flow cytometry (BD Accuri Cytometers Inc USA). Only live cells were gated according to the typical forward, and side scatter pattern (Olson et al., 2001, Dogan et al., 2004).

Percentage of Calcein AM uptake was determined using the equation below

$$\left[\frac{\text{(Calcein Fluorescence of Treated Cells)}}{\text{(Calcein Fluorescence of Untreated Cells)}}\right] \text{ X 100}$$

2.7.4 Cell Cycle Analysis:

The cells were trypsinised at 24, 48 and 72 hours, followed by fixing in 70% ethanol by single consecutive drops on vortex and incubated at 4°C for 30 min. Fixed cells were washed twice with 1xPBS in a FACS tube. The pellet was resuspended in 0.5mL of FxCycle™ PI/RNase Staining (Thermo Scientific Inc.) Solution and incubated for 30 min at room temperature. Thereafter, the DNA content was analysed by Fluorescence-activated cell sorting (FACS) analysis using the Accuri-C6 flow cytometer (BD Accuri Cytometers Inc., USA) on the DNA setting (linear FL2) on low flow.

2.8 Real-time qPCR:

MRP1-mRNA silencing was studied using a BioRad CFX Connect QRT-PCR detection system with the SYTO9 reagent to detect the level of MRP1-mRNA downregulation.

2.9 RNA Isolation:

RNA was isolated from treated and untreated cells using Trizol according to the manufacturer's protocol (Sigma-Aldrich). In summary, trypsinised cells were homogenised in 1mL of TRIzol reagent and incubated at room temperature for 5 min. Then 100µL of Bromochloropropane (BCP) was added to the homogenate, and samples were shaken vigorously by hand for 15 seconds, incubated for 10 minutes at room temperature, then centrifuged for 15 min at 12000 g at 4°C. The aqueous phase was immediately transferred carefully to a fresh tube. RNA was precipitated with 500µL isopropanol and centrifuged for 10 minutes at 12000 g at 4°C. The RNA pellet was washed with 75% ethanol and centrifuged for 5 minutes at 8000 g at 4°C.

RNA pellets were dissolved in 15 µL of DEPC treated water after being air-dried for 5-10 min.

2.9.1 Nanodrop Spectrophotometry:

3 µL of each RNA sample was taken after extraction to determine RNA purity and concentration for use in PCR, using a NanoDrop-8000 spectrophotometer (Thermo Fisher Scientific U.S.A.). 1µL of RNA was added onto the lower measurement pedestal of the NanoDrop and software measured the concentration of RNA. DEPC-water was used as a blank for RNA measurement. The samples were read in triplicate. The purity of the RNA samples should have an A260/280 ratio <1.8.

2.9.2 Reverse Transcription Polymerase Chain Reaction Amplification:

First strand cDNA was synthesised with a Moloney Murine Leukemia Virus (M-MLV) Reverse Transcriptase kit according to the manufacturer's protocol (Promega). Total RNA and random hexamer primers were used at 2.5 µg and100 ng, respectively. Nuclease-free deionised water was mixed gently to prepare a mixture up to 14µL. The mixture was heated to 70°C for 5 min to melt secondary structures within the template, then chilled immediately on ice for 5 min to prevent secondary structures from reforming.

5µL of M-MLV RT 5X Reaction Buffer, 1µL of a 20Unit/µL RNaseOUT Recombinant Ribonuclease Inhibitor (Invitrogen) and 1.25µL of 10mM dNTP mix, 1µL of 200U M-MLV Reverse Transcriptase, RNase H Minus, Point Mutant (MLV RT (H-)) were added to the mixture. The mixture was vortexed gently and water added to a final volume of 25uL, followed by incubation at 50°C for 50 minutes. The reaction was inactivated at 70°C for 15 min. First strand cDNA was stored at -20°C for subsequent use in PCR and real-time PCR.

2.9.3 Gene-specific primer design:

NCBI Primer-BLAST was used to design specific primers for target genes. The NCBI Human RefSeq database was used to check for specificity. The following parameters were considered essential for producing a unique PCR product:

- The desired PCR product size is 75 - 300bp
- Melting temperature between 56-60 °C
- Primers must span at least one intervening intron
- At least 2bp mismatch within the last 5bp of the 3' end compared to off-target mRNA
- The primers could amplify additional splice variants to capture as many transcripts as possible
- The GC content was set between 45-65%
- To minimise the formation of primer hairpins, cross-dimers and self-dimers were essential in primer sequences.

Table 2-4 summarises the designed primers and their product size.

Table 2-4 Sequences of PCR primers

Primer ID		Sequence	Product size
MRP1	Forward	5’AAG GAA TGC GCC AAG ACT AG3’	159bp
	Reverse	5’CCT TAA ACA GAG AGG GGT TC3’	
Gli1	Forward	5'AGG GAG GAA AGC AGA CTG AC3'	136bp
	Reverse	5'CCA GTC ATT TCC ACA CCA CT3'	
Gli2	Forward	5'TTGC CTC CGA GAA GCA AGA AG3'	179bp
	Reverse	5'TCG CAT GTC AAT CGG TAG GG3'	
Gli3	Forward	5'GTC TAT GGG AAG TTC GGG GA3'	120bp
	Reverse	5'TTC AGT GGT CGT GGA GCT GT3'	
SMO	Forward	5'GAA GGC TGC ACG AAT GAG GT3'	101bp
	Reverse	5'GTC CTC GTA CCA GCT CTT GG 3'	
SHH	Forward	5'GGA CAG GCT GAT GAC TCA GA3'	147bp
	Reverse	5'GCC CTC GTA GTG CAG AGA CT3'	
PTCH1	Forward	5'CCC TTT TGA GGA CAG GAC CG3'	156bp
	Reverse	5'AAC ACC ACT ACT ACC GCT GC3'	
PTCH2	Forward	5'TGT AGG CAT TGG CGT TGA GT3'	198bp
	Reverse	5'CGC CGC AAA GAA GTA CCT TAC3'	
SUFU	Forward	5’GTT ACC TTC CTC CAG ATC GT3’	200bp
	Reverse	5’ GTC TCG ATG CCT TTG TCA AC3'	
TP53	Forward	5’GCC CAA CAA CAC CAG CTC CT3'	199bp
	Reverse	5’CCT GGG CAT CCT TGA GTT CC3'	
PTEN	Forward	5’TGG ATT CGA CTT AGA CTT AGA CCT A3'	250bp

	Reverse	5’GTT TGA TAA GTT CTA GCT GTG GTG3'	
GAPDH	Forward	5’GTG AAG GTC GGA GTC AAC GG3’	240bp
	Reverse	5’TGG AGG GAT CTC GCT CCT GG3’	
ABL1	Forward	5’TTC AGC GGC CAG TAG CAT CTG ACT T3’	201bp
	Reverse	5’TGT GAT TAT AGC CTA AGA CCC GGA G3’	
18S ribosomal	Forward	5’CGG CTA CCA CAT CCA AGG AA3’	178bp
	Reverse	5’GCT GGA ATT ACC GCG GCT3’	
GUSB	Forward	5’GAA AAT ACG TGG TTG GAG AGC TCA TT3’	100bp
	Reverse	5’CCG AGT GAA GAT CCC CTT TTT A3’	
Mus_MRP1	Forward	5’TGC AGA GGC ATC TCA GCA ACT C3’	71bp
	Reverse	5’TTC GGC TAT GCT GCT GTG TT3’	
MUS_GAPDH	Forward	5’CGA CTT CAA CAG CAA CTC CCA CTC TTC C3’	284bp
	Reverse	5’TGG GTG GTC CAG GGT TTC TTA CTC CTT3’	

2.9.4 Real Time Polymerase Chain Reaction Amplification:

Quantitative real-time PCR using 1st strand cDNA derived from T98 cell line treated with MRP1 siRNA and controls was used to evaluate changes in expression of MRP1. Primer information is summarised in Table 4.

The PCR reaction mixture is described in Table 5. The first strand cDNA was diluted 1:5 and 5µL of cDNA was used in each PCR reaction. Each reaction was performed in triplicate.

Table 2-5 Real time PCR reactions per tube

For each tube	Final concentration	Volume used
10X Platinum PCR Buffer	1X	2.5 µL
50 mM $MgCl_2$	1.5 mM	0.75 µL
10 mMdNTP mix	0.4 mM	0.5 µL
100 ng/1µL Forward primer	4 ng	1 µL
100 ng/1µL Reverse primer	4 ng	1 µL
Platinum Taq DNA polymerase	1 Unit	0.2 µL
50 µM SYTO9 green fluorescent nucleic acid stain	2 µM	0.25 µL
Water	N/A	13.8 µL
TOTAL	N/A	20 µL

PCR reaction plates or tubes were then placed in thermo-cyclers (iCycler Thermo-cycler, Applied Biosystems).

Table 2-6 Thermo-cycler Real-time PCR amplification conditions

Number of Cycles	Temperature	Time	Description
1 cycle	94°C	3 min	Enzyme activation
45 cycles	94°C	1 min	Denaturation
	56°C	1 min	Annealing
	72°C	1 min	Elongation (Read FAM)
45 melting cycles	55-95°C (0.5°C per step)	6 s per step	Read FAM

2.9.5 Statistical Analysis for RT-PCR:

Statistical analysis for RT-PCR was performed using the delta-delta method for relative gene expression level normalised to control housekeeping gene. The delta-delta method is an accurate method used to detect the changes in gene expression levels, also called the comparative Ct method. It is dependent on a standard curve of a reference gene. Delta cycle threshold (ΔCt) is calculated by the differences between a target and reference gene then applying the following equation 2-ΔΔCt.

$$\Delta CT = CT \text{ target gene} - CT \text{ control}$$

Then ΔΔCT is the difference between ΔCt of the target sample and the calibrated sample. Results are expressed as fold change (Livak and Schmittgen, 2001). The data are expressed as mean + / - standard deviation (SD) and + / - standard error (SE).

2.10 RNAseq Analysis:

RNAseq analysis requires high-quality mRNA and synthesis of a low yield cDNA or degraded RNA can affect library quality or result in library failure. The Agilent Bioanalyzer and RNA Nano kit (Agilent Technologies) were used to determine the RNA quality. The RNA Integrity Number (RIN) was computed from a Bioanalyzer electrophoretic trace and was required to be greater than 8 for use in RNAseq analyses. RNA samples were quantified using a Qubit 2.0 fluorometer.

The cDNA library was synthesised by the Flinders Genomics Facility, South Australia using the Illumina TruSeq Stranded Total RNA LT Sample Prep Kit following the manufacturer's protocol. The cDNA libraries were validated, normalised and pooled with the same kit. The cDNA sequencing was 150bp paired-end read on four lanes using Nextseq 500,

Illumina. Dr Shashikanth Marri, Flinders Genomics Facility, performed Bioinformatics analysis on data generated from Nextseq 500.

2.11 Statistical Analysis:

All experiments were performed with technical replicates in triplicate such that each data point in individual experiments represents these triplicates. In addition, where possible and as stated in the relevant results section, additional independent experiments were carried out on different days. The cumulative experimental data were analysed using Excel software and GraphPad Prism 7. The quantitative data of all experiments are expressed as mean ± standard deviation. A one-way analysis of variance (ANOVA) used to evaluate the result statistically. A P-value less than 0.05 was considered statistically significant.

3 DOWNREGULATION OF MRP1 BY SIRNA AND MK-571 IN T98G GLIOBLASTOMA CELL LINE:

3.1 Introduction:

MRP1 has been studied in many cancers including glioblastoma, but it is also expressed in healthy brain tissue. Additionally, both MRP1 mRNA and protein are shown to be expressed in glioblastoma surgical specimens in high levels after chemotherapy treatment (Abe et al., 1998, Hasegawa et al., 1994). High expression of MRP1 in many cancers is linked to the important role of MRP1 in cancer biology, although the focus is largely about the role of MRPs in chemo-resistance. As would be expected from its role as a membrane bound transporter, targeting MRP1 expression in both in primary and recurrent GBM tumours, increases the chemo-sensitivity to therapy (Bähr et al., 2003, Pazinato et al., 2018, Tivnan et al., 2015, Calatozzolo et al., 2005).

RNA interference technology has been developed to specifically target and knock down genes in a range of preclinical and clinical scenarios. In the particular case of GBM, targeting MRP1 using siRNA would potentially reduce drug efflux and increase malignant cell susceptibility to chemotherapy but may also change the biology of the disease in ways that have not previously been identified or understood.

In this study, siRNA molecules targeting MRP1 were developed and employed to assess the effects of inhibition of MRP1 and to explore the biological role of MRP1 in a GBM cell line T98G. Functional inhibition of MRP1 was also explored using MK571 with the caveat that this molecule is not specific for MRP1 and has overlapping functional inhibition of other transporters. (Badagnani et al, 2008) Calcein accumulation was used as an indicator

of MRP1 activity using a flow cytometric analysis. (Olson et al. 2001) Results of these experiments are presented below demonstrating the effect of MRP1 functional inhibition on cell growth, apoptosis and cell cycle in direct comparison with the effects of inhibiting MRP1 mRNA expression and hence protein expression.

3.2 Methods:

3.2.1 Functional Inhibitor MK-571 Treatment:

T98G cells were plated as per section **Error! Reference source not found.** and incubated i n media for either 24, 48 or 72 hours with 5, 10, 25, 50, and 100uM of MK-571 to determine the optimum concentration to use in subsequent experiments. 25uM of MK-571 was established as the optimal concentration based on Calcein-AM retention and used in subsequent experiments. (see section 2.5 for further details)

3.2.2 MRP1 Functional Assay Using Calcein-AM:

See section 2.6 for further details of methodology and rationale. In brief, following treatment with either siRNA or MK-571 or no treatment, $5x10^5$ harvested cells were incubated with 0.20 µM of Calcein-AM for 30 mins at 37°C. and analysed by flow cytometry with the FL1 detector channel. The control cells were not exposed to Calcein-AM.

In other experiments, using the IncuCyte™ apparatus, cells were plated, rested overnight then treated with MK-571 at 25µM for 2 hours at which point 0.02µM of Calcein-AM was added to the cells. Cellular uptake of Calcein-AM and cell proliferation were examined and visualised continuously for 72 hours within the Incucyte™ apparatus (see section 2.7.3). Results were recorded for analysis.

3.3 Results:

3.3.1 Transient Transfection With siRNA Against MRP1:

3.3.1.1 MRP1 mRNA Expression of MRP1-siRNA Transiently Transfected T98G Cells:

The cells were harvested at the 48-hour time point for mRNA expression analysis using qRT-PCR following transfection of MRP1 siRNA (0 and 24 hrs) into T98G cells using lipofectamine only. As a result of siRNA treatment, expression of MRP1 was reduced by 60% in T98G cells treated with siRNA-MRP1 A, while the siRNA-MRP1 B showed 40% downregulation of MRP1. In addition, the non-specific control siRNA demonstrated similar expression levels as untreated T98G cells. The specific effects of the MRP1 siRNA on MRP1 expression are shown in Figure 3-1.

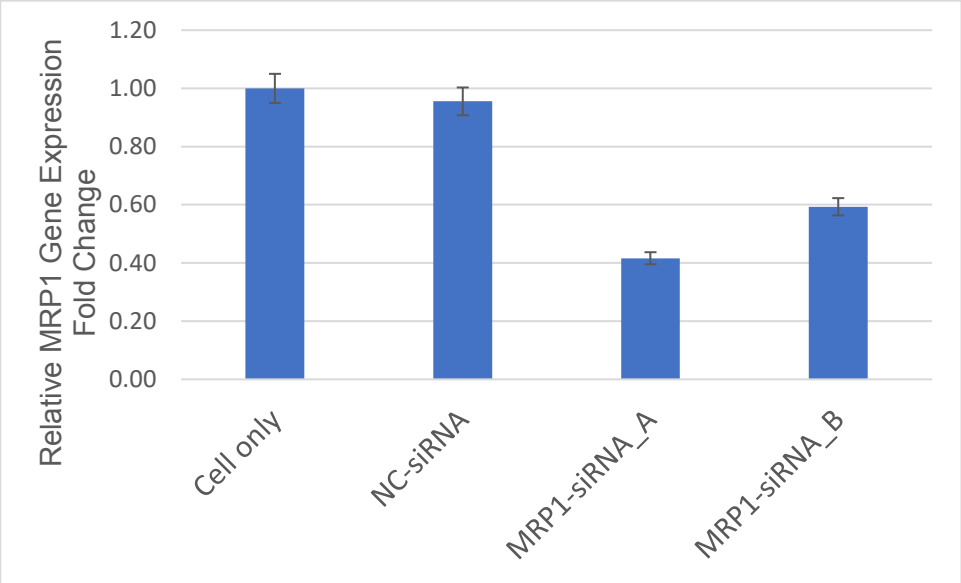

Figure 3-1 Relative qRT-PCR of MRP1 gene expression in T98G glioblastoma cell line. Quantitative RT-PCR demonstrated changes in gene expression following MRP1 siRNA treatment of cells. RNA was isolated from T98G after 48 hours of treatment with 150 nM siRNA-MRP1 or negative control siRNA. Relative MRP1 gene expression levels are displayed. Data are expressed as fold change and normalized to the GAPDH housekeeping gene. Untreated cells were used as a further control. Data shown are mean ±SD from four independent experiments. (P-Value < 0.05).

3.3.1.2 MRP1 Protein Levels Detection Following MRP1 siRNA Treatment:

Effects of siRNA-MRP1 treatment on the T98G cells were further assessed using flow cytometry at 96 hours due previous findings, representing 4 half-lives of the MRP1 protein. A reduction in MRP1 protein levels in both MRP1 siRNA treated T98G cells by almost 70% was demonstrated, compared to untreated cells. NC-siRNA showed similar MRP1 protein level to untreated cells in 3 separate experiments (Figure 3-2).

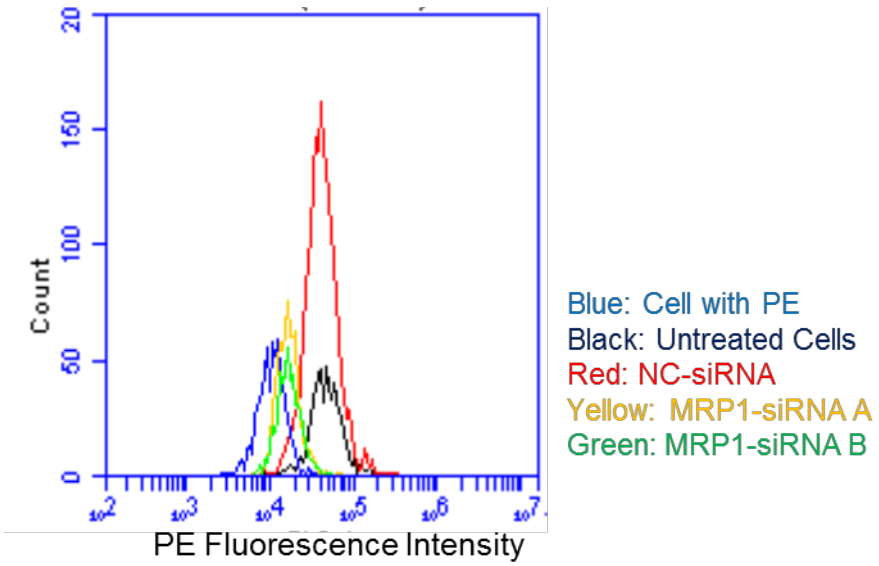

Figure 3-2 MRP1 protein expression level on the surface of T98G was determined by flow cytometry. The overlay histograms represent protein concentration in T98G cells in a single experiment. T98G cells were transfected with 150nM of either NC-siRNA (Red line), MRP1-siRNA A (Yellow line) or MRP1-siRNA B (Green line). Untreated cells (Black line) were used as a control. Cells were stained with the PE-conjugated secondary antibody (Blue line). The fluorescence intensity of PE corresponds to the MRP1 levels in the cells. Approximately 70% reduction in MRP1 protein level in both siRNA MRP1 samples were seen at 96 hours. NC-siRNA showed no change in the protein level. Data were collected from three independent experiments. (P-Value < 0.05).

3.3.1.3 MRP1 Functional Assay Using Calcein-AM:

Following treatment of T98G cells with siRNA, the inhibition of MRP1 protein level was measured by flow cytometry and the functional effect of MRP1 downregulation was assessed using Calcein-AM efflux. Cells treated with both siRNA against MRP1 exhibited greater fluorescence signals from Calcein-AM than untreated cells, indicating accumulation of Calcein-AM as a result of MRP1 inhibition. Figure 3-3 illustrates the cellular accumulation of Calcein-AM at 72 and 96 hours after treatment. Cellular accumulation increased over this time. Thus, indicating successful inhibition of MRP1 efflux due to downregulation of the MRP1 protein.

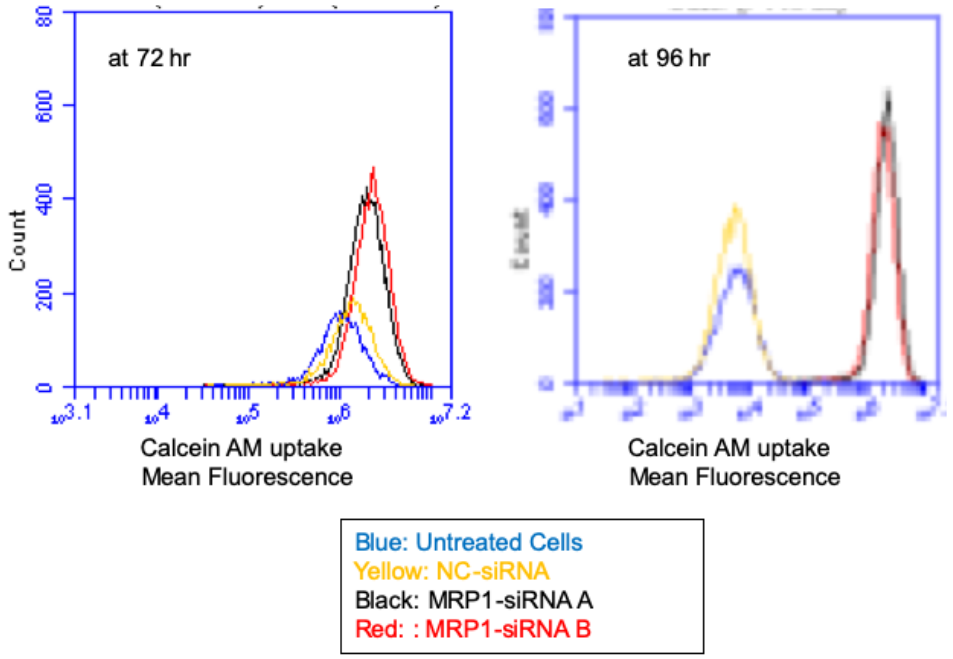

Figure 3-3 Cellular Uptake of Calcein AM after siRNA treatment. T98G cells treated with 150nM MRP1 siRNA and negative control (untreated cells and NC-siRNA) were used. Trypsinised cells were washed and incubated with 0.20 µM of Calcein-AM for 30 mins following two washes with PBS followed by flow cytometry analysis. Increase in cellular uptake was detected at 72 hours in both siRNA-MRP1 samples.

3.3.1.4 The Cytotoxicity Effect of Transient Transfection of MRP1-siRNA on T98G Cells:

NC-siRNA transfected cells demonstrated equivalent cell proliferation rates at 24, 48 hours, as observed in untreated control cells. Growth rates plateaued by 72 and 96 hours of cell culture under the conditions described in section 2.4.1 (Figure 3-4). In comparison, the proliferation curves were reduced in cells treated with either siRNA targeting MRP1 demonstrating a growth plateau from 48 to 96 hours (Figure 3-4). Both MRP1-siRNA showed approximately 30% reduction in cell growth at 24 hours and this growth impairment increased to 45% at 48 hours. At 72 and 96 hours, cell numbers were 50% of

the untreated or negative control treated cells. Thus, cellular growth was inhibited in T98G glioblastoma by transient transfection with siRNA targeting MRP1.

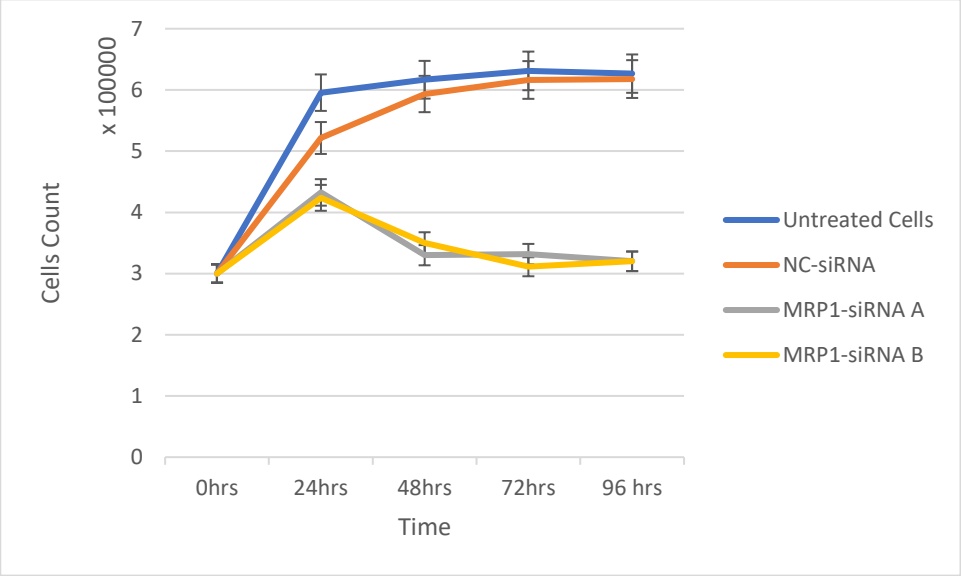

Figure 3-4 Cell count of T98G cells transiently transfected with MRP1-siRNA. T98G (3x10^5 cells /well) were transfected with 150nM of siRNA-Lipofectamine complex followed by a second siRNA treatment at 24hours. Progressive decline in cell number of siRNA-MRP1 treated samples is demonstrated at each time point. Cells growth continued to decrease slightly at 72 and 96 hours. The non-specific siRNA treated cells showed similar cell growth as untreated cells. This figure is a representative of three separate experiments that were conducted. Values represent mean ± SD at each time point 0, 24, 48, 72, and 96 hours. (P- Value < 0.05).

3.3.1.5 Apoptosis Assay in T98G Glioblastoma Cell Line Following MRP1-siRNA Treatment:

The annexin V assay was used to assess apoptosis which may be caused by MRP1 downregulation. No significant necrosis or apoptosis was seen by 24 hours in all treatments. (Figure 3-5 A). At 48 hours there was a small but statistically significant increase in apoptosis in the siRNA treated cells compared with NC treated cells but not untreated cells. However, by 72 hours this effect was no longer apparent.

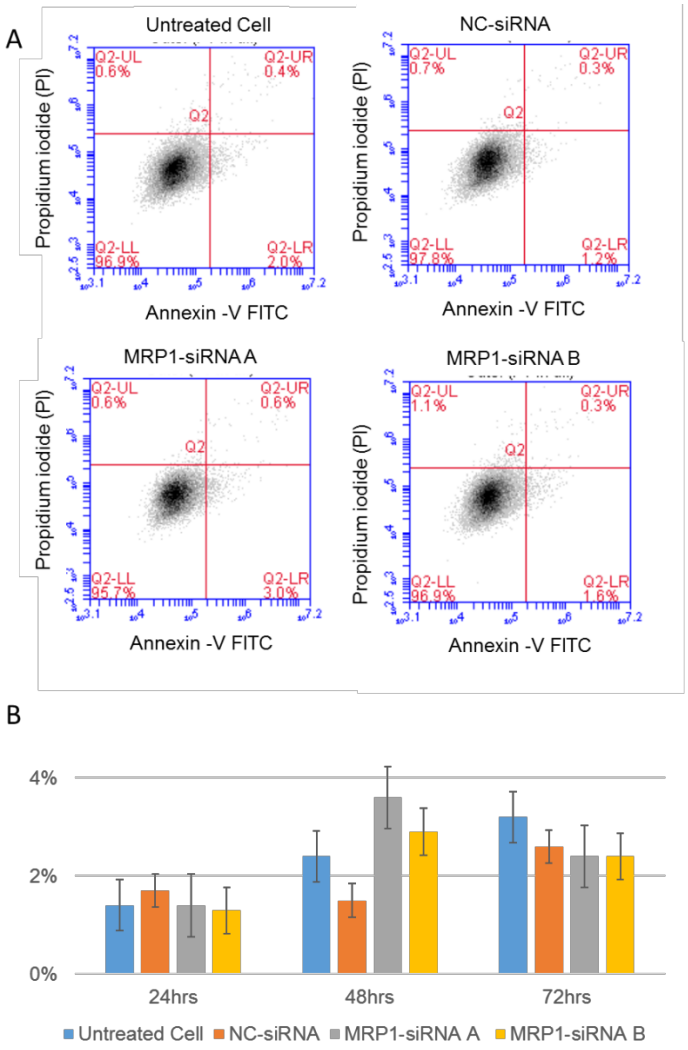

Figure 3-5 Cell Apoptosis of siRNA transfected T98G cells. The effect of transient transfection of siRNA against MRP1 in T98G cells on apoptosis was measured with Annexin V-FITC/ PI and analysed by flow cytometry. A) At the 24-hour time point, the flow cytometry profile represents early apoptosis (Annexin V-FITC staining), late apoptosis (both Annexin V-FITC and PI staining) and necrosis (PI staining). The left upper quadrant represents necrosis, the right upper quadrant represents late apoptosis and the right lowest quadrant represents early-stage apoptosis. The numbers indicate the percentage of cell death (apoptosis and necrosis). The living and dead cells are assessed by forward scatter (FSC) and side scatter and appropriately gated. B) Apoptosis was measured at 24, 48, and 72 hours. There is no significant increase in apoptosis in comparison to untreated cells at all time points. Values represent mean ± SD of 4 independent experiments. (P-Value < 0.05).

3.3.1.6 Effects of MRP1 on Cell Cycle Distribution of T98G Cells After siRNA Transient Transfection:

To further investigate the cause of cell growth retardation in T98G cells transiently transfected with siRNA toward MRP1, cell cycle distribution was analysed. The cellular fraction in each phase of cell cycle was assessed for each treatment group. The results showed that untreated cells and NC-siRNA treated cells have similar cell cycle patterns at all time points. Cells treated with siRNA-MRP1 showed an increase in S and G2/M phases and a reduction in G0/G1 phase in comparison to untreated cells.

Taking into consideration these results, it may be considered that the evident cell growth retardation occurred without a sustained induction of apoptosis but with persistent cell cycle changes apparent over 96 hours. The latter would appear to be the predominant effect of MRP1 downregulation impacting cell growth and represents a likely G2 arrest. The effects of MRP1 downregulation were then directly compared with functional blockade of MRP1 to determine if this would result in similar cell growth arrest independent of siRNA induced downregulation of MRP1 expression.

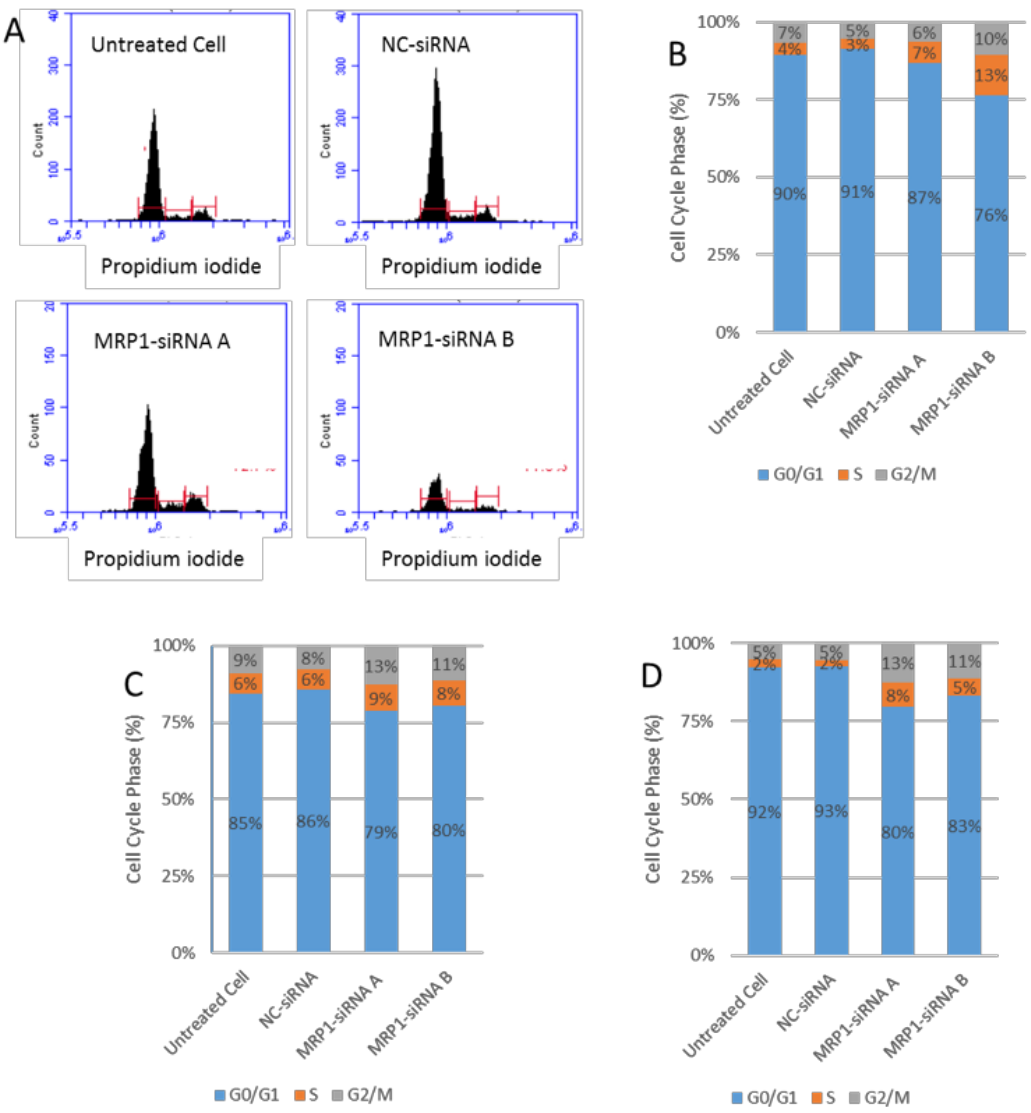

Figure 3-6 Cell Cycle analysis in T98G cells. (A) A representative histogram of T98G cells treated with 150nM of MRP1-siRNA A, MRP1-siRNA B, NC-siRNA and untreated cells at 24 hours. Stacked column charts represent the cell cycle percentage distribution in each phase (B) 24 hours (C) 48 hours and (D) 72 hours. The data shown are representative of two independent experiments.

3.3.2 Glioblastoma T98G Cell Response After the Inhibition of MRP1 Using MK-571:

MK-571 is a functional inhibitor of MRP1 and is specific for MRP proteins among the ABC transporters (specifically MRP1 and MRP4) but is also recently recognised as a CysLT receptor antagonist (formerly known as LTD4 Receptor) (Vellenga et al., 1999, Zhang et al., 2006, Robbiani et al., 2000). Its mechanism of action is through competitive inhibition

of substrate binding. In the following experiments, MK-571 was used to explore the effects of functional inhibition of MRP1 on the glioblastoma cell line T98G.

3.3.2.1 Calcein AM Cellular Accumulation Following MK-571 Treatment:

Calcein AM cellular accumulation was assessed after treatment of T98G cells with MK-571 by flow cytometric analysis for fluorescence. Cells incubated with MK-571 demonstrated increased fluorescence over non-treated control cells (Figure 3-7). Differing concentrations of MK-571 were assessed from 5 to 100µM (Figure 3-8).

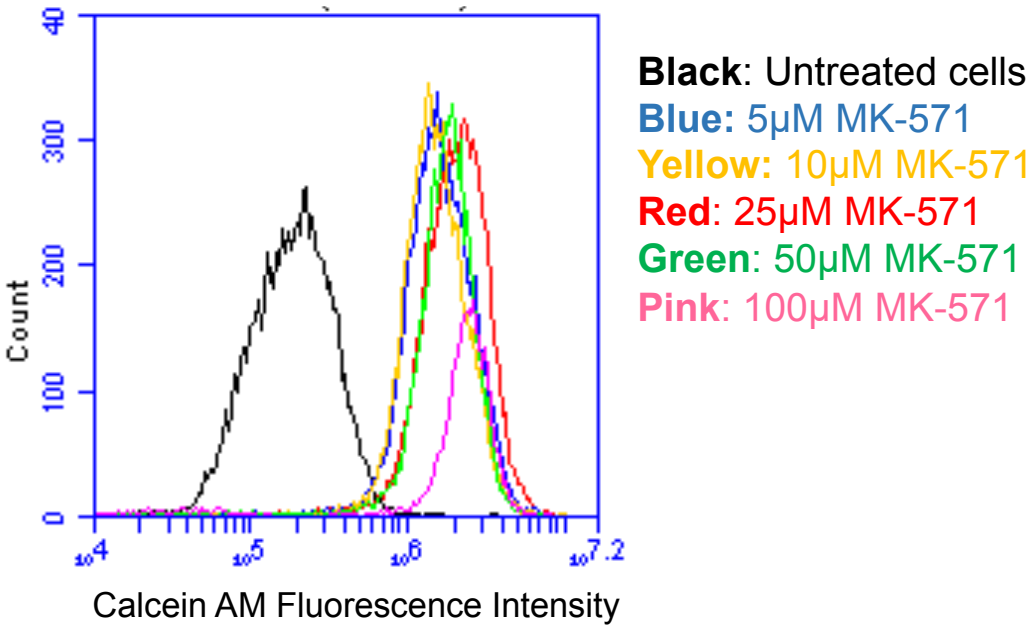

Figure 3-7 Calcein AM accumulation in T98G cells after MK-571 treatment using flow cytometry. T98G cells were incubated with different concentrations (5, 10, 25, 50 and 100 µM) of MK-571 for 24 hours. The harvested cells were washed with PBS and incubated for 30 minutes with 0.20µM of Calcein AM. Then, the cells were washed and analysed by flow cytometry. Both 5 and 10 µM of MK-571 samples showed similar accumulation of Calcein AM. However, the 25µM MK-571 sample demonstrated optimal cell accumulation without loss of cell integrity. Although 100µM of MK-571 demonstrated the highest accumulation of Calcein AM following inhibition of MRP1 by MK-571, cell viability appeared impaired (results not shown). Experiments were conducted in triplicate (n = 2). Values are a mean ± standard deviation.

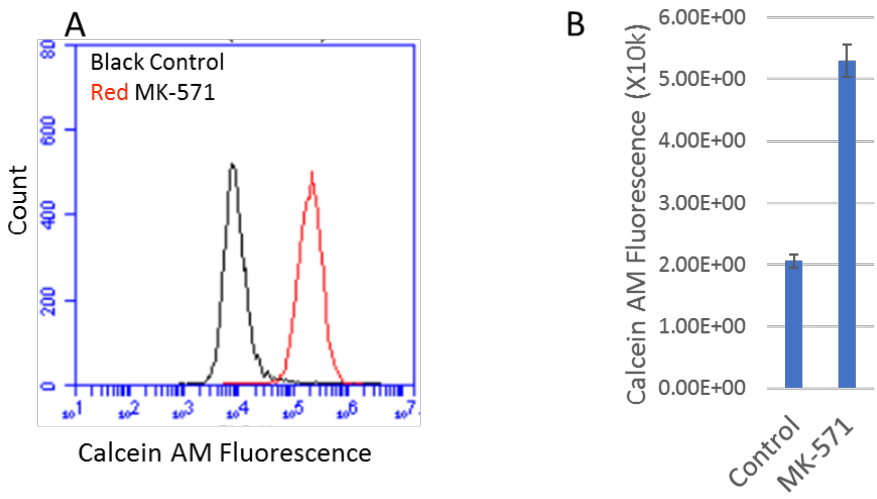

Figure 3-8 Flow cytometry analysis of Calcein AM cellular accumulation in the presence of 25µM MK-571. T98G cells were incubated with 25µM MK-571 then exposed to 0.2 µM of Calcein AM for 2 hours. Following incubation of the cell with Calcein-AM they were washed with PBS. The cells were then analysed by flow cytometry. A) Representative overlay histogram of MK-571 and control. B) Mean fluorescence of Calcein-AM in the absence or presence of MK-571. The cellular accumulation of Calcein-AM was increased 2.5-fold. Experiments were conducted in triplicate (n = 4). Values are a mean ± standard deviation. p<0.0023 compared to untreated.

3.3.2.2 Cell Growth Following MK-571 Treatment of T98G Cell Line:

Cell growth following incubation with MK-571 was assessed using an Incucyte apparatus. Figure 3-10 demonstrates a reduction in cell growth over 70 hours (Figure 3-10 A) with associated accumulation of Calcein-AM fluorescence demonstrating MRP1 functional blockade (Figure 3-10 B). Microscope derived images taken after 2 hours of incubation with MK-571 demonstrate the associated increase in cellular fluorescence Figure 3-9.

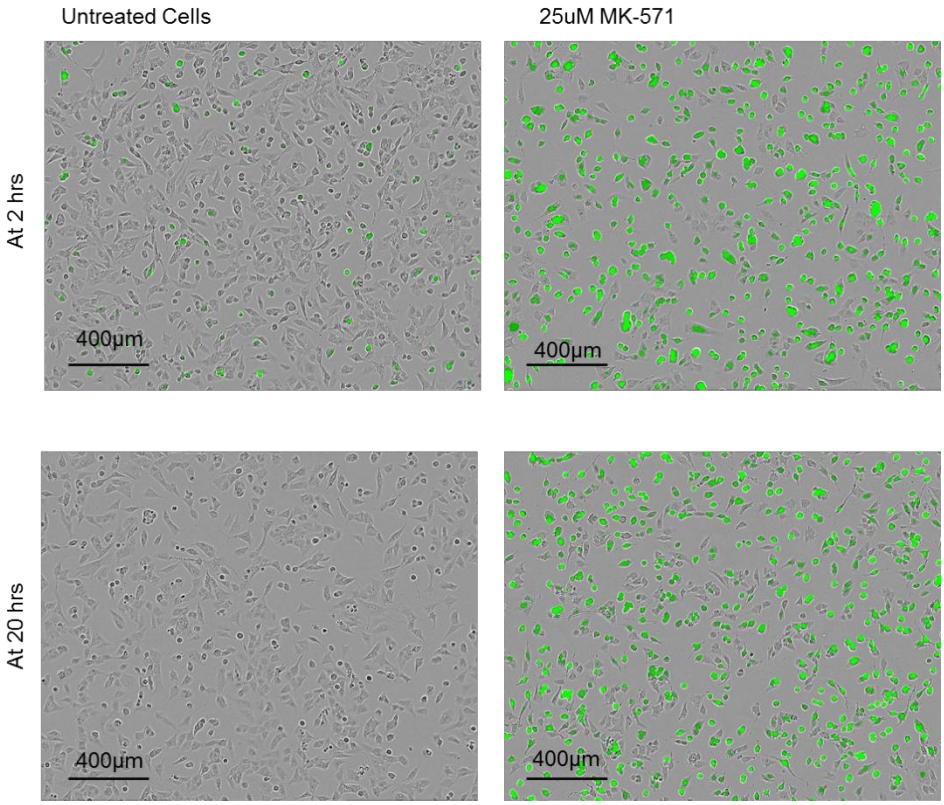

Figure 3-9 Morphology of T98G Glioblastoma cell line treated with MK-571 followed by Calcein-AM using Incucyte. The representative cells pictured here were treated with 25µM of MK-571 and the control is an untreated population of T98G cells. After two hours, the cells were exposed to 0.25µM Calcein-AM.

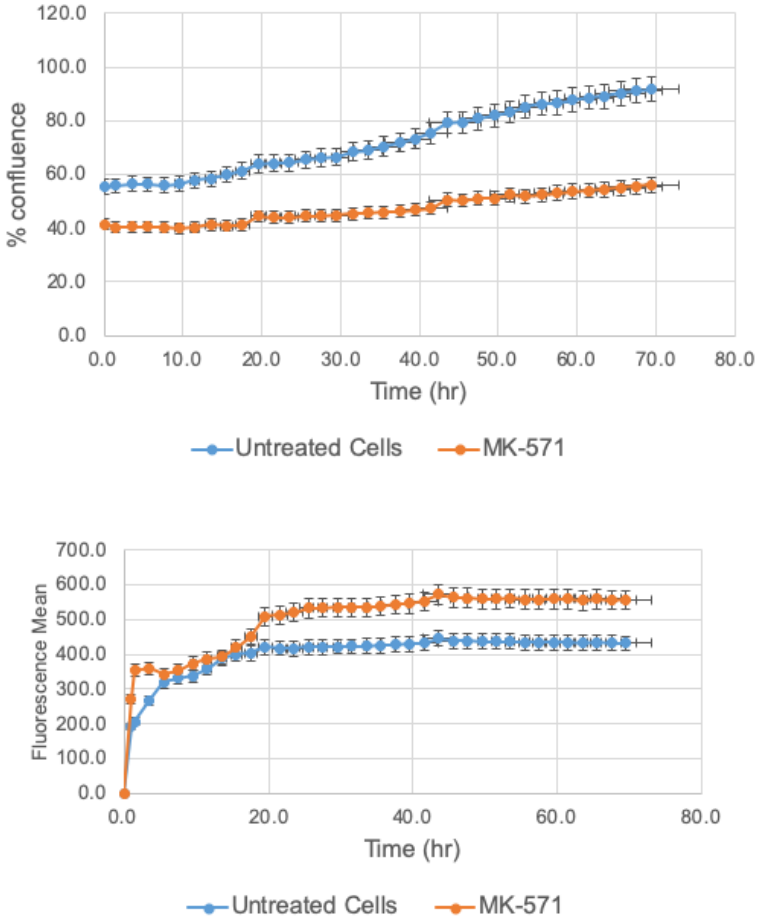

Figure 3-10 MRP1 inhibitor MK-571 effect on T98G cell line following Calcein-AM incubation using Incucyte. T98G cells were treated with 25µM of MK-571. Two hours later, 0.02µM of Calcein-AM was added to both untreated and MK-571 treated cells, incubated in Incucyte and visualised every 2 hours for 72 hours. A) Cell confluence was measured during the incubation and showed similar growth as Trypan blue assay. Cells treated with MK-571 demonstrated reduction in cell growth. B) Cellular uptake of Calcein-AM during 72 hours after treatment with 25µM of MK-571. Cells treated with MK-571 showed increase in fluorescence due to Calcein accumulation. Experiments were conducted in triplicate (n = 2). Values are mean ± standard deviation.

3.3.2.3 MRP1 Protein Inhibition by MK-571:

MRP1 protein expression was assessed in MK571 treated cells to ascertain whether functional alteration in MRP1 was associated with any change in MRP1 expression as a compensatory mechanism. No consistent alteration in protein expression was demonstrated (example shown in Figure 3.11). At the highest concentration (100 µM MK-571 represented in pink) MRP1 expression was increased at 96 hours (Figure 3-11) which may be due to an upregulation in protein to compensate for the functional blockade by MK-571. At 25 µM MK-571 there appeared to be 56 % reduction in MRP1 protein level (Figure 3-11) which is unexplained. One possible explanation would be internalisation of the bound protein which has been seen with disruption of cortical actin in lipid rafts (Kok et al., 2014, Taylor and Bebawy, 2019). This was not further explored in the thesis

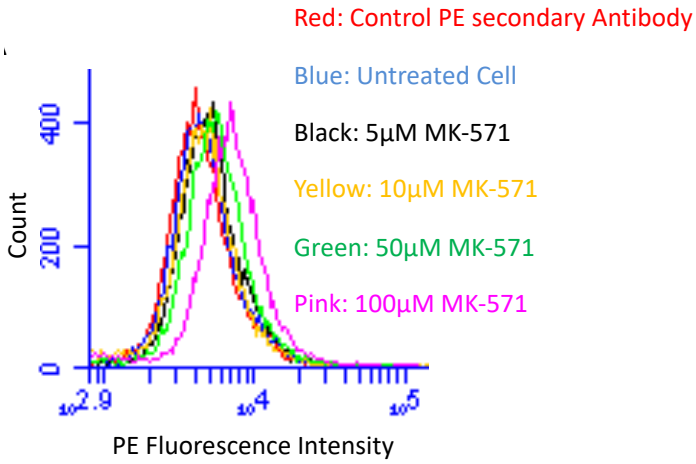

Figure 3-11 MRP1 protein level in T98G cells treated with MK-571. The overlay histograms represent MRP1 protein concentration in T98G cells. The cells were harvested at 72 and 96 hours for protein analysis using flow cytometry. T98G cells were treated with 5, 10, 25, 50, and 100µM of MK-571. Represented by the following: Red (untreated control cells stained with the PE secondary antibody); Blue - untreated cells (baseline control), black 5µM, yellow 10µM, green 50µM and Pink 100µM of MK-571 at 72 hours. The sample containing 100µM expressed a higher level of MRP1 than normal cells.

3.3.2.4 Investigation of Cytotoxicity of MK-571 Treatment

Further investigation of the role of MRP1 in GBM cell proliferation and cytotoxicity was performed following functional inhibition of MRP1. Cell growth was evaluated similarly to the siRNA experiments with cell counts using Trypan blue exclusion and cytotoxicity assessed with the Annexin V assay and Trypan blue. Results are shown in Figures 3-12 and 3-13. Similar to the effects of MRP1 downregulation, functional impairment of MRP1 leads to a reduction in cell proliferation without evidence of increased apoptotic cell death.

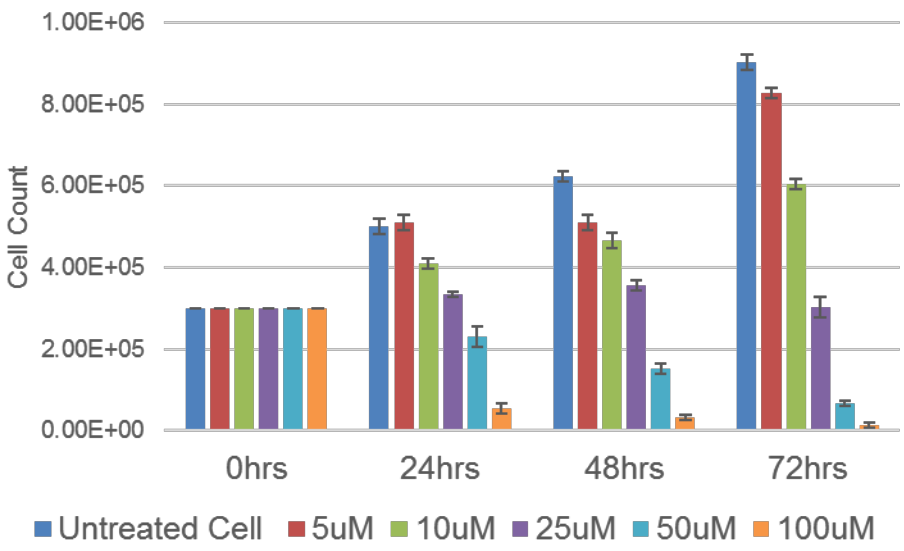

Figure 3-12 T98G cell growth evaluation following MK-571 treatment.

T98G GBM cells were incubated with 5, 10, 25, 50 and 100 µM of MK-571 for a maximum of 72 hours. Cells were harvested at 24, 48, and 72 hours and counted using the Trypan blue assay. Counts showed a reduction in cell growth in all samples. There was a clearly demonstrated relationship between drug dose and growth at all time points. 25µM of MK-571 resulted in the median reduction of cell growth at each time point. Experimental results represent the mean ± SD in triplicate at each time point 0, 24, 48, 72 hours (n=4).

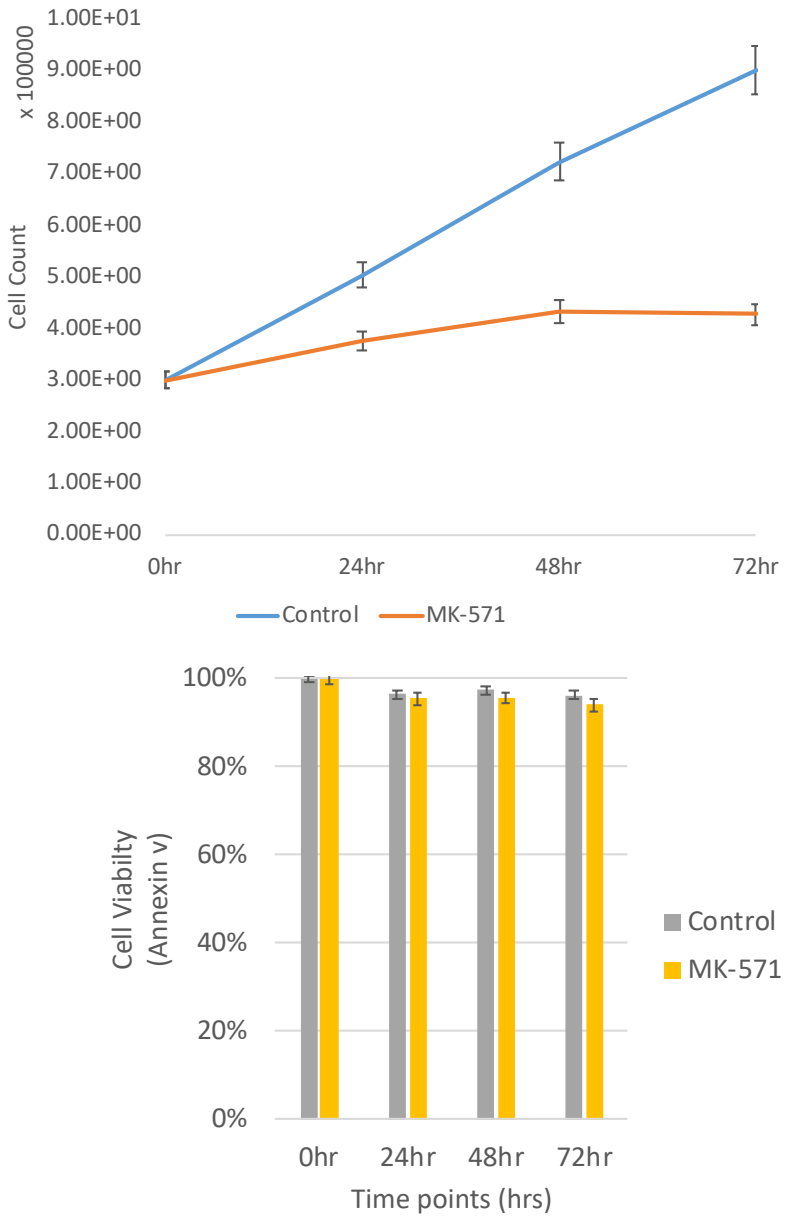

Figure 3-13 T98G cell proliferation following 25µM MK-571 treatment. T98G was incubated in medium (control) or with 25µM MK-571 for 72 hours. The cells were harvested at 24, 48, and 72 hours and analysed using Trypan Blue assay. A) Cell count showed 50% reduction in growth at 72 hours. However, B) no significant change in cell viability and no increase in cell death was observed. Cell counts were conducted using Trypan blue assay, while, cell viability was measured using Annexin-V assay. Experiments were conducted in triplicate (n = 4). Values are a mean ± standard deviation.

3.3.2.5 Morphological assessment of MK-571 treated cells:

T98G cells treated with 25µM of MK-571 generates apparent lipid vesicles in the cytoplasm of the cells (Figure 3-14). The overall shape and adherence of the cells appears the same as untreated cells. However, no lipid droplets were accumulated in the untreated cells.

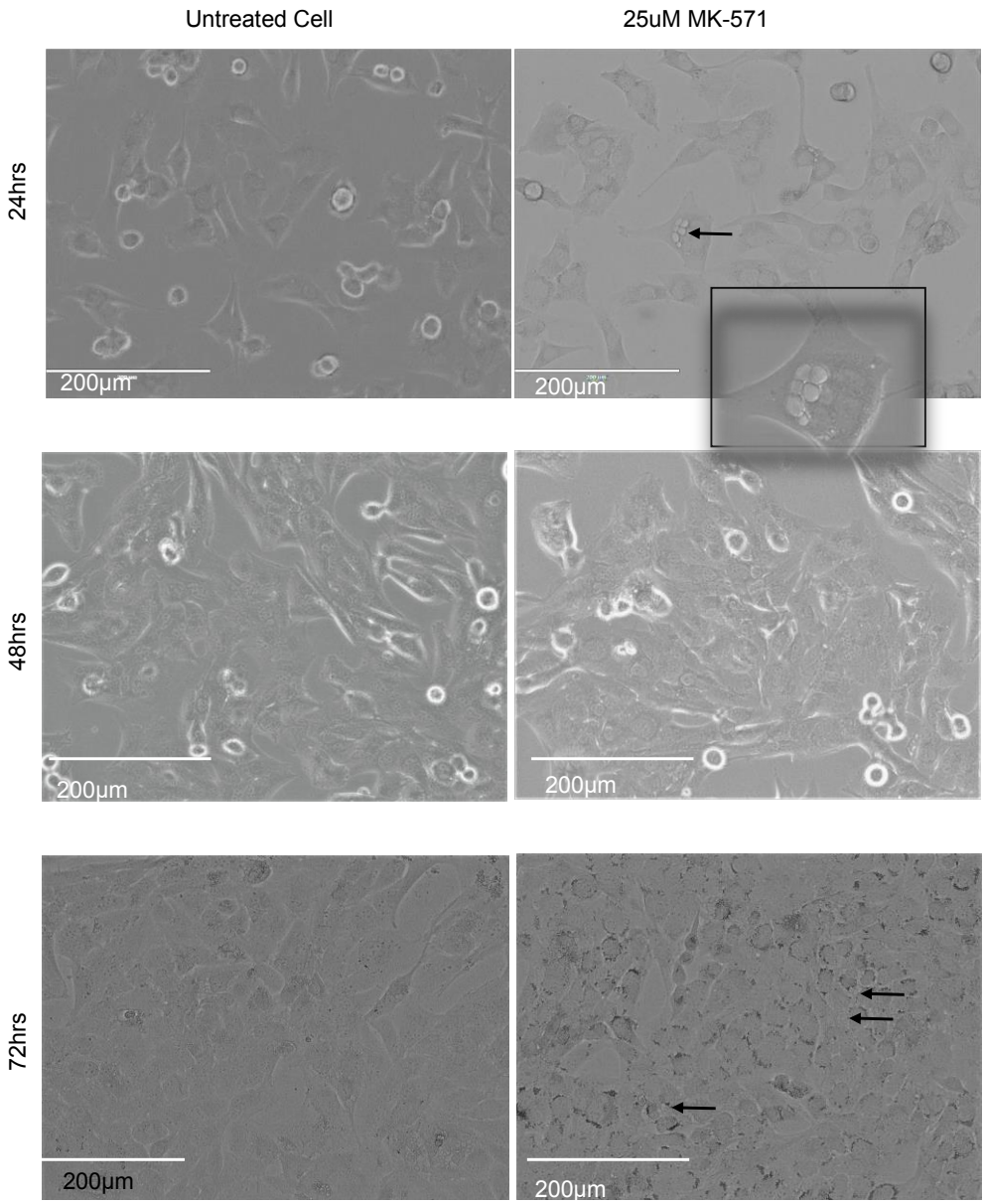

Figure 3-14 Morphology of T98G cells treated with 25µM MK-571. Black arrows point to a formation of vesicles within the cytoplasm seen after treatment.

3.4 Discussion:

The presence of the blood brain barrier and ABC transporters at cellular interfaces significantly increase the chance of treatment failure and tumour recurrence in GBM where high expression of MRP1 has been demonstrated in the primary patient cell samples, as well as patient derived cell lines (Mohri et al., 2000, Calatozzolo et al., 2005). In these particular patients, MRP1 knockdown is an attractive approach to improve drug exposure, where MRP1 expression has been documented. MRP1 is however, not uniformly overexpressed in GBM, as like so many tumours, the disease is heterogeneous at a molecular level. (Alves et al., 2011; Bahr et al., 2003; Tivnan et al., 2015) It has also been proposed that the cerebral endothelial levels of the ABC transporters may provide a stronger role for in vivo chemoresistance through these mechanisms and MRP1 levels may in fact be an artefact of long term tissue culture in some patient samples (Bahr et al., 2003).

In this study, the MRP1 expressing T98G cell line was used to carry out the in vitro experiments. This provided us with an accessible in vitro model to study the effects of MRP1 but has all of the recognised limitations of a cell line with respect to predicting a primary glioblastoma response. The study aimed to determine the biological effects of MRP1 inhibition in T98G cells. Reduction of expression of MRP1 mRNA was the initial investigative plan and two different locations within MRP1 mRNA were targeted with sequence specific siRNA, directed toward sequences within exome 7 and 17. Although no combined siRNA administration was performed this remains a possible method of improving siRNA response and MRP1 downregulation providing the delivery methods do not prove unnecessarily toxic to the cells. A non-specific siRNA was used as a control for

the study demonstrating specific effects of the targeted siRNAs. In addition, the effects of downregulation of MRP1 were directly compared with functional inhibition of MRP1 activity using MK-571 as a chemical inhibitor to further explore the effects of siRNA inhibition of MRP1 on T98G cells similar to investigations of Roundhill et al. and other authors (Roundhill et al. 2012, ST Arevalo et al., 2017).

Two doses of siRNA were used to improve the effectiveness of transfection and MRP1 inhibition as after a single dose of siRNA despite mRNA downregulation, there was inadequate protein reduction due to the long half-life of the MRP1 protein. mRNA expression was analysed using qRT-PCR. The best time point for analysis of MRP1 mRNA was reported by Golalipour to be within 36 hours after siRNA-MRP1, as this study found the effect to be reduced after 48 hours (Golalipour et al., 2006). Other studies have used different timepoints (Mohri et al., 2000, Matsumoto et al., 2004). In this study, the mRNA level of MRP1 was measured at 24 hours post the second dose of siRNA which demonstrated a reduction to 40 and 60% of baseline using MRP1-siRNA_B and MRP1-siRNA_A Resulting in significantly reduced protein expression and functional reduction in MRP1 as measured by Calcein AM using flow cytometry.

As stated, MRP1 protein levels analysed using flow-cytometry demonstrated a down-regulation of MRP1 in GBM evident at 48 hours after two transient transfections with siRNA targeted to MRP1 and the accumulation of Calcein F confirmed the loss of MRP1 function commensurate with the reduction in protein. 96 hours after siRNA treatment, protein levels were demonstrated to be 70% reduced from baseline. This result shows greater reduction compared to Golalipour's study which achieved only 25% using antisense oligonucleotides at the same time point. Tivnan reported analysing MRP1

protein at 72, 96 and 120 hours after siRNA transfection and showed an increase in protein level at 120 hours while the maximum reduction was observed at 72 hours. Thus, following several siRNA administrations, an optimum MRP1 protein analysis was seen to be at 96 hours (Tivnan et al., 2015, Henderson et al., 2011, Golalipour et al., 2006). In addition, in vitro and in vivo, siRNA inhibition has shown to be stable for five days (Tivnan, et al., 2015) In this study, although no combination of siRNA-A and siRNA-B were used due to the predicted large total dose required to deliver effective quantities of each siRNA in vitro (including lipofectamine effects on cell survival) it remains a potential option with a mixture of individually or dually loaded nanoparticles for future experiments. This would require a new exploration of pooling siRNA to maximize the siRNA efficiency (Christoph et al., 2006, Watanabe et al., 2004).

Additionally, downregulation of MRP1 and functional inhibition of MRP1 in T98G cells both affected cell proliferation. Transient transfection of T98G cells with siRNA targeted to MRP1 reduced cell growth without inducing cell death. It has been reported that in a commercial T98G cell line, either siRNA or MK-571 treatment have induced cell death (Tivnan et al., 2015, Peterson et al., 2017, Peigñan et al., 2011). However, this effect was not seen in this study, with only a transient increase in apoptosis at the 48-hour time point that was lost by the 72-hour time point.

It would be pertinent to note that only one cell line was used for these experiments. Replication in other GBM cell lines and primary cell cultures if possible, would be the next step in experimental investigation of the antisense modulation of MRP1 in this cancer subtype. In addition, new technologies such as CRISPR would provide a different approach to silencing MRP1 in these tumours.

MK-571 functional inhibition of MRP1 produced similar results demonstrating that the biological effects seen with downregulation of MRP1 are a direct effect of loss of its function. As MRP1 is a transporter predominantly of glutathione conjugated substances and lipids among other substances and also involved in the redox response of the cell, one can only infer that it is involved in the transport of a fundamental substance(s) affecting glioblastoma growth. MRP1 is known to transport lipid derived effectors and mediators of cell signalling and their receptors. MRP1 is the main transporter for the cellular excretion of the lipid metabolite leukotriene C4 (LTC4). The images of the cells treated with MK-571 (Figure 3-14) demonstrate vesicles apparently filled with lipid within the cytoplasm of the treated cells. The same effect has been seen in neuroblastoma cells in this laboratory (B. Kuss – personal communication following treatment with MRP1 antisense oligonucleotides) and in other published works. The identity of lipid droplets needs to be confirmed using specific lipid droplet antibodies and other staining techniques. However, while MRP1 (and some of the other MRPs) can indeed transport some conjugated hydrophilic lipid metabolites they do not transport lipids per se and MRP1 KO mice have no obvious phenotype such as seen in these experiments.

Given the well-known lack of specificity/selectivity of MK571 and Calcein for MRP1, these effects would need to be more fully investigated to understand their aetiology.

In addition, MRP1 contributes to the protection of some tissues against xenotoxins which may protect vital cells within the body, in particular the brain via the cerebrospinal fluid. Lipid transport by MRP1 implies a vastly different role to that of P-glycoprotein at the biological level and given that prostaglandins are felt to be an important player in GBM resistance to therapy, it is feasible that inhibition of MRP1 function in GBM cells may

affect the biology of the disease through a range of mechanisms. For example, interference in critical metabolic pathways; interference in the cell's interaction with the microenvironment through cell receptors and possibly alteration of cell growth and survival through a change in the balance of signalling molecules (Cole, 2014, Koley and Bard, 2012).

As such, the next step in this thesis was to further investigate the changes in the cellular expression profile of T98G cells following inhibition of MRP1 looking at key cell signalling pathways in GBM. Also, this experiment might be repeated with T98G cells that MRP1 knocked out completely by Crispr9. Global range of GBM cell lines that express MRP1 would be used in extended experiments.

4 DELIVERY OF MRP1-SIRNA BY POLYETHYLENEIMINE-FUNCTIONALISED POROUS SILICON NANOPARTICLES IN GLIOBLASTOMA

4.1 Introduction:

Glioblastoma multiforme (GBM) is an aggressive brain tumour with a poor clinical prognosis (Lawrence et al., 2010, Tyler et al., 2014, Yoon et al., 2010, Stukel and Caplan, 2009). Malignant glioblastoma cells divide rapidly because the tumour is surrounded by a well-developed blood supply network (Deeken and Löscher, 2007). Multimodal treatment, consisting of surgical resection, local radiotherapy and systemic chemotherapy, is the standard therapy for GBM (Tyler et al., 2014, Mrugala, 2013). Surgery can remove up to 95% of the GBM tumour, implying that 5% of the tumour remains and must be dealt with by means other than surgery. A major obstacle to treatment of cancer is overexpression of the multidrug resistance-associated proteins. MRP1 has been demonstrated to be active in a range of cancers (Kuss et al., 2002, Munoz et al., 2007, Quezada et al., 2013, Tang et al., 2004, Vos et al., 1998). Silencing MDR proteins has been tried in cancer using a variety of approaches.

Exogenously delivered siRNA has been demonstrated to silence the MRP1 gene and prevent extracellular transport of hydrophobic chemotherapeutic molecules (e.g. camptothecin and doxorubicin) across the lipid bilayer of the cell membrane (Munoz et al., 2007, DeGorter et al., 2008) The administration of naked siRNA has been shown to be effective in downregulating gene targets and in doing so increases treatment efficacy for some cancers (Devi, 2006, Guo et al., 2013). However, the negatively charged naked siRNA is subject to poor cellular uptake as well as intracellular degradation because of

endogenous enzymes in the cytoplasm (Zeng and Cullen, 2002). In order to facilitate the transfection of siRNA in a clinical setting, non-viral vectors have been used to treat cancer cells. Alternatively, the delivery of siRNAs to GBM tumour cells using nanoparticles (NPs) has been demonstrated to protect siRNAs from nucleases and promote a sustained intracellular release of the siRNA (Deeken and Löscher, 2007, Ballarin-Gonzalez et al., 2013, Shi et al., 2014).

In this chapter we investigated a possible delivery system for siRNA targeted to MRP1-mRNA using thermally hydrocarbonised porous silicon nanoparticles (THCpSiNPs). The chemistry of the nanoparticles was modified using polyethylenimine (PEI) coating to improve the release kinetics. Cell viability and cellular uptake of the treated cells *in vitro* were also examined using confocal microscopy and transmission electron microscopy (TEM). The ability of siRNA-loaded THCpSiNPs to mediate the silencing of the MRP1 gene and protein was then assessed in the T98G glioblastoma cell line.

4.2 Experimental Materials and Methods:

Porous silicon nanoparticle (THCpSiNP) fabrication, loading, coating, modification of release conditions, scanning electron microscopy and TEM imaging of loaded cells were predominantly performed by Morteza Hasanzadeh Kafshgari (Coelho et al.) in collaboration with Mohammed Alnakhli. Loading, coating and determination of the release of siRNA for all the experiments have been performed by Mohammed Alnakhli.

In vivo studies have been carried out by Wing Ying Tong (Coelho et al.) and resected mouse tissue sent to Mohammed Alnakhli for analysis of mRNA expression of MRP1 by qRT-PCR.

Table 4-1 Terms used in this chapter

	Sample abbreviation	Sample details
Controls	Untreated Cells	Untreated Cells
	THCpSiNPs	Cells with uncoated NPs
	PEI/THCpSiNPs	Cells with PEI coated NPs
	PEI/NC-siRNA/THCpSiNPs	Cells with Negative siRNA loaded on NPs and coated with PEI.
	PEI + MRP1- siRNA+ THCpSiNPs	Cells with PEI, MRP1-siRNA and NPs added separately into wells.
	PEI/ MRP1-siRNA/THCpSiNPs	Cells with MRP1-siRNA loaded on NP's and coated with PEI.
	MRP1-siRNA/THCpSiNPs	Cells with MRP1- siRNA loaded on NPs without coating.
	MRP1-siRNA/Lipofectamine	Cells transiently transfected with MRP1-siRNA using Lipofectamine.
	UN-MRP1-siRNA	Unmodified siRNA used in the first experiment. Then 2'-Fluoro modification was applied in subsequent experiments.

4.2.1 Proliferation and Viability of Cells:

The Annexin V and Trypan Blue exclusion assays were used to assess cell viabilty following treatment of the T98G cell line with PEI/siRNA/THCpSiNPs. The cells were seeded onto 6-

well plates at a density of 3×10^5 cells per well and maintained in DMEM 24 hours prior to treatment. On the experiment day, the medium was replaced with Opti-MEM™ Reduced Serum Media. Routinely, the confluence of cells used was approximately 70-80%.

- The cultured cells were incubated with prepared sterilised PEI/MRP1-siRNA/THCpSiNPs or control treatments:
- Unmodified THCpSiNPs,
- PEI coated THCpSiNPs loaded with NC-siRNA (PEI/NC-siRNA/THCpSiNPs),
- PEI coated THCpSiNPs without an siRNA payload (PEI/THCpSiNPs),
- Treatment with each single component of PEI/MRP1-siRNA/THCpSiNPs i.e. uncomplexed PEI, siRNA, non-coated THCpSiNPs (PEI + siRNA+ THCpSiNPs, separately added)
- siRNA complexed with lipofectamine (siRNA/lipofectamine)]
- Untreated cells at a concentration of 0.1 mg/mL (250 µL per well)

Cells were cultured for 24, 48 and 72 hours without change in the culture media. Effects on cell viability were determined on treated and untreated cells.

4.3 Results:

4.3.1 pSiNP Characterisation:

pSiNPs were fabricated using pulsed electrochemical etching of single-crystal doped p-type silicon wafers and subsequent ball milling of the produced pSi multilayer membranes (Figure 4-1). The average size of THCpSiNPs was measured using Dynamic light scattering (DLS). It was 145.9 nm (PDI: 0.087), with an average ζ-potential of −43 mV (at pH 7.4). The plate-like morphology of pSiNPs produced by the pulsed electrochemical etching and ball milling process was illustrated using SEM (Figure 4-2) and TEM (Figure 4-3). The size of the pSiNPs was approximately 150 nm in diameter. In general, the PEI/MRP1-siRNA/THCpSiNPs are larger than THCpSiNPs and siRNA/THCpSiNPs due to the coating (Figure 4-3). The shape of THCpSiNPs appear small and spherical at low magnification. However, upon closer examination they appear as unorganised aspheric shapes (Figure 4-2). The assessment of THCpSiNPs demonstrated the size and characteristics to be constant in all preparation experiments.

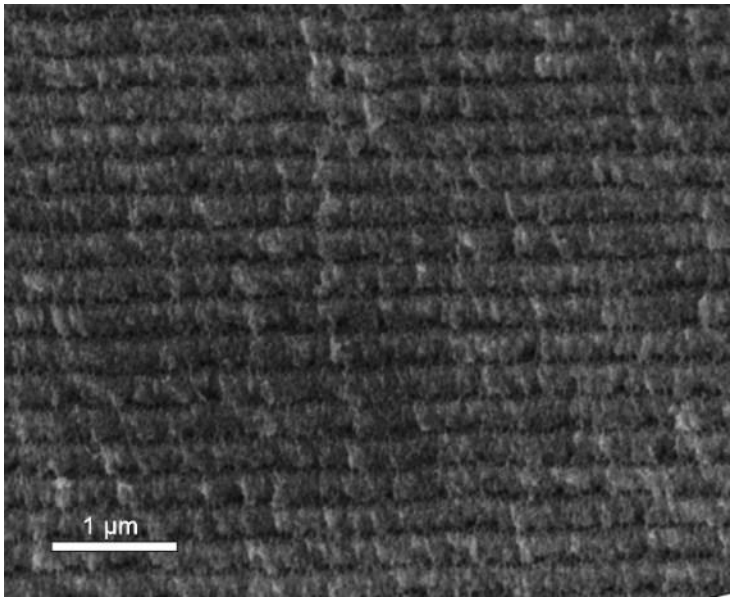

Figure 4-1 SEM image of a multilayer pSi film fabricated by pulsed electrochemical etching. (Image included in supplementary figure S1, H. Kafshgari et al., 2015)

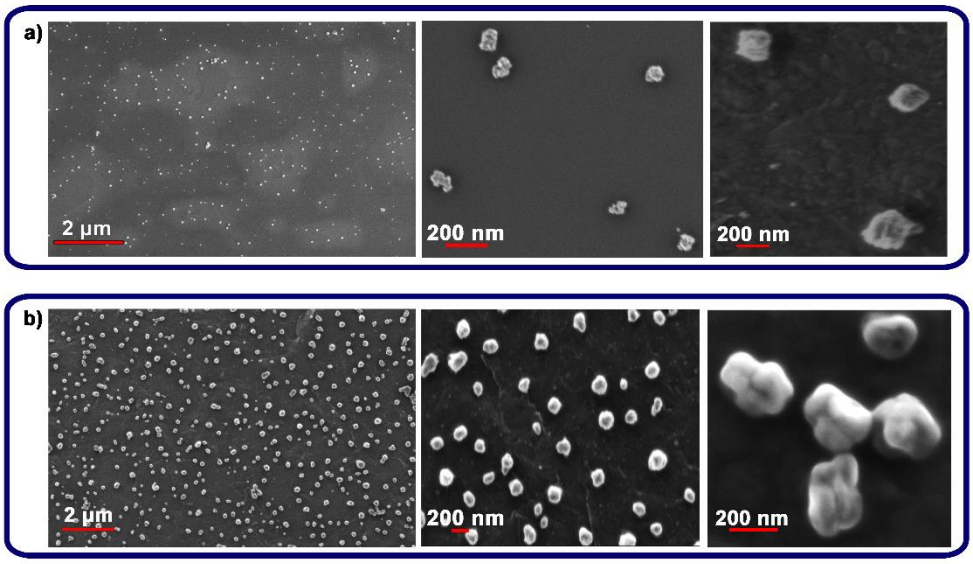

Figure 4-2 SEM images of nanoparticles. (a) THCpSiNPs, (b) PEI/siRNA/THCpSiNPs. (Image included as figure 6 H. Kafshgari et al., 2015)).

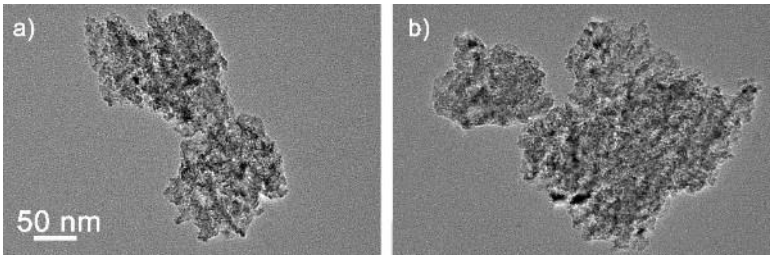

Figure 4-3 Representative TEM images of (a) THCpSiNPs, (b) PEI/siRNA/THCpSiNPs. (Image included as figure S2 H. Kafshgari et al., 2015)

THC treatment protects the pSi from oxidative hydrolysis in an aqueous medium as our interferometric reflectance spectroscopy (IRS) data show (Figure 4-4). Rapid degradation (50%, resulting in a reduced thickness of the porous film after 250 min of incubation) was observed for the hydride-terminated film. In stark contrast, the THCpSi film remained stable with only a slight reduction of its initial thickness (thickness reduction ∼4%) after 5 hours of incubation.

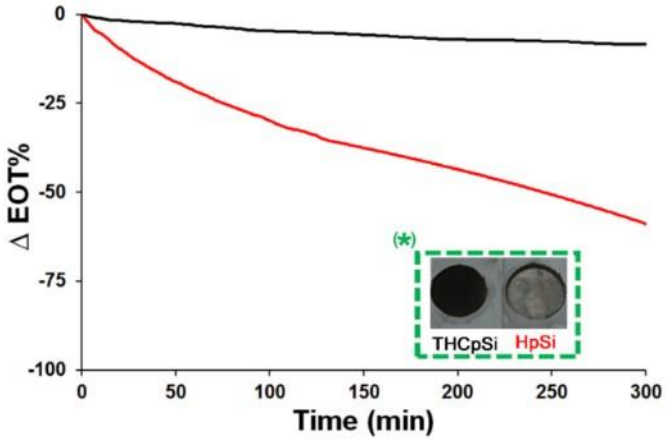

Figure 4-4 Stability of HpSi (red line) and THCpSi (black line) films as a function of time in PBS as investigated by IRS. (*) Image of HpSi and THCpSi films (representative images of the surface modifications) fixed into a flow cell with a constant flow rate (3.5 mL min^{-1}) of PBS (pH 7.4 and temperature 37 °C) after 5 hours incubation.

4.3.2 Preparing THCpSiNPs (siRNA Loading onto THCpSiNPs and Coating):

Figure 4-5 showed the kinetics of siRNA release over time. During the first few hours, all THCpSiNPs treatments showed an initial burst, followed by a sustained release. siRNA/THCpSiNPs released siRNA significantly earlier than other nanoparticle formats. However, total siRNA release showed a reduction with an increase in the coating PEI concentration from 0.05 to 0.2% w/v.

50% of siRNA were released in the medium after about 8 hours, while 100% of siRNA in the medium was observed after 35 hours. Of note, the size of THCpSiNPs increased by coating with different PEI concentrations (Table 4-2) due to the relative size of the nanoparticles and the organic polyamine coating. The variation in size as demonstrated by the increased SD although not statistically significant, likely results in some variation of siRNA release. However, all experiments demonstrate internalisation of the nanoparticles and the supernatant concentrations of siRNA did not vary significantly. Therefore, it was necessary to keep this as consistent as possible. Different THCpSiNP

sample preparations were used in different experiments to examine cellular uptake, cellular proliferation, qRT-PCR, and protein levels.

Table 4-2 Average hydrodynamic diameters, PDI and ζ-potential of THCpSiNPs after siRNA loading and PEI coating measured by DLS.(As published Hasanzadeh Kafshgari et al., 2015).

Particle	Average hydrodynamic diameter (nm)	PDI	ζ-potential (Coghlan et al.)
THCpSiNPs	**145.9 ± 32.5**	**0.087**	**-35.0 ± 4.7**
siRNA/THCpSiNPs	**193.2 ± 25.8**	**0.192**	**-11.0 ± 5.2**
PEI (0.05 w/v%)/siRNA/THCpSiNPs	**213.3 ± 78.7**	**0.120**	**53.9 ± 7.3**
PEI (0.1 w/v%)/siRNA/THCpSiNPs	**228.1 ± 77.9**	**0.085**	**59.8 ± 6.1**
PEI (0.2 w/v%)/siRNA/THCpSiNPs	**236.5 ± 81.9**	**0.080**	**56.1 ± 5.7**

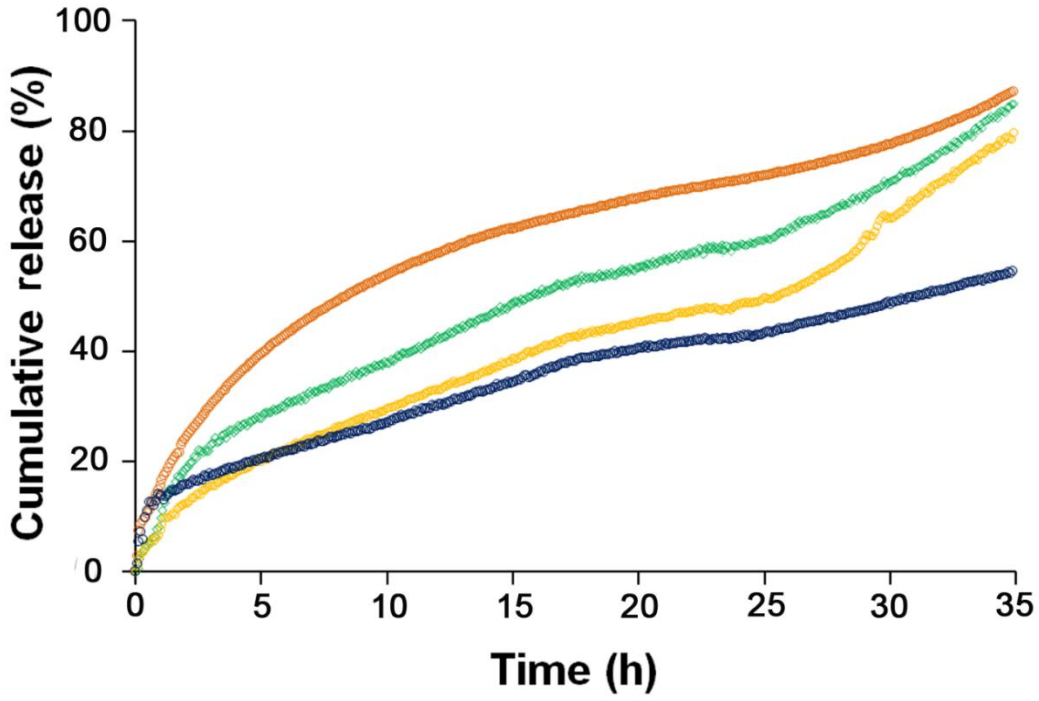

Figure 4-5 Effect of PEI coating and concentration on siRNA release profile from samples: siRNA/THCpSiNPs (red), PEI/MRP1-siRNA/THCpSiNPs (0.05% w/v, green), PEI/MRP1-siRNA/THCpSiNPs (0.1% w/v, yellow) and PEI/MRP1-siRNA/THCpSiNPs (0.2% w/v, blue). Release medium: PBS, pH 7.4, T =37°C ±0.2 (representative data, n = 3). (Data as published, Figure 6 (Hasanzadeh Kafshgari et al., 2015))

Table 4-3 Final Characteristics of THCpSiNPs for siRNA adsorption.

Characteristic	Sample
Functionalisation	THCpSiNPs
Agitation rate (rpm)	300
Type of oligonucleotide	siRNA
Average diameter (nm)	145.9
Diffusion coefficient (m^2/s)* 1, 2	≈8.39x10-11
Initial oligonucleotide concentration (µg/mL)	230
Porosity (%)	54
Solid density (g/cm^3) 3	≈2.33

pSiNPs concentration (mg/mL)	0.1
Solution bulk density (g-pSiNPs/cm^3)	≈1
Density of solvent (g/cm^3)	≈1
Temperature (°C)	25

4.3.3 Cellular Uptake of siRNA Loaded onto THCpSiNPs:

T98G control cells (not exposed to the NPs) were well-spread, displaying lamellipodia, with the typical shape and morphology of adherent T98G cells. Also no morphological changes were observed in the T98G treated cells (exposed to the PEI/NC-siRNA/THCpSiNPs) after 24 hours incubation (Figure 4-9).

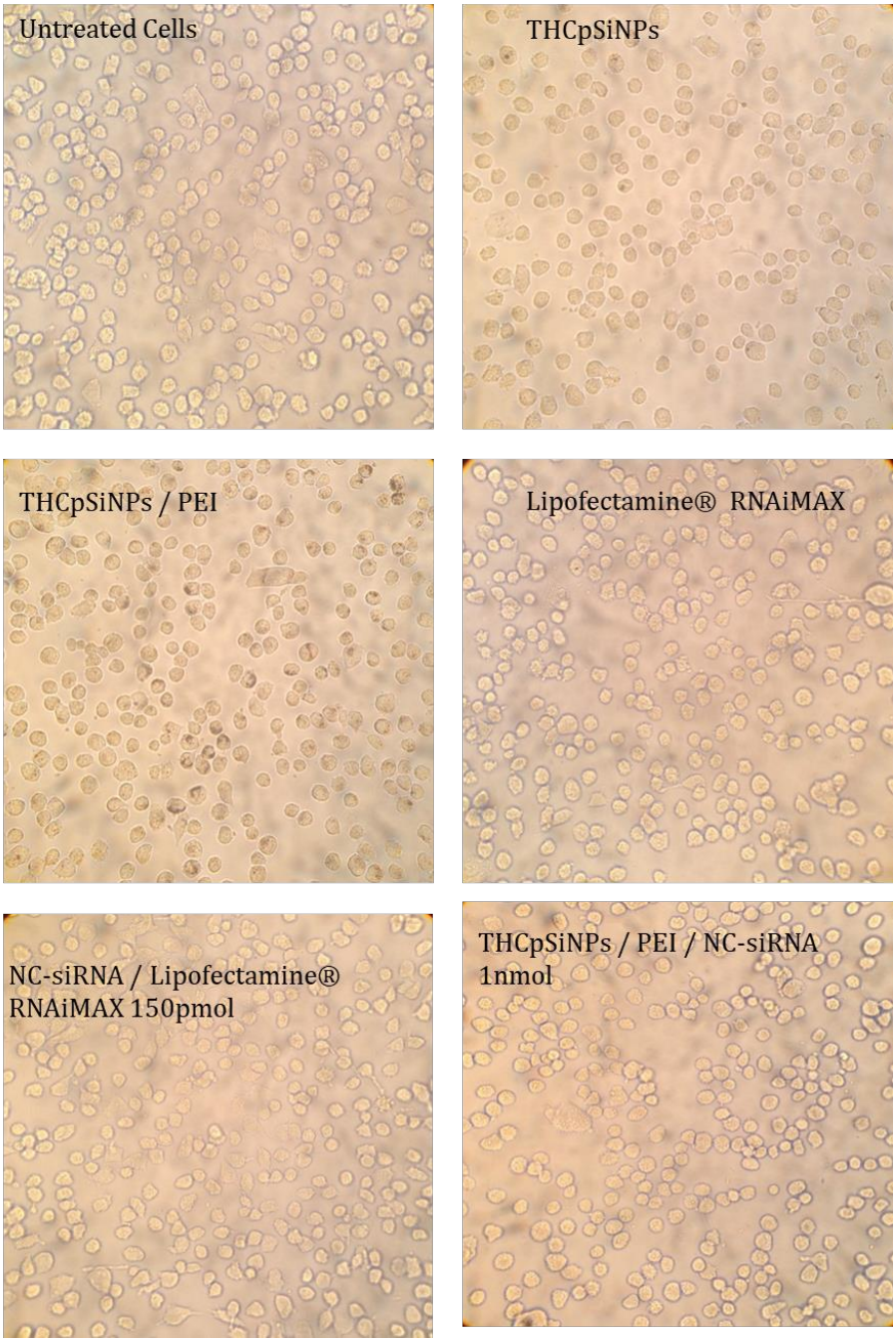
Untreated Cells
THCpSiNPs
THCpSiNPs / PEI
Lipofectamine® RNAiMAX
NC-siRNA / Lipofectamine® RNAiMAX 150pmol
THCpSiNPs / PEI / NC-siRNA 1nmol

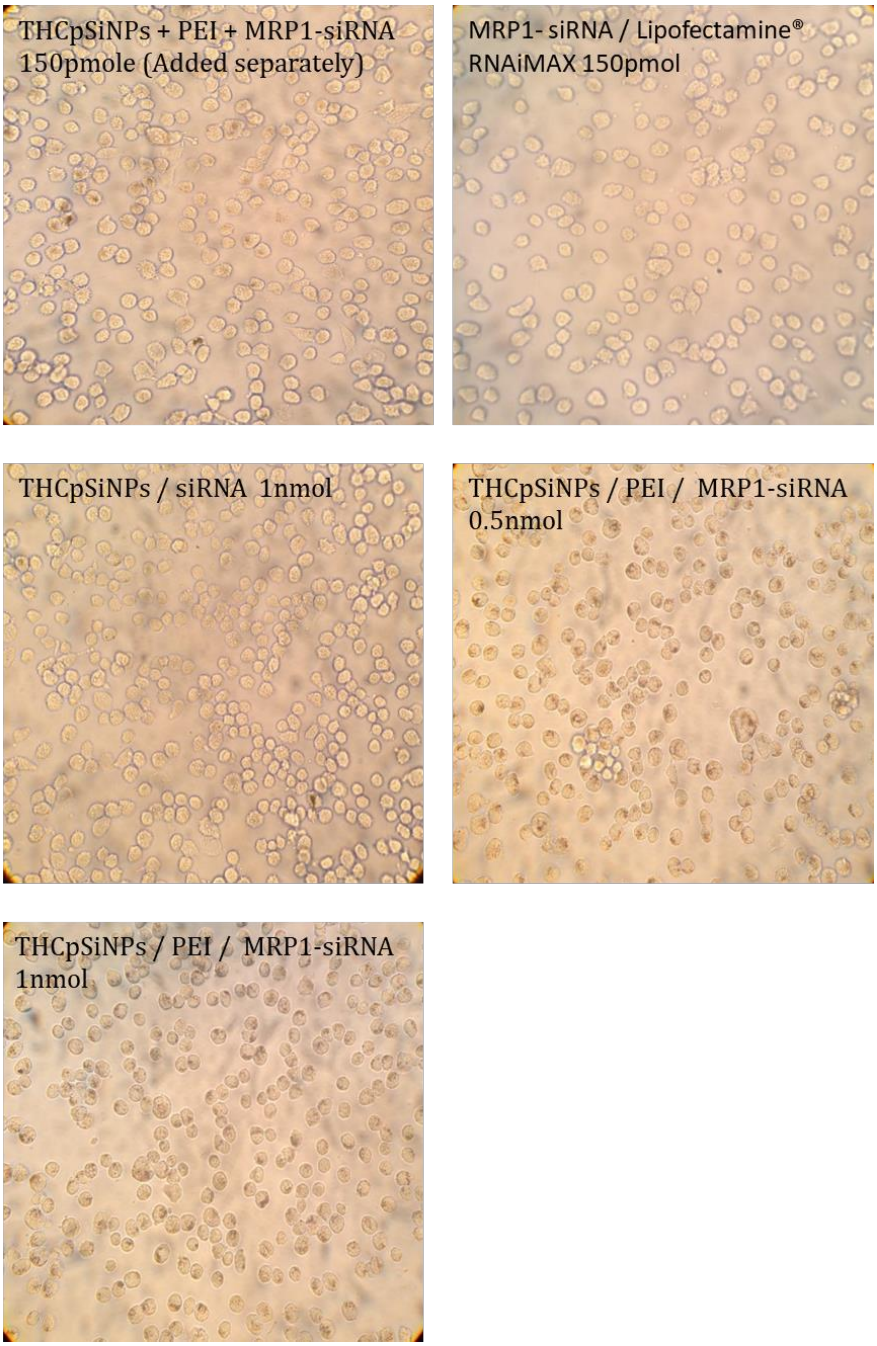

Figure 4-6 Cell morphology of T98G glioblastoma cell lines incubated with either control samples or with MRP1-siRNA at different concentrations (0.5 and 1 nmol of siRNA loaded onto THCpSiNPs). At 24 hours, cells were washed twice with PBS and Trypsin was added. Images were taken with a light microscope at 10X scale. Sample abbreviations are in Table 3-1.

Treated cells showed punctate green fluorescence, attributed to the internalisation of the PEI/MRP1-siRNA/THCpSiNPs (Figure 4-6). It is worth noting that the THC modification quenched the intrinsic luminescence of pSi, so the green fluorescence was only due to the FAM-MRP1-siRNA. Also, confirming cellular uptake, cells washed with PBS and incubated with trypsin (Figure 4-6) showed THCpSiNPs present within the cells in samples coated with PEI. Similar conditions were used to examine each sample.

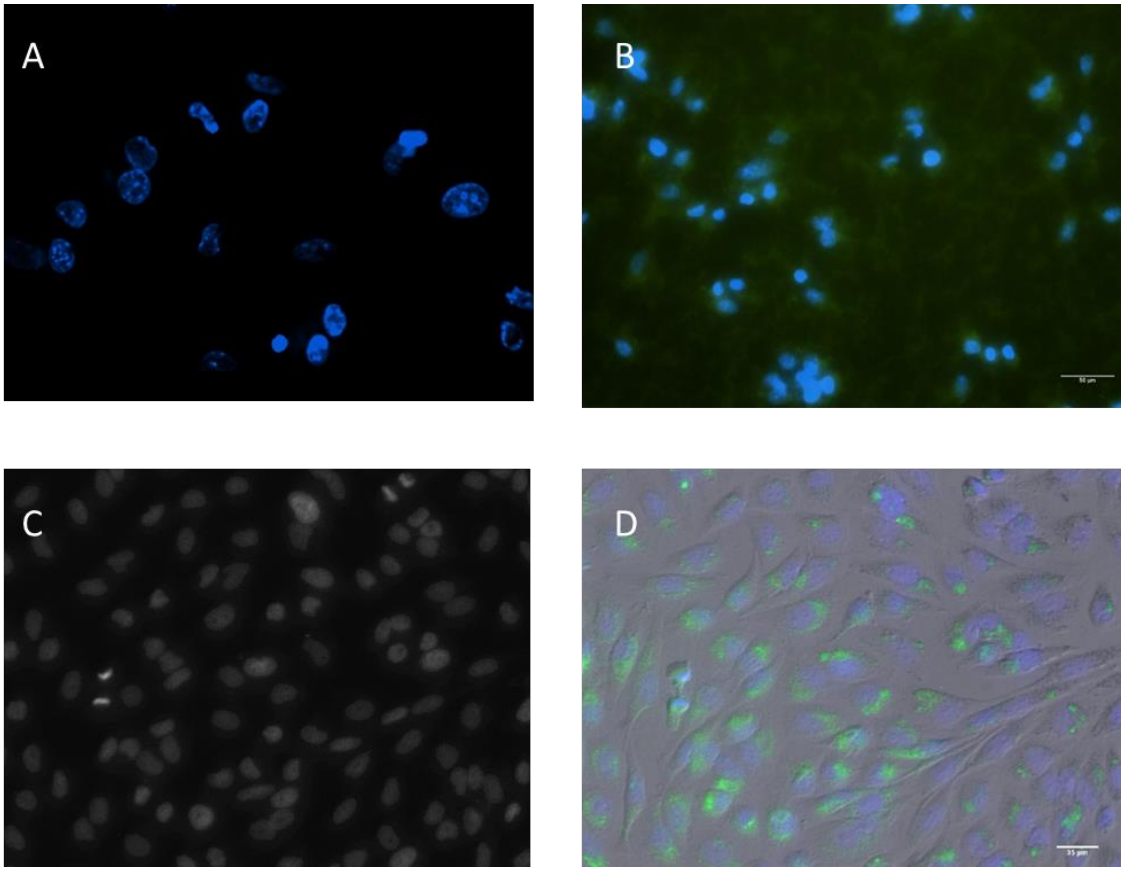

Figure 4-7 Fluorescence microscopy of T98G after transfection with PEI/FAM-MRP1-siRNA/THCpSiNPs (0.1 mg/mL). The uptake of THCpSiNPs in the cells was examined microscopically at 24 hours. Nuclear staining with DAPI. Green fluorescence represents the loaded nanoparticles taken up by cells. A & C: Untreated cells; B & D: PEI/FAM-MRP1-siRNA/THCpSiNPs treated cells. C & D represent merged grey coloured and FAM (green fluorescent) images. Image magnification: 40X.

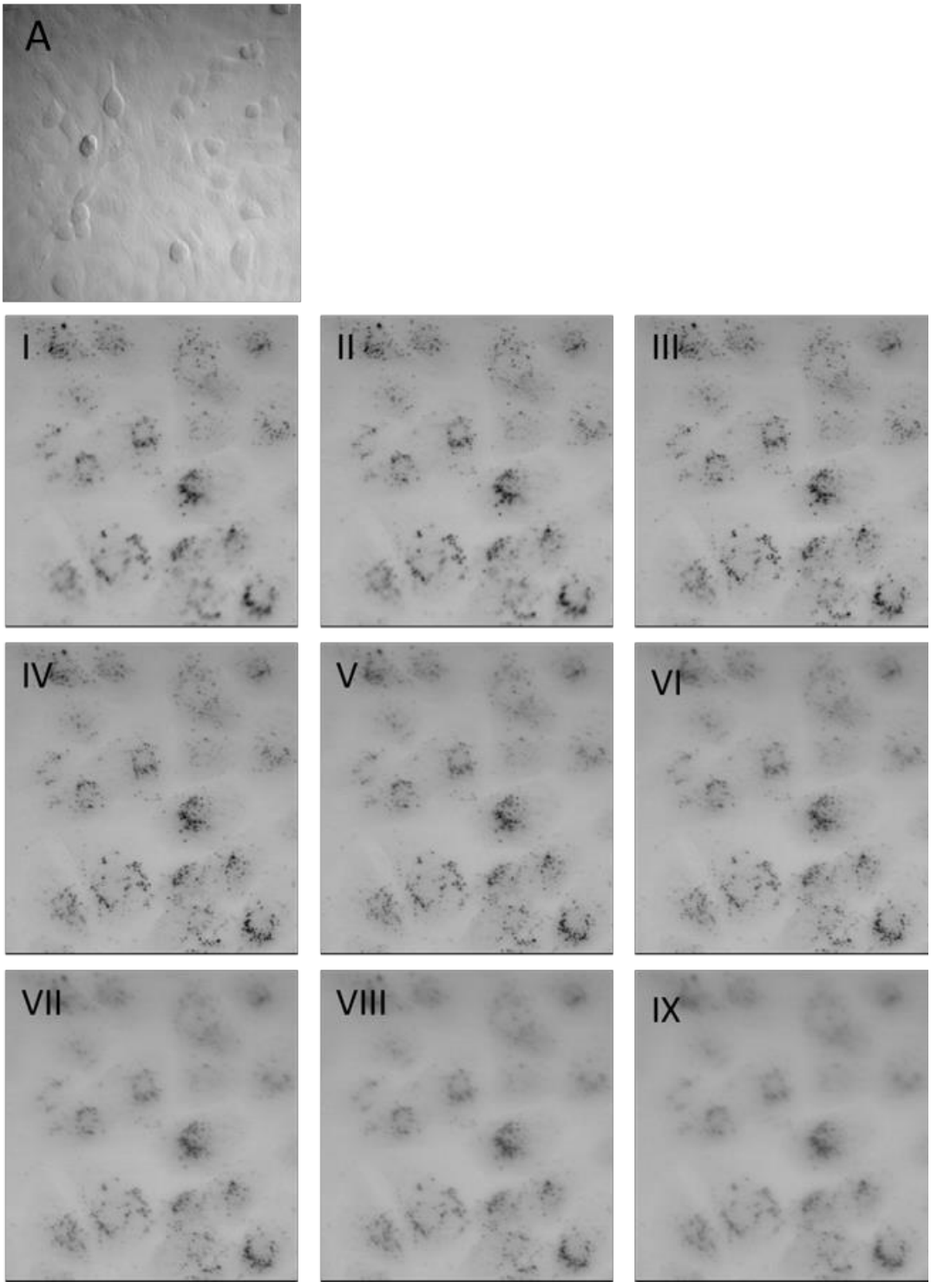

Figure 4-8 Progressive Z-stack laser-scanning confocal microscopy image series for T98G cells incubated with PEI/MRP1-siRNA/THCpSiNPs (0.1 mg/mL) (dark black dots) after 48hours. A: untreated T98G cells. The roman numbers correspond to images at different planes (height interval: 300 nm; down to up). I and IX are representative of the bottom and top plane of the treated T98G cells, respectively. Scale bars are 40X.

To confirm the cellular uptake of PEI/MRP1-siRNA/THCpSiNPs, z-stacks were acquired using confocal microscopy after 48 hours incubation (Figure 4-8).

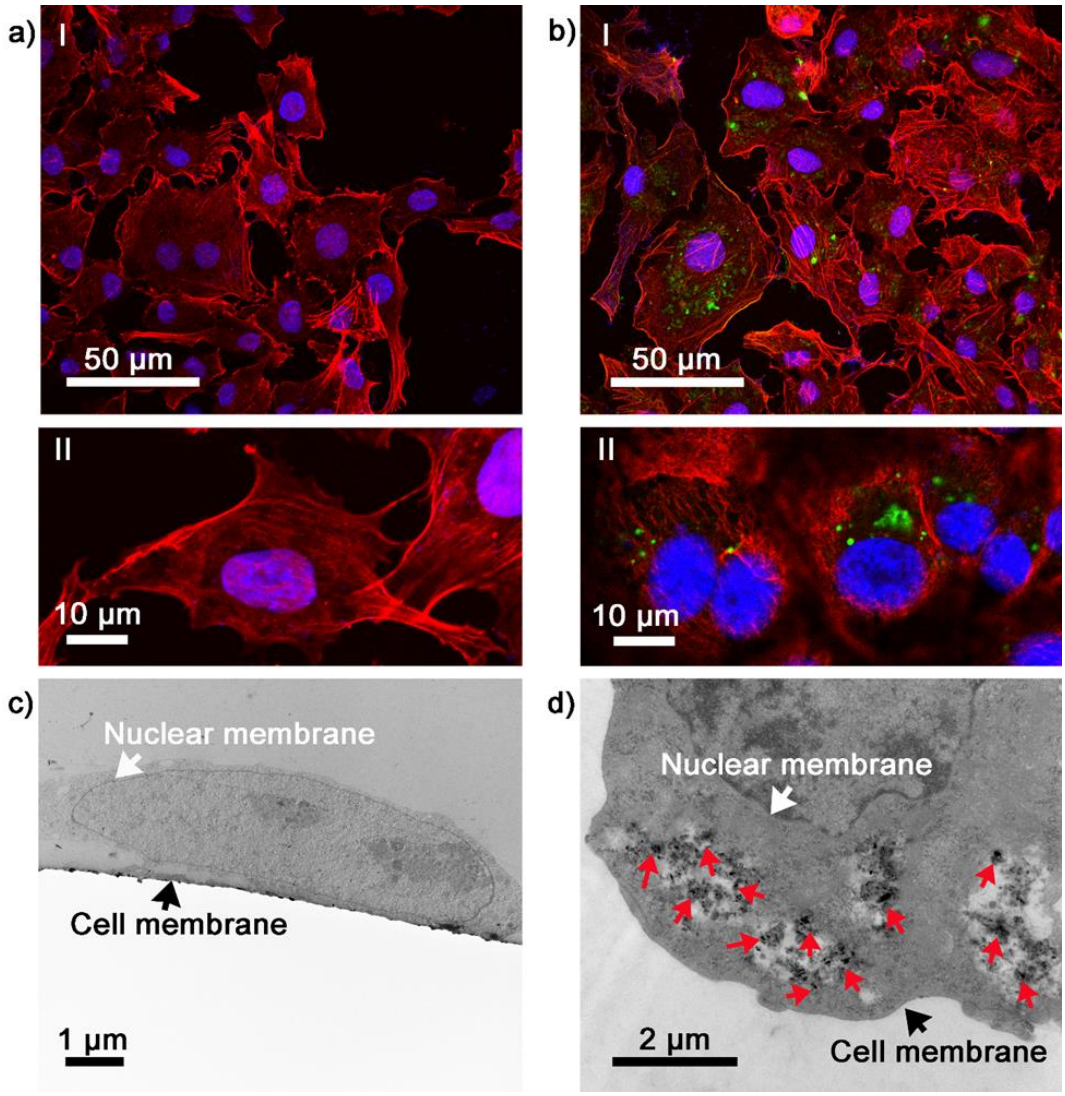

Figure 4-9 Uptake of PEI/Block-iT™/THCpSiNPs by T98G cells. Laser-scanning confocal microscopy images of (a) control T98G cells without the NPs, and (b) T98G cells incubated with PEI/Block-iT™/THCpSiNPs (I and II). The cell nucleus was stained with Hoechst 33342 (blue), PEI/Block-iT™/THCpSiNPs appeared green, and the cell cytoskeleton was stained with phalloidin-TRITC (red). TEM images of (c) control T98G cells without the NPs and (d) T98G cells incubated with PEI/Block-iT™/THCpSiNPs. The red arrows indicate the internalised NPs. (Image included as figure 6. (Hasanzadeh Kafshgari et al., 2015))

4.3.4 Proliferation and Viability of Cells:

Assessment of cell proliferation and viability were required to determine the cellular toxicity of nanoparticles as understanding the inherent toxicity is critical for a subsequent nanomedicine application. Initially one dose of treatment given 24 hours after plating the cells was investigated for its effect. 1mg of THCpSiNPs, PEI/MRP1-siRNA/THCpSiNPs (siRNA is unmodified) showed a decrease in cell growth at 24 hours, while the untreated T98G cells recovered at 72 hours with a 30% increase in cell number. Cells transiently transfected once with modified MRP1-siRNA showed a steady decrease in growth for 72 hours however, unmodified MRP1-siRNA recovered slowly after 48 hours (Figure 4-10). Thus, the THCpSiNP concentration was reduced to 0.1mg/mL and modified siRNA were used in all experiments. Again, with one treatment dose, cells started to recover after 48 hours. As a result, two doses of treatments were investigated.

T98G cells were treated twice at 0 and 24 hours. Cells treated with THCpSiNPs either coated with PEI or alone, PEI/NC-siRNA/THCpSiNPs and PEI+MRP1-siRNA+THCpSiNPs added separately showed similar proliferation to untreated cells (Figure 4-12). The growth curve of both PEI/MRP1-siRNA/THCpSiNPs and MRP1-siRNA/Lipofectamine treated cells present a similar decline in cell proliferation during the incubation period (Figure 4-12). There were no differences in cell viability observed between T98G cells treated with PEI/MRP1-siRNA/THCpSiNPs or siRNA/Lipofectamine and untreated cells (Figure 4-13). Moreover, all cells treated with control NP showed a high cell viability (>93.3%), similar to the viability of the untreated cells.

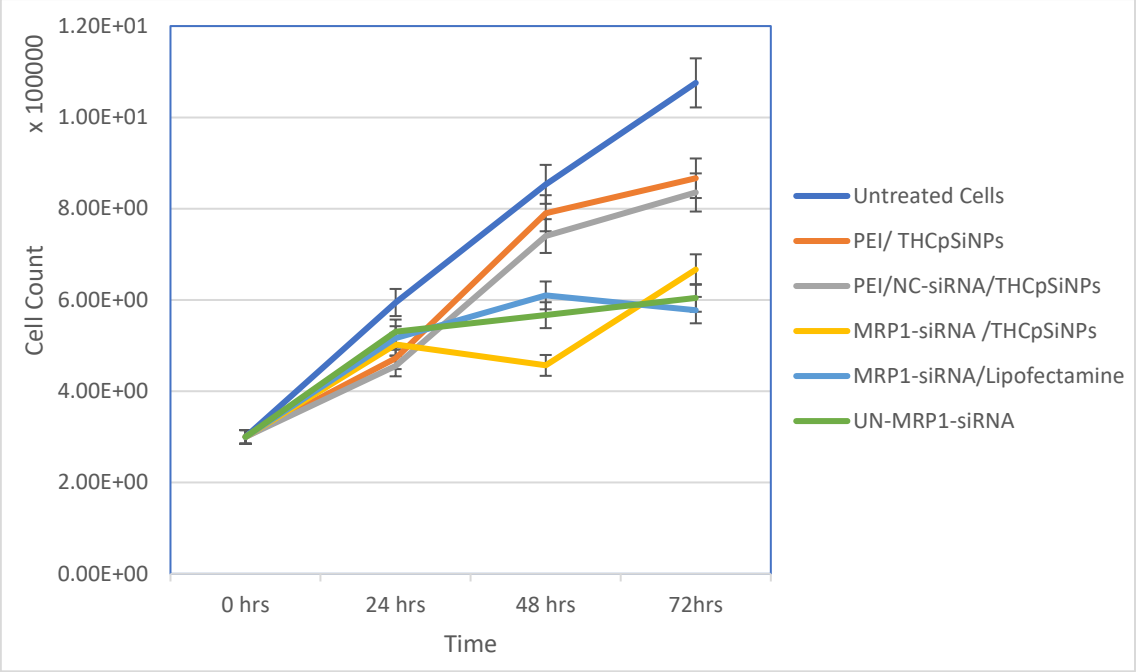

Figure 4-10 Proliferation rate of the T98G cells exposed once to NPs (1mg) and controls at different time points. Proliferation was measured using a Trypan Blue assay on a bright field microscope. Cell counts are expressed as live cell numbers. Two separate e Experiments were conducted in triplicate (n = 2; Values are mean ± standard deviation). Values are mean ± standard deviation. THCpSiNPs: Nanoparticles; NC-siRNA: negative control siRNA; MRP1-siRNA: siRNA targeting MRP1 gene; PEI: polyethyleneimine; PEI+MRP1-siRNA+ THCpSiNPs: each added separately.

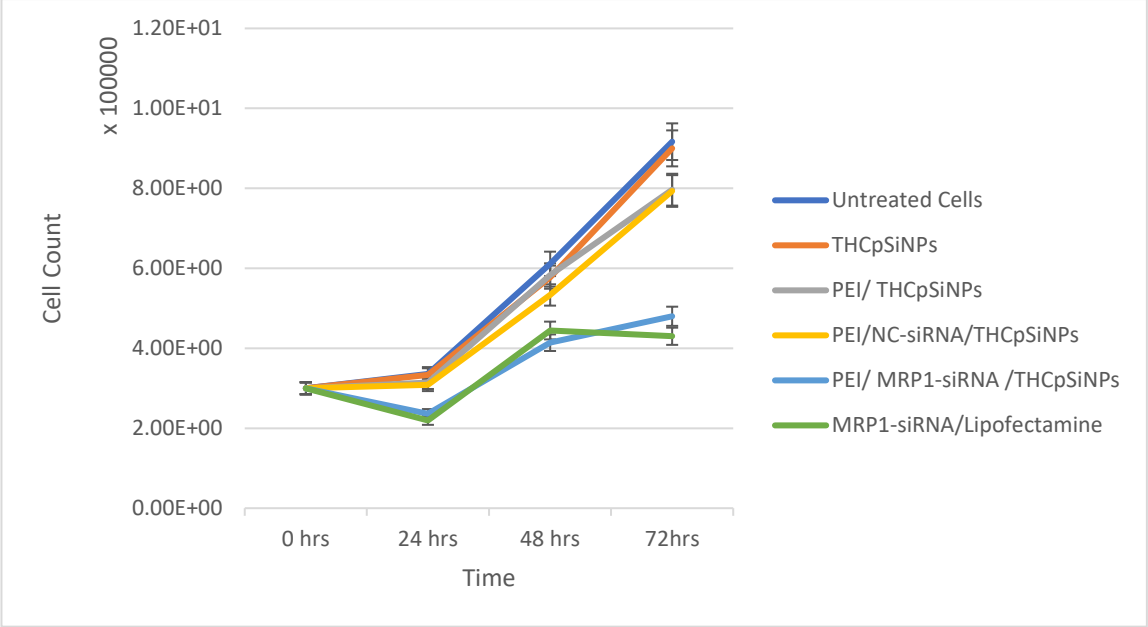

Figure 4-11 Proliferation rate of the T98G cells transfected once with the NPs (0.1mg) and controls. Viable cell number is measured at different time points by the Trypan Blue assay on a bright field microscope. Cell counts expressed as live cell numbers. Experiments were conducted in triplicate. (n = 3; Values are mean ± standard deviation). THCpSiNPs: Nanoparticles; NC-siRNA: negative control siRNA; MRP1-siRNA: siRNA targeting MRP1 gene; PEI: polyethyleneimine; PEI+MRP1-siRNA+ THCpSiNPs: each added separately.

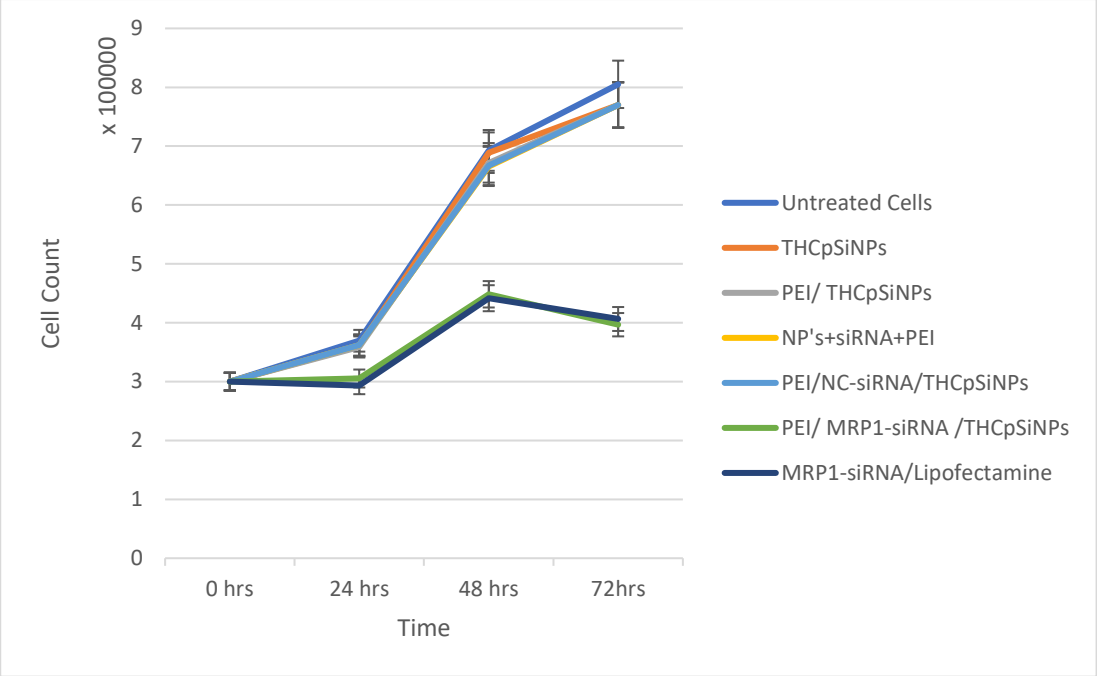

Figure 4-12 Proliferation rate of the T98G cells transfected twice with NPs (0.1mg)and controls. Cell counts measured at different time points using a Trypan Blue assay on a bright field microscope. Cell counts expressed as live cell numbers. The growth curves show a clear significant reduction in growth with PEI/MRP1-siRNA/THCpSiNPs and MRP1-siRNA/Lipofectamine treatment compared to negative controls (untreated cells, THCpSiNPs either coated with PEI or alone, PEI/NC-siRNA/THCpSiNPs and PEI+MRP1-siRNA+THCpSiNPs). Two separate experiments were conducted in triplicate. (n = 2; Values are mean ± standard deviation). THCpSiNPs: Nanoparticles; NC-siRNA: negative control siRNA; MRP1-siRNA: siRNA targeting MRP1 gene; PEI: polyethyleneimine; PEI+MRP1-siRNA+ THCpSiNPs: each added separately.

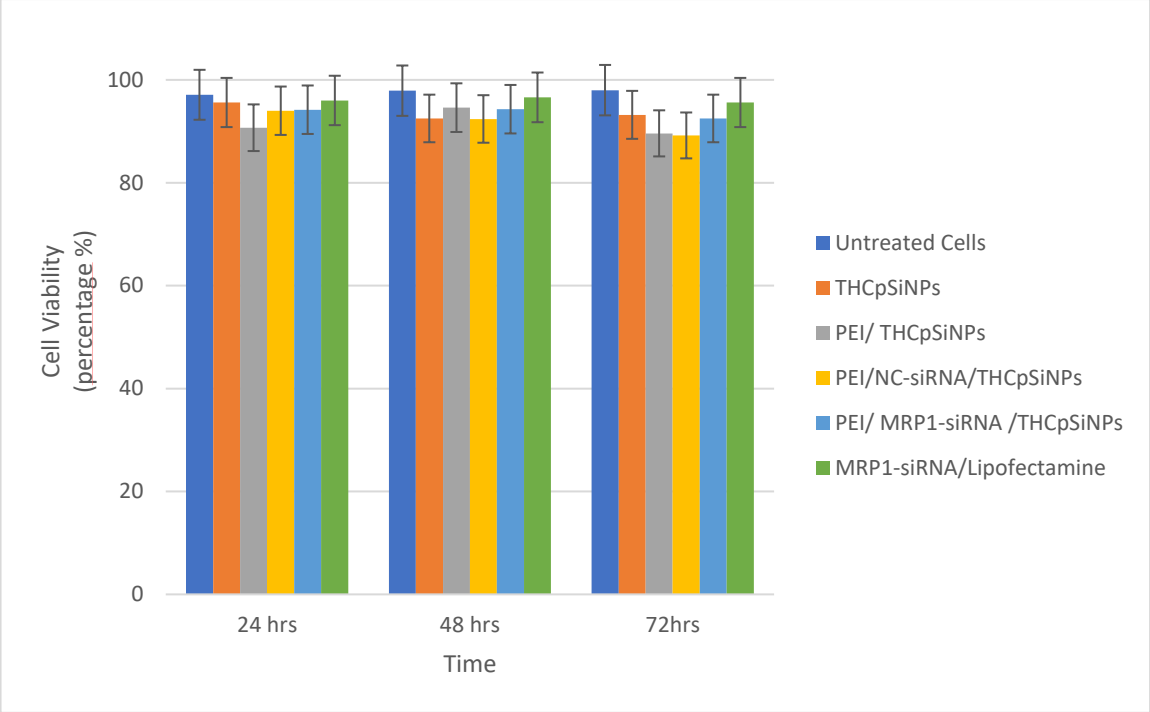

Figure 4-13 Cell Viability of the T98G cells transfected twice with the NPs and controls measured at different time points. Experiments were conducted in triplicate. (n = 2; Values are mean ± standard deviation) THCpSiNPs: Nanoparticles; NC-siRNA: negative control siRNA; MRP1-siRNA: siRNA targeting MRP1 gene; PEI: polyethyleneimine.

4.3.5 Apoptosis Assessment in T98G Following Exposure to THCpSiNPs:

In untreated cells, approximately 97% of the cells were viable at all time points however, a small increase in cell apoptosis was seen at 24 hours which could be due to the absence of serum or antibiotic in the medium. At 72 hours, untreated cells recovered as the growth medium was changed at 48 hours of treatment. Apoptosis in control samples THCpSiNPs was slightly increased over time. In contrast, apoptosis in PEI/THCpSiNP and PEI/NC-siRNA/THCpSiNPs was decreased at 24, 48 and 72 hours. Approximately 3.6 % of apoptosis in T98G cells treated with PEI/MRP1-siRNA/THCpSiNP was observed consistently during the treatment. On the other hand, cells transiently transfected with MRP1-siRNA/Lipofectamine showed levels of apoptosis 2.3%, 1.6% and 1.9% respectively at 24, 48 and 72 hours respectively (Figure 4-14).

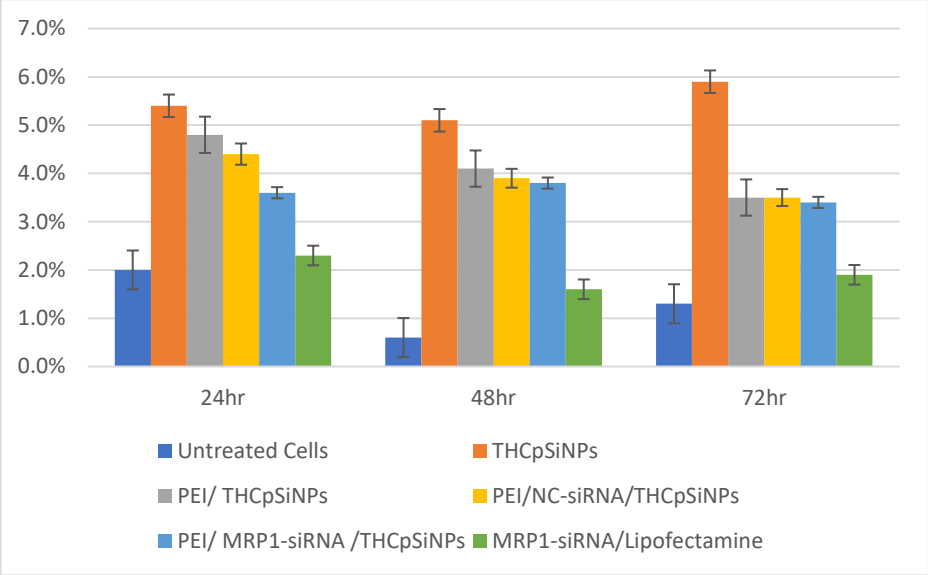

Figure 4-14 T98G cell apoptosis detection after incubation with untreated or transfected with THCpSiNPs , PEI/THCpSiNPs, PEI/NC-siRNA/THCpSiNPs, PEI/MRP1-siRNA/THCpSiNPs or MRP1-siRNA/Lipofectamine at the concentration 0.1 mg mL−1 of THCpSiNPs and 0.4 nmole of siRNA at 24, 48, and 72 hours. The T98G cell line was analysed with Annexin V-FITC/PI assay after 48 hours of the treatment. (n = 3; mean ± standard deviation shown).

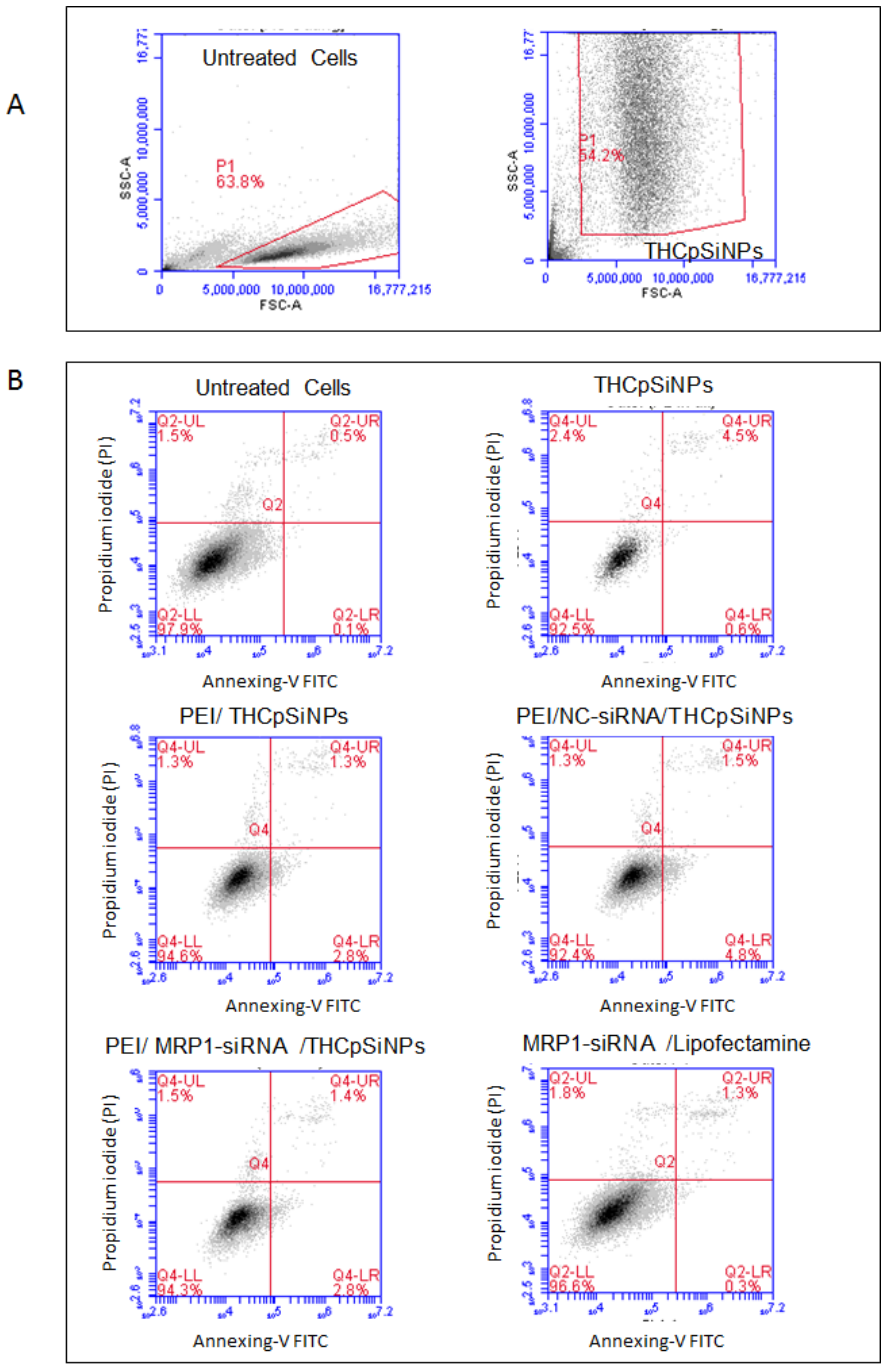

Figure 4-15 T98G cell apoptosis detection after incubation for 48 hours. A. FSC-A vs SSC-A plots of populations of gated untreated and THCpSiNP treated cells. B. Apoptosis and necrosis of untreated cells and cells treated with THCpSiNPs, PEI/THCpSiNPs, PEI/NC-siRNA/THCpSiNPs, PEI/MRP1-siRNA/THCpSiNPs or MRP1-siRNA/Lipofectamine at the concentration 0.1 mg mL−1. The T98G cell line was analysed with Annexin V-FITC/PI assay after 48 hours of treatment. The bottom left quadrant represents the viable cells, the bottom right quadrant shows the early apoptotic cells, the top left quadrant represents necrotic cells, and the top right quadrant indicates late apoptotic cells (representative data, n = 4)

4.3.6 The Effect of THCpSiNPs Loaded With siRNA on MRP1 mRNA Expression:

Multidrug resistance protein 1 (MRP1) expression was assessed in the T98G cell line and *in vivo*. T98G cells were incubated with the PEI/MRP1-siRNA/THCpSiNPs and controls for 48 hours. The effect of transient transfection of siRNA targeting MRP1 in T98G was evaluated using qRT-PCR. T98G cells were treated twice at 0 and 24 hours. MRP1 mRNA expression in both treated and untreated T98G cells was examined at 48 hours after the first transfection. PEI/MRP1-siRNA/THCpSiNPs and positive control siRNA-MRP1/Lipofectamine significantly inhibited MRP1 expression. Significant downregulation of MRP1-mRNA (63%) was observed in the PEI/MRP1-siRNA/THCpSiNPs treated cells (Figure 4-16) compared with untreated cells. Approximately 10% more reduction in MRP1 mRNA was seen in cells treated with PEI/ MRP1-siRNA /THCpSiNPs compared with cells transiently transfected using Lipofectamine. There was no downregulation of MRP1-mRNA in the negative controls or untreated cells. Meanwhile, no noticeable change was seen in cells transfected with THCpSiNPs either coated with PEI or not, and loaded with negative control siRNA.

The *in vivo* study involved mRNA extraction from tumours dissected at selected time points then quantitative analysis of MRP1 expression. According to qRT-PCR data, a reduction of MRP1 mRNA was observed at 48 and 72 hours post-treatment, with the greatest reduction being 40% at 48 hours (Figure 4-17 A). The expression began to recover between 48 and 72 hours, reaching approximately 90% at 72 hrs (Figure 4-17 B). Kidney and duodenum, which express MRP1 at physiological levels were also harvested. qRT-PCR results suggested that the reduction of MRP1 mRNA in the kidney reached as much as 60% at 48 hours post MRP1 siRNA treatment, and 55% (n=2) at 72 hours (Figure 4-17). The reduction in the duodenum was even more pronounced, being 80% (n=2) at

48 hours, with no recovery observed after 72 hours post-treatment (Figure 4-17). Therefore, we conclude that MRP1 siRNA delivered in non-targeted nanoparticles, PEI-THCpSiNPs in this case, induces MRP1 knockdown in kidney and duodenum. This demonstrates that the PEI- THCpSiNPs successfully delivered siRNA to the tumour (s.c. xenografts) and yielded significant MRP1 knockdown.

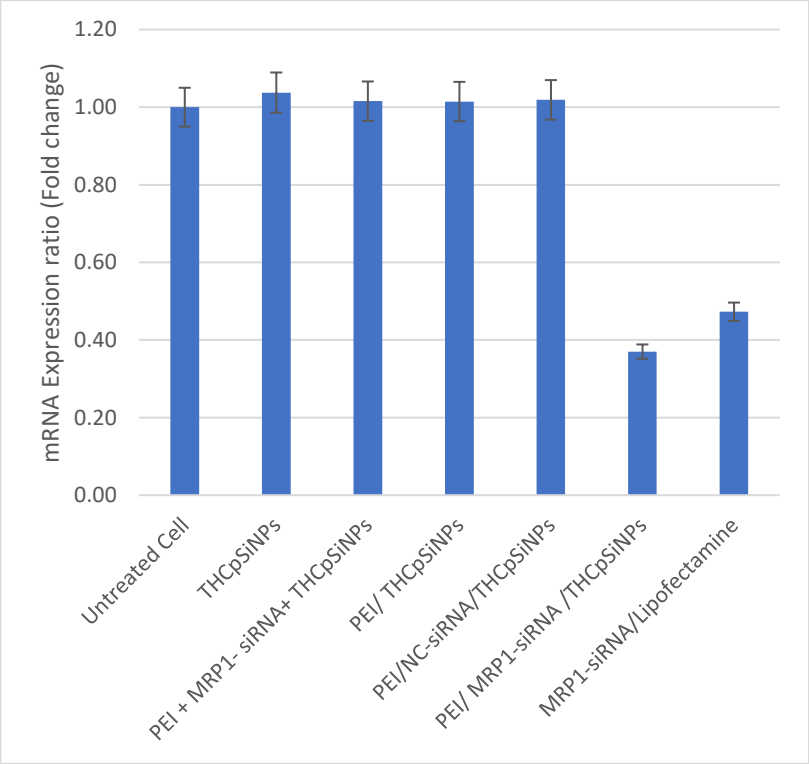

Figure 4-16 qRT–PCR demonstrating knock-down effects on MRP1 in T98G cell line at 48 hours, after the incubation of T98G with PEI/MRP1-siRNA/THCpSiNPs and controls.

These data were calculated using the delta delta Ct method. Average of triplicates (± Standard Deviation). Difference in expression between MRP1 and GAPDH reference housekeeping gene. THCpSiNPs: Nanoparticles; NC-siRNA: negative control siRNA; MRP1-siRNA: siRNA targeting MRP1 gene; PEI: polyethyleneimine; PEI+MRP1-siRNA+ THCpSiNPs: each one added separately.

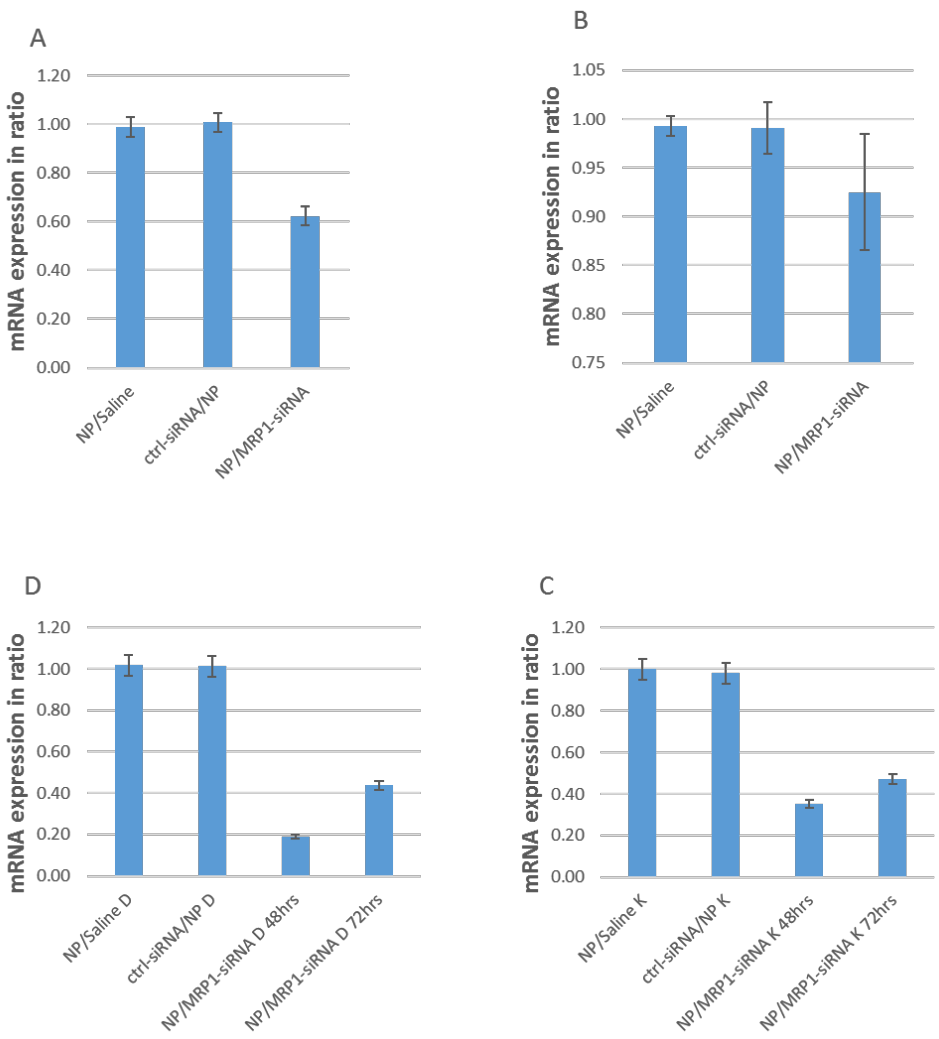

Figure 4-17 qRT–PCR demonstrating knock-down effects on MRP1 in vivo. mRNA expression data of two mice injected intraperitoneally with 1nmole siRNA-MRP1 loaded onto THCpSiNP and PEI coated. Mice had U87MG cells grown on both left and right flanks. The expression of MRP1 mRNA A. 48 hours and B. 72 hours after siRNA/ THCpSiNP injection into mice. Samples were from 4 different tumours grown in two mice. C. MRP1 expression in mouse Kidney (K) and D. mouse Duodenum (D). Both Kidney and Duodenum samples were harvested at 48 and 72 hours. These data were calculated using the delta delta Ct method. Average of triplicates (with± SD). MRP1 expression difference between MRP1 and GAPDH reference housekeeping gene n=4 tumour using 2 mice.

4.3.7 MRP1 Protein level:

MRP1 protein level in T98G cells was evaluated by flow cytometry analysis. See Table 4-1 for the relevant details. Flow cytometry demonstrated a significant reduction in MRP1 protein level in both PEI/MRP1-siRNA/THCpSiNPs and MRP1-siRNA/Lipofectamine treated T98G cells at 96 hrs (~70% reduction of the average protein level compared with the untreated cells) (Figure 4-18) also consistent with the demonstrated downregulation of the MRP1-mRNA in T98 cells *in vitro* (Figure 4-16). A difference in protein level in the negative controls treated cells was not observed. A reduction of MRP1-protein was not detected at 48 and 72 hours of incubation with THCpSiNPs (Figure 4-18 A and B). Data are a representative of one of three independent experiments.

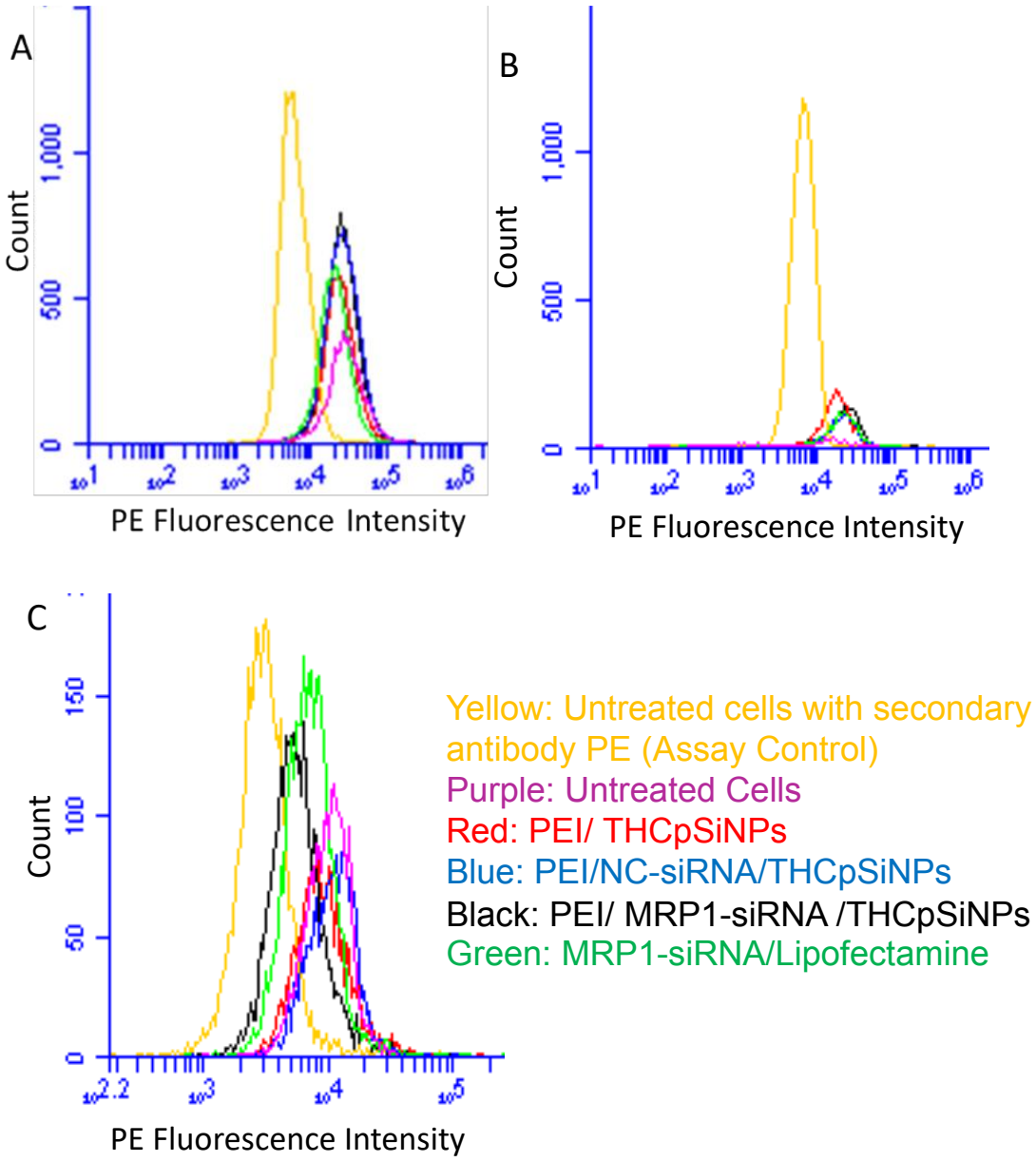

Figure 4-18 Flow cytometry histograms evaluating MRP1 protein concentration in T98G cells. Cells were harvested at A. 48 hours, B. 72 hours and C. 96 hours after treatment with nanoparticles and say all the treatments. Histograms represent the cell count numbers versus fluorescence intensity expressed as log relative fluorescence.

4.4 Discussion:

Glioblastomas are aggressive cancers that affect the central nervous system. They are characterised as highly chemo-resistant tumours protected from chemotherapy exposure by the BBB and ABC transporters within the tumour cells themselves. A delivery vehicle may help overcome several resistance mechanisms exhibited by glioblastoma. The ultimate aim of the experimental work described in this chapter was to develop a system (in this case using nanoparticles) to deliver siRNA across the BBB *in vivo*. To achieve this, initially siRNA targeted towards MRP1 were loaded onto nanoparticles coated with PEI and delivered to T98G glioblastoma cell line *in vitro*. This work demonstrated that designed MRP1 siRNA molecules were effective in reducing expression of MRP1 mRNA by 60% and that with 2 separate treatments at 24 and 48 hours, protein downregulation could also be achieved when measured at 96 hours post-treatment. It is noteworthy that the half-life of the mature MRP1 protein is 20 hours (Almquist et al., 1995) which explains why between 72 – 96 hours there is a measurable downregulation of the MRP1 protein by flow cytometry. The effects of a single transfection appear to be insufficient to knock down protein and demonstrate functional effects of MRP1 downregulation on T98G cells *in vitro*. A single transfection however did result in a transient reduction in mRNA, as shown in (Figure 4-16).

In vivo experiments were initiated on the strength of the *in vitro* results and were planned to provide adequate siRNA to the mice bearing xenografted U87MG cell tumours. Several cell lines were trialled prior to the U87MG. However growth was most consistent with this cell line and experiments were carried forward as such. While statistical analysis was limited, there were 4 tumours per grouping allowing some statistical analysis in this

essentially pilot in vivo study. An orthoptic model has been considered, the most relevant being a rat model with injected cerebral tumours. However, this was beyond the scope of this thesis. Mice were injected with these nanoparticles *in vivo* without the aid of any transfection agents and demonstrated downregulation of target tumours as well as endogenous cells. The relative inefficiency of the tumour downregulation may relate to reduces blood supply. (Meng et al., 2013, Gordon et al., 2010, Yu et al., 2018, Van Woensel et al., 2016). Almost all cells can internalize NPs by a form of pinocytosis. This includes macropinocytosis, clathrin-mediated endocytosis, caveolae-mediated endocytosis and mechanisms independent of clathrin and caveolin (Treuel et al., 2013). Physico-chemical properties of NPs including size, shape, surface charge and surface chemistry strongly modulate the cellular uptake efficiency. Various nanoparticle delivery systems have been developed to deliver modulators of MRP1 in glioma cells (Xu et al., 2015, Saad et al., 2008). It was hypothesised that siRNA-MRP1 loaded onto nanoparticles administered during resected glioblastoma surgery would allow significant tissue penetration due to the disruption of the BBB. Delivery at the site of the tumour bed would then potentially result in the reduction of MRP1 expression, at the mRNA and protein level consequently increasing the chemosenstivity of the residual tumour cells. No cerebral spinal fluid or brain samples were taken during the in vivo experiments to know if systemic administration has the potential to cross the blood brain barrier but this would be an important next step in the project.

Our studies have also demonstrated reduced cell proliferation in vitro following MRP1 downregulation which has the potential to result in slowed tumour growth. Although this has not been confidently demonstrated in the presented work, this effect has been seen

in other tumour types: breast and neuroblastoma (Endo, 2019; Kuss, 2002) MRP1 downregulation also has been shown to increase cell proliferation in mucoepidermoid carcinoma. (Cai, 2016) The underlying cellular effects clearly require further investigation. Greater levels of retained nanoparticles would be required to affect sustained MRP1 reduction and determine the effect on tumour growth and apoptosis as well as adequately powered mouse experiments to allow confident analysis of the data.

In this study, nanoparticles were modified, loaded and coated followed by biological in vitro and in vivo studies. We used PEI-coated pSiNPs as the siRNA delivery vehicle to study the knockdown and phenotypic changes, both in cell lines, tumours and collateral organs. The pSiNP delivery vehicle for MRP1 siRNA was used due to a number of inherent desirable properties including high loading capacity, biodegradability and biocompatibility. Furthermore, successful *in vitro* knockdown of MRP1 with siRNA delivered using pSiNPs has previously been demonstrated (Wan et al., 2014, Kafshgari et al., 2015). The average size of THCpSiNPs used was 145.9 – 170 nm. For gene delivery by means of nanocarriers, a particle size between 100–300 nm is optimal in order to achieve high permeability into tumours, to accelerate cell binding and internalisation, and to avoid renal clearance. In addition, it is smaller than the tumour vasculature average size ranging from 380 – 780 nm (Hobbs et al., 1998). In our case, the pSiNPs are neither so small that they are subject to rapid renal clearance nor so large (>400 nm in diameter) that they are captured by the inter-endothelial gap defence in tumours (Alexis et al., 2010, Wan et al., 2014). Also, they are within the range of 100nm which allows them to be longer lasting in the circulatory system. A different process of filtration and

ultracentrifugation was used to concentrate nanoparticles to obtain best results (Blanco et al., 2015, Malhotra et al., 2014).

During the siRNA loading onto THCpSiNPs, multiple steps of sonication were applied. Sonication increases the possibility of siRNA degradation. Thus, a chemical modification of siRNA was undertaken. 2-Fluoro modification has been shown to increase serum stability, binding affinity, and nuclease stability (Shen et al., 2015). Also, samples were kept at 4°C to reduce siRNA degradation (Van Woensel et al., 2016). The cationic polymer PEI was subsequently coated onto the surface of the THCpSiNPs preloaded with siRNA (PEI/siRNA/THCpSiNPs). PEI has been reported to be the polymer most used in siRNA delivery studies and has been considered the "gold standard'' in non-viral nucleic acid delivery (Aliabadi and Uludağ, 2016, Aliabadi et al., 2012). PEI caps the pores instead of penetrating them due to the large gyration radius of PEI (∼39 nm) while the THCpSiNPs average pore size is ∼9 nm (Lü et al., 2016, Ekhorutomwen et al., 2004). Modification of THCpSiNPs through PEI-coating decelerated siRNA release based on several mechanisms: (Węglarz et al.) a slow disintegration and dissolution of the PEI cap, (Abel et al.) the attractive electrostatic forces between positively charged PEI and negatively charged loaded siRNA, and (3) a decelerated wetting of the hydrophobic surface of THCpSiNPs (Wan et al., 2014, Kovalainen et al., 2012). Also, the PEI capping facilitated an obvious improvement of cell uptake in GBM cells. The PEI/MRP1-siRNA/THCpSiNPs were attached to cells rapidly (Bernkop-Schnurch and Dunnhaupt, 2012, Ragelle et al., 2013).

Cytotoxicity of PEI has been a concern for clinical translation. However, there is no significant cytotoxicity observed during THCpSiNPs delivery. Although the mechanism of such diminished toxicity remains unclear, a similar observation was reported by Yuen

Shan et al., who evaluated PMMA nanoparticles coated with branched 25 kDa PEI for gene delivery and showed efficient transfection and low cytotoxicity (Siu et al., 2012). Additionally, in this thesis MRP1 silencing by employing PEI-THCpSiNPs delivery of siRNA alone resulted in a reduced proliferation rate of GBM cells without causing significant cell death. The consistent decrease in total cell counts in in vitro MRP1 siRNA transfected T98G cells, without significant increase in apoptotic cell death was further investigated. Although, the primary action of MRP1 in glioblastoma has been ascribed to chemotherapeutic efflux from the cell, others have described a decrease in malignant cell proliferation and tumour growth when MRP1 action is attenuated in the absence of chemotherapeutic agents. Thus, in the absence of significantly increased cell cytotoxicity from the nanoparticles alone, this delivery system may be considered to be a potentially applicable system and the effects of MRP1 downregulation could be further explored with only minimal effects of the nanoparticles on the cells themselves.

Following cell transfection, we used qRT-PCR to evaluate MRP1 mRNA expression and flow cytometry to measure the reduction in MRP1 protein level. High precision multichannel flow cytometry allows quantitative studies at single cell level as transfection may not be equivalent in all cells and provides a better understanding of the range of potential transfection efficiencies. Additionally, it may be correlated with Calcein AM functional data (Szeremy et al, 2019). While immunoblotting was also briefly investigated, the size of MRP protein was found to make immunoblotting less reliable (data not shown). Significant downregulation of MRP1 mRNA expression resulted from treatment with both PEI/MRP1-siRNA/THCpSiNPs and MRP1-siRNA/Lipofectamine. This downregulation implies internalisation of PEI/MRP1-siRNA/THCpSiNPs into cells, and

subsequent release of the loaded siRNA into the cytoplasm exploiting the known proton sponge effect (Kafshgari et al., 2015, Akinc et al., 2005). On the other hand, there was no significant change in MRP1 expression in the negative control samples.

The reduction in MRP1-protein level was observed after 96 hours of treatment due to time taken for protein translation to be inhibited following the halted expression of the MRP1-mRNA. The 48- and 72-hour time points did not show any changes in MRP1 protein level, despite anticipation of the 72-hour timepoint to show downregulation, being approximately 3 half-lives of the mature MRP1 protein. (Wan et al., 2014, Almquist et al., 1995).

Since PEI-pSiNP delivery of siRNA is a biocompatible and versatile platform, it allowed us to characterise the MRP1 knockdown approach and to validate the decrease in proliferation of GBM *in vivo* as being a direct effect of MRP1 down regulation at both the mRNA and protein levels. (Carthew and Sontheimer, 2009). Hence, it can be concluded that the PEI-pSiNPs successfully accumulated and delivered the siRNA into the subcutaneous xenograft GBM tumour. The best model is a rat brain tumour model. However, this experiment was meant as a proof of principle of delivering nanoparticles containing siRNA to a whole organism and demonstrating effective delivery to a tumour. The next stage of these experiments would be the use of the rat model. This was out of scope for this thesis.

Bio-distribution of the cationic nanoparticle is well-documented to indicate accumulation in the liver, spleen, kidney, and lung (Knudsen et al., 2014), and both kidney and in Brunner's glands of duodenum tissues are known to express MRP1 as their physiological phenotype (Evers et al., 1996, Tyden et al., 2010). We observed significant

downregulation of MRP1 in these two organs, which was even more long-lasting than the silencing in the S.C. GBM tumour, which may be due to an expected accumulation profile of the non-targeted PEI-pSiNPs. It is reported that the physiological function of MRP1 in kidney and the digestive system is related to protection from natural toxins (Broker et al., 2004). However, histology of the various tissues was preserved during the treatment period with no ostensible effects on the health and metabolism of the treated mice. Additionally, if the nanoparticles were to be delivered via an Omaya reservoir allowing direct delivery to the tumour bed, systemic delivery of drug would be markedly reduced compared with the intravenously injected nanoparticles given to the mice. Clearly further investigation of the delivery of nanoparticles containing MRP1 siRNA would be required before embarking upon human studies.

5 THE ROLE OF MRP1 AND SONIC HEDGEHOG PATHWAY EXPRESSION IN GLIOBLASTOMA:

5.1 Introduction:

Glioblastomas are inherently drug resistant tumours. The relationship between drug resistance and glial tumours is likely to be multifactorial. Cancer stem cells are frequently held responsible for the drug resistance of cancers. These stem cells are present in gliomas and may be responsible for the high death rates of these incurable brain tumours. Human gliomas have been demonstrated to display a stem cell associated signature in their expression profiling. As such, it has been suggested that HEDGEHOG (HH)-GLI signalling regulates the expression of "stemness" genes in glioblastoma (Clement et al., 2007). HH-GLI signalling is also required for sustained glioma growth and survival, and HH inhibitors such as cyclopamine display additive and synergistic effects with temozolomide, the current chemotherapeutic agent of choice for CNS tumour therapy. Within the Sonic Hedgehog signalling pathway, expression of human Patch (Ptc) confers resistance to growth inhibition by a variety of chemotherapeutic drugs such as doxorubicin, methotrexate, temozolomide, and 5-fluorouracil (Bidet et al., 2012). Studies have also shown that the MDR phenotype can be induced when the SHH pathway is activated, and importantly SHH signalling appears to promote MDR by increasing the transcription of a subset of ABC transporter proteins (Xu et al., 2013, Das et al., 2013, Sims-Mourtada et al., 2007, Bidet et al., 2012)

Interference of HH-GLI signalling with various agents suggests that the tumorigenicity of human gliomas requires an active SHH pathway of which HH/Gli1 are critical members. But the demonstrated link between HH-Gli1 and chemoresistance is not currently fully

explained however it appears to also involve glucuronidation of drugs and alteration of MRP1 expression (Zahreddine et al., 2014, Shahi et al., 2016)

HH-GLI signalling therefore may be significant in the inherent drug resistance and biology of glioblastoma and other CNS tumours.

This chapter therefore aimed to explore whether there is a relationship between the SHH pathway and MRP1 mediated drug resistance, hypothesising that downregulation of MRP1 could result in altered expression of key genes of SHH signalling pathway. PTEN and TP53 were explored as additional key players in the biology of glioblastoma and in the T98G Glioblastoma cell line. Cells that were treated previously (see results of chapter 4) were utilised to further investigate expression pathways in the glioblastoma cell line. MRP1 mRNA expression and protein levels were reduced more than 60% and 70% respectively in these experiments. Extracted RNA was analysed for quality. qRT-PCR and RNAseq were used to explore the effect of MRP1 knock down on global glioblastoma gene expression.

5.2 Methodology:

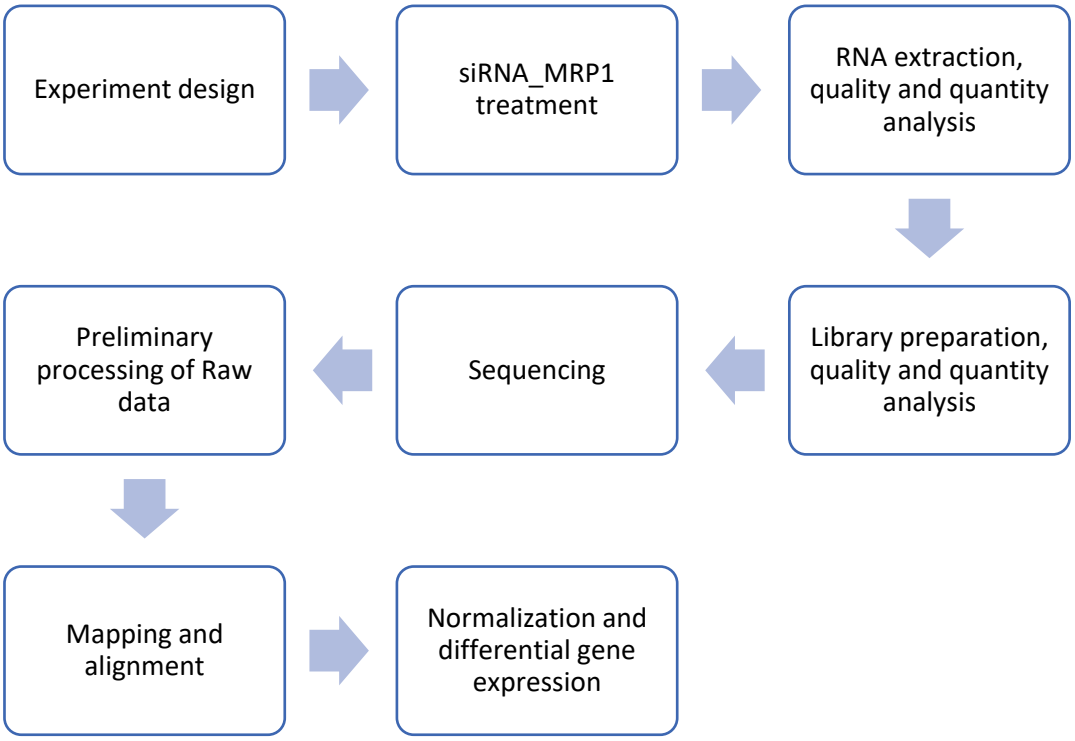

Figure 5-1 Typical RNA-seq Data analysis pipeline.

Table 5-1 Abbreviations specifically used in RNAseq assay in this chapter.

Sample abbreviation		Sample details	Experiments
M01	Un_EX1	Untreated Cell	Experiment 1
M02	NC_EX1	Negative control siRNA	
M03	MRP1_A_EX1	siRNA against MRP1 set1	
M04	MRP1_B_EX1	siRNA against MRP1 set2	
M05	Un_EX2	Untreated Cell	Experiment 2
M06	NC_EX2	Negative control siRNA	
M07	MRP1_A_EX2	siRNA against MRP1 set1	
M08	MRP1_B_EX2	siRNA against MRP1 set2	
M09	Un_EX3	Untreated Cell	Experiment 3
M10	NC_EX3	Negative control siRNA	
M11	MRP1_A_EX3	siRNA against MRP1 set1	
M12	MRP1_B_EX3	siRNA against MRP1 set2	

5.2.1 qRT-PCR assay:

SiRNA and control treated T98G cells were harvested at 48 hours (24 hours following the second transfection) for mRNA analysis by qRT-PCR, using the delta-delta method for quantification (See 2.8). Briefly, RNA was extracted using TRIzol® (see section 2.9). First strand cDNA was synthesised with a Moloney Murine Leukemia Virus (M-MLV) Reverse Transcriptase kit according to the manufacturer's protocol (see section 2.9.2). Quantitative real-time PCR using 1st strand cDNA derived from T98 cell line treated with MRP1 siRNA and controls was used to evaluate changes in expression of MRP1 and SHH key genes. Primer information is summarised in (Table 2-4). The target genes and control were performed at same time for every experimental samples. The PCR reaction mixture is described in (Table 2-5). PCR reaction plates were then placed in thermo-cyclers (iCycler Thermo-cycler, Applied Biosystems) and run according to the conditions in Table 2-6.

5.2.2 Quality and Quantity Assessments:

5.2.2.1 Total RNA Bioanalyzer Assessment:

For quality and quantity analysis of RNA, Agilent RNA 6000 Nano Kit were used for all samples according to manufacturer's protocol. Samples were run on Agilent 2100 Bioanalyzer machine.

5.2.3 Sequencing:

Following sample preparation, quantity and quality of libraries were assessed. The Bioanalyser was used to determine the final size of libraries. Sequencing samples were prepared in Flinders Genomic Facility and run at SAHMRI (South Australia Health and Medical Research Institute Ltd) Genomic Facility. NextSeq 500 platform were used. A loading concentration of 10 nM on TruSeqLT kit (Illumina) using individual 150-cycle

(paired-end 75 bp) was prepared. Paired-end reads containing both ends of the same RNA fragment were used, and the resulting raw read data was saved in two files. Data then underwent computational quality controls analysis.

5.2.4 Computational Quality:

A standard pipeline of sequencing facility, adapter trimming was performed. The sequencing reads passed the quality control requirements for analysis and a FastQC report was generated including quality analysis plots and metrics.

5.2.5 Reads Mapping

The cleaned sequence reads were then aligned against the Human Genome release 24 (https://www.gencodegenes.org/releases). The BWA aligner (v0.7.12-r1039) was used to map reads to the genomic sequences. The alignment files are sorted and compressed in BAM format. Mapping was summarised for the human genome and the known gene annotation. All the annotated features from the human gene annotation (Ensemble ftp://ftp.sanger.ac.uk/pub/gencode/Gencode_human/) were used. The uniquely mapping and non-mapping reads to the known genes have been reported.

The counts are generated based on the annotation information from the gene code using the htseq-count tool (http://htseq.readthedocs.io/en/master/count.html). The ratio of calculated RPKM (Reads Per Kilobase of transcript per Million mapped reads) values for each library and filtered low count genes is taken and transformed into log2 values to obtain fold change in expression. Due to the low number of samples further statistics could not be applied to the data.

5.3 Results:

5.3.1 Quality and Quantity Assessments:

5.3.1.1 Total RNA Bioanalyzer Assessment:

A total RNA Bioanalyzer assay was performed on all RNA samples prior to qRT-PCR and RNA. This analysis determines the fragments quality, purity and quantity of RNA samples. Ribosomal RNA (18S and 28S) was calculated. The two peaks indicate 18S and 28S ribosomal RNA are visible in

Figure 5-2. These were also detected on the generated gel seen in Figure 5-3. The calculated RIN (RNA integrity number) is 9 implying that the RNA is of high integrity seen in Figure 5-3. Thus, the RNA was determined to be pure and not containing any significant degradation.

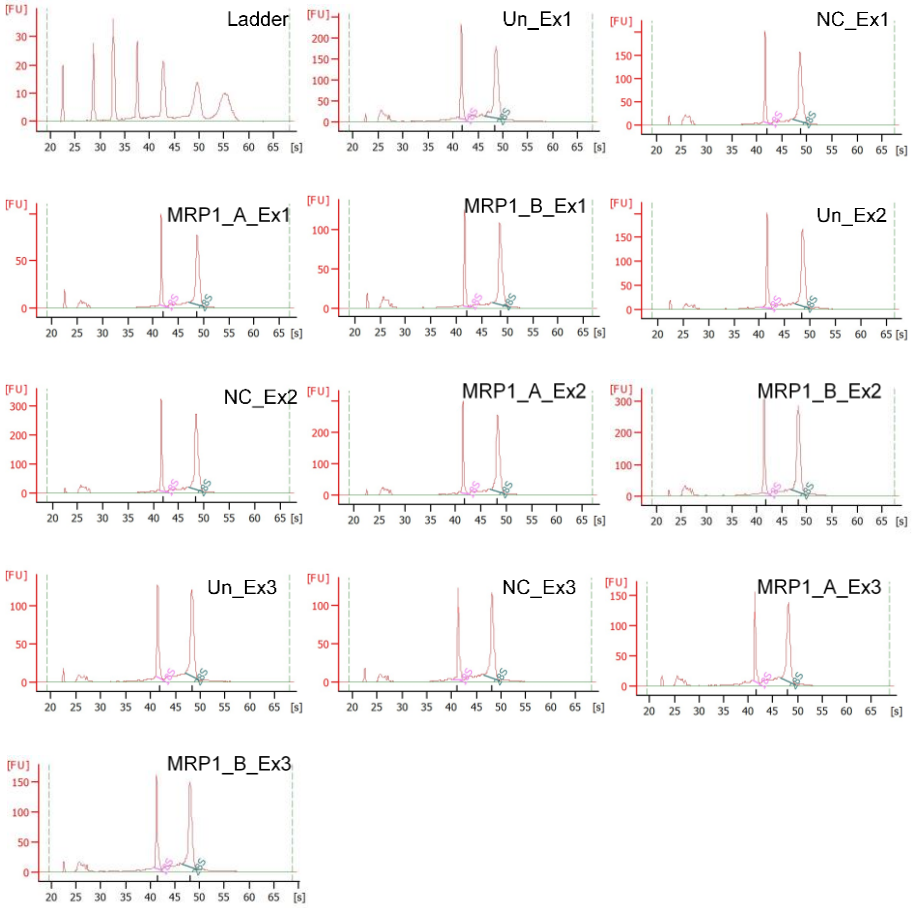

Figure 5-2 Bioanalyzer assessment of RNA integrity.

Representative of RNA integrity results after Bioanalyzer assessment. RNAs extracted from the three different biological experiments were analysed using an Agilent 2100 bioanalyzer and Agilent RNA 6000 Nano Chips. Software set on Eukaryote total RNA series II sensitivity. All samples are uncontaminated. Data indicates the 18S and 28S rRNA subunit. Samples were run on a single chip. FU stands for fluorescence units. Un; untreated cells, NC; negative control siRNA, MRP1_A; siRNA target MRP1 set A, MRP1_B; siRNA target MRP1 set B.

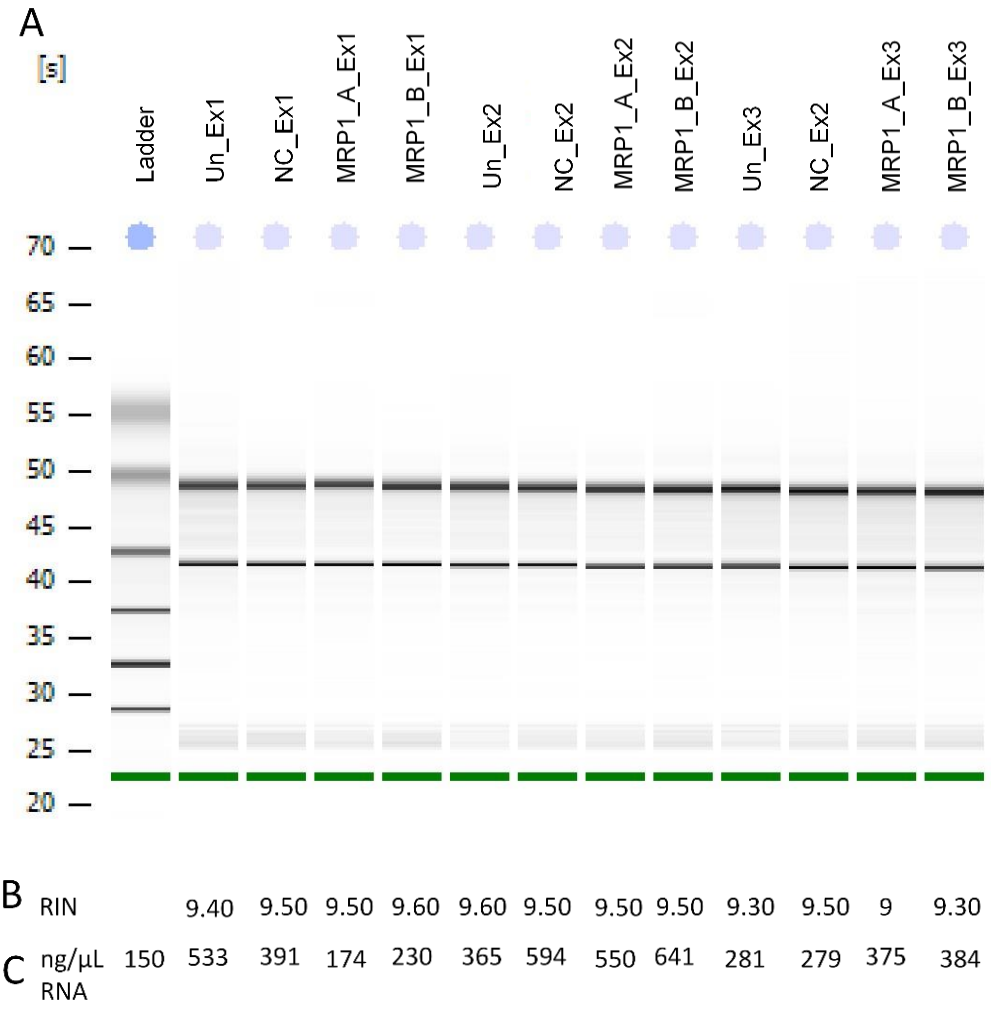

Figure 5-3 Bioanalyzer Agilent RNA 6000 gel-like image of total RNA. A) The gel image generated by the bioanalyser and present a total RNA gel-like image. B) RNA concentration and C) RNA integrity number (RIN) as determined by the Agilent Bioanalyzer. All samples showed clear 28S and 18s distinctive ribosomal RNA bands. Also, gel-like image indicated no contamination in total RNA found. In addition, RIN of samples were more than 9 which RNAseq requires and, implies there is no RNA degradation. Samples were run on a single chip. Un; untreated cells, NC; negative control siRNA, MRP1_A; siRNA target MRP1 set A, MRP1_B; siRNA target MRP1 set B. L; RNA Ladder.

5.3.2 Quantitative Real-time Polymerase Chain Reaction (qRT-PCR):

5.3.2.1 Internal Controls Validation:

RNA isolated from T98G cells treated as per Chapter 4 (section 4.2.2) The expression of three different housekeeping genes was analysed: GUSB, 18S and GAPDH. The three genes were chosen to represent a range of expression levels within the glioblastoma cell lines to cater for different levels of gene expression. The observed housekeeping gene amplification threshold (Ct) was found to be constant in all treated and control samples.

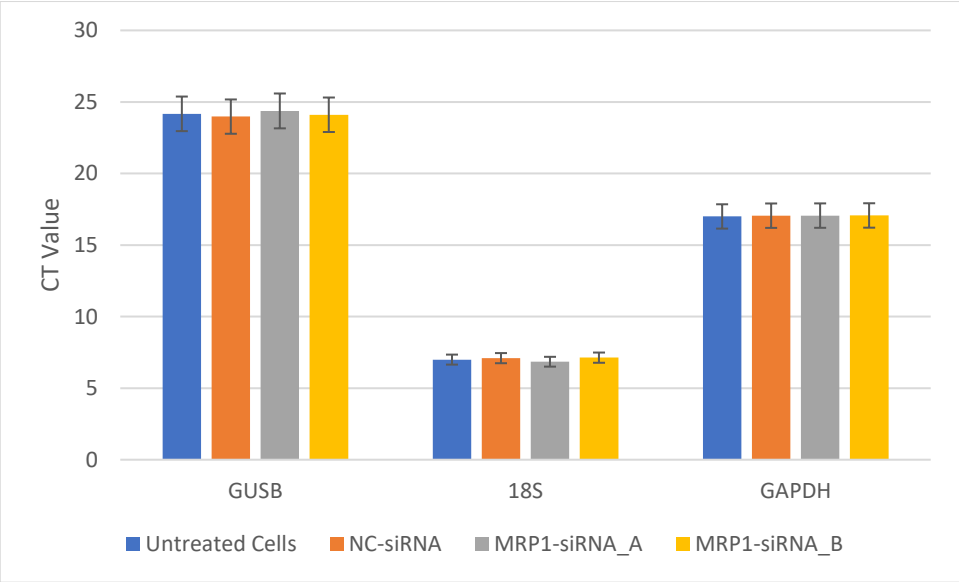

Figure 5-4 Real-time PCR CT values of reference genes. The bars represent the candidate reference genes expression level average in T98G cell transient transfected with either siRNA-MRP1 or negative control siRNA. Data shown are mean ±SD from (GUSB and 18S n=2) and GAPDH n=4 independent experiments. Housekeeping gene expression was found to be consistent and independent of the therapy applied to the cells.

5.3.2.2 Impact of MRP1 Knockdown by MRP1-siRNA on SHH Signalling Pathway Genes:

Target gene analysis. Components of SHH pathway were analysed for gene expression changes following MRP1 siRNA engineered MRP1 knockdown. Figure 5-5 shows the resultant effects expressed as relative fold change of key members of the pathway. The Ct values are also given. Gli1, Gli2, Gli3, PATCH 1 and 2, and SUFU were significantly reduced in expression in the treated cells. SMO, SHH and PTEN were not significantly altered. Interestingly, TP53 was also altered. A similar analysis was conducted on MK571 T98G treated cells. This also demonstrated a reduction in the expression of key members of the SHH pathway. In these cells, the majority have completed or very high inhibition of MRP1 as judged by Calcein retention which occurs very clearly with MK571 treatment. In these cells all genes analysed were reduced in expression but particularly Gli2 and Gli3 where expression was almost completely lost.

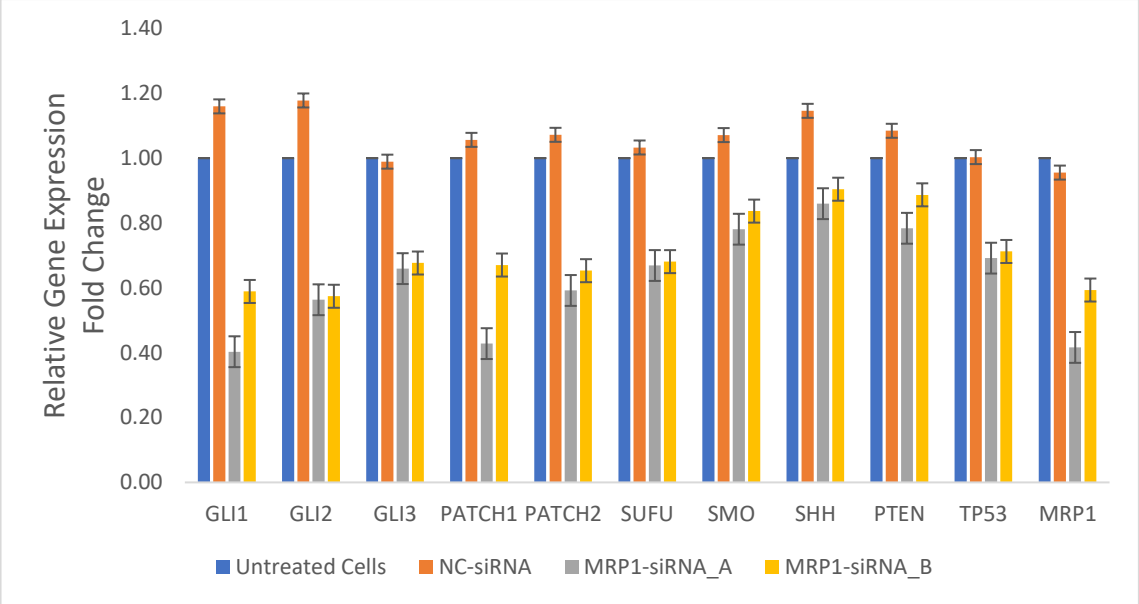

Figure 5-5 Relative qRT-PCR of MRP1, SHH key genes, PTEN, and TP53 gene expression in T98G glioblastoma cell line. Quantitative RT-PCR demonstrated changes in gene expression following MRP1 siRNA treatment of cells. RNA was isolated from T98G after 48 hours of treatment with 150 nM siRNA-MRP1 or negative control siRNA. Relative gene expression levels are displayed. Data are expressed as fold change and normalized to the GAPDH housekeeping gene. Untreated cells were used as a further control. Data shown are mean ± SD from four independent experiments.

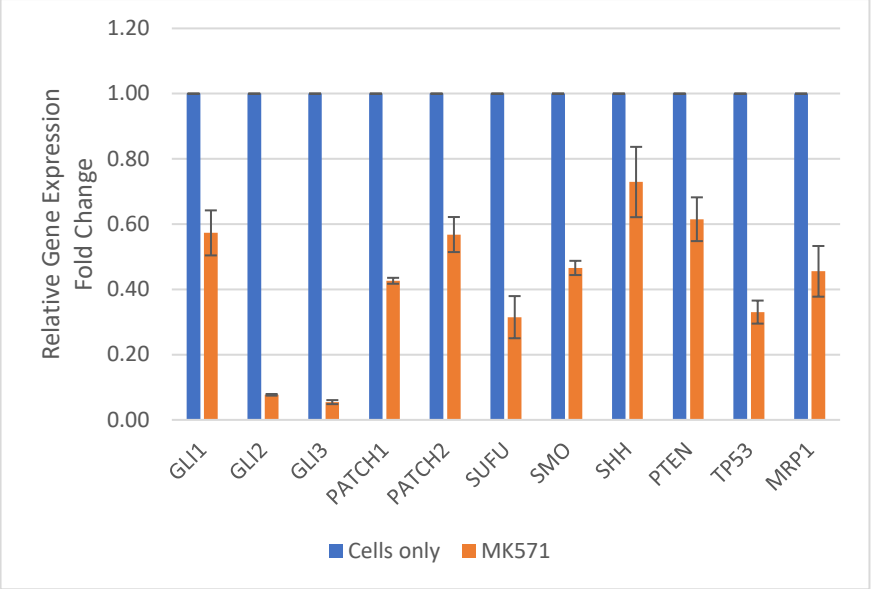

Figure 5-6 Relative QRT-PCR of MRP1, SHH key genes, PTEN, and TP53 gene expression in T98G glioblastoma cell line treated with MK-571. RNA was isolated from T98G after 48 hours of treatment with 25µM of MK-571. Relative gene expression levels are displayed. Data are expressed as fold change and normalized to the GAPDH housekeeping gene. Untreated cells were used as a further control. Data shown are mean ±SD from two independent experiments.

5.3.3 RNAseq Analysis:

5.3.3.1 NGS cDNA Library Quality and Quantity Assessment:

The LabChip assay was carried by Flinders Genomics Facility to validate the integrity and provide quantification of NGS libraries. Libraries were shown to be of good quality in this analysis (see Figure 5-7).

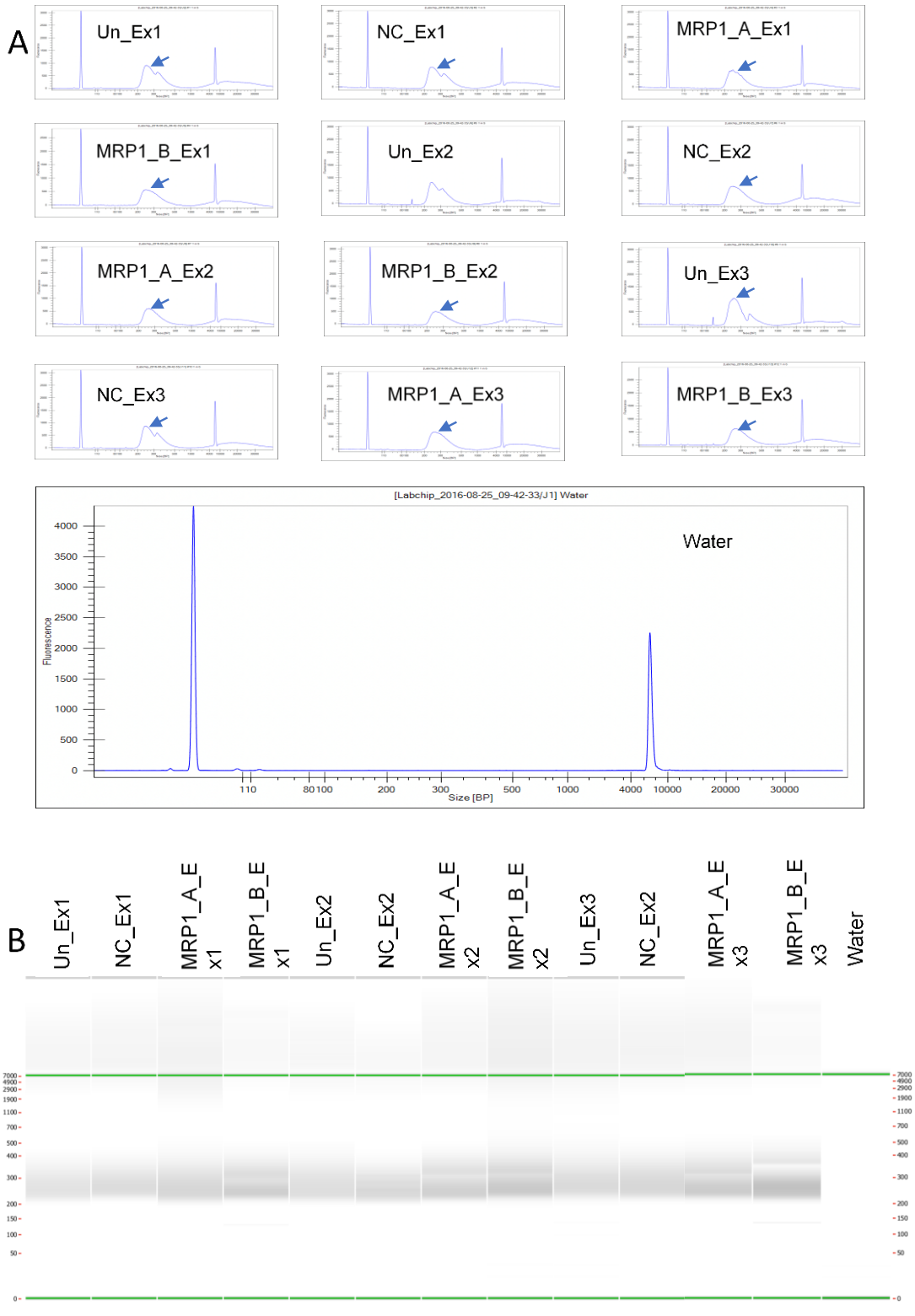

Figure 5-7 TruSeq Stranded Total RNA Sample Preparation quality and size distribution.
A) bioanalyser RNA B) electrophoresis gel of cDNA. Samples were loaded on Labchip and analysed using LabChip GX Software Version 4.2.1748.0 SP1. Samples required to be 260bp in length. Water was used as a negative control.

5.3.3.2 Quality Control and Sequence Data Evaluation:

The reads per base sequence quality for the 12 pair-end sequenced samples appeared excellent, with >96% bases above Q30 across all sample and no end trimming required. The reads were also screened for the presence of any Illumina adaptor/overrepresented sequences and cross species contamination. Adaptors were trimmed and retained a length of 35-76nt. Quality analysis plots and metrics were generated by FastQC software, which analyses the sequencing issues that are arising from library preparation and the sequencing process.

5.3.3.3 Quality Control (FastQC):

Report generated by FAstQC study different basic statistical values. Plots are of an untreated cell sample and are representative of all 12 samples. The first plot is per base sequence quality (see Figure 5-8), which studies the quality value range through all bases. The reads that sit within the green section imply a high quality, the orange represents medium quality and the red is an area of poor quality. All samples were within the green region implying high quality scores across all bases.

The next plot is the per tile sequence quality (Figure 5-8). The best quality achieved and demonstrated by this plot is when the background is clear dark blue. If there is some coloured bubble present, this implies there is a loss of sequence in the region. Our sequencing showed dark blue in all samples implying high sequence quality (Figure 5-9).

Per sequence quality scores plot is present the read quality. A good quality read is represented by a value above 27, whilst under 20 is considered to be failed sequencing. Sequencing samples in this study showed a high number of good quality reads (Figure 5-10).

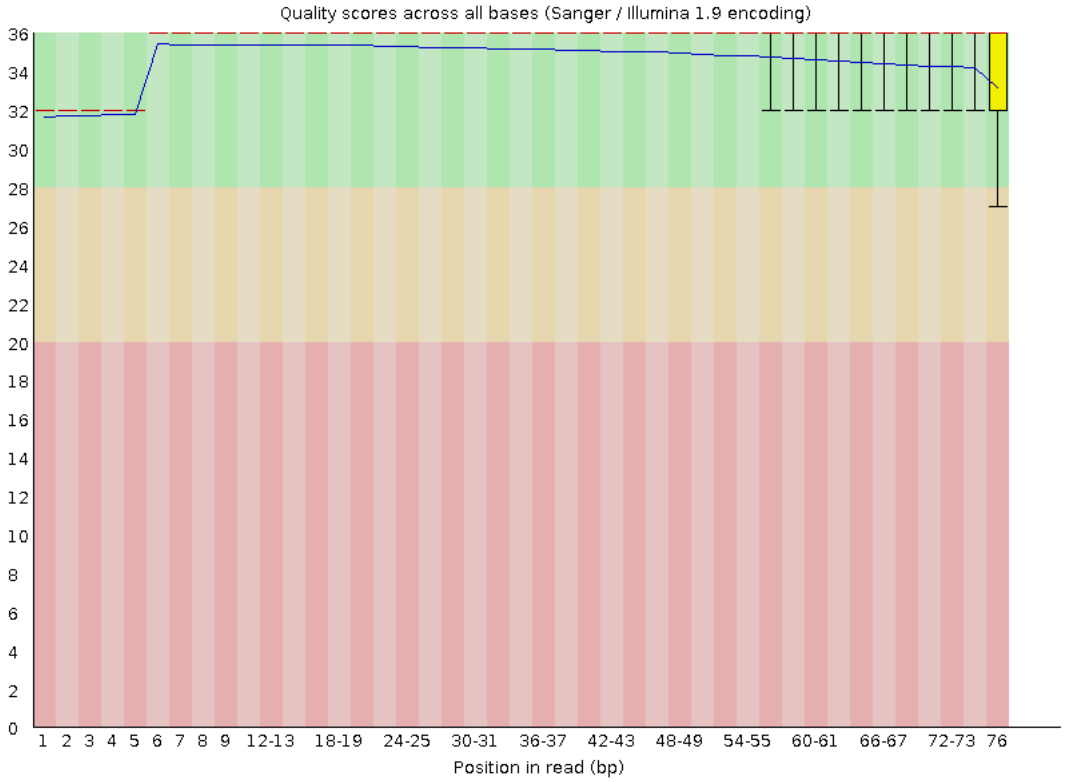

Figure 5-8 Per base sequence quality. showing the quality value range through all bases. All reads sit within the green section, implying high quality scores across the bases.

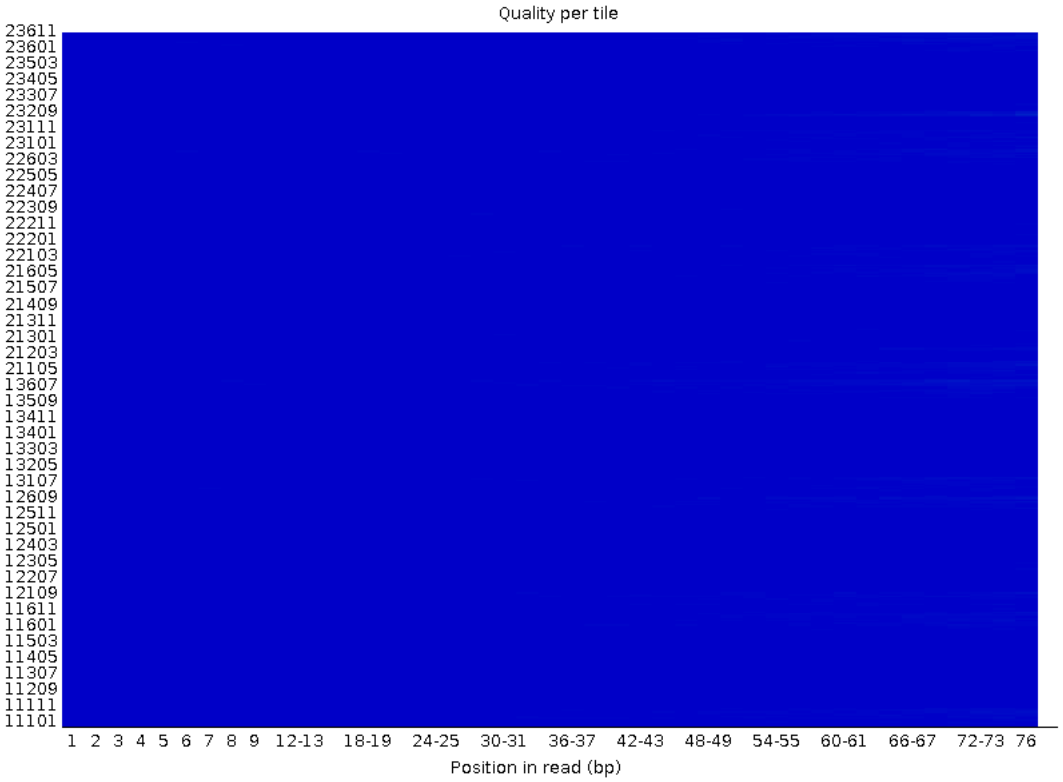

Figure 5-9 Per tile sequence quality. The best quality achieved and demonstrated by this plot is when the background is clear dark blue which was obtained from the samples submitted for sequencing.

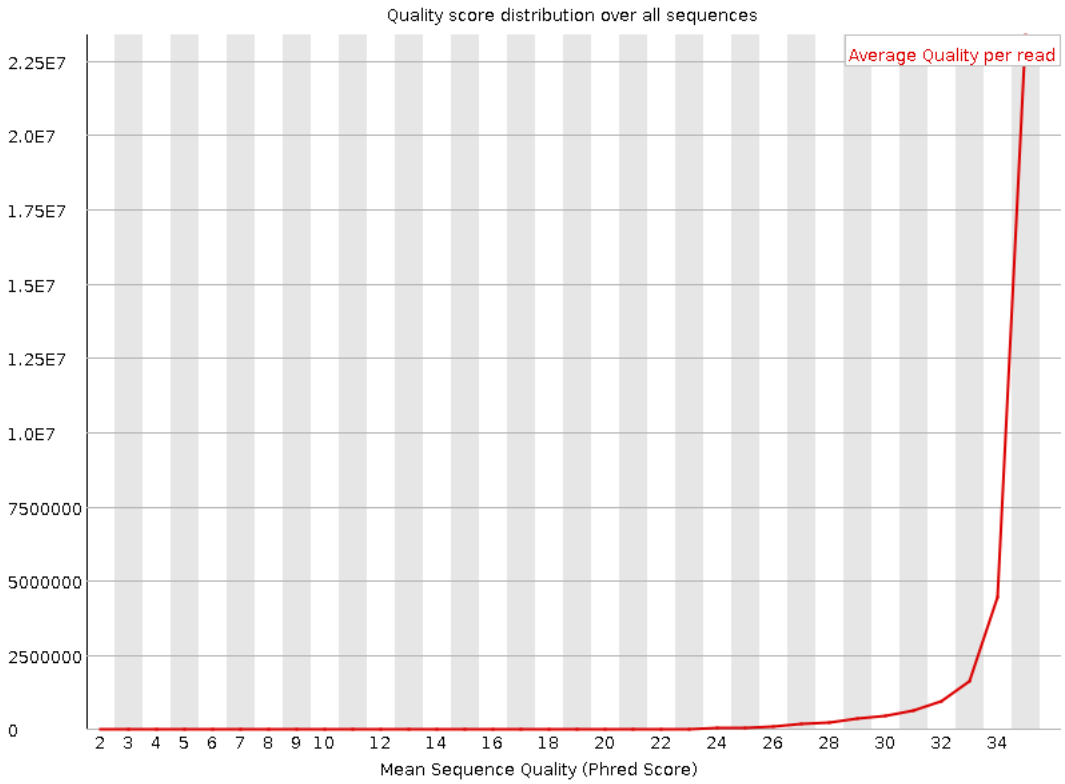

Figure 5-10 Per sequence quality scores. A good quality read is represented by a value above 27, whilst under 20 is considered to be failed sequencing. Hence all scores were of satisfactory quality.

Per base sequence content is the analysis of the AT and CG nucleotide content in the samples. Good quality sequencing should have approximately equal AT and GC content. The RNA samples showed a consistent nucleotide bias at the 5' end of the sequencing reads, which is not considered an issue as they are consistent within samples (Figure 5-11). Sometime this bias is referring to overrepresented sequence which in this case is expected to be due to long non-coding RNA.

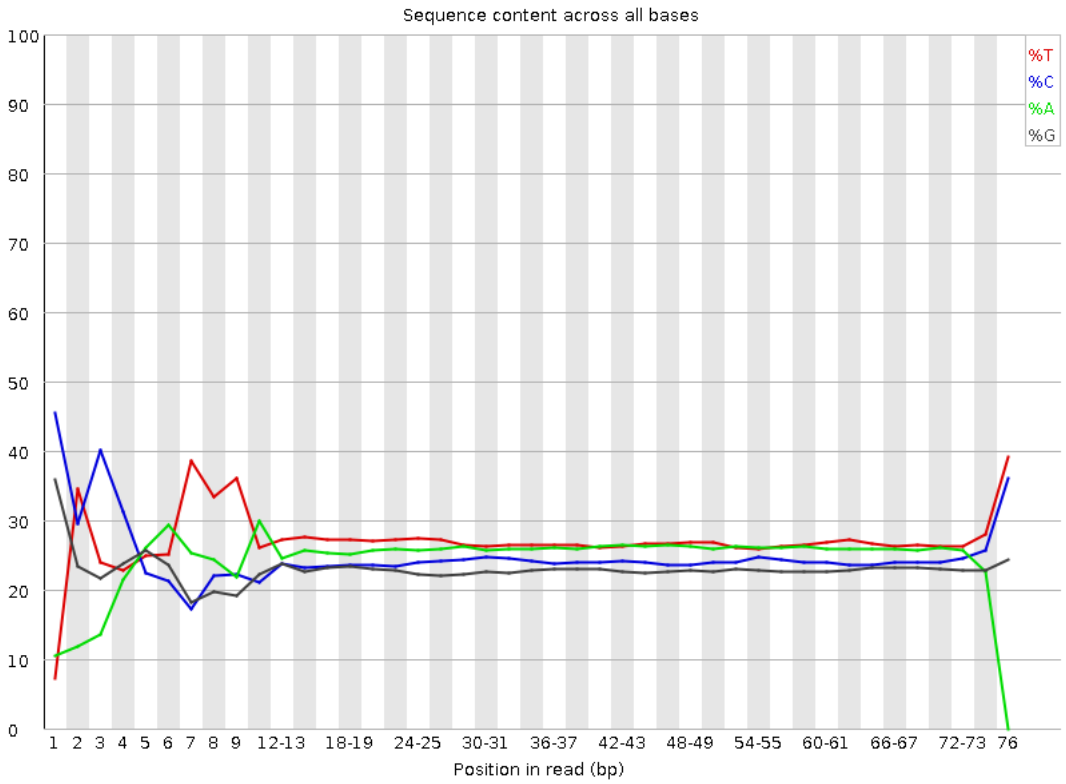

Figure 5-11 Per base sequence content: The RNA samples showed a consistent nucleotide bias at the 5' end of the sequencing reads which should not affect read quality.

The poly(A)+ data plot shows the GC content at each base position through the entire sequence. Figure 5-12 presents a normal distribution of GC content. The red peak corresponds to the overall GC content of the underlying genome. The overall GC content of the genome was calculated from the reference distribution of previous data. This plot showed that the data was of good quality.

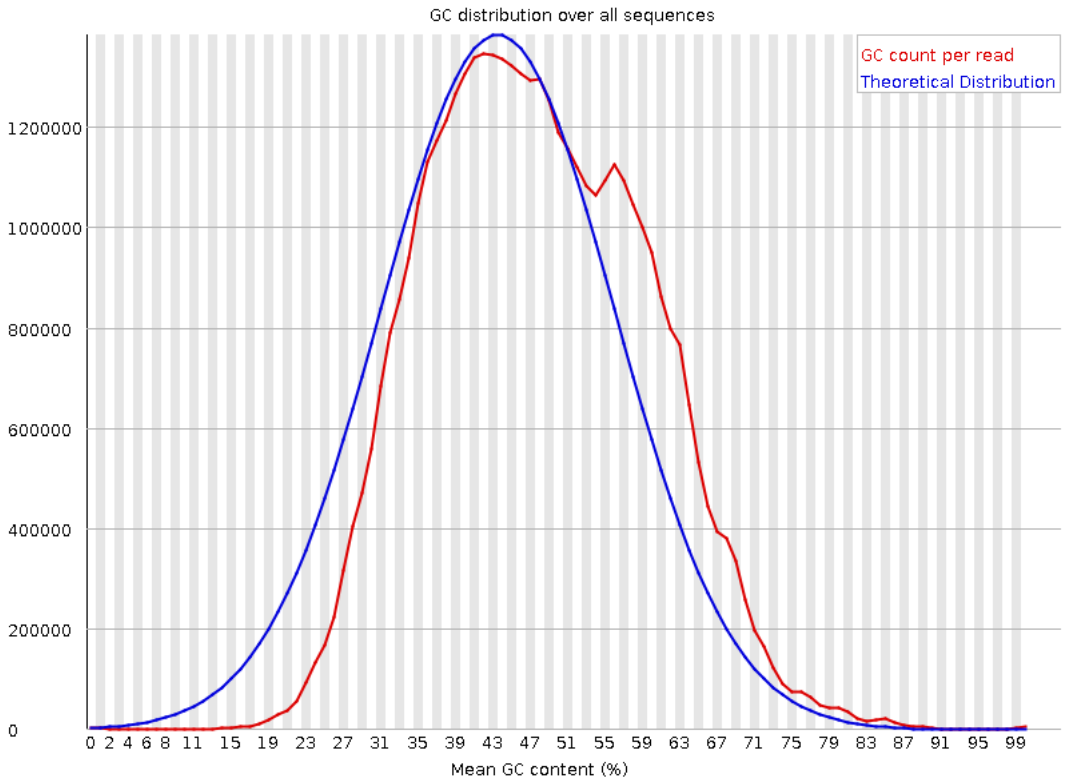

Figure 5-12 Per sequence GC content - poly(A)+ data of the actual sequence data per read compared with the theoretical distribution shows good alignment.

The next plot is the Per base N nucleotides. The sequencing machine creates an N base when it is unable to make a base call with sufficient confidence. Thus, this plot base line which shows a line at zero indicates excellent quality reads with no replacement of the bases with N content (Figure 5-13).

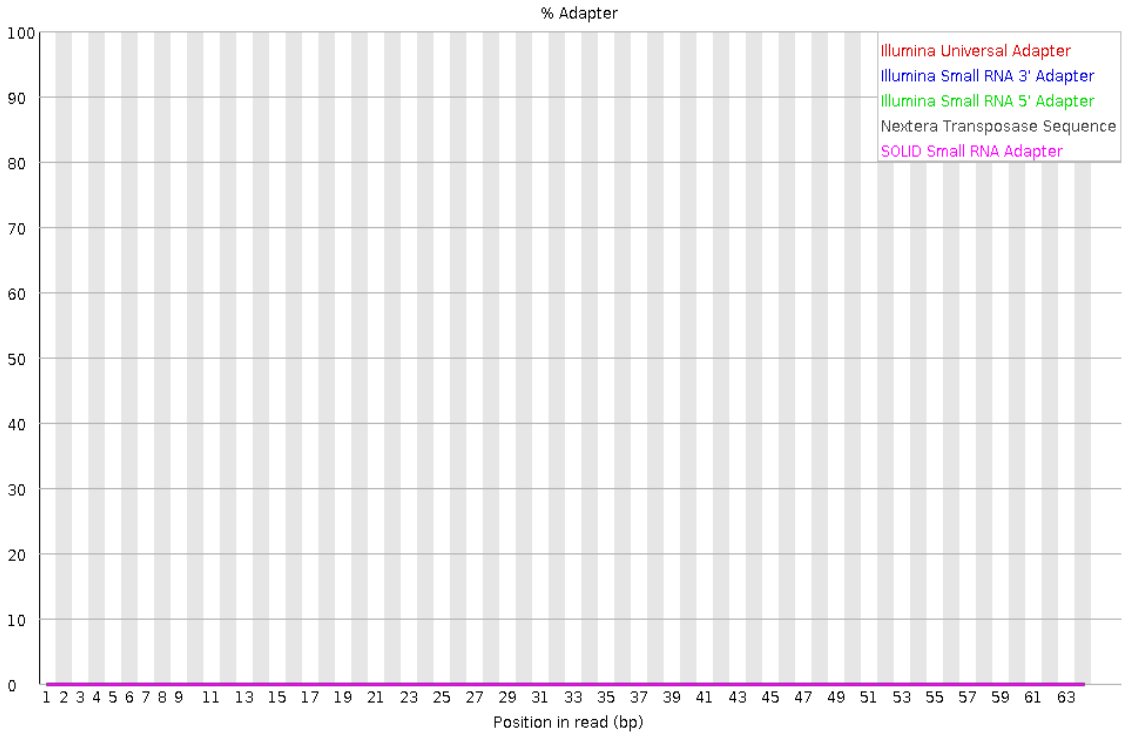

Figure 5-13 Per base N content

Sequence length distribution is useful for detecting any sequence fragments of uniform length. This uniform length is usually trimmed after the sequencing to avoid any poor-quality base calls at the end. Thus, the graph represents the fragment size distribution in the sequencing data. All sequence showed the same size which means good quality (Figure 5-14).

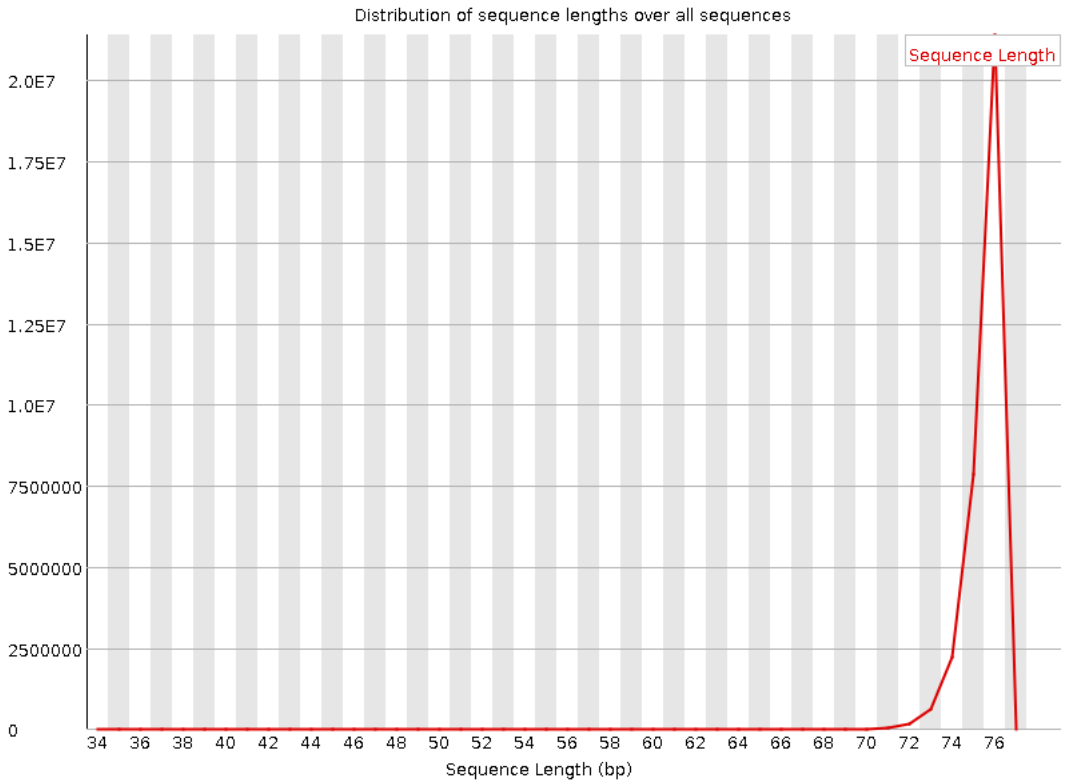

Figure 5-14 Sequence length distribution.

The final plot in FastQC is the PCR products duplication level. The lower duplication persentage means a higher target sequencing coverage. Figure 5-15 is representative of untreated cells from Experiment One. This analysis showed a low level of duplicates in the whole sequencing. A similar level of duplication was also detected in all other samples.

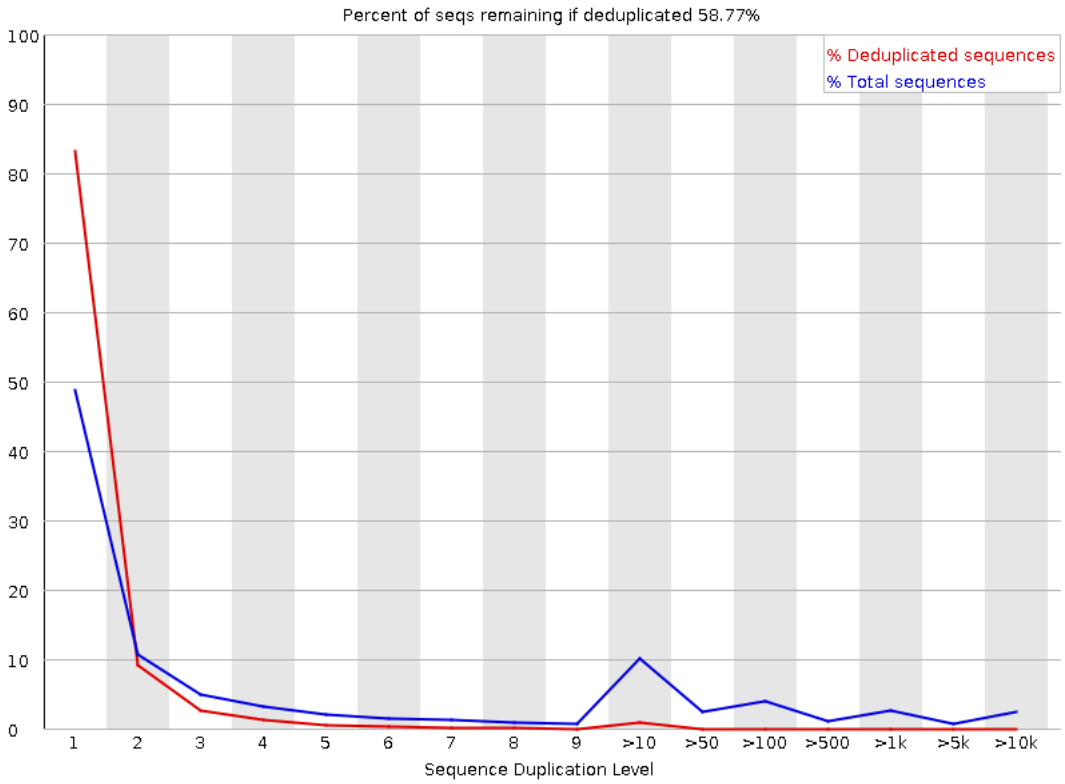

Figure 5-15 PCR products duplication level.

5.3.3.4 Principal Components Analysis:

Principal component analysis (PCA) is a statistical method to reduce a large set of variables to a small set, whilst still retaining all relevant information. Unfortunately, samples with the same treatments did not cluster together as expected. No apparent explanation has been provided by the bioinformatic analyst for this result despite all quality data being excellent and qRT-PCR providing results with apparent clustering of outcomes. Further replicates would be required to interrogate this data but were not possible due to time constraints.

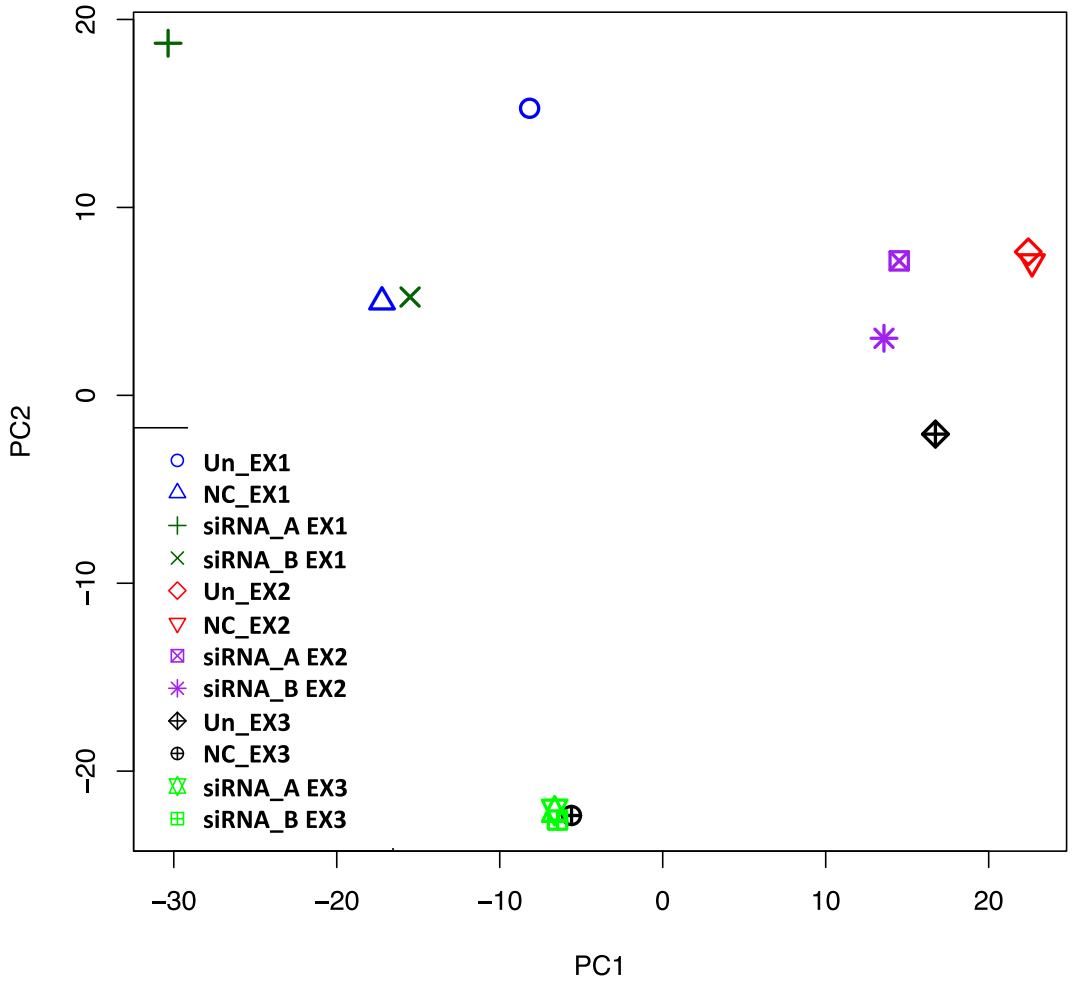

Figure 5-16 Principal components analysis of RNA-seq. Representative of three independent experiments. It expresses the relationship of samples. In this case it appears that each experiment clustered with itself rather than the treated cells clustering with similarly treated cells. No apparent explanation could be provided for this occurrence in the analysis of the data set.

5.3.3.5 Mapping

The cleaned sequence reads were then aligned against the Human Genome release 24 (https://www.gencodegenes.org/releases). The Burrows-Wheeler (BWA) aligner (v0.7.12-r1039) was used to map reads to the genomic sequences. The alignment files are sorted and compressed in BAM format. Mapping was summarised for the human genome and the known gene annotation. All the annotated features from the human gene annotation (Ensembl ftp://ftp.sanger.ac.uk/pub/gencode/Gencode_human/) were used. The uniquely mapping and non-mapping reads to the known genes have been reported. Only sample M03 showed a significant reduction in uniquely mapped reads (26.73%) compared with other samples where the mapped reads frequency varied from 77% to 85% approximately which is considered to be a satisfactory outcome.

Table 5-2 Summary of the RNAseq reads.

Sample	Total Reads	Uniquely Mapped Reads	Multi Mapped Reads	Unmapped Reads
M01	32743839	27799776 (84.90%)	4443106 (13.57%)	500957 (1.53%)
M02	35851470	29878469 (83.34%)	5340454 (14.90%)	632547 (1.76%)
M03	39380876	10525159 (26.73%)	28175675 (71.55%)	680042 (1.73%)
M04	37574999	31510239 (83.86%)	5439057 (14.48%)	625703 (1.67%)
M05	30818495	24203505 (78.54%)	5323161 (17.27%)	1291829 (4.19%)
M06	40229452	32886818 (81.75%)	6639266 (16.50%)	703368 (1.75%)
M07	38640688	30985423 (80.19%)	6991871 (18.09%)	663394 (1.72%)
M08	38131286	31915539 (83.70%)	5559695 (14.58%)	656052 (1.72%)
M09	27230390	21012661 (77.17%)	4985649 (18.31%)	1232080 (4.52%)
M10	29284521	24833260 (84.80%)	3786563 (12.93%)	664698 (2.27%)
M11	32818902	27906561 (85.03%)	4344545 (13.24%)	567796 (1.73%)
M12	35196850	29455440 (83.69%)	4823286 (13.70%)	918124 (2.61%)

Table 5-3 Summary of the Mapping statistics reads on genome

Sample	Total Reads	Mapped Reads	Unmapped reads
M01	32743839	32242882 (98.47%)	500957 (1.53%)
M02	35851470	35218923 (98.24%)	632547 (1.76%)
M03	39380876	38700834 (98.27%)	680042 (1.73%)
M04	37574999	36949296 (98.33%)	625703 (1.67%)
M05	30818495	29526666 (95.81%)	1291829 (4.19%)
M06	40229452	39526084 (98.25%)	703368 (1.75%)
M07	38640688	37977294 (98.28%)	663394 (1.72%)
M08	38131286	37475234 (98.28%)	656052 (1.72%)
M09	27230390	25998310 (95.48%)	1232080 (4.52%)
M10	29284521	28619823 (97.73%)	664698 (2.27%)
M11	32818902	32251106 (98.27%)	567796 (1.73%)
M12	35196850	34278726 (97.39%)	918124 (2.61%)

Table 5-4 shows the distribution of the reads based on human biotype genes. All samples' reads showed approximately 90-92.55% of protein coding. In addition, RNAseq analysis

identified long non-coding RNAs at various percentages throughout the samples (1.2% to 3.15%).

Table 5-4 The distribution of the reads based on human biotype genes.

Biotype	M01	M02	M03	M04	M05	M06	M07	M08	M09	M10	M11	M12
transcribed_unprocessed_pseudogene	0.15%	0.15%	0.14%	0.14%	0.16%	0.18%	0.15%	0.15%	0.14%	0.14%	0.15%	0.15%
unprocessed_pseudogene	0.05%	0.05%	0.06%	0.05%	0.05%	0.05%	0.05%	0.05%	0.05%	0.05%	0.05%	0.05%
miRNA	0.02%	0.02%	0.02%	0.02%	0.02%	0.02%	0.02%	0.01%	0.02%	0.02%	0.02%	0.02%
lincRNA	1.40%	1.29%	1.49%	1.27%	2.67%	3.15%	1.95%	1.61%	1.98%	1.59%	1.78%	1.78%
protein_coding	92.37%	91.96%	90.27%	92.12%	90.09%	90.26%	90.90%	92.25%	90.57%	92.56%	92.55%	92.57%
processed_pseudogene	2.30%	2.19%	2.02%	2.22%	2.26%	2.08%	2.27%	2.29%	2.09%	1.89%	1.83%	1.79%

antisense_RNA	processed_transcript	snRNA	transcribed_processed_pseudogene	sense_intronic	misc_RNA	TEC
0.53%	0.19%	0.10%	0.12%	0.11%	1.30%	0.10%
0.53%	0.18%	0.09%	0.12%	0.11%	1.36%	0.10%
0.52%	0.18%	0.09%	0.12%	0.10%	1.43%	0.10%
0.52%	0.20%	0.12%	0.13%	0.10%	1.30%	0.10%
0.47%	0.21%	0.11%	0.13%	0.09%	1.39%	0.08%
0.48%	0.21%	0.09%	0.13%	0.09%	1.45%	0.08%
0.58%	0.23%	0.14%	0.13%	0.11%	1.37%	0.09%
0.54%	0.23%	0.10%	0.13%	0.10%	1.56%	0.08%
0.48%	0.21%	0.12%	0.14%	0.09%	1.59%	0.08%
0.47%	0.20%	0.27%	0.13%	0.09%	0.91%	0.08%
0.50%	0.22%	0.11%	0.15%	0.09%	1.68%	0.08%
0.51%	0.22%	0.07%	0.16%	0.10%	1.09%	0.09%

transcribed_unitary_pseudogene	0.02%	0.02%	0.02%	0.02%	0.03%	0.03%	0.02%	0.02%	0.03%	0.02%	0.02%	0.02%
snoRNA	0.83%	1.09%	0.68%	1.11%	1.12%	0.91%	0.95%	0.92%	1.12%	0.99%	0.87%	0.85%
scaRNA	0.01%	0.02%	0.02%	0.02%	0.02%	0.02%	0.02%	0.02%	0.02%	0.02%	0.02%	0.02%
rRNA	0.00%	0.00%	0.01%	0.00%	0.00%	0.00%	0.00%	0.00%	0.00%	0.00%	0.00%	0.00%
unitary_pseudogene	0.00%	0.00%	0.00%	0.00%	0.00%	0.00%	0.00%	0.00%	0.00%	0.00%	0.00%	0.00%
3prime_overlapping_ncRNA	0.00%	0.00%	0.00%	0.00%	0.00%	0.00%	0.00%	0.00%	0.00%	0.00%	0.00%	0.00%
polymorphic_pseudogene	0.00%	0.00%	0.00%	0.00%	0.00%	0.00%	0.00%	0.00%	0.00%	0.00%	0.00%	0.00%

bidirectional_promoter_lncRNA	0.00%	0.00%	0.00%	0.00%	0.00%	0.00%	0.00%	0.00%	0.00%	0.00%	0.00%
sense_overlapping	0.03%	0.03%	0.02%	0.02%	0.03%	0.03%	0.03%	0.03%	0.03%	0.03%	0.03%
pseudogene	0.00%	0.00%	0.00%	0.00%	0.00%	0.00%	0.00%	0.00%	0.00%	0.00%	0.00%
IG_V_pseudogene	0.00%	0.00%	0.00%	0.00%	0.00%	0.00%	0.00%	0.00%	0.00%	0.00%	0.00%
scRNA	0.00%	0.00%	0.00%	0.00%	0.00%	0.00%	0.00%	0.00%	0.00%	0.00%	0.00%
IG_V_gene	0.00%	0.00%	0.00%	0.00%	0.00%	0.00%	0.00%	0.00%	0.00%	0.00%	0.00%
IG_C_gene	0.00%	0.00%	0.00%	0.00%	0.00%	0.00%	0.00%	0.00%	0.00%	0.00%	0.00%

IG_J_gene	0.00%	0.00%	0.00%	0.00%	0.00%	0.00%	0.00%	0.00%	0.00%	0.00%	0.00%
sRNA	0.00%	0.00%	0.00%	0.00%	0.00%	0.00%	0.00%	0.00%	0.00%	0.00%	0.00%
ribozyme	0.00%	0.00%	0.00%	0.00%	0.00%	0.00%	0.00%	0.00%	0.00%	0.00%	0.00%
translated_processed_pseudogene	0.00%	0.00%	0.00%	0.00%	0.00%	0.00%	0.00%	0.00%	0.00%	0.00%	0.00%
vaultRNA	0.00%	0.00%	0.00%	0.00%	0.00%	0.00%	0.00%	0.00%	0.00%	0.00%	0.00%
non_coding	0.00%	0.00%	0.00%	0.00%	0.00%	0.00%	0.00%	0.00%	0.00%	0.00%	0.00%
TR_C_gene	0.00%	0.00%	0.00%	0.00%	0.00%	0.00%	0.00%	0.00%	0.00%	0.00%	0.00%

TR_J_gene	0.00%	0.00%	0.00%	0.00%	0.00%	0.00%	0.00%	0.00%	0.00%	0.00%	0.00%
TR_V_gene	0.00%	0.00%	0.00%	0.00%	0.00%	0.00%	0.00%	0.00%	0.00%	0.00%	0.00%
TR_V_pseudogene	0.00%	0.00%	0.00%	0.00%	0.00%	0.00%	0.00%	0.00%	0.00%	0.00%	0.00%
TR_D_gene	0.00%	0.00%	0.00%	0.00%	0.00%	0.00%	0.00%	0.00%	0.00%	0.00%	0.00%
IG_C_pseudogene	0.00%	0.00%	0.00%	0.00%	0.00%	0.00%	0.00%	0.00%	0.00%	0.00%	0.00%
macro_lncRNA	0.00%	0.00%	0.00%	0.00%	0.00%	0.00%	0.00%	0.00%	0.00%	0.00%	0.00%
TR_J_pseudogene	0.00%	0.00%	0.00%	0.00%	0.00%	0.00%	0.00%	0.00%	0.00%	0.00%	0.00%

IG_J_pseudogene	IG_D_gene	IG_pseudogene	Mt_tRNA	Mt_rRNA
0.00%	0.00%	0.00%	0.02%	0.25%
0.00%	0.00%	0.00%	0.02%	0.17%
0.00%	0.00%	0.00%	0.02%	0.11%
0.00%	0.00%	0.00%	0.03%	1.45%
0.00%	0.00%	0.00%	0.03%	0.12%
0.00%	0.00%	0.00%	0.03%	1.07%
0.00%	0.00%	0.00%	0.03%	0.59%
0.00%	0.00%	0.00%	0.03%	0.76%
0.00%	0.00%	0.00%	0.02%	0.25%
0.00%	0.00%	0.00%	0.03%	3.04%
0.00%	0.00%	0.00%	0.02%	0.33%
0.00%	0.00%	0.00%	0.02%	0.54%

Table 5-5 raw counts (read counts for each gene)

	Experiment 1				Experiment 2				Experiment 3			
Gene Id	**M01**	**M02**	**M03**	**M04**	**M05**	**M06**	**M07**	**M08**	**M09**	**M10**	**M11**	**M12**
MRP1	334	331	55	311	376	421	283	404	366	427	419	451
GAPDH	44141	48139	15442	51619	35823	45599	60468	63558	36806	41538	43147	45293
GUSB	865	1046	329	1153	554	770	813	907	470	715	751	795
GLI1	46	50	9	45	42	59	31	48	23	31	35	35
GLI2	58	69	33	49	29	49	32	29	58	50	50	42
GLI3	560	492	264	544	483	659	620	649	568	535	621	602
PTCH1	266	312	109	307	172	240	269	253	188	218	248	277
PTCH2	45	43	25	43	56	66	76	69	85	116	127	100
SHH	1	2	0	4	0	3	1	2	1	3	6	4

SMO	762	803	192	781	1224	1567	1168	1447	953	921	1023	970
SUFU	181	177	53	146	147	206	158	169	143	123	132	110
TP53	1754	1726	501	1671	1130	1342	1544	1641	1044	1320	1297	1398
PTEN	0	0	0	0	0	0	0	0	0	0	0	0

Table 5.5 shows the raw read counts for each gene that was analysed by real time PCR prior to RNAseq analysis (Figure 5.5 and 5.6). Unfortunately the read counts did not correlate with the real time PCR data, and therefore it was deemed that this data was not reliable for identifying global downstream gene expression changes in response to *MRP1* knockdo

5.4 Discussion:

To study the gene expression changes in SHH signalling pathway, qRT-PCR was chosen as representing the most sensitive and quantitatively accurate assay. Gene specific primers were designed to amplify RNA sequences and following RT-PCR, the resultant products were analysed by melting curve and gel electrophoresis to confirm the singularity of the product and the lack of non-specific products arising.

Housekeeping genes used in normalising the qRT-PCR results of the target genes were relatively constant and not influenced by treatment in all experiments. Different housekeeping genes with different levels of expression were used to avoid skewed results as studies have shown some housekeeping genes cannot be generally used as a suitable endogenous control for quantification assays. However, all 3 housekeeping genes showed consistent CT values (Węglarz et al., 2006, Blanquicett et al., 2002, Thellin et al., 1999). The Lemma group studied 15 housekeeping genes, with GAPDH showing the most stable result compared to 18S and GUSB in their analysis. However, in our cell line model all genes showed consistent values (Lemma et al., 2016).

It is acknowledged that the siRNA induced knock-down of MRP1 was incomplete (60%) However, despite this MRP1 knockdown showed variant reduction in SHH signalling pathway key genes. GLI1, GLI2, PATCH 1 and PATCH 2 showed more than 40% reduction in mRNA expression (p values < 0.001). In addition, GLI3 and SUFU mRNA expression reduced by 30% (p values <0.03). However, SMO and SHH were reduced by less than 20% and this was not significant (p values < 0.01). TP53 expression appeared to be affected by the inhibition of MRP1 and was downregulated by 30% (p values < 0.022) while PTEN

is showing approximately 15% downregulation but did not reach significance (p values = 0.43).

These findings are novel and have not been previously reported in the literature. However, other interesting associations between the SHH pathway and ABC transporters have been found. HhAntag691 (vismodegib) is a small molecular inhibitor of the SHH signalling pathway through inhibition of SMO. It was discovered by high throughput screening of a library of small molecule compounds and then optimised through medicinal chemistry. Its chemical formulation is as follows: 2-chloro-N-(4-chloro-3-(pyridin-2-yl) phenyl)-4-(methylsulfonyl) benzamide = $C_{19}H_{14}Cl_2N_2O_3S$. HhAntag691 has been demonstrated to be around 10-times more potent than cyclopamine (another known inhibitor of the SHH pathway) and has been used to treat medulloblastoma in animal models. It was employed in clinical trials for a variety of solid tumours (Zhang et al., 2009, Su and Pasternak, 2013) and more recently as an inhibitor in Basal Cell Carcinoma with the original data being published in 2015 with follow up in 2018 and 2019 as neoadjuvant therapy in this disease (Koelblinger and Lang, 2018, Woltsche et al., 2019). Additionally, there are reports with this inhibitor documenting the role of SHH pathway in embryonic palatal development and its role in cleft palate (Abramyan, 2019). Other *in vivo* studies have also demonstrated GLI1 inhibition and SHH signalling pathway deregulation when this inhibitor is used (Romer et al., 2004). Interestingly, HhAntag691 is also a potent inhibitor of two ABC transporters, ABCG2/BCRP and ABCB1/Pgp, and is a mild inhibitor of ABCC1/MRP1. Several studies go on to report that it also successfully inhibited MRP1 activity which is expressed highly at the blood brain barrier in their experiments (Romer et al., 2004, Gabay et al., 2003). However, no studies using an siRNA

approach targeting SHH pathway members have demonstrated a reduction in MRP1 expression and therefore it is likely that MRP1 inhibition by this molecule is the direct effect of binding to MRP1. This fact is not made clear in the publications discussing HhAntag691 leaving open to speculation the exact mechanism of action. No recent studies in cancer therapeutics are reported.

Thus, the downregulation of the key genes of SHH signalling pathway and TP53 due to the transient transfection with MRP1-siRNA suggests that critical cellular pathways could be affected by knocking down MRP1. This is further supported by the finding that MK571 inhibition of MRP1 also results in SHH pathway member downregulation. The broad range of molecules transported by MRP1 including lipids and cell signalling regulators make it possible that these effects are part of a cell signalling pathway disruption following MRP1 functional loss. To better understand the magnitude of gene expression changes occurring after MRP1 downregulation RNAseq analysis was attempted.

RNA samples from the same experiments were analysed using the Bioanalyzer to validate the quality of RNA. As demonstrated above, all samples showed good quality RNA (represented by a RIN score greater than 9). RNAseq libraries were prepared and assessed by the LabCHIP assay, demonstrating clean libraries which should have provided satisfactory data for the RNAseq assay (Langmead et al., 2009, Sultan et al., 2014). RNAseq data was trimmed and FastQC report was generated. The FastQC report presented a good quality read integrity and sequencing. However, Principal Component Analysis (PCA) showed un-clustering of samples even though they were treated the same way and the same cell line model was used for all experiments (T98G cell line).

Sequencing of the samples yielded 27 to 40 million reads with good quality coverage of the reads being gained (77-85%) of the uniquely mapped reads except for one sample treated with MRP1-siRNA_A in experiment 1 (M03) which only provided 26% uniquely mapping reads and 71% of multi-mapped reads (Dobin et al., 2013). The multi-mapped reads of all other samples were approximately 13-18%. Cleaned sequence reads were aligned to the reference human genome (Langmead et al., 2009). The coverage was high with 97-98%. The protein coding coverage was 90-92.55% for all samples. In addition, a low percentage of long non-coding RNA and processed pseudogenes were also detected.

However, to evaluate gene expression, we commenced by comparing housekeeping genes (GAPDH and GUSB) in all samples and discovered that these housekeeping genes were inconsistent throughout the experimental samples by this methodology. Additionally, other genes such as MRP1, which we had previously demonstrated to be downregulated in the siRNA treated samples by qRT-PCR failed to show a similar downregulation by RNAseq. In addition, the images generated specifically for exons (2, 7, 17 and 28) of the MRP1 (ABCC1) gene for each experiment were interrogated for expected read loss surrounding the exons targeted by siRNAs A and B. For the exons, 17 and 28 there was complete knockdown in all the experiments but this included the non-treated controls. In comparison, for exons 2 and 7 variable knockdown is observed. This irregularity also extended to a complete absence of mapped reads for the exons 17 and 28 and relatively low numbers of mapped reads to exons 2 and 7 (See appendix A). Thus, the detailed analysis of housekeeping genes and MRP1 gene expression failed to demonstrate a consistent interpretable result meaning that analysis of other gene

expression would be meaningless. Therefore, the sequence data obtained did not meet the requirements for further analysis despite high QC analysis of the respective samples.

Despite several attempts to interrogate the data with bio-informatician assistance this aspect of the thesis was unable to be completed. Additional approaches including proteomics and potentially lipidomics may further assist in understanding the changes that have been seen and could be the foundation for future studies. The results of the transciptome analysis were clearly disappointing, however the fact remains that there appears to be an interdependence of SHH signalling pathway members and MRP1 function which warrants further investigation and that this association is not due to non-specific siRNA knockdown effects as functional inhibition also results in reduced expression of the SHH pathway members.

6 FINAL CONCLUSION:

From the literature review, we found that GBM clinical treatment continues to remain a challenge worldwide, which is disappointing as it accounts for 75% of gliomas. Poor prognosis is a result of chemo-resistance and difficulties or delays in diagnosis. Micro-neurosurgery in combination with radio-, chemo-immunotherapies and adjuvant chemotherapy with temozolomide (TMZ) are the gold standard treatment for GBM (Saran et al., 2016). However, survival rates remain dismal, with less than 4% of glioblastoma patients surviving for five years.

The first results chapter, Chapter 3, highlighted the effects of inhibition MRP1 using two different sets of siRNA and MK-571 (inhibitor of MRP1 and other transporters) on the cellular biology of a GBM cell line. Results demonstrating the reduction of mRNA (40 and 60%) and protein levels (70%) were associated with increasing Calcein AM cellular accumulation, validating the effect of two doses of siRNA causing downregulation of the protein with a resultant reduction in function. While Calcein accumulation is not specific for MRP1 function, the siRNA knockdown was specific for MRP1, therefore changes in calcein AM accumulation are representative of a loss in MRP1 protein in these experiments. The use of a functional inhibitor of MRP1, MK-571 also resulted in similar findings of Calcein accumulation, and attenuated cell growth without evidence of affecting protein expression. This functional inhibition is however less specific for MRP1 inhibition and this needs to be taken in to account when interpreting the results. Additionally, Calcein changes do not predict for inhibition of all drugs and substances transported by MRP1 which need to be substantiated by cytotoxic studies, as present in the literature.

Interestingly, T98G cell line growth was reduced with slight increase in apoptosis at the 48-hour time point, but with no increase in cell death over a 96-hour period. However, demonstration of an increase in S and G2 cell cycle phase is consistent with a G2 arrest in treated samples which may explain the cell proliferation results. As MRP1 is a transporter of intracellular substances, one can only hypothesise that it is involved in the transport of key elements in GBM proliferation. These findings remain to be replicated in different GBM cell lines and if possible, primary cell lines from patients.

The second results chapter of this thesis (Chapter 4) sought to explore a possible delivery system for siRNA that may ultimately be utilised in a clinical setting. A PEI-pSiNP siRNA delivery system was effectively synthesised and applied to an *in vitro* and *in vivo* model. This delivery system maintained and prolonged the effectiveness of siRNA and rapidly delivered siRNA directly into the GBM cells. In addition, MRP1 silencing effected by employing PEI-pSiNP delivery of siRNA alone resulted in a reduction of cell proliferation rate of GBM cells without cytotoxic drug co-treatment, indicating that MRP1 expression has a more fundamental role in the biology of GBM cells than simply a xenobiotic transporter. Additionally, in terms of transfection efficiency PEI-pSiNP compared favourably to lipofectamine transfection without significant toxic effects apparent either *in vitro* or in vivo. Since the effect of siRNA subsides over time mainly due to the dilution of intracellular siRNA (Bartlett and Davis, 2006), the proliferation attenuation effect associated with MRP1 silencing would be transient. Slow sustained nanoparticle delivery of siRNA may assist in prolongation of the cellular effects. This needs to be explored further in association with radiotherapy and or chemotherapy in an orthoptic model such as the Sprague Dawley rat brain tumour model (Connolly et al., 2017, Yang et al., 2018).

In this thesis, MRP1 knockdown in a GBM cell line was demonstrated in vivo in a xenografted mouse model, and the proliferation attenuation was also observed in the tumour, highlighting the potential utility of MRP1 as a therapeutic intervention in the future. This is envisaged to be possible by installation of the nanoparticles to the tumour bed after tumour resection and immediately prior to chemo or radiotherapy. A direct delivery system to the tumour bed would avoid systemic exposure to the siRNA. However, in the limited experimental tissues investigated there was no end organ damage in the mouse despite downregulation of MRP1 in the duodenum and kidney. A more thorough investigation of systemic effects would need to be undertaken in any subsequent animal models. The long-term effect of repeated exposure to MRP1 downregulation systemically is unknown.

During the study of qRT-PCR of MRP1 mRNA expression, SHH signalling pathway key genes (GLI1, GLI2, PATCH 1 and PATCH 2) were investigated to assist in the explanation of the cell proliferation events. These were initially planned as a second target for siRNA downregulation in this thesis. Unexpectedly SHH pathway members demonstrated a similar reduction to MRP1 mRNA expression in the siRNA experiments. This has not previously been reported. Thus, the present study provides novel evidence for a significant inhibition of SHH signalling pathway genes by targeting MRP1. These studies will need to be repeated using additional cell lines and further explored in global expression changes.

SHH signalling pathway contributes to chemo- and radio-resistance (Sims-Mourtada et al., 2006). However, there are some agents and herbs were used to target MRP1 and SHH, such as HhAntag691 and Curcumin. (Meng et al., 2017, Shanmugam et al., 2015).

Studies demonstrated that SHH Hedgehog signalling pathway key genes of GLI1, SMO, and Sufu protein expression were facilitated by Curcumin treatment in a pancreatic cancer cell line and Glioma (Yin et al., 2018, Cao et al., 2016). Interestingly, it also inhibits MRP1 expression, involving the glutathione and GSTs conjugation mechanism required for MRP1 transport although these effects are likely to be non-specific (Chearwae et al., 2006, Wortelboer et al., 2003).

The connection between SHH and MRP1 remain to be explained. The original aim of the thesis was to explore more broadly the effects of MRP1 downregulation on gene expression in GBM cell lines however this work must now be taken up in future studies. Given the wide array of substances transported by MRP1 it is likely that gene expression may be changed by transport of regulatory molecules by MRP1. However, from this work it is evident that the multidrug resistance phenotype of glioblastoma cells is enhanced by a relationship of the SHH pathway genes and MRP1 expression and that this warrants further investigation. Thus, the MRP1 siRNA drug delivery system explored in this thesis provides an avenue of drug delivery to GBM sufferers which may improve drug sensitivity in glioblastoma but may also change fundamental biology of the tumours through regulation of key factors including the SHH pathway members and others yet unknown.

APPENDIX A: IGV SNAPSHOT OF MRP1 EXONS:

Experiment one:

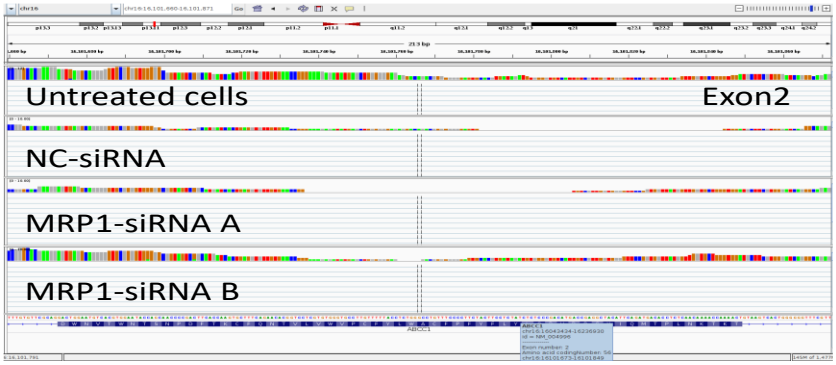

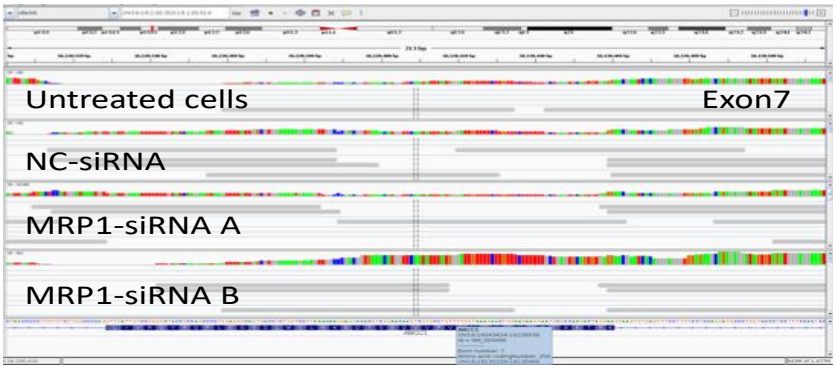

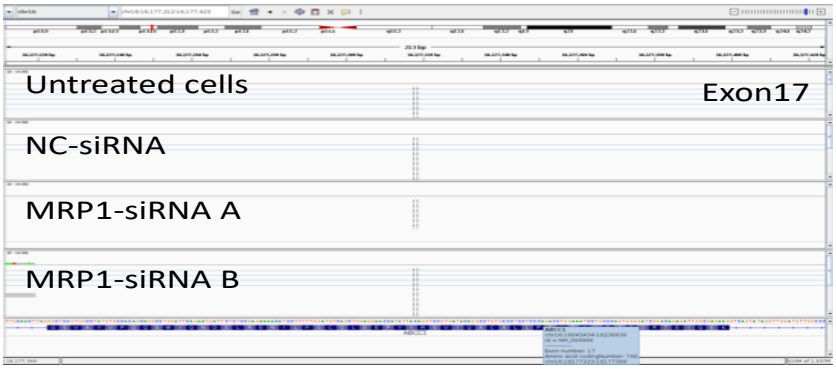

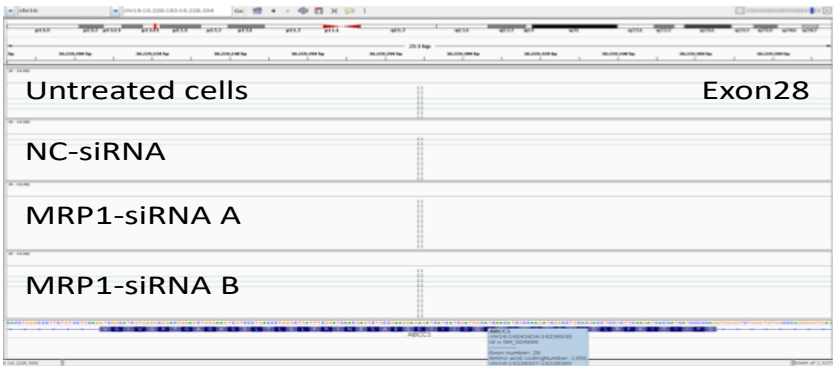

Experiment two:

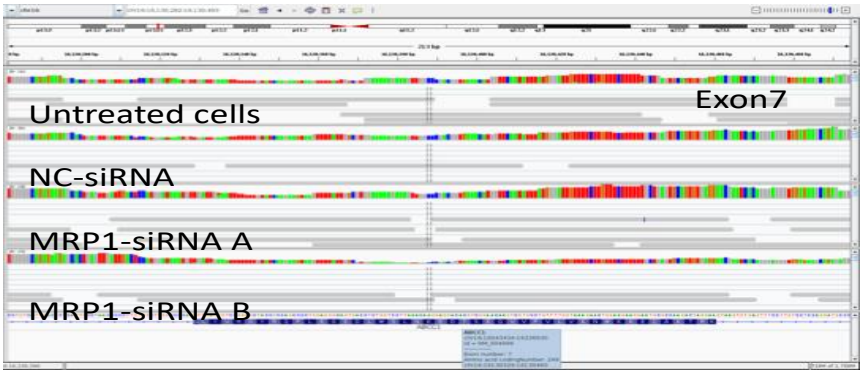

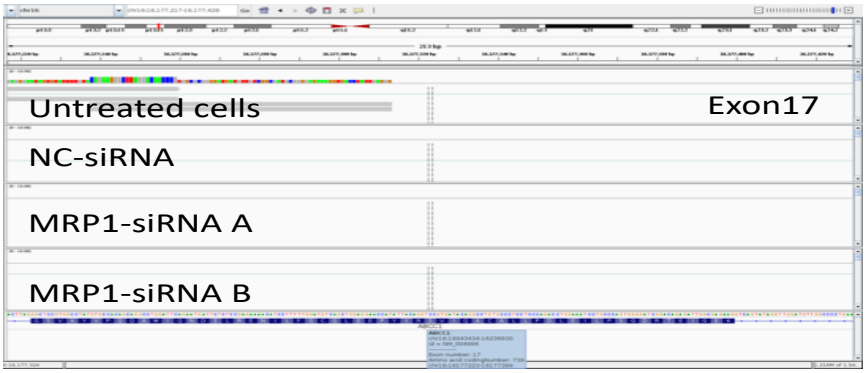

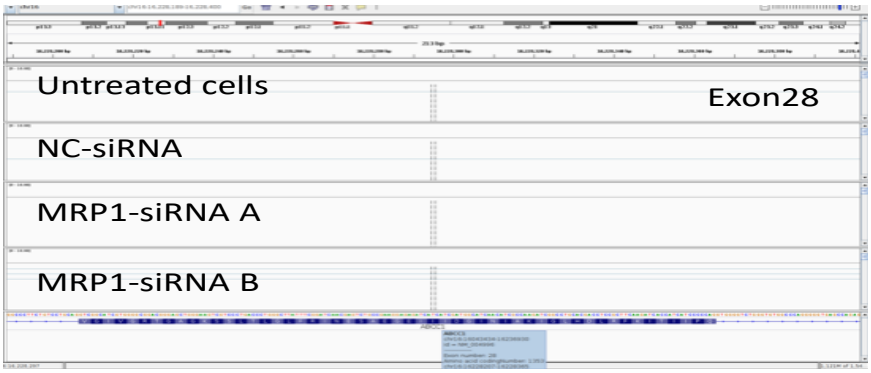

Experiment three:

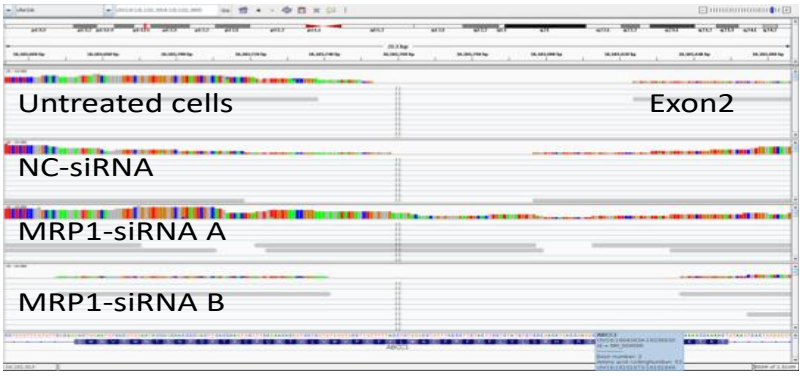

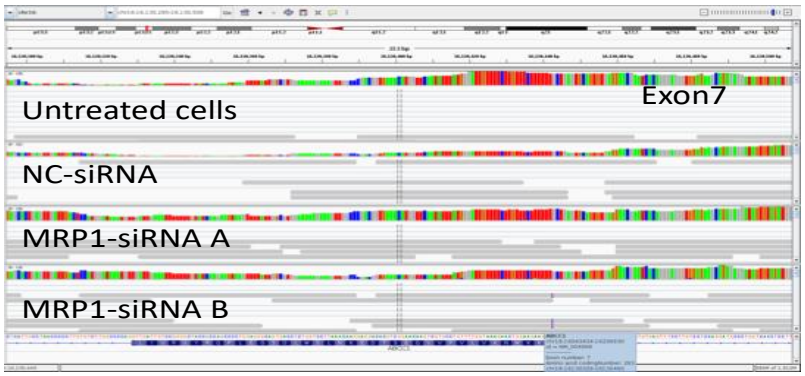

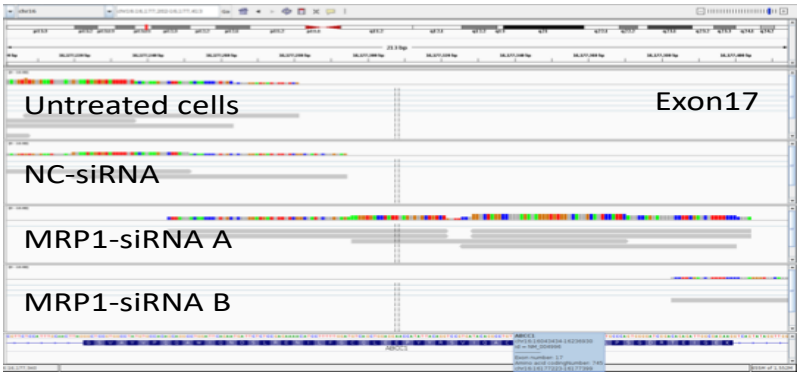

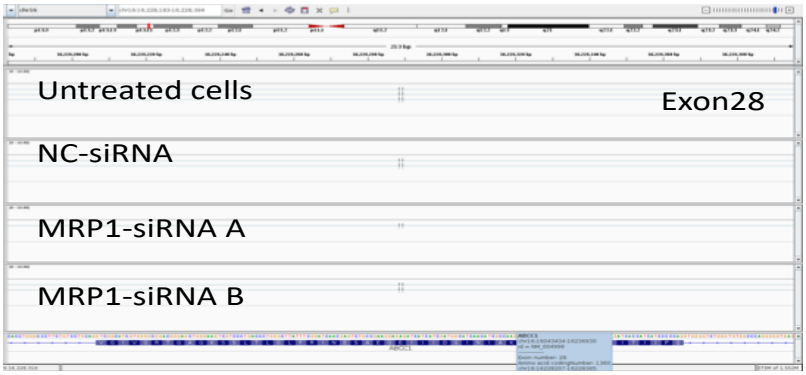

APPENDIX B: PUBLICATION DURING CANDIDATURE

Kafshgari, M.H., Alnakhli, M., Delalat, B., Apostolou, S., Harding, F.J., Mäkilä, E., Salonen, J.J., Kuss, B.J. and Voelcker, N.H., 2015. *Small interfering RNA delivery by polyethylenimine-functionalised porous silicon nanoparticles. Biomaterials Science*, 3(12), pp.1555-1565.

Tong, WY, **Alnakhli, M**, Bhardwaj, R, Apostolou, S, Sinha, S, Fraser, C, Kuchel, T, Kuss, B & Voelcker, NH 2018, *Delivery of siRNA in vitro and in vivo using PEI-capped porous silicon nanoparticles to silence MRP1 and inhibit proliferation in glioblastoma*. Journal of Nanobiotechnology, 16(Węglarz et al.), p. 38.

Biomaterials Science

PAPER

View Article Online
View Journal | View Issue

Cite this: *Biomater. Sci.*, 2015, **3**, 1555

Small interfering RNA delivery by polyethylenimine-functionalised porous silicon nanoparticles†

M. Hasanzadeh Kafshgari,‡[a] M. Alnakhli,‡[b] B. Delalat,[a] S. Apostolou,[b] F. J. Harding,[a] E. Mäkilä,[c] J. J. Salonen,[c] B. J. Kuss[b] and N. H. Voelcker*[a]

Received 24th June 2015,
Accepted 14th August 2015

DOI: 10.1039/c5bm00204d

www.rsc.org/biomaterialsscience

In this study, thermally hydrocarbonised porous silicon nanoparticles (THCpSiNPs) capped with polyethylenimine (PEI) were fabricated, and their potential for small interfering RNA (siRNA) delivery was investigated in an *in vitro* glioblastoma model. PEI coating following siRNA loading enhanced the sustained release of siRNA, and suppressed burst release effects. The positively-charged surface improved the internalisation of the nanoparticles across the cell membrane. THCpSiNP-mediated siRNA delivery reduced mRNA expression of the MRP1 gene, linked to the resistence of glioblastoma to chemotherapy, by 63% and reduced MRP1-protein levels by 70%. MRP1 siRNA loaded nanoparticles did not induce cytotoxicity in glioblastoma cells, but markedly reduced cell proliferation. In summary, the results demonstrated that non-cytotoxic cationic THCpSiNPs are promising vehicles for therapeutic siRNA delivery.

Introduction

Glioblastoma multiforme (GBM) is an aggressive brain tumour with a poor clinical prognosis.[1–4] Malignant glioblastoma cells divide rapidly because the tumour is surrounded by a well-developed blood supply network.[5] Multimodal treatment, consisting of surgical resection, local radiotherapy and systemic chemotherapy, is the standard therapy for GBM.[2,6] Surgery can remove up to 95% of the GBM tumours; however, a major obstacle to treatment of this cancer is overexpression of the multidrug resistance associated protein 1 (MRP1) which reduces the susceptibility of GBM tumours to chemotherapy.[7–11] As a result, GBM treatment employs intensive chemotherapy regimens which induce systemic toxicity and associated side effects.[1,12,13]

Exogenously delivered siRNA can silence the MRP1 gene and facilitate diffusion of hydrophobic chemotherapeutic molecules (*e.g.* camptothecin and doxorubicin) across the lipid bilayer of the cell membrane.[8,14] The administration of naked siRNA increases treatment efficacy for some cancers.[15,16] However, the negatively charged naked siRNA is subject to poor cellular uptake as well as intracellular degradation because of endogenous enzymes in the cytoplasm.[17] Therefore, to facilitate the transfection of siRNA in a clinical setting, non-viral vectors have been used to treat cancer cells. The delivery of siRNAs to GBM tumour cells using nanoparticles (NPs) has been demonstrated to protect siRNAs from nucleases and promote sustained release of the siRNA.[5,18,19]

Porous silicon (pSi) is an increasingly popular biomaterial for use in therapeutic agent delivery.[20,21] SiNPs are biodegradable and undergo complete degradation to produce silicic acid ($Si(OH)_4$), a non-toxic soluble form of silicon.[20,22] Moreover, the fabrication of pSiNPs from bulk single crystal silicon wafers by means of electrochemical anodisation in hydrofluoric acid (HF) produces a nanostructured material with a surface area of up to 800 $m^2\ g^{-1}$.[23] The structural tunability of pSiNPs allowing macroporous (>50 nm), mesoporous (5–50 nm), and microporous (<5 nm) pores to be created, affords an opportunity for the loading and controlled release of a wide range of different therapeutic agents, such as anticancer drugs, oligonucleotides and high molecular weight proteins.[22,24,25]

Adsorption of siRNA and oligonucleotides to the pSiNP surface is mediated by electrostatic interactions.[26,27] Suitable particle surface functionalisation facilitates electrostatically driven nucleotide loading.[20,21,28,29] For example, siRNA loading into oxidised pSiNPs could be improved 10-fold by amine-modification of the pSiNPs.[21] Alternatively, other pSi nanostructures, including nanowires and mesoporous microparticles, have been successfully used to deliver functional

[a]*ARC Centre of Excellence in Convergent Bio-Nano Science and Technology, Mawson Institute, University of South Australia, GPO Box 2471, Adelaide SA 5001, Australia. E-mail: nico.voelcker@unisa.edu.au*
[b]*School of Medicine, Flinders University, Bedford Park, Adelaide, SA 5042, Australia*
[c]*Department of Physics and Astronomy, University of Turku, FI-20014 Turku, Finland*

†Electronic supplementary information (ESI) available: SEM and TEM images, IRS study, batch adsorption capacity, adsorption kinetics, human plasma protein adsorption (effects on average hydrodynamic diameter of the NPs), cell proliferation assay, cell apoptosis by annexin V analysis and cellular uptake (Z-stack confocal microscopy). See DOI: 10.1039/c5bm00204d

‡These authors contributed equally to this work.

siRNA into cancer cells.[30,31] We recently succeeded in increasing adsorption of oligonucleotides into thermally hydrocarbonised porous silicon nanoparticles (THCpSiNPs) even further (to the level of 17 μg mg^{-1}) by exploiting the surface properties and porous structure of the NP.[29]

In contrast to the rapid degradation of freshly prepared pSiNPs in aqueous solutions (within minutes), which accelerates the release of loaded oligonucleotides, thermal hydrocarbonisation of pSiNPs post-fabrication produces a stable Si–C layer on the pSi surface.[29] As a result, release of peptides, oligonucleotides and hydrophobic model drugs from THCpSiNPs is sustained, *in vitro* and *in vivo*.[24,25] Capping NP pores after loading with positively charged polymers such as polyethylenimine (PEI) further extends release and also promotes the cellular uptake of negatively charged siRNA.[26,32]

The endosomal escape of siRNA-loaded nanocarriers is crucial to silencing the target gene.[33,34] The pH-responsiveness of PEI also aids endosomal escape of pSiNPs *via* the proton sponge effect,[35] allowing the oligonucleotide payload to reach its cytoplasmic target. Recently, an siRNA delivery model using mesoporous silica NPs (MSNs) coated with PEI demonstrated the downregulation of green fluorescent protein gene expression.[26] However, the well-documented cytotoxicity of MSNs due to the disruption of mitochondrial membranes and generation of reactive oxygen species (ROS) is a major limitation for their use.[36–39] pSiNPs do not show this level of toxicity *in vitro* and *in vivo*.[40] PEI facilitated cellular accumulation and internalisation of pSiNPs has been shown to accelerate the apoptosis of solid tumours.[41] Although post-fabrications such as amine and oxidised modifications on the surface of pSiNPs may induce inflammation, such toxicity can be eliminated through the final polymeric coating.[29,42,43]

Here, we investigated the loading of siRNA targeted to MRP1-mRNA and its release from THCpSiNPs with and without PEI coating. Cell viability and cellular uptake, *in vitro*, of the treated cells were also examined using confocal microscopy and transmission electron microscopy (TEM). The ability of siRNA-loaded THCpSiNPs to mediate the silencing of the MRP1 gene and protein was then assessed in the T98G glioblastoma cell line.

Experimental

Materials

Ethanol (EtOH), PEI (MW: 25 kDa), 1-decene, phosphate buffered saline (PBS), human plasma serum, dodecenylsuccinic anhydride (DDSA), Araldite® 502 epoxy resin, Embed812 resin (procure 812), tris-2,3,6-(dimethylaminomethyl)phenol (DMP-30), osmium tetroxide solution (for electron microscopy, 4% in H_2O), sucrose and uranyl acetate were obtained from Sigma-Aldrich (St. Louis, MO, USA). Silicon wafers (p+ type, 0.01–0.02 Ω cm) and hydrofluoric acid (HF, 38%) were obtained from Siegert Consulting Co. (Aachen, Germany) and Merck (Darmstadt, Germany), respectively. Cellulose membrane dialysis tube (Mw cut-off 50 kDa; flat width 10 mm; diameter 6.4 mm, Spectra/Por Biotech-Grade CE dialysis tubing) was purchased from Cole-Parmer (Chicago, IL, USA). All oligonucleotides used are shown in Table 1. The Block-iT™ Fluorescent oligo, a fluorescein-labelled double-stranded RNA duplex (16.1 kDa), is designed as a detection tool for siRNA internalization (Invitrogen, Mulgrave, VIC, Australia). DMEM culture medium, Opti-MEM culture medium, fetal bovine serum (FBS), L-glutamine, penicillin, streptomycin, amphotericin B, Hoechst 33342, Annexin V/FITC, Alexa Fluor® 488 conjugate, Annexin binding buffer (5×), sheep anti-Mouse Ig (R-phycoerythrin (PE) conjugated F (ab′) secondary antibody), trypsin (0.05%, EDTA 0.53 mM) and Lipofectamine® RNAiMAX transfection reagent were also purchased from Invitrogen (Carlsbad, CA, USA). Sterile 0.01 M PBS (pH 7.4), Triton X-100, propidium iodide (PI), phalloidin-TRITC were also obtained from Sigma-Aldrich. Paraformaldehyde solution 4% v/v was obtained from Electron Microscopy Science, Ft Washington, MD, USA. Fluoro-gel mounting medium was purchased from ProSciTech, Kirwan, Qld, Australia. The BD Cytofix/Cytoperm™ kit was obtained from BD Biosciences (San Jose, CA, USA). MRP1 antibody (QCRL-1) was purchased from Santa Cruz Biotechnology, Inc. (Dallas, TX, USA). All solutions were prepared using ultra purified water supplied by a Milli-Q system (Millipore, Billerica, MA, USA). T98G GBM cell line (ATCC® CRL-1690™) from the American Type Culture Collection (Manassas, VA, USA) was used in the experiments. Incubation of cells with all samples took place at 37 °C unless otherwise stated.

Fabrication of THCpSiNPs

p+ Type (0.01–0.02 Ω cm) silicon wafers were used to fabricate pSiNPs by periodically etching at 50 mA cm^{-2} (2.2 s period) and 200 mA cm^{-2} (0.35 s period) in an aqueous 1 : 1 HF (38%) : EtOH electrolyte for a total etching time of 20 min. The pSi films were detached from the silicon substrate by increasing the current density to electropolishing conditions (250 mA cm^{-2}, 3 s period). In order to stabilise freshly etched hydride

Table 1 Sequence of oligonucleotides used in this study

Oligonucleotide ID		Sequence	Company
2′-Fluoro modified ABCC1 siRNA (siRNA)	Sense	5′→GAGGCUUUGAUCGUCAAGUTT→3′	GenePharma, Shanghai, China
	Antisense	5′→ACUUGACGAUCAAAGCCUCTT→3′	
Negative control siRNA (NC-siRNA)	Sense	5′→UUCUCCGAACGUGUCACGUTT→3′	
	Antisense	5′→ACGUGACACGUUCGGAGAATT→3′	
Block-iT™	—	FITC labeled oligonucleotide	Invitrogen

terminated pSi membranes, the detached multilayer films were thermally hydrocarbonised under N_2/acetylene (1 : 1) flow at 500 °C for 15 min, and then cooled down to room temperature under a stream of N_2 gas. Films were subsequently converted to THCpSiNPs using wet ball-milling with a ZrO_2 grinding jar (Pulverisette 7, Fritsch GmbH, Idar-Oberstein, Germany) in 1-decene. THCpSiNPs were harvested by centrifugation (1500*g*, 5 min).

siRNA loading

To load Block-iT™ (40 μL of 322 μg mL^{-1} in water) and siRNA (25 μL of 500 μg mL^{-1} in water) into the THCpSiNPs (0.1 mg mL^{-1}, 250 μL, suspended in EtOH) for the cellular uptake and reverse transcription polymerase chain reaction (RT-PCR) experiments, the particles were dispersed by sonication for 1 min, then incubated at 5 °C overnight. Following incubation, the supernatant was separated from NPs by centrifugation (5000 rpm, 5 min) and the THCpSiNPs with the loaded siRNA (siRNA/THCpSiNPs) or the loaded Block-iT™ (Block-iT™/THCpSiNPs) were collected. The amount of absorbed oligonucleotide was measured by UV-Vis spectrophotometry (HP8453, Agilent Technologies, Santa Clara, CA, USA) at 260 nm from three replicates.

The concentration of oligonucleotide in the supernatant was subtracted from the initial concentration of oligonucleotide in the loading solution. The amount of oligonucleotides absorbed onto the pSiNPs, P (mg mg^{-1}) was calculated using the following equation:

$$P = \frac{V(C_0 - C)}{W_D} \quad (1)$$

where V (mL) is volume of the oligonucleotide solution. C_0 and C (μg mL^{-1}) are the initial oligonucleotide concentration and the oligonucleotide concentration at the measurement time, respectively. W_D (mg) is the weight of the pSiNPs.

All siRNA loading processes were performed in a biosafety cabinet (Aura 2000, Microprocessor Automatic Control, Firenze, Italy) to keep the NPs sterile for subsequent cell uptake studies.

PEI coating of siRNA/THCpSiNPs

To coat siRNA/THCpSiNPs with PEI (PEI/siRNA/THCpSiNPs), the sterile siRNA/THCpSiNPs (0.1 mg mL^{-1}) were dispersed by 1 min sonication into PEI solutions (250 μL) of concentrations 0.05 and 0.1 and 0.2% w/v. Coating was performed at pH 5.7, above the IEP (= 5.2) of siRNA/THCpSiNPs but below the pK_a of PEI (= 9.08 (ref. 44)). The pSiNP suspension was incubated at 5 °C for 20 min, and then centrifuged at 5000 rpm at 5 °C for 5 min to collect the coated NPs. After removing the supernatant containing the unconjugated PEI, the amount of siRNA released during the coating process was measured using UV-Vis spectrophotometry at 260 nm to determine the final amount of loaded siRNA into the NPs. The sterile PEI/siRNA/THCpSiNPs were kept at 5 °C until use in siRNA release and cell uptake studies. The mean particle size and size distribution of the prepared PEI/siRNA/THCpSiNPs were determined by DLS and scanning electron microscopy (SEM). The surface charge after PEI coating was determined from zeta potential measurements. The same procedure was carried out for the PEI coating of the Block-iT™/THCpSiNPs (PEI/Block-iT™/THCpSiNPs). All PEI coating processes were carried out in the bio-safety cabinet to keep the NPs sterile for future cell uptake studies.

Nitrogen sorption measurements

The pore volume, average pore diameter, and specific surface area of THCpSiNPs were calculated from nitrogen sorption measurements performed using a Tristar 3000 porosimeter (Micromeritics Inc., Norcross, GA, USA).

Dynamic light scattering and zeta potential

Mean hydrodynamic diameter of NPs, size distribution along with the polydispersity index (PDI) and surface zeta (ζ)-potential of NPs were determined by dynamic light scattering (DLS) using a Zetasizer Nano ZS (Malvern, Worcestershire, UK). A scattering angle of 90° and a temperature of 25 °C was used with NPs dispersed in Milli-Q water.

Scanning electron microscopy (SEM)

Images of THCpSiNPs and PEI-coated siRNA/THCpSiNPs (PEI/siRNA/THCpSiNPs) were acquired on a SEM (Crossbeam 540, Carl Zeiss AG, Oberkochen, Germany) by collecting the back-scattered electrons (0.7 kV beam energy under high vacuum 2×10^{-4} Pa). The samples were prepared by allowing a single drop of nanoparticle suspension to dry overnight at room temperature on a thin layer graphite attached to a standard SEM holder by double-sided carbon tape.

siRNA release experiments

To study release kinetics, the prepared siRNA/THCpSiNPs and PEI/siRNA/THCpSiNPs (coated with PEI solution at concentrations 0.05, 0.1 and 0.2% w/v) were suspended at 0.1 mg mL^{-1} in PBS (100 μL). The solution was transferred into a cellulose membrane dialysis "bag" (to avoid NP interference in UV absorbance measurements) fitted inside of a quartz cuvette (3 mL) filled with PBS and maintained at 37 ± 0.5 °C. The amount of oligonucleotide released was measured using the UV/Vis spectrophotometry every 5 min for 35 h. All release experiments were conducted in triplicate. siRNA release data was fitted to a Higuchi model. The simplified Higuchi's model (eqn (2)) describes the drug release from an insoluble matrix of THCpSiNPs as a square root of a time-dependent process linked to the Fickian diffusion.[45,46]

$$Q = K_H \times t^{0.5} \quad (2)$$

where Q is the cumulative release drug in time t, K_H (h$^{-0.5}$) is a dissolution constant and t is time (h). The critical release parameter K_H was calculated for each release experiment independently. Differences in K_H were analyzed using one-way

ANOVA, followed by Tukey HSD *post hoc* tests (Kaleidagragh software, Synergy).

Confocal microscopy

T98G cells were seeded onto flat-bottomed 24-well tissue culture plates (Thermo Fisher Scientific Inc., SA, Australia) at a density of 3×10^4 cells per cm^2 in DMEM supplemented with 10% v/v FBS, 2 mM L-glutamine, 100 U per mL penicillin, 100 μg per mL streptomycin and cultured in a 37 °C, 5% CO_2 humidified atmosphere for 24 h prior to incubation with NPs. Cells were grown to 80% confluence before exposure to NPs. After 24 h, the medium was removed and cells were exposed to Opti-MEM culture medium supplemented with 5% (v/v) FBS containing 0.1 mg mL^{-1} of PEI/Block-iT™/THCpSiNPs at 37 °C, 5% CO_2 as specified above. The cell culture medium did not contain antibiotics. Controls (untreated cells) were generated by incubating T98G GBM cells in Opti-MEM without NPs for an identical time period. Following incubation (24 h), the cells were washed with PBS to remove the non-internalised NPs. Subsequently, the cells were fixed in 4% paraformaldehyde solution for 30 min, then permeablised with 0.25% Triton X-100 for 5 min at room temperature. The nuclei of cells were stained with 2 μg mL^{-1} Hoechst 33342 for 15 min at room temperature. Cells were also stained with 100 μM phalloidin-TRITC for 45 min. After washing with PBS, cells were mounted with Fluoro-gel mounting reagent. Cells were imaged using a Nikon A1 laser scanning confocal microscope (Nikon Inc., Rhodes, NSW, Australia) equipped with the appropriate filters. The efficiency of cellular uptake of NPs was assessed by counting the number of cells that exhibited green fluorescence (from the Block-iT™), together with the total number of cells present.

TEM of cells

Cellular uptake was illustrated by means of TEM imaging as described previously.[29] Briefly, cellulose membrane dialysis tubes were placed into a 24-well plate, then T98G cells were seeded at a density of 3×10^4 cells per cm^2 for 24 h in DMEM supplemented (see section confocal microscopy). After incubation, the medium was removed and cells were exposed to Opti-MEM culture medium supplemented with 5% v/v FBS containing 0.1 mg mL^{-1} of PEI/siRNA/THCpSiNPs for 24 h at 37 °C, 5% CO_2. For control experiments, medium without the NPs was used. After incubation, T98G cells cultured on the cellulose membrane were fixed using 4% paraformaldehyde with 4% sucrose in 0.1 M PBS (pH 7.2) overnight. Aqueous osmium tetroxide solution (2.0% w/v) was added to the fixed cells before dehydrating cells by exposure to a series of ethanol/water mixtures (70% to 100% ethanol with 5% step increases). The dehydrated cells were embedded in absolute ethanol and resin mixture (Araldite 502, procure 812, D.D.S.A., DMP-30) (1 : 1) then incubated in pure resin mixture. The cells were transferred to embedding moulds containing fresh pure resin mixture, which was then polymerised for 24 h at 70 °C. Samples were cut with a diamond knife (sectioned of 60–100 nm thickness) and placed on a 200-mesh copper grid ProSciTech Co., Thuringowa, Qld, Australia). The cells placed on the grids were stained with uranyl acetate for 15 min, and rinsed with de-ionised water, subsequently stained with lead citrate for 3–5 min, and then rinsed with de-ionised water. The samples were imaged on a Tecnai™ Spirit Philips TEM (Hillsboro, OR, USA) at 20–120 kV beam energy under high vacuum (1×10^{-5} Pa).

Cell viability and proliferation

In vitro cellular toxicity and proliferation of T98G GBM cells treated with PEI/siRNA/THCpSiNPs were evaluated using Annexin V assay and Trypan Blue exclusion assay. The cells were seeded onto 6-well plates at a density of 3×10^5 cells per cm^2 and maintained in DMEM supplemented (see section confocal microscopy). The cultured cells were incubated with prepared sterilised PEI/siRNA/THCpSiNPs or control treatments [(a) unmodified THCpSiNPs, (b) PEI coated THCpSiNPs loaded with NC-siRNA (PEI/NC-siRNA/THCpSiNPs), (c) PEI coated THCpSiNPs without an siRNA payload (PEI/THCpSiNPs), (d) treatment with each single component of PEI/siRNA/THCpSiNPs *i.e.* uncomplexed PEI, siRNA, non-coated THCpSiNPs (PEI + siRNA + THCpSiNPs, separately added), and (e) siRNA complexed with lipofectamine (siRNA/lipofectamine)] and untreated cells at a concentration of 0.1 mg mL^{-1} (250 μL per well) for 24, 48 and 72 h to determine the effect of the treatment on cell viability. Afterward, the cells (1.5×10^6 cells per tube) were resuspended in 500 μL of the Annexin V binding buffer (final concentration 3×10^5 cells per 100 μL). The suspension was then divided into each of four FACS tubes (Falcon™ round-bottom tube, Thermo Fisher Scientific Inc., Waltham, MA, USA) including the cells without Annexin V-FITC or PI, cells with 10 μL of PI (2.5 mg mL^{-1}), cells with 5 μL of Annexin V-FITC (1 mg mL^{-1}), and cells with both PI and Annexin V-FITC. Subsequently, the tubes were incubated for 30 min at ambient temperature and protected from light before being assayed using an Accuri-C6 flow cytometer (BD Accuri Cytometers Inc., USA). The same treatment was repeated for all control.

To assess proliferation, the treated cells were trypsinised, and then 50 μL of the suspended cells was taken and mixed with an equal volume of Trypan Blue. Cells were counted using a haemocytometer (Abcam plc, Cambridge, UK) on a bright field microscope (Leitz Wetzlar SM-LUX reflected light microscope, Wetzlar, Germany). The same was done for the control samples (THCpSiNPs, PEI/NC-siRNA/THCpSiNPs, PEI/THCpSiNPs, PEI + siRNA + THCpSiNPs, siRNA/lipofectamine and untreated cells). All experiments were repeated at least three times, and the cell viability and proliferation were reported as the average of duplicate wells ± standard deviation.

Quantitative real time-polymerase chain reaction (QRT-PCR)

MRP1-mRNA silencing was studied through the use of a BioRad CFX Connect QRT-PCR detection system with SYTO9 reagent to detect the level of MRP1-mRNA downregulation. The QRT-PCR study was performed as described previously.[21] Briefly, the T98G cells treated with PEI/siRNA/THCpSiNPs

Table 2 Sequences of primers for MRP1 and GAPDH

Primer ID		Sequence	Exon number
siMohb	Forward	5′→AAGGAATGCGCCAAGACTAG→3′	7
	Reverse	5′→CCTTAAACAGAGAGGGGTTC→3′	8
GAPDH	Forward	5′→GTGAAGGTCGGAGTCAACGG→3′	N/A
	Reverse	5′→TGGAGGGATCTCGCTCCTGG→3′	N/A

were trypsinised (see section cell viability and proliferation), washed twice with PBS then centrifuged (1200*g* for 5 min). Subsequently, total mRNA was extracted using TRI Reagent® (Sigma-Aldrich) according to the manufacturer's protocol. cDNA was synthesised by means of M-MLV H(−) reverse transcriptase (Promega, Alexandria, NSW, Australia). The coincident measurement of the "housekeeping" gene glyceraldehyde-3-phosphate dehydrogenase (GAPDH) was used to control the experimental variations in the amount of RNA and to normalise the MRP1-mRNA expression data, which was calculated using the $\Delta\Delta C_t$ method. The primers were designed *via* the primer-blast web tool (http://www.ncbi.nlm.nih.gov/tools/primer-blast/). All primers used for QRT-PCR of MRP1-mRNA are shown in Table 2. The same procedure was repeated for the T98G cells treated with negative control samples (THCpSiNPs, PEI/NC-siRNA/THCpSiNPs, PEI/THCpSiNPs, PEI + siRNA + THCpSiNPs and untreated T98G cells) and positive control (siRNA/lipofectamine T98G treated cells). All experiments were performed at least in triplicate.

MRP1-protein level analysis

Flow cytometry of MRP1 protein levels was performed as described previously.[21] The T98G cells treated with PEI/siRNA/THCpSiNPs were trypsinised and washed twice with PBS then centrifuged (1200*g*) for 5 min (see section cell viability and proliferation). Subsequently, 300 μL of BD Cytofix/Cytoperm solution was added to each tube containing the trypsinised cells (3×10^5 per tube). The cells were incubated in the dark at −20 °C for 30 min, washed twice with the BD Perm/Wash buffer (1 mL) then centrifuged at 1200*g* (3 min). Afterward, treated cells were incubated with 10 μL of MRP1 antibody (QCRL-1; 200 μg mL^{-1}) for 90 min (−20 °C in the dark), then washed twice with the BD Perm/Wash buffer. Next, 50 μL of the 1/50 sheep anti-Mouse Ig secondary antibody was added to the cells and kept for 30 min at room temperature. Before the protein level was analysed using flow cytometry, cells were rinsed twice with PBS. The same procedure was performed for all control samples (THCpSiNPs, PEI/NC-siRNA/THCpSiNPs, PEI/THCpSiNPs, PEI + siRNA + THCpSiNPs, siRNA/lipofectamine and untreated cells. All experiments were performed at least in triplicate.

Results and discussion

Characterisation of the pSiNPs

pSiNPs were fabricated by means of pulsed electrochemical etching of single-crystal doped p-type silicon wafers and subsequent ball milling of the produced pSi multilayer membranes (Fig. S1 in the ESI†), previously described.[22,24,25] DLS showed the average size of THCpSiNPs to be 145.9 nm (PDI: 0.087), accompanied by an average ζ-potential of −43 mV (at pH 7.4). The plate-like morphology of pSiNPs produced by the pulsed electrochemical etching and ball milling process[47] was illustrated by means of SEM (see Fig. 2a and b) and TEM (Fig. S2 in the ESI†), and the depicted sizes were found to be in agreement with the sizes measured by DLS. For gene delivery by means of nanocarriers, a particle size between 100–300 nm is optimal in order to achieve high permeability into tumours, to accelerate cell binding and internalisation, and to avoid renal clearance.[21] In our case, the pSiNPs are neither so small that they are subject to rapid renal clearance nor so large (>400 nm in diameter) that they are captured by the interendothelial gap defense in tumours.[48]

THC treatment protects the pSi from oxidative hydrolysis in aqueous medium as our interferometric reflectance spectroxscopy (IRS) data show (Fig. S3 in the ESI†). Rapid degradation (50%, resulting in reduced thickness of the porous film after 250 min of incubation) was observed for the hydride-terminated film. In stark contrast, the THCpSi film remained stable with only a slight reduction of its initial thickness (thickness reduction ~4%) after 5 h of incubation.

siRNA loading into THCpSiNPs

Equilibrium adsorption studies were performed to investigate the adsorption capacity of siRNA into THCpSiNPs. Increasing siRNA concentration from 28.65 to 229.2 μg mL^{-1} increased the adsorption capacity (see Fig. 2a). Data were fitted to a Langmuir isotherm ($R^2 > 0.9943$, Table S1 in the ESI†), producing a theoretical model for the adsorption of siRNAs into the THCpSiNPs.[49]

The adsorption kinetics (Table S2 in the ESI†) were studied and modelled to methodically assess the loading mechanism (see Fig. 2b). The rate of adsorption of siRNA was higher at the beginning of the loading process due to the large unoccupied surface area (specific surface area of 202 m^2 g^{-1} and pore volume 0.51 cm^3 g^{-1}) of the pSiNPs. Two most commonly used pseudo adsorption kinetic models (Lagergren's first- and pseudo second-order)[50] were applied to ascertain the mechanism of the sorption process (Table S3 in the ESI†). With respect to the lowest root mean square deviation (σRMSD) between the experimental data and the model, the pseudo second-order model showed a better convergence at the equilibrium time rather than the Lagergren's first-order model (see Table S4 in the ESI†). Goodness-of-fit to the pseudo-second order kinetic model implies that siRNA loading is rate-limited by sorption to the THCpSiNPs solid phase.

PEI coating on siRNA/THCpSiNPs

The cationic polymer PEI was subsequently coated onto the surface of the THCpSiNPs preloaded with siRNA (PEI/siRNA/THCpSiNPs). The size and ζ-potential of the siRNA/THCpSiNPs increased after coating with PEI solutions of 0.05, 0.1 and 0.2% w/v PEI concentration (Table 3). An asymmetric

Table 3 Average hydrodynamic diameter, PDI and ζ-potential of THCpSiNPs after siRNA loading and PEI coating measured by DLS

Particle	Average hydrodynamic diameter (nm)	PDI	ζ-Potential (mV)
THCpSiNPs	145.9 ± 32.5	0.087	−35.0 ± 4.7
siRNA/THCpSiNPs	193.2 ± 25.8	0.192	−11.0 ± 5.2
PEI (0.05 w/v%)/siRNA/THCpSiNPs	213.3 ± 78.7	0.120	53.9 ± 7.3
PEI (0.1 w/v%)/siRNA/THCpSiNPs	228.1 ± 77.9	0.085	59.8 ± 6.1
PEI (0.2 w/v%)/siRNA/THCpSiNPs	236.5 ± 81.9	0.080	56.1 ± 5.7

cylindrical morphology was observed for PEI-coated siRNA/THCpSiNPs, and the diameter measured by SEM and TEM (Fig. 1b and S2b in the ESI†) was in agreement with the DLS data. Indeed, we expected the PEI to cap the pores rather than penetrate into them because of the large gyration radius of PEI (~39 nm (ref. 51)) compared to the average pore size of THCpSiNPs (~9 nm). Since the actual size and surface charge of NPs can change upon injection into the bloodstream because of the adsorption of blood components, we examined the effect of incubation in human plasma on particle size and ζ-potential.[52] The adsorption of serum proteins on the surface led to an increase in the size (to 325 nm in diameter) and dispersity (PDI) of both THCpSiNPs and PEI/siRNA/THCpSiNPs after 30 min of incubation, and also changed the ζ-potentials (Fig. S4 in the ESI†).

The effect of PEI coating on the adsorption capacity of siRNA into THCpSiNPs was evaluated. The adsorption capacity gradually decreased with PEI concentration: PEI/siRNA/THCpSiNPs coated with 0.05% w/v PEI solution gave an adsorption capacity of 49.5 μg mg^{-1}, 0.1% w/v PEI solution showed an adsorption capacity: 39.9 μg mg^{-1}, and for 0.2% w/v PEI solution the adsorption capacity was only 24.2 μg mg^{-1}. In comparison, the adsorption capacity for bare siRNA/THCpSiNPs was 57.2 μg mg^{-1}. Release of the negatively charged siRNA from the pores and surfaces into the surrounding aqueous environment during the PEI coating increased with increasing concentration of PEI, presumably because the cationic PEI was able to bind and release siRNA loaded into the THCpSiNPs. Our results compare favourably with previous siRNA loading studies using PEI coated MSNs and pSiNPs, where the adsorption capacity was found to be 27 and 8 μg mg^{-1} for PEI coated MSNs and amine-modified pSiNPs, respectively.[21,26]

Sustained siRNA release from PEI/siRNA/THCpSiNPs

The amount of siRNA released from siRNA/THCpSiNPs coated using PEI (concentrations 0.05, 0.1 and 0.2% w/v) over 35 h was determined by measuring the absorbance of the PBS solution (37 °C, pH 7.4) containing the released siRNA at 260 nm. These release kinetics are shown as a function of time in Fig. 3. An initial burst was observed from each type of THCpSiNPs in the first few hours, followed by a sustained release. The rate of siRNA release in the initial 24 h decreased when the coating PEI concentration was increased from 0.05 to 0.2% w/v. In all cases, the release rate for PEI/siRNA/THCpSiNPs was notably decreased compared to siRNA/THCpSiNPs. Release data were fitted to the simplified Higuchi's model, which describes drug release based on Fickian diffusion. The critical model parameter (K_H) and fit (R^2) calculated for each coating condition are shown in Table 4. The K_H parameters calculated for siRNA from PEI coated THCpSiNPs were significantly lower than that calculated for the uncoated THCpSiNPs ($p < 0.0001$, Tukey HSD test), consistent with the retardation of siRNA release after PEI capping. Modification of THCpSiNPs through a PEI-coating decelerated siRNA release based on several mechanisms: (1) a slow disintegration and dissolution of the PEI cap, (2) the attractive electrostatic forces between positively charged PEI and negatively charged loaded siRNA, and (3) a decelerated wetting of the hydrophobic surface of THCpSiNPs.

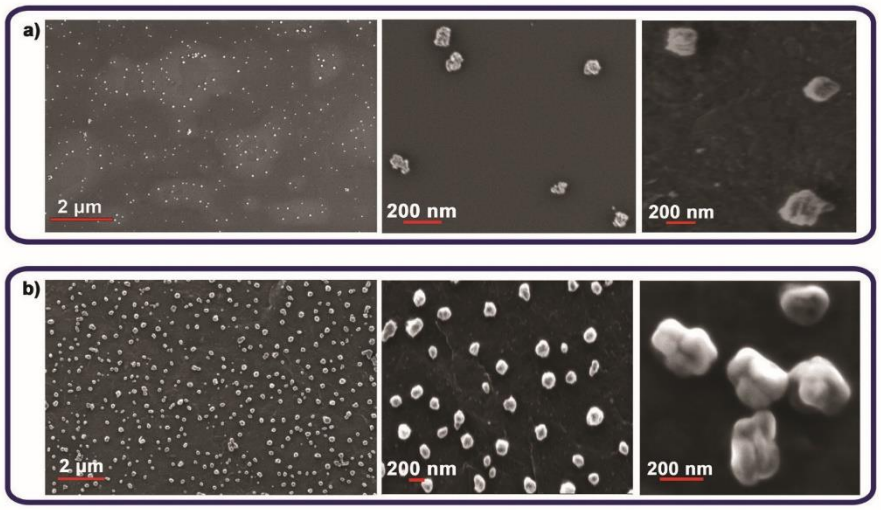

Fig. 1 Representative SEM images of (a) THCpSiNPs, (b) PEI/siRNA/THCpSiNPs.

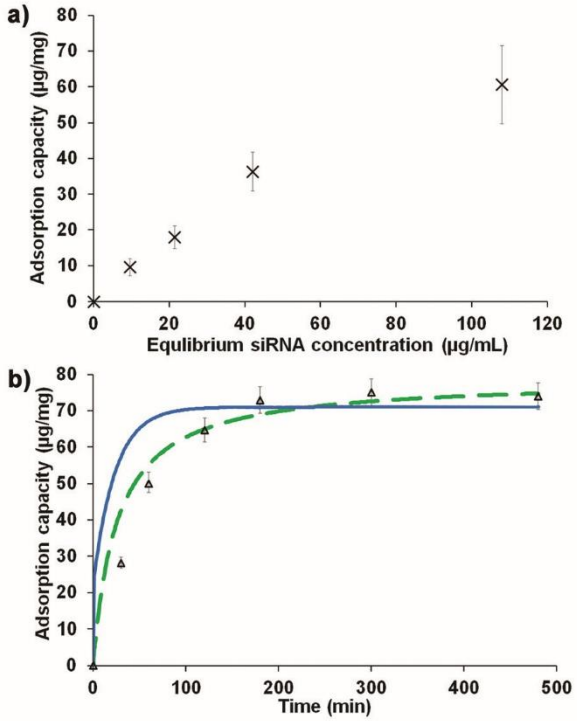

Fig. 2 (a) Adsorption of siRNA from EtOH/water solution to THCpSiNPs and (b) rate of adsorption of siRNA into THCpSiNPs. Curves show data fit to Lagergren's first-order (blue line) and pseudo second-order (dash green line) kinetic models. Concentration of the pSiNPs = 0.1 mg mL^{-1}, loading medium: EtOH/water (48/2 v/v), agitation rate (300 rpm) at ambient temperature (n = 3; mean ± standard deviation shown).

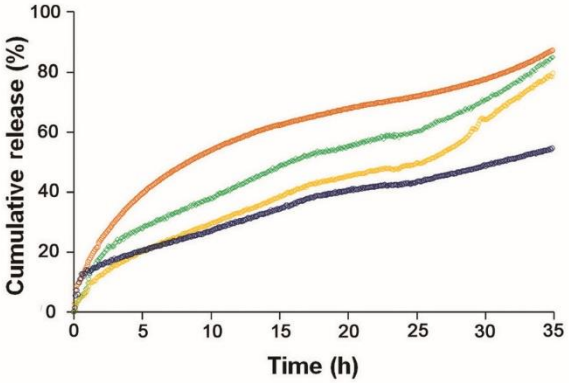

Fig. 3 Effect of PEI coating and concentration on siRNA release profile from samples: siRNA/THCpSiNPs (red), PEI/siRNA/THCpSiNPs (0.05% w/v, green), PEI/siRNA/THCpSiNPs (0.1% w/v, yellow) and PEI/siRNA/THCpSiNPs (0.2% w/v, blue). Release medium: PBS, pH 7.4, T = 37 °C ± 0.2 (representative data, n = 3).

Cell viability and proliferation

We examined the cytotoxicity induced by THCpSiNPs loaded with anti-MRP1 siRNA and control oligonucleototide sequences using the glioblastoma cell line, T98G. T98G cells were incubated with PEI/siRNA/THCpSiNPs and negative controls (THCpSiNPs, PEI/NC-siRNA/THCpSiNPs, PEI/THCpSiNPs and PEI + siRNA + THCpSiNPs) at a concentration of 0.1 mg mL^{-1}, and compared with siRNA/lipofectamine (positive control) and untreated cells for 48 and 72 h. T98G cells were incubated at a NP concentration of 0.1 mg mL^{-1} for 48 and 72 h.

No differences in cell viability were observed between T98G treated with PEI/siRNA/THCpSiNPs or siRNA/lipofectamine and untreated cells (see Fig. 4 and S5†). Moreover, all cells treated with control NP showed a high cell viability (>93.3%), similar to the viability of the untreated cells (see Fig. 4 and S5 in the ESI†). In our earlier work, cells incubated with siRNA-loaded amine-modified pSiNPs showed a significant amount of cell death (33% after 48 h).[21] Here the PEI/siRNA/THCpSiNPs induced negligible cell death, as measured by the Annexin V assay, after the 48 and 72 h incubation, indicating that the vector with loaded MRP1 siRNA is not in itself toxic to glioblastoma cells. pSi and its degradation by-product, silicic acid, are known to be non-toxic, and the biocompatibility of THCpSiNPs has been shown *in vitro* and *in vivo*.[29]

We next evaluated the influence of the siRNA delivery system on the proliferation of glioblastoma cells, by treating T98G cells with PEI/siRNA/THCpSiNPs at a concentration of 0.1 mg mL^{-1} for 24, 48 and 72 h. The THCpSiNP treated showed similar proliferation to untreated cells (see Fig. 5). Moreover, treating cells with siRNA/THCpSiNPs did not influence cell proliferation (Fig. S6 in the ESI†). This is expected since the internalization of the NPs without PEI coating would be negligible as shown in previous work.[29,47] However, the PEI/siRNA/THCpSiNPs and siRNA/lipofectamine (siRNA 390 nmole per 3 × 10^5 cells per cm^2) treatments showed reduction in cell proliferation compared with the control cultures. Although, the primary action of MRP1 in glioblastoma has been ascribed to chemotherapeutic efflux from the cell, others have described a decrease in malignant cell proliferation and

Table 4 Results of fitting drug release kinetics data to the simplified Higuchi model

Models and parameters		siRNA/THCpSiNPs (uncoated)	PEI (0.05% w/v) siRNA/THCpSiNPs	PEI (0.1% w/v) siRNA/THCpSiNPs	PEI (0.2% w/v) siRNA/THCpSiNPs
Higuchi	K_H ($h^{-0.5}$)	17.11 ± 0.23[a]	11.91 ± 0.35	10.44 ± 0.49	8.12 ± 0.35
	R^2	0.995	0.994	0.994	0.991

[a] K_H is reported ± standard deviation from triplicate release experiments.

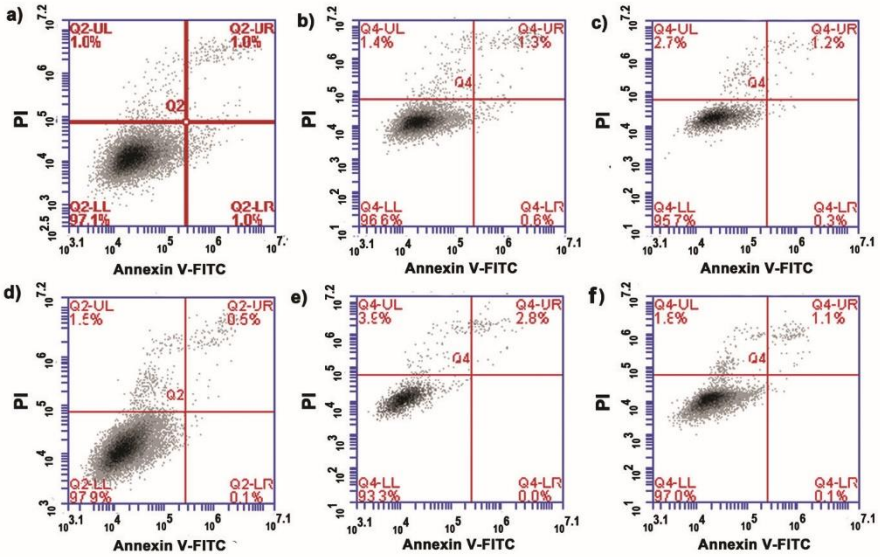

Fig. 4 T98G cell apoptosis detection after incubation with (a and d) untreated cells, (b and e) THCpSiNPs and (c and f) PEI/siRNA/THCpSiNPs at the concentration 0.1 mg mL^{-1}. (n = 3; mean ± standard deviation shown). T98G cells line was analysed with Annexin V-FITC/PI assay after 48 h (a–c) and 72 h (d–f) of the treatment. The bottom left quadrant represents the viable cells, the bottom right quadrant shows the early apoptotic cells, the top left quadrant represents necrotic cells, and the top right quadrant indicates late apoptotic cells (representative data, n = 3).

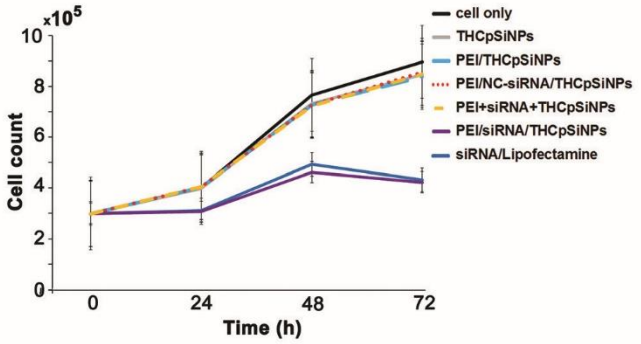

Fig. 5 Proliferation rate of the T98G cells transfected with the NPs and controls at different time points. Proliferation was measured though the use of the Trypan Blue assay on a bright field microscope (n = 4; mean ± standard deviation).

tumour growth when MRP1 action is attenuated in the absence of chemotherapeutic agents.[7,53]

Cell uptake of NPs

The internalisation of PEI/THCpSiNPs preloaded with Block-iT™ (PEI/Block-iT™/THCpSiNPs) was studied in T98G cells using laser-scanning confocal microscopy. T98G control cells (not exposed to the NPs) were well-spread, displaying lamellipodia, with the typical shape and morphology of adherent T98G cells (see Fig. 6a). No morphological changes were also observed in the T98G treated cells (exposed to the PEI/Block-iT™/THCpSiNPs) after 24 h incubation (see Fig. 6b). Treated cells showed punctate green fluorescence, attributed to the internalisation of the PEI/Block-iT™/THCpSiNPs. To confirm the uptake of PEI/Block-iT™/THCpSiNPs by cells, z-stacks were acquired using confocal microscopy (Fig. S7 in the ESI†).

It is worth noting that the THC modification quenched the intrinsic luminescence of pSi, so the green fluorescence was only due to the Block-iT™.[29] However, green fluorescence intensity was not observed in the GBM cells treated with the Block-iT™/THCpSiNPs without the PEI capping, therefore showing negligible internalisation of uncoated THCpSiNPs into the cell interior. TEM was performed to confirm the cell uptake and distribution of intracellular PEI/siRNA/THCpSiNPs (see Fig. 4c and d). The internalised NPs were not observed within the cell nucleus. This can be explained by the fact that the central pore of the nuclear complex has a diameter of 50 nm,[54] smaller than the average size of the NPs (236.5 nm), thus NP are excluded from transport into the nucleus.

MRP1-mRNA downregulation

MRP1-mRNA expression was investigated following incubation of T98G GBM cells with the PEI/siRNA/THCpSiNPs and controls for 48 h. Both treated and untreated T98G cells expressed MRP1-mRNA at 48 h (Table 5). However, significant downregulation of MRP1-mRNA (63%) was observed in the PEI/siRNA/THCpSiNPs treated cells. This downregulation implies internalisation of PEI/siRNA/THCpSiNPs into cells, and subsequent release of the loaded siRNA into the cytoplasm exploiting the known proton sponge effect.[35] There was no downregulation of MRP1-mRNA in the negative controls or untreated cells.

MRP1-protein downregulation

We validated the down-regulation of the MRP1-mRNA expression by measuring the protein expression of MRP1 using flow cytometry 98 h after incubation with the PEI/siRNA/

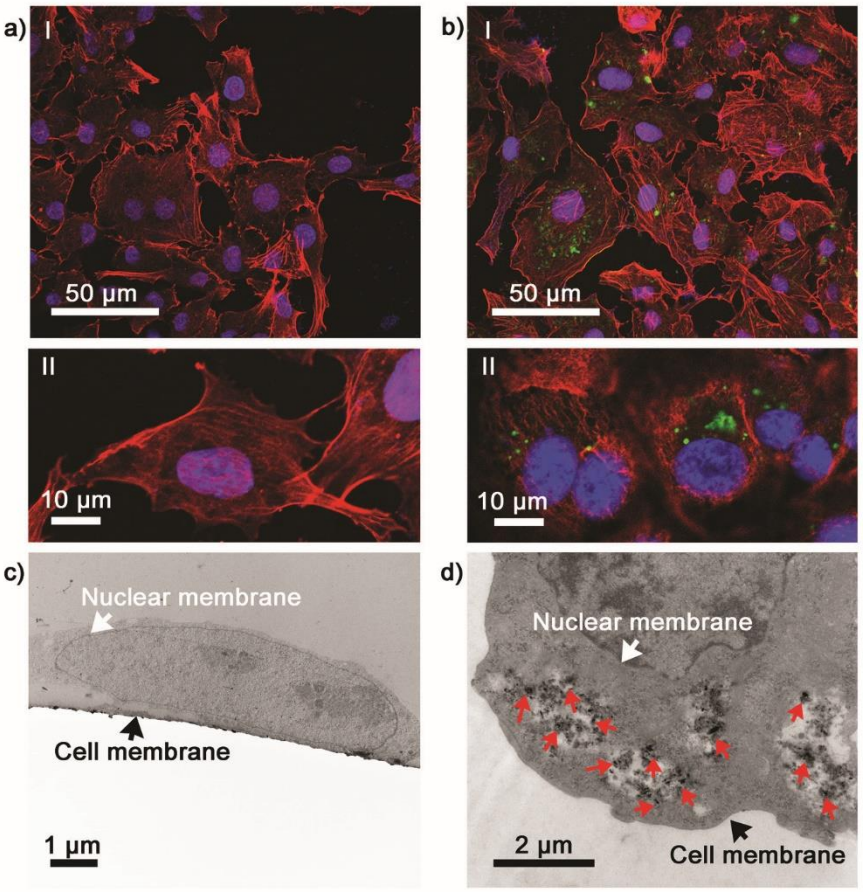

Fig. 6 Uptake of PEI/Block-iT™/THCpSiNPs by T98G cells. Laser-scanning confocal microscopy images of (a) control T98G cells without the NPs, and (b) T98G cells incubated with PEI/Block-iT™/THCpSiNPs (I and II). The cell nucleus was stained with Hoechst 33342 (blue), PEI/Block-iT™/THCpSiNPs appeared green and the cell cytoskeleton was stained with phalloidin-TRITC (red). TEM images of (c) control T98G cells without the NPs and (d) T98G cells incubated with PEI/Block-iT™/THCpSiNPs. The red arrows indicate the internalised NPs.

Table 5 Fold change of expression 48 h after the incubation with PEI/siRNA/THCpSiNPs and controls. (n = 7; mean ± standard deviation shown)

Sample ID	Fold change of expression	Role[a]
Untreated cells	1.00 ± 0.05	NC
THCpSiNPs	1.04 ± 0.17	NC
PEI + siRNA + THCpSiNPs	1.12 ± 0.30	NC
PEI/THCpSiNPs	1.11 ± 0.26	NC
PEI/NC-siRNA/THCpSiNPs	1.12 ± 0.13	NC
PEI/siRNA/THCpSiNPs	0.37 ± 0.14	MS
siRNA/Lipofectamine	0.47 ± 0.16	PC

[a] Abbreviation: NC: negative control; MS: main sample; PC: positive control.

THCpSiNPs. Downregulation of MRP1 protein (70% reduction of the average protein level compared with the untreated cells) was significant and also consistent with the demonstrated downregulation of the MRP1-mRNA (see Fig. 7). The reduction of the MRP1-protein level was observed after 96 h of incubation due protein translation inhibition following the halted expression of the MRP1-mRNA.[21]

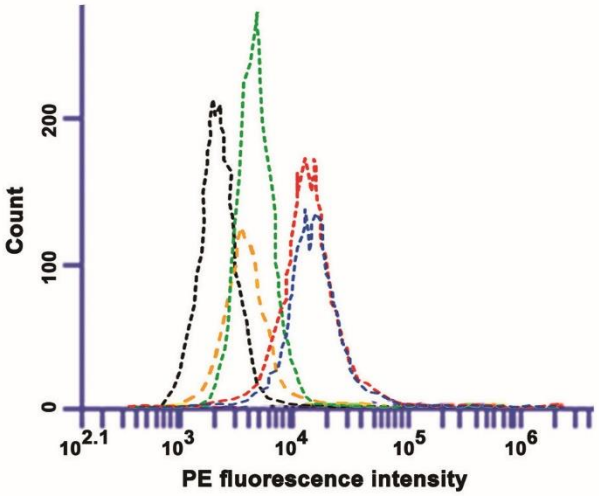

Fig. 7 Flow cytometry histograms evaluating MRP1 protein concentration in T98G cells. Black: untreated cells incubated with the secondary antibody; blue: untreated cell; red: cells incubated with the PEI/NC-siRNA/THCpSiNPs; yellow: cells incubated with siRNA/Lipofectamine (positive control); green: cells incubated with PEI/siRNA/THCpSiNPs. Cells were harvested 96 h after treatment with nanoparticles.

No reduction of MRP1-protein was detected at 48 and 72 h of the incubation (data not shown), presumably due to the long half-life of MRP1-protein.[55,56] Taken together, our fabricated PEI/siRNA/THCpSiNPs reduced T98G cell growth, MRP1-mRNA and MRP1-protein expression without inducing direct cell toxicity proving efficiency for gene silencing *in vitro*.

Conclusions

We have reported on a promising nanocarrier for controlled siRNA delivery, based on the electrochemically etched pSiNPs, which were subsequently modified by the surface-stabilising THC process. These mesoporous NPs showed a remarkable capacity for siRNA loading (up to 57 μg siRNA per mg pSiNP loaded). The sorption of siRNA within mesopores was best described by a pseudo second-order kinetics model. To improve the release of siRNA *in vitro*, cellular uptake of the NPs, and endosomal escape, the siRNA loaded NPs were coated with PEI. The PEI capping not only demonstrated sustained release kinetics of the loaded siRNA from the NPs over 35 h but also suppressed burst release to below 11%. TEM and confocal microscopy imaging confirmed the uptake of PEI/Block-iT™/THCpSiNPs into T98G cells. Intracellular siRNA release was demonstrated by significant MRP1 gene downregulation (63%) and protein silencing (70%). The PEI coated NPs did not induce cytotoxicity in T98G cells after 72 h of the treatment. Taken together, our polymer-coated mesoporous silicon NPs can be potentially used as biocompatible nanocarriers for efficient gene silencing.

Acknowledgements

This research was conducted with funding the Australian Research Council Centre of Excellence in Convergent Bio-Nano Science and Technology (project number CE140100036) and the Channel 7 Children's Research Foundation. MA thanks the Saudi Arabia Higher Education Ministry for awarding him a King Abdullah Scholarship.

Notes and references

1 Y. R. Lawrence, X. A. Li, I. e. Naqa, C. A. Hahn, L. B. Marks, T. E. Merchant and A. P. Dicker, *Int. J. Radiat. Oncol. Biol. Phys.*, 2010, **76**, S20–S27.
2 B. M. Tyler, G. Pradilla, U. Hadelsberg, H. Bow, I. Suk and H. Brem, in *Focal Controlled Drug Delivery*, ed. A. J. Domb and W. Khan, Springer, US, 2014, ch. 7, pp. 169–194, DOI: 10.1007/978-1-4614-9434-8_7.
3 D. J. Yoon, B. H. Kwan, F. C. Chao, T. P. Nicolaides, J. J. Phillips, G. Y. Lam, A. B. Mason, W. A. Weiss and D. T. Kamei, *Cancer Res.*, 2010, **70**, 4520–4527.
4 J. M. Stukel and M. R. Caplan, *Expert Opin. Drug Deliv.*, 2009, **6**, 705–718.
5 J. F. Deeken and W. Loscher, *Clin. Cancer Res.*, 2007, **13**, 1663–1674.
6 M. M. Mrugala, *Discov. Med.*, 2013, **15**, 221–230.
7 B. J. Kuss, M. Corbo, W. M. Lau, D. A. Fennell, N. M. Dean and F. E. Cotter, *Int. J. Cancer*, 2002, **98**, 128–133.
8 M. Munoz, M. Henderson, M. Haber and M. Norri, *IUBMB Life*, 2007, **59**, 752–757.
9 C. Quezada, W. Garrido, C. Oyarzún, K. Fernández, R. Segura, R. Melo, P. Casanello, L. Sobrevia and R. San Martín, *J. Cell. Physiol.*, 2013, **228**, 602–608.
10 R. Tang, A. M. Faussat, P. Majdak, J. Y. Perrot, D. Chaoui, O. Legrand and J. P. Marie, *Leukemia*, 2004, **18**, 1246–1251.
11 T. A. Vos, G. J. Hooiveld, H. Koning, S. Childs, D. K. Meijer, H. Moshage, P. L. Jansen and M. Müller, *Hepatology*, 1998, **28**, 1637–1644.
12 Y. R. Lawrence, W. Shi and A. P. Dicker, *Expert Rev. Neurother.*, 2010, **10**, 1493–1495.
13 Y. R. Lawrence, M. Wang, A. P. Dicker, D. Andrews, W. J. Curran, J. M. Michalski, L. Souhami, W.-Ka. Yung and M. Mehta, *Br. J. Cancer*, 2011, **104**, 1365–1371.
14 M. K. DeGorter, G. Conseil, R. G. Deeley, R. L. Campbell and S. P. C. Cole, *Biochem. Biophys. Res. Commun.*, 2008, **365**, 29–34.
15 G. R. Devi, *Cancer Gene Ther.*, 2006, **13**, 819–829.
16 W. Guo, W. Chen, W. Yu, W. Huang and W. Deng, *Chin. J. Cancer*, 2013, **32**, 488–493.
17 Y. Zeng and B. R. Cullen, *RNA*, 2002, **8**, 855–860.
18 B. Ballarín-González, F. Dagnaes-Hansen, R. A. Fenton, S. Gao, S. Hein, M. Dong, J. Kjems and K. A. Howard, *Mol. Ther. Nucleic Acids*, 2013, **2**, 1–8.
19 J. Shi, Y. Xu, X. Xu, X. Zhu, E. Pridgen, J. Wu, A. R. Votruba, A. Swami, B. R. Zetter and O. C. Farokhzad, *Nanomed. Nanotechnol. Biol. Med.*, 2014, **10**, 897–900.
20 E. J. Anglin, L. Cheng, W. R. Freeman and M. J. Sailor, *Adv. Drug Delivery Rev.*, 2008, **60**, 1266–1277.
21 Y. Wan, S. Apostolou, R. Dronov, B. Kuss and N. Voelcker, *Nanomedicine*, 2014, **9**, 2309–2321.
22 M. H. Kafshgari, A. Cavallaro, B. Delalat, F. J. Harding, S. J. P. McInnes, E. Mäkilä, J. Salonen, K. Vasilev and N. H. Voelcker, *Nanoscale Res. Lett.*, 2014, **9**, 333.
23 R. B. Vasani, S. J. P. McInnes, M. A. Cole, A. M. M. Jan, A. V. Ellis and N. H. Voelcker, *Langmuir*, 2011, **27**, 7843–7853.
24 D. Liu, L. M. Bimbo, E. Mäkilä, F. Villanova, M. Kaasalainen, B. Herranz-Blanco, C. M. Caramella, V.-P. Lehto, J. Salonen, K.-H. Herzig, J. Hirvonen and H. A. Santos, *J. Controlled Release*, 2013, **170**, 268–278.
25 M. Kovalainen, J. Mönkäre, M. Kaasalainen, J. Riikonen, V.-P. Lehto, J. Salonen, K.-H. Herzig and K. Järvinen, *Mol. Pharmaceutics*, 2013, **10**, 353–359.
26 X. Li, Q. R. Xie, J. Zhang, W. Xia and H. Gu, *Biomaterials*, 2011, **32**, 9546–9556.
27 X. Li, J. Zhang and H. Gu, *Langmuir*, 2011, **27**, 6099–6106.

28 C. Chiappini Dottore, Doctor of Philosophy, University of Texas at Austin, 2011.
29 M. H. Kafshgari, B. Delalat, W. Y. Tong, F. J. Harding, M. Kaasalainen, J. Salonen and N. H. Voelcker, *Nano Res.*, 2015, **8**, 2033–2046.
30 C. Chiappini, E. De Rosa, J. O. Martinez, X. Liu, J. Steele, M. M. Stevens and E. Tasciotti, *Nat. Mater.*, 2015, **14**, 532–539.
31 T. Tanaka, L. S. Mangala, P. E. Vivas-Mejia, R. Nieves-Alicea, A. P. Mann, E. Mora, H.-D. Han, M. M. K. Shahzad, X. Liu, R. Bhavane, J. Gu, J. R. Fakhoury, C. Chiappini, C. Lu, K. Matsuo, B. Godin, R. L. Stone, A. M. Nick, G. Lopez-Berestein, A. K. Sood and M. Ferrari, *Cancer Res.*, 2010, **70**, 3687–3696.
32 T. Xia, M. Kovochich, M. Liong, H. Meng, S. Kabehie, S. George, J. I. Zink and A. E. Nel, *ACS Nano*, 2009, **3**, 3273–3286.
33 D. Ma, *Nanoscale*, 2014, **6**, 6415–6425.
34 J. Gilleron, W. Querbes, A. Zeigerer, A. Borodovsky, G. Marsico, U. Schubert, K. Manygoats, S. Seifert, C. Andree, M. Stöter, H. Epstein-Barash, L. Zhang, V. Koteliansky, K. Fitzgerald, E. Fava, M. Bickle, Y. Kalaidzidis, A. Akinc, M. Maier and M. Zerial, *Nat. Biotechnol.*, 2013, **31**, 638–646.
35 M. H. Kafshgari, F. J. Harding and N. H. Voelcker, *Curr. Drug Delivery*, 2015, **12**, 63–77.
36 S. Lee, M.-S. Kim, D. Lee, T. K. Kwon, D. Khang, H.-S. Yun and S.-H. Kim, *Int. J. Nanomedicine*, 2013, **8**, 147–158.
37 S. Jambhrunkar, S. Karmakar, A. Popat, M. Yu and C. Yu, *RSC Adv.*, 2014, **4**, 709–712.
38 A. J. Di Pasqua, K. K. Sharma, Y.-L. Shi, B. B. Toms, W. Ouellette, J. C. Dabrowiak and T. Asefa, *J. Inorg. Biochem.*, 2008, **102**, 1416–1423.
39 K. M. Dunnick, M. A. Badding, D. Schwegler-Berry, J. M. Patete, C. Koenigsmann, S. S. Wong and S. S. Leonard, *J. Toxicol. Environ. Health, Part A*, 2014, 77, 1251–1268.
40 J.-H. Park, L. Gu, G. v. Maltzahn, E. Ruoslahti, S. N. Bhatia and M. J. Sailor, *Nat. Mater.*, 2009, **8**, 331–336.
41 J. Shen, R. Xu, J. Mai, H.-C. Kim, X. Guo, G. Qin, Y. Yang, J. Wolfram, C. Mu, X. Xia, J. Gu, X. Liu, Z.-W. Mao, M. Ferrari and H. Shen, *ACS Nano*, 2013, 7, 9867–9880.
42 D. V. Bax, A. Kondyurin, A. Waterhouse, D. R. McKenzie, A. S. Weiss and M. M. M. Bilek, *Biomaterials*, 2014, **35**, 6797–6809.
43 M. Licciardi, C. Scialabba, G. Cavallaro, C. Sangregorio, E. Fantechi and G. Giammona, *J. Biomed. Nanotechnol.*, 2013, **9**, 949–964.
44 M. Ikonen, L. Murtomäki and K. Kontturi, *Colloids Surf., B*, 2008, **66**, 77–83.
45 Y. Fu and W. J. Kao, *Expert Opin. Drug Deliv.*, 2010, 7, 429–444.
46 S. Dash, P. N. Murthy, L. Nath and P. Chowdhury, *Acta Pol. Pharm.*, 2010, **67**, 217–223.
47 L. M. Bimbo, M. Sarparanta, H. A. Santos, A. J. Airaksinen, E. Makila, T. Laaksonen, L. Peltonen, V.-P. Lehto, J. Hirvonen and J. Salonen, *ACS Nano*, 2010, 4, 3023–3032.
48 F. Alexis, E. Pridgen, R. Langer and O. C. Farokhzad, in *Drug Delivery*, ed. M. Schäfer-Korting, Springer, Berlin, Heidelberg, 2010, ch. 2, vol. 197, pp. 55–86.
49 E. R. Monazam, L. J. Shadle, D. C. Miller, H. W. Pennline, D. J. Fauth, J. S. Hoffman and M. L. Gray, *AIChE J.*, 2013, **59**, 923–935.
50 M. Kafshgari, M. Mansouri, M. Khorram and S. Kashani, *Int. J. Ind. Chem.*, 2013, **4**, 5.
51 S. A. Ekhorutomwen, S. P. Sawan, B. F. Smith, T. W. Robison and K. V. Wilson, *Solution behavior of modified polyethylenimine (PEI) polymers by light scattering investigations*, 2004.
52 M. Sarparanta, L. M. Bimbo, J. Rytkönen, E. Mäkilä, T. J. Laaksonen, P. Laaksonen, M. Nyman, J. Salonen, M. B. Linder, J. Hirvonen, H. A. Santos and A. J. Airaksinen, *Mol. Pharmaceutics*, 2012, **9**, 654–663.
53 L. Peigñan, W. Garrido, R. Segura, R. Melo, D. Rojas, J. Cárcamo, R. San Martín and C. Quezada, *Neurochem. Res.*, 2011, **36**, 1397–1406.
54 S. K. Vasu and D. J. Forbes, *Curr. Opin. Cell Biol.*, 2001, **13**, 363–375.
55 W. Yue, K. Abe and K. L. R. Brouwer, *Mol. Pharm.*, 2009, **6**, 134–143.
56 C. Alemán, J.-P. Annereau, X.-J. Liang, C. O. Cardarelli, B. Taylor, J. J. Yin, A. Aszalos and M. M. Gottesman, *Cancer Res.*, 2003, **63**, 3084–3091.

Supporting Information

Small interfering RNA delivery by polyethylenimine-functionalised porous silicon nanoparticles

M. Hasanzadeh Kafshgari[1,#], M. Alnakhli[2,#], B. Delalat[1], S. Apostolou[2], F. J. Harding[1], E. Mäkilä[3], J. J. Salonen[3], B. Kuss[2], N. H. Voelcker[1,]*

[1]ARC Centre of Excellence in Convergent Bio-Nano Science and Technology, Mawson Institute, University of South Australia, GPO Box 2471, Adelaide SA 5001, Australia

[2]School of Medicine, Flinders University, Bedford Park, Adelaide, SA 5042, Australia

[3]Department of Physics and Astronomy, University of Turku, FI-20014 Turku, Finland

SEM imaging of multilayer pSi film

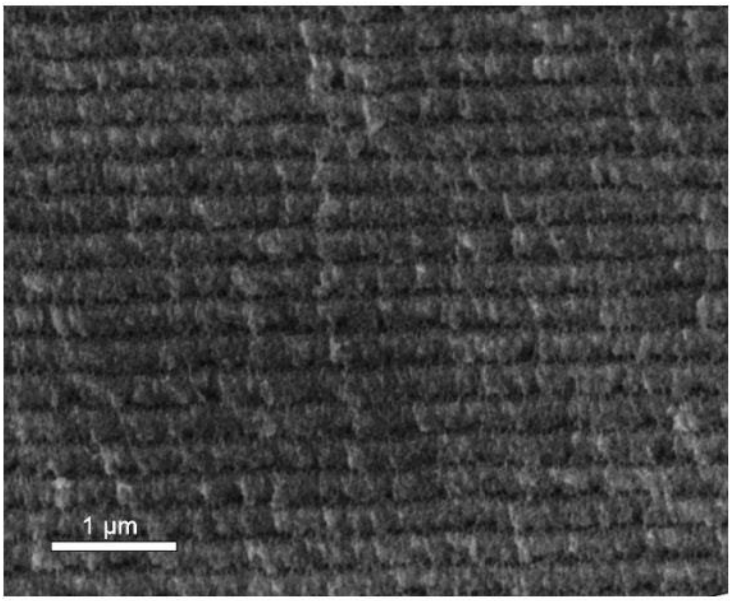

Fig. S1. Representative SEM image of a multilayer pSi film fabricated by the pulsed electrochemical etching.

TEM imaging of THCpSiNPs and PEI/siRNA/THCpSiNPs

The morphology of THCpSiNPs and PEI/siRNA/THCpSiNPs (Fig. S2) was investigated by means of TEM (JEM-2100F TEM, JEOL USA, Inc., MA, USA) with 20–120 kV beam energy under high vacuum 1×10^{-5} Pa. Both samples were prepared by allowing a single drop of the nanoparticle suspension (in EtOH) to dry overnight at room temperature on 200-mesh copper grids (ProSciTech Co., Thuringowa, Qld, Australia).

# These authors contributed equally to this work.
* Corresponding authors: Nicolas H. Voelcker
Tel.: +61 8 8302 5508, Fax: +61 8 8302 5613.
Email: nico.voelcker@unisa.edu.au

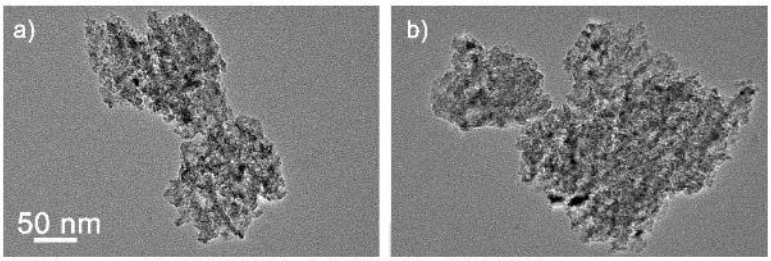

Fig. S2. Representative TEM images of (a) THCpSiNPs, (b) PEI/siRNA/THCpSiNPs.

Interferometric Reflectance Spectroscopy (IRS)

To measure stability of the surface modifications (THC and hydride terminated), interferometric reflectance spectra were acquired using an Ocean Optics USB2000 spectrometer equipped with a tungsten halogen lamp (Ocean Optics, LS-1). Light from the lamp was focused onto the surface of the sample using a collimating lens. pSi membranes (THC and hydride terminated) were clamped into a custom-built closed flow cell, through which PBS solution at 37 °C was circulated via a peristaltic pump (LongerPump BT100-1J, Baoding Longer Precision Pump Co. Ltd., Hebei, China) with a flow rate of 3.5 mL min^{-1}. Initial effective optical thickness (EOT) readings (obtained from interferometric reflectance spectra by fast Fourier transformation using IGOR software from Wavemetrics Inc., Portland, OR, USA) were recorded every 1 min for a period of 5 h (Fig. S3).

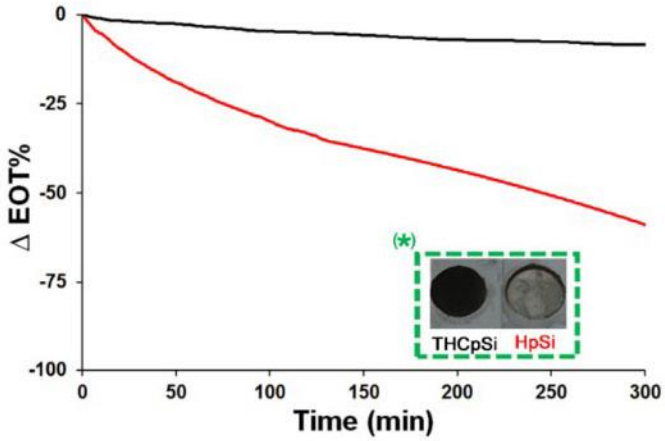

Fig. S3. Stability of HpSi (red line) and THCpSi (black line) films as a function of time in PBS as investigated by IRS. (*) Image of HpSi and THCpSi films (representatives of the surface modifications) fixed into a flow cell with a constant flow rate (3.5 mL min^{-1}) of PBS (pH 7.4 and temperature 37 °C) after 5 h incubation.

Equilibrium adsorption capacity

To load the siRNA into the THCpSiNPs (0.1 mg/mL, 0.050 mL, suspended in EtOH) for the batch adsorption experiments, the solution (initial concentrations 28, 57, 114 and 229 µg/mL) was dispersed by sonication for 1 min, then incubated at ambient temperature overnight (300 rpm). After the incubation, the supernatant was removed by centrifugation (5000 rpm, 5 min). The loaded pSiNPs were then collected. The amount of absorbed siRNA was calculated via UV-Vis spectrophotometry at 260 nm from three replicates. The amount of absorbed siRNA onto the THCpSiNPs was calculated based on Equation S1. The adsorption capacity was then examined by means of Langmuir isotherm given as

$$P = \frac{P_{\max} K_f C}{1 + K_f C} \quad \text{(S1)}$$

where P_{max} (µg/mg) and K_f (mL/µg) are the maximum amount of adsorption and the sorption equilibrium constant, respectively. C (µg/mL) and P (µg-solute/mg-THCpSiNPs) are the concentration and amount of adsorption.

Table S1. Langmuir isotherm constants for the adsorption of siRNA from EtOH/water solution to THCpSiNPs.

K_f (mL/mg)	P_{max} (µg/mg)	R^2
0.0172	72.46	0.9943

Adsorption kinetics

siRNA solution was added to 0.1 mg/mL THCpSiNPs suspension (50 µL, EtOH) at a volumetric ratio of 48/2 THCpSiNPs suspension/siRNA solution. Subsequently, the suspension solution was well dispersed by sonication for 1 min before the incubation (see Table S2) at ambient temperature for different predetermined incubation times (30, 60, 120, 180, 300 and 480 min). Afterward, the loaded THCpSiNPs were collected by centrifugation (5000 rpm, 5 min). The amount of the absorbed siRNA was measured by UV-Vis at 260 nm from three replicates. The amount of siRNA absorbed onto the THCpSiNPs, P (mg/mg), was calculated based on the Equation S1.

Table S2. Characteristics of THCpSiNPs for siRNA adsorption.

Characteristic	Sample
Functionalisation	THCpSiNPs
Agitation rate (rpm)	300
Type of oligonucleotide	siRNA
Average diameter (nm)	145.9
Diffusion coefficient (m^2/s)* [1, 2]	≈8.39×10^{-11}
Initial oligonucleotides concentration (µg/mL)	230
Porosity (%)	54
Solid density (g/cm^3) [3]	≈2.33
pSiNPs concentration (mg/mL)	0.1
Solution bulk density (g-pSiNPs/cm^3)	≈1
Density of solvent (g/cm^3)	≈1
Temperature (°C)	25

Modeling of siRNA adsorption

Pseudo first and second-order models

The pseudo first and second-order models were used to assess the experimental data in order to evaluate the mechanisms involved in the adsorption of siRNA into THCpSiNPs (Table S2). The first-order rate expression of Lagergren is given as:

$$\log(P_e - P) = \log P_e - \frac{k_1 t}{2.303} \quad \text{(S2)}$$

Where P_e and P (μg/mg) are the amounts of siRNA adsorbed into the THCpSiNPs at equilibrium and at time t, respectively, and k_1 (1/min) is the rate constant of pseudo first-order model.[4] The measured data are able to fit to a straight line that is calculated by drawing log (P_e-P) versus t.

The second-order kinetic model can fit a range of sorption data without input parameters beforehand:[4,5]

$$\frac{t}{P} = \frac{1}{k_2 P_e^2} + \frac{t}{P_e} \quad \text{(S3)}$$

where k_2 (μg/mg min) is the rate constant of pseudo second-order model. Accordingly, there is a linear relationship in the plot of t/P versus t in the agreement with the second-order model. The slopes and intercepts of the plots are indicating the second-order rate constant k_2 and P_e. To determine the deviations among data, σ_{RMSD} (Root Mean Square Deviation) was applied:

$$\sigma_{RMSD} = \left[\frac{1}{n} \sum_{i=1}^{n} \left(\frac{P_{Exp} - P_{Cal}}{P_{Exp}} \right)_i^2 \right]^{0.5} \times 100 \quad \text{(S4)}$$

.

Table S3. Pseudo first and second-order adsorption rate constant and P_e,value.

Sample	Pseudo second-order kinetic model			Lagergren pseudo first-order kinetic model		
	K_1 (1/min)	$P_{e,Cal}$ (μg/mg)	R^2	K_2 (μg/mg·min)	$P_{e,Cal}$ (μg/mg)	R^2
	0.0005	**78.74**	**0.996**	**1.68**	**71**	**0.889**

Table S4. Calculated σ_{RMSD} of the kinetic models.

Kinetic models	σ_{RMSD} of sample
Pseudo first-order kinetic model	0.1487
Pseudo second-order kinetic model	**0.0223**

Human plasma protein adsorption

The behavior of nanoparticles in the circulating blood is subjected to the adsorption of proteins of the plasma.[6] The adsorption of human plasma proteins towards THCpSiNPs (0.1 mg/mL) before and after the PEI coating (with 0.1% w/v) was evaluated by measuring hydrodynamic diameter, PDI and ζ-potential. Thus, PEI coated and uncoated THCpSiNPs were suspended in 1 mL of human plasma. The samples were sonicated (30 s) to be well-dispersed, and then incubated at 37 °C for 0, 30, 60, and 120 min. NPs were then sedimented by centrifugation (5000 rpm, 5 min) and washed with de-ionised water. For DLS measurement, the treated NPs were resuspended in de-ionised water (1 mL) to measure their hydrodynamic diameter, PDI and ζ-potential. The sorption of serum proteins on the surface led to increase of the primary size and aggregation (PDI) of THCpSiNPs and PEI/siRNA/THCpSiNPs, and also changed the primary ζ-potential (Fig. S4). These changes occurred within 30 min of incubation.

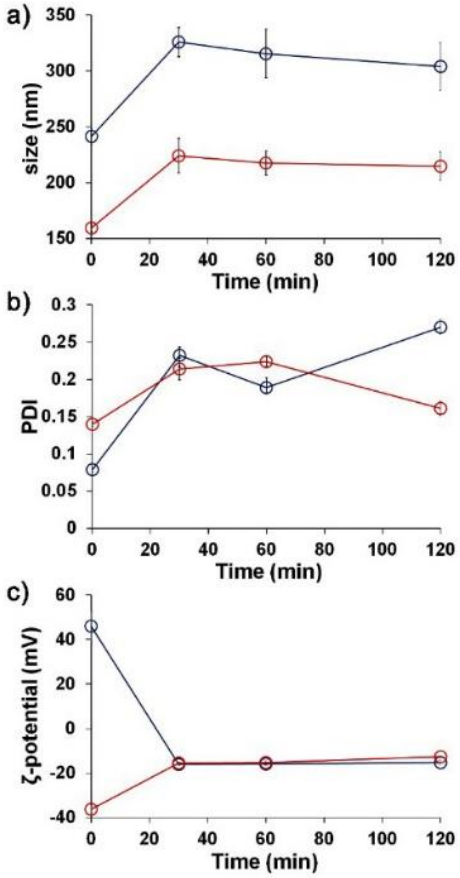

Fig. S4. Effect of human plasma protein adsorption on (a) the average hydrodynamic diameter, (b) PDI and (c) ζ-potential of THCpSiNPs (red line) and PEI/siRNA/THCpSiNPs (blue line) as a function of time.

Tong et al. J Nanobiotechnol (2018) 16:38
https://doi.org/10.1186/s12951-018-0365-y

Journal of Nanobiotechnology

RESEARCH

Open Access

Delivery of siRNA in vitro and in vivo using PEI-capped porous silicon nanoparticles to silence MRP1 and inhibit proliferation in glioblastoma

Wing Yin Tong[1,2,3], Mohammed Alnakhli[4], Richa Bhardwaj[2], Sinoula Apostolou[4], Sougata Sinha[2], Cara Fraser[5], Tim Kuchel[5], Bryone Kuss[4*] and Nicolas H. Voelcker[1,2,3*]

Abstract

Background: Multidrug resistance-associated protein 1 (MRP1) overexpression plays a major role in chemoresistance in glioblastoma multiforme (GBM) contributing to its notorious deadly nature. Although MRP1-siRNA transfection to GBM in vitro has been shown to sensitise the cells to drug, MRP1 silencing in vivo and the phenotypic influence on the tumour and normal tissues upon MRP1 down-regulation have not been established. Here, porous silicon nanoparticles (pSiNPs) that enable high-capacity loading and delivery of siRNA are applied in vitro and in vivo.

Result: We established pSiNPs with polyethyleneimine (PEI) capping that enables high-capacity loading of siRNA (92 µg of siRNA/mg PEI-pSiNPs), and optimised release profile (70% released between 24 and 48 h). These pSiNPs are biocompatible, and demonstrate cellular uptake and effective knockdown of MRP1 expression in GBM by 30%. Also, siRNA delivery was found to significantly reduce GBM proliferation as an associated effect. This effect is likely mediated by the attenuation of MRP1 transmembrane transport, followed by cell cycle arrest. MRP1 silencing in GBM tumour using MRP1-siRNA loaded pSiNPs was demonstrated in mice (82% reduction at the protein level 48 h post-injection), and it also produced antiproliferative effect in GBM by reducing the population of proliferative cells. These results indicate that in vitro observations are translatable in vivo. No histopathological signs of acute damage were observed in other MRP1-expressing organs despite collateral downregulations.

Conclusions: This study proposes the potential of efficient MRP1-siRNA delivery by using PEI-capped pSiNPs in achieving a dual therapeutic role of directly attenuating the growth of GBM while sensitising residual tumour cells to the effects of chemotherapy post-resection.

Keywords: Brain tumour, Gene delivery, Nanoparticles, Multidrug resistance-associated protein, siRNA, Cell proliferation

Background

Glioblastoma multiforme (GBM) is a deadly form of brain cancer with only a 5% survival rate at 5 years [1] and the age-standardised mortality rate of brain cancer in 2012 remains the same as in 1982 [2]. The mainstay of therapy is surgical resection. Factors that contribute to the deadly nature of this cancer include the invasiveness of GBM cells, and therefore residual disease, at the resection margins; the selective permeability of the blood–brain barrier (BBB), and the inherent chemoresistance in the endothelial layer at the BBB and in the GBM cells [3, 4]. As the drug fails to penetrate and accumulate, it leads to poor chemotherapy effectiveness in both consolidation and treatment of unresectable tumours.

*Correspondence: Bryone.Kuss@sa.gov.au; nicolas.voelcker@monash.edu
[1] Monash Institute of Pharmaceutical Sciences, Monash University, 381 Royal Parade, Parkville, VIC 3052, Australia[4] School of Medicine, Flinders University, Bedford Park, Adelaide, SA 5042, Australia
Full list of author information is available at the end of the article

Chemoresistance results from the expression of membrane-bound efflux transporters, such as the multidrug resistance protein (MRP) superfamily [5]. Multidrug resistance-associated protein 1 (MRP1), a MRP subtype, is a 190 kDa protein, through the hydrolysis of ATP, it actively removes substrates from cytoplasm [6]. It's overexpression in certain tumours removes drugs from cancer cells compromising treatment effectiveness [7]. Conventional drugs for GBM treatment, such as temozolomide (TMZ) and vincristine (VCR), are substrates of MRP1 which is overexpressed in brain tumours [8] and on the apical surface of endothelial cells of the BBB [9]. These drugs are transported out of the tumour and out of the intracranial space, contributing significantly to the multidrug resistant phenotype of GBM.

Inhibition of MRP1 is a strategy for chemosensitisation and this approach has been substantiated in lung carcinoma in vitro and in vivo [10]. Small molecules are discovered to target and attenuate MRP1 function in various carcinomas over the last decade [11–13]. In comparison, small interfering RNA (siRNA) are more economical, versatile and effective in specific knockdown of protein [14], however its susceptibility to degradation and incapability in penetrating cell plasma membrane are the main obstacles for translation into clinical practice [15]. Nanoparticle delivery is a way to overcome those pharmacokinetic limitations, in which we demonstrated the use of bare porous silicon nanoparticles (pSiNPs) to deliver siRNA into cells [16]. In particular, pSiNPs were used as the delivery vehicle due to their high biocompatibility and degradability, and their degradation product, silicic acid, is non-toxic and is cleared rapidly [17, 18]. The high porosity and surface area of pSiNPs enables high concentrations of therapeutics to be delivered per weight of pSiNP [19, 20]. These pSiNPs have been employed in drug delivery applications such as delivery of enzymes [21], small molecules [22], and nucleotides [23]. The release of the drug can be easily tailored by controlling the degradation rate of pSiNPs and their surface chemistry [24, 25]. Thermal hydrocarbonisation (THC) treatment is a well-established modification to improve the hydrolytic stability of pSiNPs [26–28]. Owing to the polyanionic nature of siRNA, cationic surface treatments are believed to be more favourable to retain siRNA inside pSiNP [29].

MRP1 knockdown in GBM cells in vitro using various polymeric vectors as transfection method has suggested that such anti-chemoresistance approach is viable, however, the inhibition of MRP1 in GBM tumours has not yet been established. Moreover, the side-effect of MRP1 knockdown on phenotypes of GBM cells and on other MRP1-expressing cells has not yet been investigated. Here, we studied the extend of MRP1 silencing and associated effects using siRNA delivered in pSiNPs with PEI optimised capping to control its release, and also report the effect and mechanism of this on the inhibition of proliferation of GBM cells in vitro and in vivo. At the same time, we also evaluated the side effects of MRP1 silencing in the organs that the nanoparticles may accumulate in. We anticipate that the results will provide insights into the potential of MRP1 gene therapy in GBM treatment, and unlock the door to eradication of this fatal disease.

Methods

Porous silicon nanoparticle (pSiNP) fabrication

pSiNPs were fabricated according to the previously reported procedure [23, 27] from p+ type (0.01–0.02 Ω cm) silicon wafers (Siegert Consulting Co., Aachen, Germany) by periodically etching at 50 (2.2 s period) and 200 (0.35 s period) mA/cm^2 in a solution of 1:1 hydrofluoric acid (38%):ethanol (EtOH) for 20 min. Afterwards, the porous silicon (pSi) films were detached from the substrate by abruptly increasing the current density to electropolishing conditions (250 mA/cm^2, 3 s period). The detached multilayer pSi films were then thermally hydrocarbonised under N_2/acetylene (1:1, vol.) flow at 500 °C for 15 min, and cooled down to room temperature under a stream N_2 gas. Subsequently, pSiNPs were produced by wet ball-milling (ZrO_2 grinding jar, Pulverisette 7, Fritsch GmbH, Idar-Oberstein, Germany) of the thermally hydrocarbonised pSi films in 1-decene. The completion of THC surface treatment was confirmed by FTIR analysis via the disappearance of Si-H_x species (2200 cm^{-1}) and strong signal corresponding to C–H (3000 cm^{-1}) and Si–C (770 cm^{-1}) species (Additional file 1: Figure S1). pSiNPs were harvested by centrifugation (1500×*g*, 5 min). pSiNP stock solutions were prepared in EtOH at 20 mg/ml.

siRNA loading, PEI capping and release kinetics

After pSiNP fabrication and characterisation, siRNA was loaded and particles were coated with polyetherimine (PEI). Both test siRNA (siRNA) and scramble siRNA (ctrl siRNA) were purchased from GenePharma Co. Ltd. (Shanghai, China). siRNA is complementary to mRNA sequence encoding for MRP1 (5′ GAGGCUUUG AUCGUCAAGUTT 3′), while ctrl siRNA sequence (5′ UUCUCCGAACGUGUCACGUTT 3′), lacks homology to all other genes. These siRNAs were solubilised in molecular biology grade water to make stock solutions (500 µg/ml). siRNA loading was performed by our previously established protocol [23]. Briefly, siRNA (100 µl of 500 µg/ml in water) was added to pSiNPs (250 µl of 1 mg/ml in EtOH), mixed by sonication for 1 min, then incubated overnight at 4 °C. Following the incubation, the

loaded pSiNPs were isolated by centrifugation at 5000 rcf at 4 °C then resuspended in EtOH and centrifuged two more times to wash off unbound siRNA. To cap the siRNA loaded pSiNPs with PEI, the pellet was then resuspended in 0.05% PEI of 25 kDa (Sigma-Aldrich, 408727) diluted in EtOH and incubated for 20 min. pSiNPs were centrifuged, and the pellet was washed with EtOH for three times to wash off excess PEI.

To measure the loading efficiency of siRNA into pSiNPs, siRNA concentration in the supernatant was measured at 260 nm by using a Nanodrop spectrophotometer (ND2000, ThermoFisher) and the amount of siRNA was then back calculated. The loading efficiency (%) = (the siRNA amount in loading buffer − the siRNA amount in supernatant)/(the siRNA amount in loading buffer) × 100%.

The release kinetics were determined by incubating PEI-pSiNPs/siRNA (MRP1 and ctrl) in PBS at 37 °C for 120 h. The supernatant was extracted at designated time points, and the amount released was back calculated from the absorbance measurement at 260 nm. The in vitro and in vivo treatment schedule was based on the release kinetics. The reason for conducting release kinetic assay in PBS, instead of culture medium is that quantitating siRNA released in protein containing medium is problematic owing to the masking of the RNA absorbance at 260 nm. Quantitation in PBS is reliable and its physiological relevant pH and osmolality are suitable for demonstrating the siRNA release from PEI-capped pSiNP.

To compare the siRNA knockdown efficacy and to delineate the cell phenotypes influenced by the nanoparticle of choice, lipofectamine (Invitrogen, 11668-019) was used in parallel as a delivery agent. The loading of siRNA to form a siRNA-lipid complex with lipofectamine was performed following the supplier's protocol. Briefly, siRNA was first diluted in Opti-MEM (Gibco, 51985091). It was then mixed with lipofectamine at a 1:1 ratio to form siRNA-lipid complex. All siRNA loadings were carried out immediately prior to cell exposure under sterile conditions.

Size and zeta-potential characterisation of pSiNPs

To reveal the size distribution and zeta-potential of pSiNPs, the particles were first washed and resuspended into MilliQ and sonicated for 5 min. The particles were then analysed using a Zetasizer Nano ZS (Malvern, Worcestershire, UK). The analysis was carried out at a scattering angle of 90° at a temperature of 25 °C.

TEM characterisation

Transmission electron microscopy (TEM) was done to visually examine the size and structure of pSiNPs prepared. pSiNP stock solution was first sonicated to homogenise particles. PEI-pSiNPs and pSiNPs without coating, siRNA-loaded or empty were diluted in EtOH. 10 µl of solution was spotted onto each 300 mesh Cu grid (ProSciTech Co.) and air-dried. The samples were then observed under a field-emission TEM (JEOL, JEM-2100F, Japan). The average pore size of pSiNP was determined firstly by SEM imaging freshly etched pSi film before detachment and ball milling. TEM images was taken to further confirm the pore size by measuring pores of pSiNP. The pore diameter is determined by measuring wall-to-wall distance of individual pores using ImageJ. The average was taken from 50 measurements of randomly selected particles.

Cell culture

In this study we used U87 cells of human origin that stably express cytoplasmic mCherry, a kind gift from Bakhos A. Tannous, MGH, Massachusetts, USA, and T98G cells of human origin (ATCC® CRL-1690™). Both are well-recognised model cell lines representing GBM, mCherry expressing GBM cells allow live cell imaging of nanoparticle uptake. It is documented that both cell lines demonstrate a similar cell growth rate [30]. Cell lines were maintained in Dulbecco's Modified Eagle Medium (DMEM, Sigma-Aldrich D6546) supplemented with 10% foetal bovine serum (Invitrogen), 1% antibiotic–antimycotic (Invitrogen) at 37 °C and 5% CO_2 in a humidified incubator. For lipofectamine-based siRNA delivery, Opti-MEM reduced serum medium was used in culture. For tumour xenograft inoculation preparation, 10 mM HEPES buffer (Sigma-Aldrich, H0887) was supplemented in DMEM for stabilising the pH of high confluence culture. All experiments were conducted following at least two passages after thawing cells.

For the functional inhibition assay, MK-571, the MRP1 inhibitor (a leukotriene receptor ligand), was used to determine the functional activity of MRP1 in T98G GBM cell line, followed by a Calcein-AM (Santa Cruz Biotechnology, Inc., Dallas, TX, USA) accumulation assay [31]. Calcein AM was used to measure the multidrug transporter-mediated activity. It is a non-fluorescent probe, but when it permeates the cells, it hydrolyses to a fluorescent molecule. Cells were seeded at 3×10^5 cells/well in 6 well-plates and allowed to adhere overnight. Subsequently, a total of 25 µM MK-571 was added to each well and incubated for a further 72 h. The cells were analysed at 24, 48, 72 h. At the 24 h time point, cells were incubated with 0.20 µM of Calcein AM staining solution at 37 °C. After incubation for 30 min, cell samples were immediately washed and analysed by Accuri-C6 flow cytometer (BD Accuri Cytometers Inc., USA) to determine cellular uptake of Calcein AM. The

control experiment was performed under identical conditions. 1×10^4 events were collected by flow cytometry. Cell viability was measured by trypan blue and Annexin V as described previously [32].

The cells were seeded into 6-well plates at a density of 5×10^4 cells/cm^2 and maintained in DMEM for 24 h after which the cultured cells were exposed to sterilised pSiNPs (bare/capped with PEI/loaded with siRNA) at a concentration of 0.125 mg/ml (250 µl per well of 1 mg/ml) for 24 h. After 24 h, cells were washed with sterile PBS and a second dose of pSiNPs was added (0.125 mg/ml) for another 24 h, followed by cells washed with sterile PBS then maintained in DMEM for another 24 h before harvesting for different studies.

Cellular uptake of pSiNPs

To visualise the uptake of pSiNPs in U87 cells, nanoparticles fabricated as described above, were fluorescently labelled with fluorescein-5-thiosemicarbazide. pSiNPs were first hydrosilylated to obtain an activated carboxyl group on the surface by incubating with neat undecylenic acid (UA) for 16 h at 120 °C [33]. The pSiNPs were extracted from UA via centrifugation after the reaction and washed with EtOH five times to ensure complete removal of excess UA. Next, the carboxy-functional pSiNP surface was covalently modified with fluorescein-5-thiosemicarbazide dye by means of ethyl(dimethylaminopropyl)carbodiimide (EDC)/*N*-hydroxysuccinimide (NHS) coupling reaction. EtOH was removed from UA-functionalised pSiNPs by centrifugation and the particles were rinsed with DMF twice. An 8 mM solution of EDC in anhydrous DMF was prepared and 0.2 equivalents of triethylamine were added to the solution. In the meantime, 8 mM solution of NHS was prepared in anhydrous DMF. 500 µl of each solution was removed, mixed well and added to the UA-functionalised pSiNPs, followed by addition of 1 ml of fluorescein-5-thiosemicarbazide solution (4 mM). The entire reaction mixture was allowed to react for 24 h at RT in the dark with stirring. Excess cross linking agent, dye and DMF were removed by centrifugation and the nanoparticles were copiously washed with cold water, followed by an EtOH wash and stored in EtOH. An alternative of tracking the subcellular delivery of siRNA is by loading pSiNP with FAM-labelled siRNA. However, this is not reported here since the change of physical/chemical properties of siRNA and the resulting changes in release profile is unknown.

After fluorescence labelling, pSiNPs were either coated with PEI as described above, or left uncoated. The zeta-potential, hydrodynamic size and release profile of fluorescence labelled pSiNPs/PEI capped pSiNP were unaltered. U87 cells were then exposed to these particles for 3 h, then washed three times with warm PBS to remove excess pSiNPs. Cells were cultured for another 24 h before fixation, counterstained, mounted and imaged under a confocal microscope (ELYRA super-resolution microscope, Zeiss Elyra PS.1).

Trypan Blue viability assay

A Trypan Blue exclusion assay was performed to study the effect of PEI-pSiNP delivery on the viability of cells. Briefly, U87 cells exposed to PEI capped or bare pSiNPs were washed, trypsinised, diluted, and mixed 1:1 with sterile filtered 0.4% Trypan Blue solution (T8154, Sigma). After 5 min incubation, cells were counted using a haemocytometer under a bright field microscope. The proportion of the viable cells to total cells are reported.

EdU assay of cells

The proliferation rate of U87 cells receiving siRNA delivery by lipofectamine or PEI-pSiNPs, and respective controls were assessed through pulse labelling of cells using the Click-iT EdU Imaging Kit (Invitrogen, C10337). Briefly, cells were seeded on the poly-L-lysine coated coverslips at a density of 5×10^4 cells/cm^2. At 24 h post exposure, cells were incubated with 10 mM of EdU (5-ethynyl-2-deoxyuridine) in DMEM for 1 h. Cells were then washed and fixed in 4% PFA and permeabilised in 0.5% Triton X-100 in PBS. S-phase cells, which are EdU positive, were visualised following the protocol specified by the manufacturer. All cells were counter-stained by Hoechst 33342, and mounted on a glass slide with fluorescence mounting medium (Dako, S3023). Images were taken under widefield Olympus IX83 fluorescence microscope using a 10× objective. Image analysis was done using Fiji ImageJ v.2.0.0. to automatically count nuclei with positive staining. The averaged ratio of EdU positive nuclei to the total number of cells is reported as "EdU positive nuclei proportion (%)". This directly reflects the proliferation rate of cells.

Immunofluorescence

The cells were seeded onto poly-L-lysine coated glass coverslips, in a 6-well plate, at the cell density described, and were exposed to PEI-pSiNPs with or without siRNA, or lipofectamine carrying siRNA, or left untreated. After 24 h, cells were fixed for 10 min with 4% freshly prepared PFA at room temperature, quenched with 100 mM glycine in PBS for 15 min and washed twice with PBS before permeabilisation in 0.05% Triton X-100 in PBS for 5 min at room temperature. After permeabilisation, the cells were washed twice with PBS and blocked with 3% bovine serum albumin (BSA) in PBS for 30 min at room temperature. The cells were then incubated with primary antibodies overnight, washed, and incubated

with fluorochrome-conjugated secondary antibodies for 60 min. The slides were washed in PBS then counterstained for 15 min. The primary antibody used was mouse anti-ki67 (Abcam, ab8191). The secondary antibody used was Alexa 488 goat anti-mouse (Invitrogen, A11001). Rhodamine-phalloidin (Invitrogen, R415) and Hoechst (Sigma-Aldrich, B2261) were used to counter label the actin filaments and nuclei, respectively. After washing, cells on coverslips were mounted on a glass slide. These samples were then imaged at high magnification using a confocal microscope (ELYRA Superresolution Microscope, Zeiss Elyra PS.1).

For statistical analysis, images were taken under a widefield Olympus IX83 fluorescence microscope, and counted using the image analysis technique described above. The averaged ratio of ki67 positive nuclei to the total number of nuclei was calculated, directly indicating the progression of the cell cycle.

Western blotting

To study the relative protein expression of MRP1 and cell cycle checkpoints, protein lysates were analysed by Western blotting. The cells that were exposed to PEI-pSiNPs with MRP1 siRNA or control siRNA, or siRNA delivered in lipofectamine, or left untreated were washed in warm PBS and directly lysed in a sodium dodecyl sulphate (SDS) lysis buffer (2% SDS, 50 mM Tris pH 6.8) supplemented with protease inhibitor cocktail (Sigma, P8340). Tissue samples were thawed and homogenised using Navy Bead Lysis Kits using a tissue homogeniser (Bullet Blender, BB24-AU). The protein concentration was quantified by an EZQ protein quantitation kit (Invitrogen, R3320). The proteins were then mixed with Laemmli loading buffer (BioRad, 161-0747) with β-mercaptoethanol, and boiled at 95 °C for 10 min. To analyse MRP1, proteins were electrophoresed in 10% bis-acrylamide gels, and transferred onto nitrocellulose membranes overnight. For pCdk2 and pHistone H3 analysis, electrophoresis was performed with 14% bis-acrylamide gel. Membranes were blocked with 5% (w/v) non-fat milk powder (Devondale) in PBST (0.05% Tween-20 in PBS) for 60 min, followed by washing with PBST and incubation with a primary antibody in blocking buffer overnight with rocking at 4 °C. The primary antibodies used were mouse anti-MRP1, rabbit anti-Cdk2 pTyr15, and rabbit anti-Histone H3 pSer10 (Abcam, ab24102 and ab136810, respectively). The secondary antibodies used were horseradish peroxidase conjugated Immun-Star goat anti-mouse immunoglobulin G (BioRad, 1705047) and goat anti-rabbit immunoglobulin G (Agrisera, AS09602). The membranes were washed and incubated with the secondary antibodies for 60 min. After washing, membranes were developed with Clarity™ Western ECL Substrate (BioRad, 1705061) and imaged by using a Chemi-Doc with a cool CCD camera (Syngene, G:BOX Chemi XRQ). Expression was measured by densitometry analysis of the bands using Fiji ImageJ, deducting the background intensity, and normalised to the integrated density of the β-actin housekeeping protein band. Knockdown efficiency was calculated as test group/control group x 100%.

To illustrate the distribution of the cell cycle population upon exposure to PEI-pSiNPs with MRP1 siRNA, cells were analysed using flow cytometry, and a histogram of DNA content plotted. Briefly, the exposed cells were trypsinised, PBS rinsed, and fixed dropwise in 100% ethanol. The cells in single cells were rinsed and stained with PI (50 μg/ml), and subsequently analysed using ImageStream flow cytometer (Amnis). Cell populations is gated and measured using Amnis software.

Mice tumour model

To assess the siRNA delivery, MRP1 knockdown and its subsequent influence on the proliferative state, and the effect of knockdown on distal organs, a subcutaneous xenograft tumour model was established using nude mice. Animal procedures were performed according to a protocol approved by South Australian Health & Medical Research Institute Animal Ethics Committee (Approval number, SAM#98). U87 cells were trypsinised, washed with warm PBS and counted. 5×10^6 cells in chilled PBS were then mixed 1:1 with Matrigel (E1270, Sigma) to a total volume of 100 μl. CD-1 nude mice of mixed gender, between 6 and 8 weeks of age, were then subcutaneously inoculated with the prepared cells on both flanks. Food and water were provided ad libitum, and since CD-1 nudes are immunocompromised, they were housed in individually-ventilated cages (IVC). On week 4 post-inoculation, mice bearing tumours reaching 250 mm^3 were paired into groups to receive either pSiNPs/Saline, pSiNPs/ctrl siRNA, or pSiNPs/siRNA (MRP1). Each group and time point contained at least two mice, each bearing (four tumours total per treatment). No statistical difference in tumour size was observed between the groups (data not shown). Each group of mice received 2 intravenous doses delivered 24 h apart. Each mouse received 31.25 mg/kg of pSiNPs loaded with siRNA, or the same amount of unloaded pSiNPs, per dose. Mice were humanely killed at 24, 72 h post-treatment. Tumours, kidneys and duodenums were harvested. For histological analysis, tissues were immediately fixed in neutral buffered formalin (NBF, Sigma-Aldrich) at 4 °C for 2 d, followed by paraffin embedding. For protein level analysis, tissues were immediately cut into small cubes, 1 mm^3, immersed in SDS sample buffer, and snap-frozen. For mRNA level analysis, tissues were immersed

into RNAlater (AM7023, ThermoFisher) and stored at −20 °C.

Quantitative real time-polymerase chain reaction (qRT-PCR)

MRP1-mRNA silencing was studied using a BioRad CFX Connect QRT-PCR detection system with a SYTO9 reagent to detect the level of MRP1-mRNA expression. In summary, tissue sections were homogenised using TRI Reagent® (Sigma-Aldrich) (1 ml per 50–100 mg of tissue). TissueLyser II Qiagen (QIAGEN®, Hilden, Germany) was used to disrupt and homogenise tissue. Total mRNA was extracted using TRI Reagent, according to the manufacturer's protocol. cDNA was synthesised from mRNA using M-MLV H (−) reverse transcriptase (Promega Corporation, Alexandria, NSW, Australia). The coincident measurement of the "housekeeping" gene glyceraldehyde-3-phosphate dehydrogenase (GAPDH) was used to control the experimental variations of RNA and to normalise the MRP1-mRNA expression data, which was calculated using the ΔΔCt method. The primers were designed via the web tool (http://www.ncbi.nlm.nih.gov). All primers used for QRT-PCR of MRP1-mRNA are shown in Table 1.

Immunohistochemistry

Histological sections were immunohistochemically stained to visualise the MRP1 expression and to study the proliferative state of the tumours. Microtome sectioned tissue specimens of 5 µm were dehydrated at 50 °C overnight, followed by deparaffinisation and rehydration. Rehydrated slides were first incubated in sodium citrate buffer pH 6 at 95 °C for 30 min for antigen retrieval and cooled down to room temperature. For ki67 staining, slides were additionally incubated with 0.1% Triton X-100 in PBS for 10 min to permeablise the nuclear envelope. Slides were then incubated in 1% H_2O_2 for 15 min to quench endogenous peroxidase activity, followed by serum blocking for 1 h. Goat anti-mouse IgG Fab (Abcam, ab6668) was added for 1 h to block endogenous IgG. After washing in PBST, slides were incubated with primary against ki67 (Abcam, ab8191) or primary against MRP1 (Santa Cruz, sc-18835) overnight in a moisture chamber at 4 °C. Slides were then incubated with biotinylated mouse-rabbit polyvalent secondary (Abcam, ab64264), followed by streptavidin peroxidase (Abcam, ab64264) incubation. After washing, slides were developed using 3,3′-diaminobenzidine (DAB) substrate for 15 min then counterstained with Mayer's haematoxylin QS (Vector, H-3404), and eventually mounted in coverslips with DPX.

Table 1 Sequences of the primers used in qRT-PCR analysis

Primer ID		
MRP1_Human	Forward	5′→ AAGGAATGCGCCAAGACTAG → 3′
	Reverse	5′→ CCTTAAACAGAGAGGGGTTC → 3′
GAPDH_Human	Forward	5′→ GTGAAGGTCGGAGTCAACGG → 3′
	Reverse	5′→ TGGAGGGATCTCGCTCCTGG → 3′
MRP1_Mice	Forward	5′→ TGCAGAGGCATCTCAGCAACTC → 3′
	Reverse	5′→ TTCGGCTATGCTGCTGTGTT → 3′
GAPDH_Mice	Forward	5′→ CGACTTCAACAGCAACTCC-CACTCTTCC → 3′
	Reverse	5′→ TGGGTGGTCCAGGGTTTCTTACTC-CTT → 3′

Hematoxylin and Eosin (H&E) staining

To study the side-effect of MRP1 knockdown in distal organs, kidney and duodenum were excised and sectioned for histological characterisation. Deparaffinised and rehydrated sections were stained with Lillie-Mayer's H&E (Australian Biostain P/L) following standard protocols. H&E and immunohistological stained tissue sections were imaged using a bright-field microscope.

Statistics

Experiments were conducted in triplicate unless otherwise stated. Error bars presented in charts equal ± 1 standard deviation (SD). Statistical differences were tested by non-parametric Kruskal–Wallis 1-way ANOVA test. The hypothesis was accepted at a 95% significant level ($p < 0.05$).

Results

Characteristics of pSiNPs and siRNA release from pSiNPs

pSiNPs were fabricated as a vehicle to deliver siRNA for MRP1 silencing. The cellular uptake and biodistribution of the siRNA loaded pSiNP is dependent on the size and surface characteristics [34]. Their size, pore structure and colloidal stability were characterised by means of TEM, dynamic light scattering (DLS), and a zeta-potential analyser. TEM images show that plate-shaped pSiNPs were successfully fabricated at the desired size of approximately 110 nm (Fig. 1a). These particles contained pores of approximately 15 nm in size. The achieved pore dimensions were suitable for loading siRNAs, which are approximately 7.5 nm long and 2.5 nm wide [35, 36]. Judging from TEM images, there was no observable difference in size between PEI-coated and non-coated pSiNPs. The hydrodynamic diameter distribution of these particles was further analysed using DLS in aqueous media (Fig. 1b). This confirmed that particle size distribution was small, where 70% of pSiNP sized

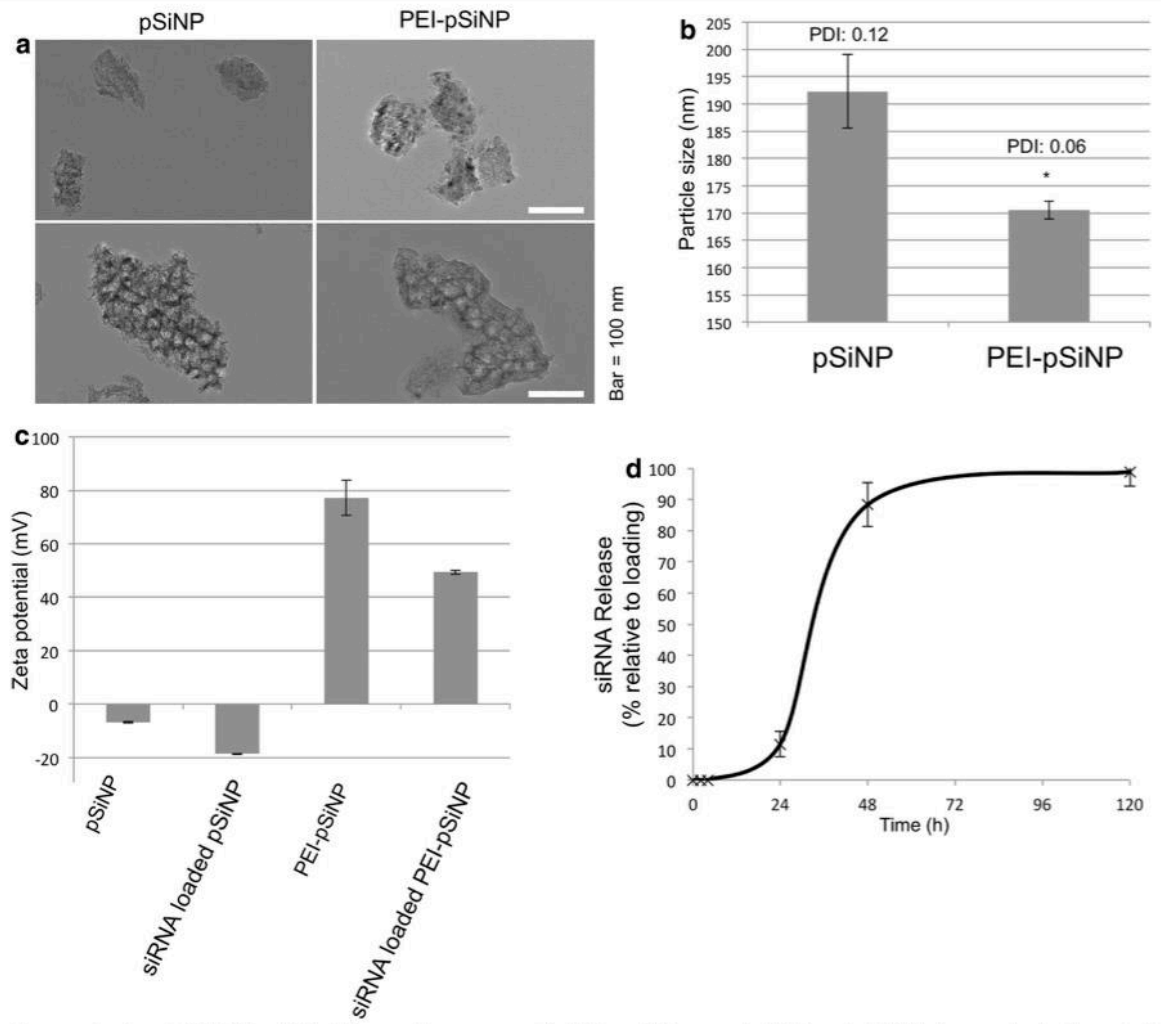

Fig. 1 Characterisation of pSiNPs for siRNA delivery. **a** The structure of pSiNPs and PEI-capped pSiNPs under TEM. **b** Average hydrodynamic diameter in MilliQ. **c** Zeta potential of empty pSiNPs and pSiNPs loaded with siRNA. **d** siRNA release kinetics of PEI-coated pSiNPs. (*n* = 3; *mean* ± *standard deviation*; **p* < 0.05)

between 186 and 198 nm (PDI: 0.12), and 70% of PEI-pSiNP sized between 169 and 173 nm (PDI: 0.06). The PEI-pSiNPs were statistically smaller than the uncoated pSiNPs, and this was attributed to the improved colloidal stability of PEI-pSiNPs in an aqueous medium. To investigate this phenomenon further, we determined the surface zeta potential of pSiNPs. Fabricated pSiNP had a slightly negative zeta potential of −7 mV (Fig. 1c). As expected, PEI-capped pSiNPs had an overall positive charge, with zeta-potential reaching 80 mV. Loading with siRNA resulted in both types of particles becoming more negatively charged with −20 and 50 mV in pSiNPs and PEI-pSiNPs, respectively. Nanoparticles with a zeta-potential of more than ±30 mV are predicted to be colloidal stable [37, 38], which explains the higher stability of PEI-pSiNPs.

Based on the colloidal stability and the advantage in facilitating cellular uptake, we chose PEI-capped pSiNPs for further study. siRNA was loaded into pSiNPs and capped with PEI, and the loading efficiency was calculated as 70 ± 9%, effectively carrying 23 µg of siRNA per 250 µg of PEI-pSiNPs. This loading capacity is much higher than pSiNP loading documented without cationic PEI capping, which was only 1.75 µg per 250 µg of pSiNPs [16]. The release of siRNA in PBS was followed for up to 120 h (Fig. 1d). Substantial siRNA release was observed between 24 and 48 h, where 70% siRNA was released within this period. The release plateaued from 72 h onwards. These kinetics indicated a suitable release profile that allowed uptake and accumulation of PEI-pSiNPs in tumours before releasing most of the siRNA [39].

Intracellular siRNA delivery by pSiNPs

After confirming that the surface chemistry and siRNA release profile of PEI-pSiNPs were suitable, pSiNPs were fluorescently labelled and exposed to the U87 GBM cell line to characterise cellular uptake. As anticipated, greater uptake was observed for positively charged PEI-capped pSiNPs as compared to uncapped pSiNPs (Fig. 2a). Although PEI-capping benefits the loading, favourable release profile, and cellular uptake, it is essential that the nanoparticle delivery by itself is biocompatible to cells. The viability of U87 cells exposed to both types of pSiNPs by Trypan Blue exclusion showed no significant difference between untreated cells and cells exposed to pSiNPs or PEI-pSiNPs (Fig. 2b). This indicate that the cytotoxicity of PEI-capped pSiNPs is minimal and that these particles are fairly biocompatible.

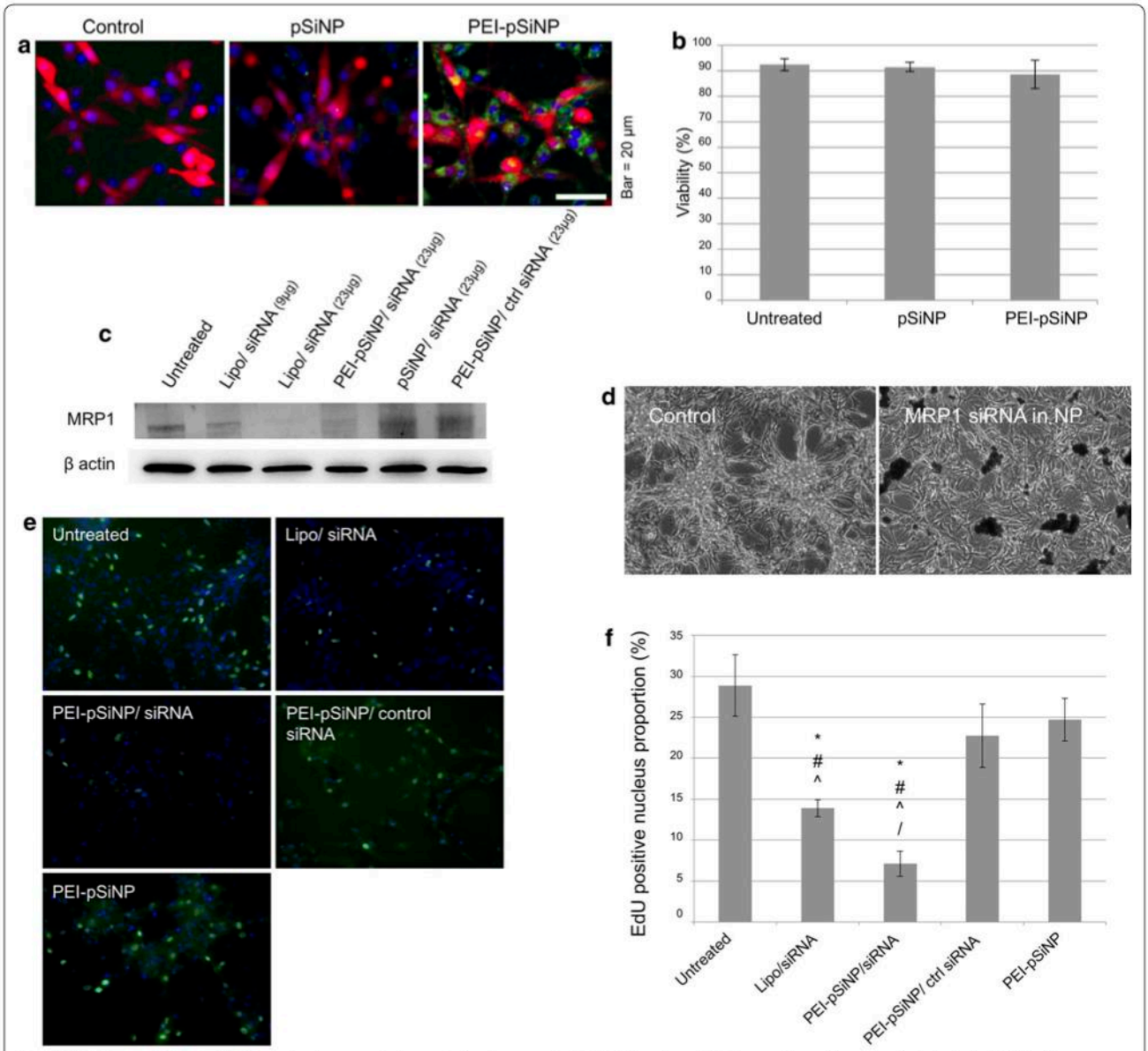

Fig. 2 Cellular uptake of pSiNPs and subsequent phenotypic changes in U87 GBM cells. **a** Cellular uptake of fluorescein labelled pSiNPs. Green: pSiNPs; red: cytoplasmic mCherry; blue: nucleus. **b** The viability of U87 cells exposed to pSiNPs measured by Trypan Blue exclusion assay. **c** MRP1 expression in U87 cells exposed to siRNA via lipofectamine (Lipo/siRNA) or nanoparticle (pSiNP) delivery by immunoblotting. **d** Phase contrast image of U87 cells exposed to PEI-pSiNPs carrying MRP1 siRNA and untreated at day 3 post-exposure. **e** The proliferation of U87 cells as measured by EdU labelling of cells in S-phase. Green: EdU positive nuclei; Blue: nuclei. **f** Quantitation of S-phase cell proportions. (*, #, ^, / $p < 0.05$ *as compared to untreated, PEI-pSiNPs/ctrl siRNA, PEI-pSiNPs and Lipo/siRNA, respectively*)

In vitro MRP1 silencing

Next, we employed PEI-pSiNPs to deliver MRP1 siRNA into U87 cells to study downregulation of MRP1 via immunoblotting. For comparison, we used lipofectamine(Lipo)-based transfection. Results illustrate that the MRP1 expression was downregulated in cells transfected with MRP1 siRNA as compared to untreated controls, with 51 and 30% downregulation in Lipo/siRNA (23 μg siRNA) and PEI-pSiNP/siRNA (23 μg siRNA) treated cells, respectively (Fig. 2c). In contrast, control siRNA delivered via PEI-pSiNPs did not knock down MRP1 in U87 cells, ruling out non-specific effects of the siRNA and of its delivery system. Additionally, the extent of downregulation was dependent on the concentration of siRNA delivered as the cells receiving less Lipo/siRNA (9 μg) expressed more MRP1 as compared to 23 μg delivered via lipofectamine and PEI-pSiNPs (Fig. 2c). To demonstrate the effect of MRP1 downregulation by PEI-pSiNPs/siRNA on drug efflux, we exposed U87 cells to either DOX, or PEI-pSiNPs/siRNA, or co-treatment, or left untreated. Result showed that MRP1 silencing using PEI-pSiNP/siRNA sensitised U87 cells to DOX (Additional file 2: Figure S2). This indicates PEI-pSiNPs delivering MRP1 siRNA is a viable approach to reduce chemoresistance.

Prolonged culture of U87 cells transfected by PEI-pSiNPs/siRNA for 2 more days, resulted in an observable reduction in total cell population as seen in a representative phase contrast image (Fig. 2d). However, such effect of MRP1 on cancer cell growth has not been well documented. We speculated that MRP1 knockdown attenuates cell proliferation in parallel to chemosensitisation. To quantitatively study cell proliferation, U87 cells transfected with siRNA were pulse-labelled by EdU to identify the population of U87 cells that entered S-phase of the cell cycle at a given time (Fig. 2e). Significantly less EdU positive nuclei were observed in Lipo/siRNA and PEI-pSiNP/siRNA treated cells as compared to untreated or PEI-pSiNP/ctrl siRNA treated cells (Fig. 2f). Although there was also a reduction in proliferation rate in PEI-pSiNP and PEI-pSiNP/ctrl siRNA treated cells as compared to untreated cells, this effect was not significant ($p=0.127$). In particular, the EdU proportion of cells receiving siRNA delivered by PEI-pSiNPs was significantly lower than for cells receiving siRNA in lipofectamine ($p=0.034$). Collectively, these results indicate a decrease in proliferation rate of GBM cells with MRP1 knockdown by siRNA, which this effect was independent of the siRNA delivery method.

MRP1 functional inhibitor MK-571

To further elucidate the role of MRP1 in GBM cell proliferation, we exposed them to the functional inhibitor MK-571 which attenuates transmembrane transport of MRP-specific ligands. Unlike MRP1 siRNA, MK-571 did not inhibit the translation of MRP1 proteins. It was observed that exposure of cells to 25 μM MK-571 was sufficient to suppress cell growth without causing cell death (Fig. 3a, b). The inhibition of MRP1 transmembrane transport by 25 μM MK-571 was assessed by monitoring the export of intracellular Calcein AM, a fluorescent dye that is a substrate of MRP1, from GBM cells [40]. When MRP1 is functionally active in the cell, Calcein AM is exported by MRP1 as an indicator of its transporter function. We observed that the cells treated with MK-571 exhibited greater fluorescence signals from Calcein AM than untreated cells, indicating accumulation of Calcein-AM as a result of MRP1 inhibition (Fig. 3c, d).

Decrease in proliferation rate and cell cycle arrest

We further studied the proliferation of U87 cells under MRP1 silencing by monitoring the expression of Ki67, which plays an important role during mitosis, and hence serves as a marker for cell proliferation [41]. For all treatment groups, Ki67 expression in the nucleolus and chromosomes was observed during interphase and mitotic phase, respectively (Fig. 4a). However, the ratio between the Ki67 positive nuclei and the total population of nuclei was significantly reduced in Lipo/siRNA and PEI-pSiNP/siRNA treated U87 cells as compared to untreated controls, but not in PEI-pSiNP/ctrl siRNA ($p=0.275$) and PEI-pSiNP treated cells ($p=0.127$) (Fig. 4b). This is consistent with the observed reduction of EdU labelling and confirms that the reduced proliferation rate of U87 cells can be attributed to MRP1 knockdown.

This observation prompted us to study the effect of MRP1 silencing on cell cycle progression of U87 cells by probing the activation of cell cycle regulatory kinases. The elevated abundance of phosphorylated cyclin-dependent kinases 2 (pCdk2) and histone H3 (pHH3) in U87 cells implicate cells arresting at G1/S, and G2/M, respectively [42, 43]. By means of Western blot, we observed that the abundance of pCdk2 was higher in Lipo/siRNA and PEI-pSiNPs/siRNA treated U87 cells than for untreated cells by a factor of 2 and 1.8, respectively. The abundance of pHH3 was similar among the groups (Fig. 4c). Treatment with pSiNPs/siRNA and PEI-pSiNPs/ctrl siRNA resulted in only a slight pCdk2 elevation as compared to untreated cells by a factor of 1.2. Since the inhibitory phosphorylation on Cdk2 is maximal during G1/S [42], the elevated abundance of pCdk2 may suggest that the observed halt in proliferation is related to cells arresting at G1/S. A histogram of DNA content generated from flow cytometry also illustrates an increase in G1 cell population (from 34 to 56%), and a decrease of G2/M population (from 33 to 15%) upon MRP1 knockdown via PEI-capped pSiNP

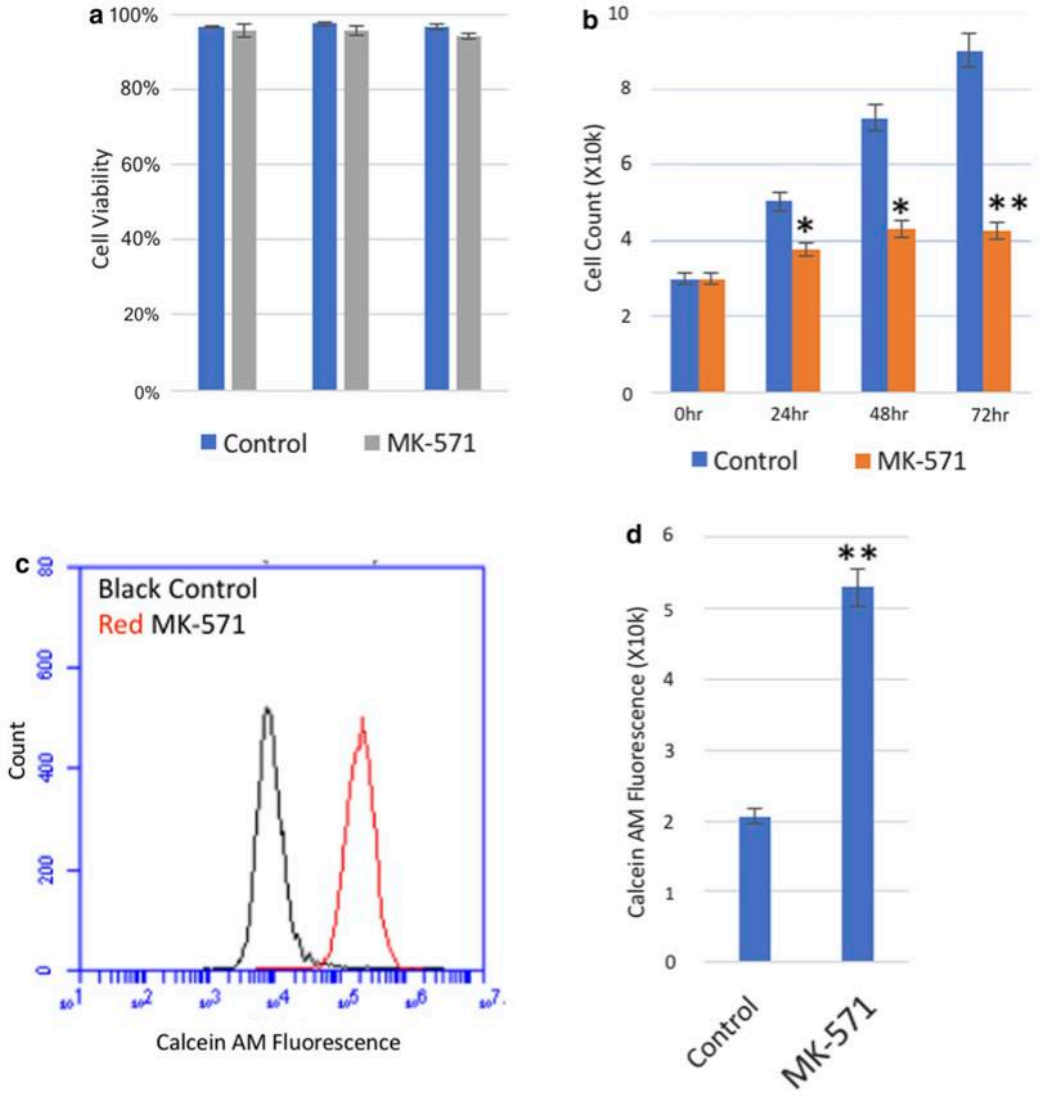

Fig. 3 Functional inhibition of MRP1 transmembrane transport and GBM cell proliferation. T98G was treated with 25 μM of MK-571 for 72 h and untreated cells were used as a control. **a** The cell viability was measured by the Annexin-V assay and **b** cells were counted using the Trypan Blue assay. **c**, **d** At the 24 h time point, cells were incubated in 0.20 μM of Calcein AM staining solution at 37 °C. After incubation for 30 min, cell samples were immediately washed and analysed by flow cytometry to determine cellular uptake of Calcein AM. (*$p < 0.0329$, **$p < 0.0023$ *compared to untreated*) ($n = 4$; *mean* ± *standard deviation*)

siRNA delivery (Fig. 4d). Collectively, the observed cell cycle arrest aligns with the results of cell cycle checkpoint proteins expression, EdU and Ki67 studies, which indicate an obvious reduction in cell proliferation upon MRP1 downregulation.

MRP1 knockdown and proliferative state in tumours

The relationship between GBM proliferation and MRP1 downregulation was further investigated in a tumour bearing mouse model. CD-1 nude mice were subcutaneously (S.C.) inoculated with U87 cells, and the tumour growth kinetics were characterised (data not shown). Once the tumours reached a minimum size of 250 mm^3, mice were treated with PEI-pSiNPs carrying either siRNA, ctrl siRNA, or saline intravenously for two consecutive days (2 mice and 4 tumours per group). mRNA extracted from tumours dissected at selected time points was analysed quantitatively for MRP1 expression. According to qRTPCR data, a reduction of MRP1 mRNA was observed at 48 and 72 h post-treatment, with the greatest reduction being 40% at 48 h (Fig. 5a). The expression began to recover between 48 and 72 h, reaching approximately 90% at 72 h. Reduction of MRP1 was also observed by immunoblotting at the protein level,

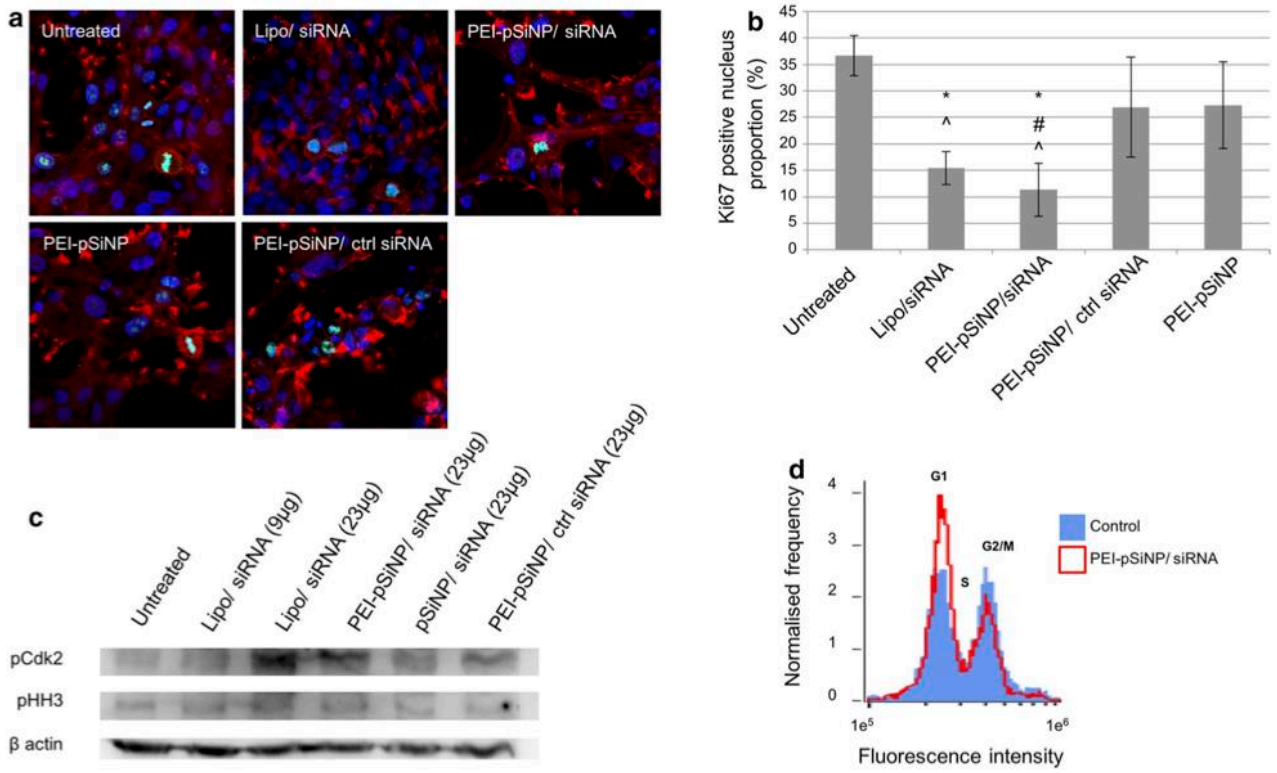

Fig. 4 Effect of MRP1 silencing on the proliferative state of U87 cells. **a** Immunofluorescence of Ki67 imaged with confocal microscopy. **b** Quantitation of Ki67 positive cell proportion. (*, #, ^ *p* < 0.05 *as compared to untreated, PEI-pSiNPs loaded with ctrl siRNA, and PEI-pSiNPs, respectively*) (*n* = 3, *mean* ± *standard deviation*). **c** Distribution of cells in G1/S and M phases as indicated by relative expression of phospho-tyr15 Cdk2 and phospho-ser10 histone H3 revealed by immunoblotting. **d** Distribution of cell cycle populations as illustrated by DNA content histogram

consistent with gene expression level. The protein expression of MRP1 in tumours observed at 48 and 72 h post-treatment with PEI-pSiNPs/siRNA was reduced, by 82 and 65%, respectively, compared to the levels observed in tumours treated with PEI-pSiNPs delivering control siRNA (Fig. 5b). This demonstrates that the PEI-pSiNP successfully delivered siRNA to the tumour and yielded significant MRP1 knockdown.

To further evaluate the siRNA delivery and knockdown in vivo, we histologically compared the MRP1 protein distribution in tumours receiving PEI-pSiNPs/siRNA and control treatments. Immunohistochemical images correspond with qRTPCR and immunoblotting results, demonstrating a general downregulation of MRP1 in PEI-pSiNP/siRNA treated mice as compared to controls (Fig. 5c). Downregulation of MRP1 was also observed in mouse epidermis and dermis above the S.C. tumour in mice receiving MRP1 siRNA but not in control animals (Fig. 5c, arrows). Within the tumours, there was variation in downregulation of MRP1. Less MRP1 expression was seen in the GBM cells adjacent to the dermis, where blood vessels are abundant, while downregulation was less effective on the side adjacent to the peritoneum (Fig. 5c, squares). This gradient may reflect the penetration profile of PEI-pSiNPs into solid tumours.

The use of an untargeted delivery by nanoparticles allows investigation of the collateral downregulation of MRP1 in distal organs. We harvested kidney and duodenum, which also express MRP1 at physiological levels [44, 45]. qRT-PCR result suggested that the reduction of MRP1 mRNA in the kidney reached as much as 60% at 48 h post MRP1 siRNA treatment, and 55% ($n = 2$) at 72 h (Fig. 5d). The reduction in the duodenum was even more pronounced, being 80% ($n = 2$) at 48 h, with no recovery observed after 72 h post-treatment (Fig. 5e). Therefore, we conclude that MRP1 siRNA delivered in non-targeted nanoparticles, PEI-pSiNPs in this case, induces MRP1 knockdown in kidney and duodenum.

Ki67 expression in GBM tumours was also examined to study the proliferation potential of GBM cells experiencing MRP1 knockdown. Consistent with the in vitro results, Ki67 expression in the tumours of PEI-pSiNP/siRNA treated mice was reduced compared to controls (Fig. 5f). Such reduction in Ki67 was observed at both 48 and 72 h post-treatment, indicating that the proliferation retardation was sustained after nascent MRP1 mRNA,

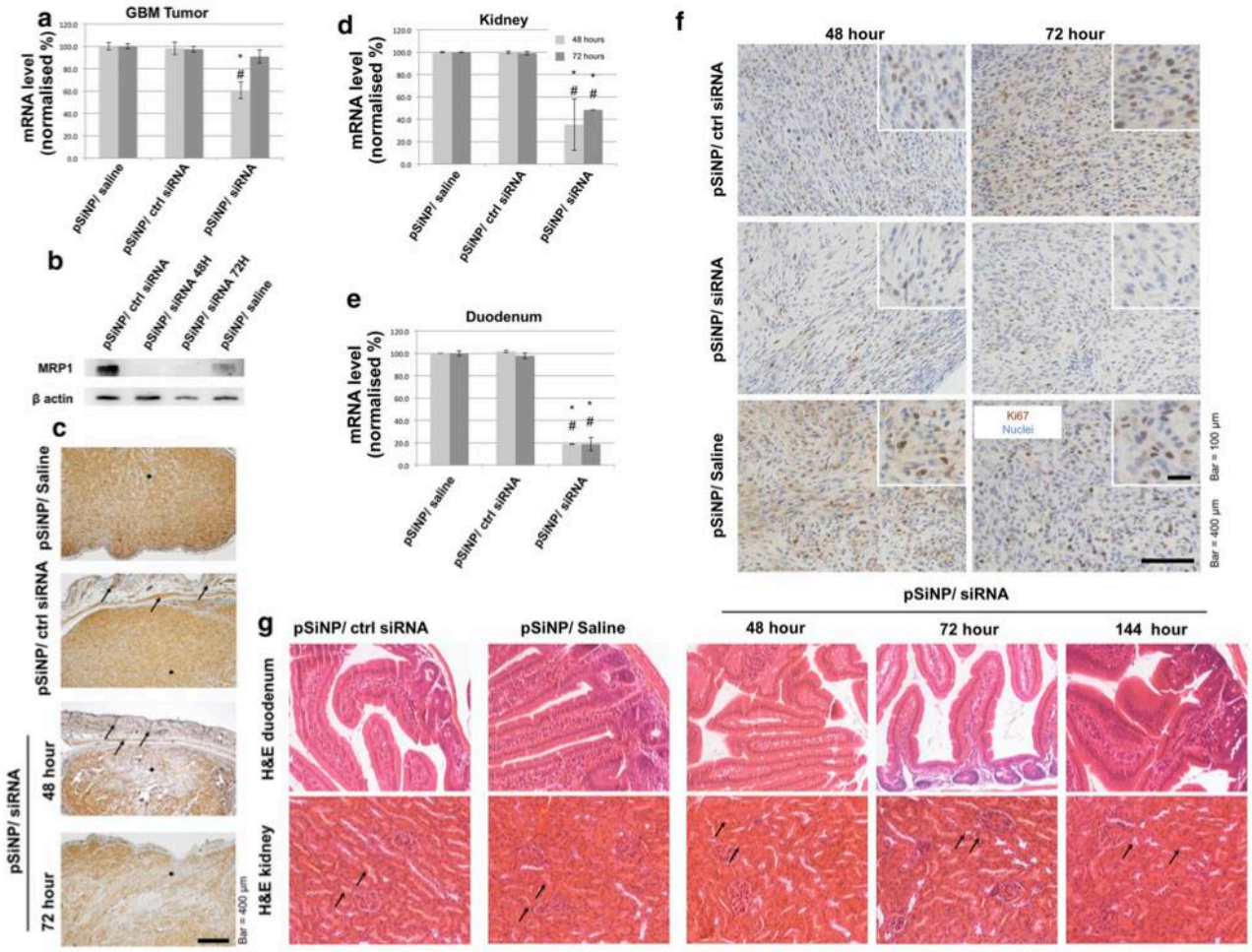

Fig. 5 Effect of MRP1 silencing in vivo. MRP1 mRNA and protein expression level in tumours of mice being treated with siRNA-loaded PEI-pSiNPs at 48 and 72 h post-injection (intravenous) as revealed by **a** qRTPCR ($n=4$), **b** immunoblotting, and **c** immunohistochemistry. MRP1 mRNA expression level in **d** kidney ($n=2$) and **e** duodenum ($n=2$). **f** Immunohistochemistry of Ki67 expression in the tumour to reveal the proliferative state of U87 cells in mice receiving different treatments. **g** H&E staining of kidney and duodenum of mice treated with PEI-pSiNPs with MRP1 siRNA or ctrl siRNA, or none, revealing the histopathology of MRP1 downregulation in distal organs over 144 h (6 d) post-injection. (*, #$p < 0.05$ *as compared to controls pSiNPs/saline and pSiNPs/ctrl siRNA, respectively*)

and protein levels started to restore. A longer time point analysis will be performed in future studies.

Histopathology of MRP1 expressing organs

Since there is no definite conclusion to date as to the function of MRP1 in organs physiologically expressing MRP1, we performed histopathology analysis on the kidney and duodenum, in which MRP1 was shown to be collaterally downregulated, for signs of acute necrosis. The histological sections representing 48 h up to 144 h post-treatment were H&E stained. Histological analysis of kidney was focused on signs of acute tubular necrosis, which have been reported for nanotoxicity [46]. There were no observable differences between kidneys receiving ctrl-siRNA and MRP1-siRNA. All of them show no damage to endothelial cells, nor was an eosinophilic staining pattern or pyknosis of nuclei observed around proximal and distal convoluted tubule (Fig. 5g, arrows), indicating the absence of damage to tubular cells [47]. In the duodenum, we did not observe accumulation of lymphocytes in villi of both the controls and MRP1 silenced groups at all the time points. Neither did we observe differences in the population of goblet cells. These results indicate that there was no sign of acute duodenitis [48].

Discussion

MRP1 expression has been identified in a variety of tumours and is being comprehensively studied as a therapeutic target for chemosensitisation. Various modulators have been pursued over the last two decades [11, 12].

Combination therapy has already shown effectiveness in vitro and in vivo in lung carcinoma [10] and breast cancers [49]. Clinical trials exploring MRP1 knockdown with a small molecule modulator in patients with breast, lung, bowel, melanoma, renal and ovarian cancers are ongoing [50].

GBM remains poorly treated, therefore exploring the promise and effect of MRP1 downregulation using a nanoparticle delivery approach has merit. To date, there are only a handful of reports based on in vitro trials. For example, patient derived GBM cells were chemosensitised in vitro using an MRP1 inhibitor [13]. A study by Tivnan et al. tested chemosensitisation with GBM cells derived from relapsed patients, demonstrating some effectiveness in this setting [8]. Additionally, various nanoparticle delivery systems, including ours, have been developed to deliver modulators of MRP1 in glioma cells [51, 52]. However, in vivo effectiveness and effects on other cells remains to be investigated. Although the correlation between MRP1 expression and more aggressive phenotype of cancer has been observed [53], phenotypic effects of the knockdown of MRP1 remain unknown.

In this study, we used PEI-capped pSiNPs as a siRNA delivery vehicle in vitro and in vivo in order to study the knockdown and phenotypic changes, both in tumour and collateral organs. The reason for choosing the pSiNP delivery vehicle for MRP1 siRNA is due to a number of inherent desirable properties including high loading capacity, biodegradability and biocompatibility. Furthermore, we have previously documented the successful in vitro knockdown of MRP1 with siRNA delivered using pSiNPs [16, 23]. The PEI-pSiNPs in this study were of an average size of 170 nm, smaller than the average size of tumour vasculature ranging from 380 to 780 nm [54]. Additionally, nanoparticles at 100 nm range have generally proven to be long-lasting in the circulation [34]. We optimised the release profile for in vivo delivery through optimising the pSiNP capping and washing procedure. The percentage siRNA released after 24 h was found to be only 10%, while 80% of the siRNA was released between 24 and 48 h. In view of previous studies that have shown PEI nanoparticles, such as JetPEI, to facilitate distribution to the respective organs at 24 h [39], we believe that the release profile of the PEI-pSiNPs used here would prevent immature burst release, and thus deliver most of the siRNA into the tissues. As compared to other reported nanoparticles of comparable size, chitosan nanoparticles showed siRNA burst release before 24 h with only 10% siRNA being released between 24 and 48 h [55], whilst for PLGA nanoparticles release of 50% of the loaded amount was reported before 24 h, and only 10% was released between 24 and 48 h [56].

The superior siRNA retention for the first 24 h is thought to be due to the electrostatic interaction between PEI and siRNA and the packing of the siRNA into the pores of the pSiNPs [57]. The PEI capping also facilitated an obvious improvement of cell uptake in GBM cells as expected. Whilst the risk of cytotoxicity associated with branched PEI gene delivery due to the charge density has been a concern for clinical translation [58], cytotoxicity was not observed with our pSiNP delivery. This is consistent with our previous study in terms of a lack of observable apoptotic and cytotoxic phenotypes [32]. Although the mechanism of such diminished toxicity remains unclear, a similar observation was reported by Yuen Shan et al., who evaluated PMMA nanoparticles coated with branched 25 kDa PEI for gene delivery and showed efficient transfection and low cytotoxicity [59].

MRP1 protein expression was downregulated with MRP1 siRNA but not with the scrambled siRNA sequence, indicating specific MRP1 effects. While the knockdown efficiency of siRNA delivered with lipofectamine (51%±4%) was observed to be higher than that of PEI-pSiNPs (30±9%) in vitro, 30% of downregulation was found to be sufficient to sensitise U87 cells to doxorubicin and reduce the viability by 70% as compared to exposure to doxorubicin only. While this level of downregulation is comparable to our previous in vitro study [16], the delivery vehicle used here did not cause cytotoxicity by itself, indicating that it is potentially applicable for systemic delivery.

The consistent decrease in total cell counts in MRP1 siRNA transfected U87 cells, without an increase in apoptotic cell death was further investigated. We demonstrated that the proliferation of GBM cells was proportional to MRP1 expression level by means of an EdU incorporation assay and Ki67 immunofluorescence, indicating that U87 cells have a much slower proliferation rate when MRP1 is silenced. Similar studies of MRP1 downregulation in neuroblastoma cells using antisense expression vectors revealed spontaneous cell death and a reduction in cell proliferation [60, 61]. For ovarian carcinoma cells, Mahdizadeh et al. characterised the effect of saffron extract-crocin exposure and observed both MRP1 silencing, cytotoxicity, and a reduction in cell proliferation [62]. However, the mechanism of the observed proliferation retardation in those cancer types was not further investigated. In contrast, we observed no glioma cell death upon transfection.

Here, the cell cycle arrest at G1/S observed in GBM was demonstrated to be associated with MRP1 silencing by determining the relative abundance of phosphorylated Cdk2 and the increase in G1 cell population. This observation differs from multidrug transporter P-glycoprotein (Pgp) knockdown, which was shown to cause cell cycle

arrest at G2/M in leukaemia cells with apoptosis induction [63]. Since MRP1 and Pgp transport different substrates across the plasma membrane [64], we speculate that the effect of MRP1 knockdown on proliferation is mediated through the inhibition of transmembrane trafficking. The functional inhibition of MRP1 using MK-571 also resulting in attenuation of proliferation appears to support such speculation.

Since PEI-pSiNP delivery of siRNA is a biocompatible and versatile platform, it allowed us to characterise the MRP1 knockdown approach and to validate the decrease in proliferation of GBM in vivo. We demonstrated that the siRNA delivery resulted in MRP1 downregulation at both mRNA and protein level. The observed siRNA-induced knockdown indicates that the siRNA was delivered into the cytoplasm where it forms RNA-induced silencing complex (RISC) with the complementary mRNA before the translation [65]. Hence, it can be concluded that the PEI-pSiNPs successfully accumulated and delivered the siRNA into the subcutaneous xenograft GBM tumour.

The MRP1 downregulation was observed throughout most of the tumour under histological study, indicating that the size of PEI-pSiNPs (~ 170 nm) was generally able to penetrate the GBM tumour mass and deliver the payload. The penetration of nanoparticles into solid tumour depends on the size and surface chemistry of the nanoparticles, and also the architecture of the tumour [66]. Although S.C. tumours do not replicate the complexity of orthotropic GBM, such as the requirement to transverse the BBB, our results serve as the first step translating the promise of the MRP1 silencing approach reported based on in vitro studies under GBM-specific in vivo tumour microenvironment. For example, this approach could be promising for coating the resected bed of the tumour at the completion of surgery and to use an Omaya reservoir for MRP1-siRNA delivery to minimise GBM recurrence through its anti-proliferative and chemosensitising properties, since the BBB is not intact at glioblastoma progression, and at post-surgery [67–69].

For the effectiveness of the delivery to early stage of glioma, where the BBB is intact, such approach remains to be further optimised and evaluated in suitable orthotropic models.

It has been reported that the expression of Ki67 in brain cancers correlates with histological malignancy grade in all glioma subtypes [70]. It is also clinically accepted that Ki67 generally reflects the cancer aggressiveness, as its function is closely linked to cell division [41]. The diminished Ki67 positive proportion in tumours of the mice receiving PEI-pSiNPs/siRNA indicates that MRP1 downregulation correlates with GBM proliferation, in agreement with the in vitro result. Thus, we believe our observations highlight the potential that suppression of GBM proliferation associated with MRP1 silencing could be exploited to suppress the progression of the residual GBM, in parallel to chemosensitising the tumour.

Biodistribution of the cationic nanoparticle is well-documented to indicate accumulation in the liver, spleen, kidney, and lung [71], and both kidney and duodenum tissues are known to express MRP1 as their physiological phenotype [44, 45]. We observed significant downregulation of MRP1 in these two organs, which was even more long-lasting than the silencing in the S.C. GBM tumour, which may be due to the expected accumulation profile of the non-targeted PEI-pSiNPs. It is reported that the physiological function of MRP1 in kidney and digestive system is related to protection from natural toxins, cholehepatic and enterohepatic circulation of bile, and in the protection of the biliary tree tissues against toxic bile constituents [72]. However, no histopathological signs that would indicate tissue damage such as necrosis in these two organs was observed over 6 days post-treatment. Since MRP1 knockdown in tumour and proliferation inhibition were observed as early as 48 h post-injection and sustained despite nascent mRNA started recovering, this may indicate a possible treatment window. Future studies should investigate the collateral damage of MRP1 siRNA plus cytotoxic drug co-treatments in other organs, such as heart which is susceptible to oxidative damage, while MRP1 knockdown would further decrease the tolerance in normal organs to cytotoxic drugs [73]. In addition, targeted delivery of MRP1 siRNA should be explored in follow-up studies to minimise the undesired silencing of MRP1 in other organs. Given that MRP1 expression also causes radiation resistance, we speculate that localised delivery at the site of primary tumour resection may provide a means of sensitisation towards chemo- and radiotherapy and obviate the need for systemic exposure and potential toxicity from MRP1 downregulation in other organs.

This study highlights the relationship between MRP1 and GBM cell proliferation, and provides insights into the relationship between MRP1 expression and malignancy grade. In addition, we demonstrated that MRP1 silencing by employing PEI-pSiNP delivery of siRNA alone would reduce the proliferation rate of GBM cells by attenuating the cell cycle at G1/S, without cytotoxic drug co-treatment, indicating the importance of MRP1 expression in the biology of GBM. Since the effect of siRNA subsides over time mainly due to the dilution of intracellular siRNA owing to cell division [74], the proliferation attenuation effect associated with MRP1 silencing may intensify the therapeutic effect of this approach. MRP1 knockdown of GBM was demonstrated here for the first time in vivo, and the proliferation attenuation

was also observed in the tumour, highlighting the promise of MRP1 as a treatment to GBM.

Conclusion

Chemoresistance in GBM, partially mediated by MRP1 overexpression in the brain, renders GBM a fatal disease that is notoriously difficult to eradicate. Gene therapy aimed at MRP1 silencing has been showing promising results in sensitising other drug-resistant cancers while its effect on brain cancers have not been thoroughly investigated. Here, we demonstrated that the MRP1 silencing using pSiNP-based delivery of MRP1 siRNA not only drug-sensitised, but also inhibited GBM cell proliferation by arresting cell cycle at G1/S on its own. The reduction in proliferation rate was independent of the siRNA delivery method. This effect may be mediated via transmembrane transporters as suggested by a MRP1 functional inhibition assay. Through the use of PEI-capped pSiNP delivery of siRNA, we established MRP1 silencing in GBM tumours in mice. Consistently, the reduction of ki67 positive staining in GBM correlated with MRP1 silencing in the tumour. MRP1 siRNA delivery was not targeted to tumours and hence also showed silencing in MRP1-expressing organs such as kidney and duodenum. However, no histopathological signs were observed. In conclusion, this study illustrated, for the first time, the correlations between MRP1 expression and GBM proliferation. This provides insights into residual GBM eradication through highlighting the potential that, apart from chemotherapeutics sensitising, MRP1 silencing itself may deliver therapeutic effects by attenuating the growth of GBM.

Additional files

Additional file 1: Figure S1. FTIR-ATR surface chemical analysis of pSiNP indicating the completion of thermal hydrocarbonisation of pSiNP.

Additional file 2: Figure S2. Chemosensitisation of which GBM cells as indicated by the viability of cells treated by pSiNP/siRNA, or DOX, or combination treatment, or untreated.

Authors' contributions

WYT, RB, MA, performed in vitro study. WYT, CF, TK, MA, and SA performed in vivo study. SS, RB, WYT performed nanoparticles fabrication, modification and biophysical characterisations. WYT, NHV, and BK designed and planned the experiments. All authors provided input in the interpretation of results. All authors read and approved the final manuscript.

Author details

[1] Monash Institute of Pharmaceutical Sciences, Monash University, 381 Royal Parade, Parkville, VIC 3052, Australia. [2] Future Industries Institute, University of South Australia, Mawson Lakes, Adelaide, SA 5095, Australia. [3] Melbourne Centre for Nanofabrication, Victorian Node of the Australian National Fabrication Facility, Clayton, VIC 3168, Australia. [4] School of Medicine, Flinders University, Bedford Park, Adelaide, SA 5042, Australia. [5] South Australian Health and Medical Research Institute, North Terrace, Adelaide, SA 5000, Australia.

Competing interests

The authors declare that they have no competing interests.

Availability of data and materials

Not applicable.

Consent for publication

All authors read and approved the final manuscript.

Ethics approval and consent to participate

Animal procedures were performed according to a protocol approved by South Australian Health & Medical Research Institute Animal Ethics Committee (Approval Number, SAM#98).

Funding

Funding support of this study was provided by Channel 7 Children's Research Foundation, Foundation for Children (2016-081) and partially supported by Science and Industry Endowment Fund John Stocker Postdoctoral Fellowship (PF16-072). This work was performed in part at the Melbourne Centre for Nanofabrication (MCN) in the Victorian Node of the Australian National Fabrication Facility (ANFF).

Publisher's Note

Received: 19 September 2017 Accepted: 31 March 2018
Published online: 13 April 2018

References

1. Mrugala MM. Advances and challenges in the treatment of glioblastoma: a clinician's perspective. Discov Med. 2013;15(83):221–30.
2. Australian cancer incidence and mortality (ACIM) books, brain cancer for Australia (ICD10 C71).
3. Mohri M, Nitta H, Yamashita J. Expression of multidrug resistance-associated protein (MRP) in human gliomas. J Neurooncol. 2000;49(2):105–15.
4. Sugiyama D, Kusuhara H, Lee YJ, Sugiyama Y. Involvement of multidrug resistance associated protein 1 (Mrp1) in the efflux transport of 17beta estradiol-D-17beta-glucuronide (E217betaG) across the blood–brain barrier. Pharm Res. 2003;20(9):1394–400.
5. Dallas S, Miller DS, Bendayan R. Multidrug resistance-associated proteins: expression and function in the central nervous system. Pharmacol Rev. 2006;58(2):140–61.
6. Rosenberg MF, Mao Q, Holzenburg A, Ford RC, Deeley RG, Cole SP. The structure of the multidrug resistance protein 1 (MRP1/ABCC1). crystallization and single-particle analysis. J Biol Chem. 2001;276(19):16076–82.
7. Munoz M, Henderson M, Haber M, Norris M. Role of the MRP1/ABCC1 multidrug transporter protein in cancer. IUBMB Life. 2007;59(12):752–7.
8. Tivnan A, Zakaria Z, O'Leary C, Kogel D, Pokorny JL, Sarkaria JN, Prehn JH. Inhibition of multidrug resistance protein 1 (MRP1) improves chemotherapy drug response in primary and recurrent glioblastoma multiforme. Front Neurosci. 2015;9:218.
9. Schinkel AH. The roles of P-glycoprotein and MRP1 in the blood–brain and blood–cerebrospinal fluid barriers. In: Dansette PM, Snyder R, Delaforge M, Gibson GG, Greim H, Jollow DJ, Monks TJ, Sipes IG, editors. Biological reactive intermediates VI: chemical and biological mechanisms in susceptibility to and prevention of environmental diseases. US: Springer; 2001. p. 365–72.
10. Ganesh S, Iyer AK, Weiler J, Morrissey DV, Amiji MM. Combination of siRNA-directed gene silencing with cisplatin reverses drug resistance in human non-small cell lung cancer. Mol Ther Nucleic Acids. 2013;2:e110.
11. Burkhart CA, Watt F, Murray J, Pajic M, Prokvolit A, Xue C, Flemming C, Smith J, Purmal A, Isachenko N, Komarov PG, Gurova KV, Sartorelli AC, Marshall GM, Norris MD, Gudkov AV, Haber M. Small molecule MRP1 inhibitor reversan increases the therapeutic index of chemotherapy in mouse model of neuroblastoma. Can Res. 2009;69(16):6573–80.
12. Persidis A. Cancer multidrug resistance. Nat Biotech. 1999;17(1):94–5.

13. Peigñan L, Garrido W, Segura R, Melo R, Rojas D, Cárcamo JG, San Martín R, Quezada C. Combined use of anticancer drugs and an inhibitor of multiple drug resistance-associated protein-1 increases sensitivity and decreases survival of glioblastoma multiforme cells in vitro. Neurochem Res. 2011;36(8):1397–406.
14. Bumcrot D, Manoharan M, Koteliansky V, Sah DW. RNAi therapeutics: a potential new class of pharmaceutical drugs. Nat Chem Biol. 2006;2(12):711–9.
15. Hickerson RP, Vlassov AV, Wang Q, Leake D, Ilves H, Gonzalez-Gonzalez E, Contag CH, Johnston BH, Kaspar RL. Stability study of unmodified siRNA and relevance to clinical use. Oligonucleotides. 2008;18(4):345–54.
16. Wan Y, Apostolou S, Dronov R, Kuss B, Voelcker NH. Cancer-targeting siRNA delivery from porous silicon nanoparticles. Nanomedicine. 2014;9(15):2309–21.
17. Dalilottojari A, Tong WY, McInnes SJP, Voelcker NH. Biocompatibility, bioactive biomaterials. In: Korotcentkov G, editor. Porous silicon: from formation to application, vol. 3. Boca Raton: CRC Press; 2016. p. 1328.
18. Santos HA, Makila E, Airaksinen AJ, Bimbo LM, Hirvonen J. Porous silicon nanoparticles for nanomedicine: preparation and biomedical applications. Nanomedicine. 2014;9(4):535–54.
19. Vallet-Regi M. Nanostructured mesoporous silica matrices in nanomedicine. J Intern Med. 2010;267(1):22–43.
20. Salonen J, Kaukonen AM, Hirvonen J, Lehto VP. Mesoporous silicon in drug delivery applications. J Pharm Sci. 2008;97(2):632–53.
21. Daneshjou S, Dabirmanesh B, Rahimi F, Khajeh K. Porous silicon nanoparticle as a stabilizing support for chondroitinase. Int J Biol Macromol. 2017;94:852–8.
22. Liu D, Bimbo LM, Makila E, Villanova F, Kaasalainen M, Herranz-Blanco B, Caramella CM, Lehto VP, Salonen J, Herzig KH, Hirvonen J, Santos HA. Co-delivery of a hydrophobic small molecule and a hydrophilic peptide by porous silicon nanoparticles. J Control Release. 2013;170(2):268–78.
23. Kafshgari M, Delalat B, Tong WY, Harding F, Kaasalainen M, Salonen J, Voelcker N. Oligonucleotide delivery by chitosan-functionalized porous silicon nanoparticles. Nano Res. 2015;8(6):2033–46.
24. Wang Y, Cui H, Sun C, Zhao X, Cui B. Construction and evaluation of controlled-release delivery system of Abamectin using porous silica nanoparticles as carriers. Nanoscale Res Lett. 2014;9:655.
25. Wang C-F, Mäkilä EM, Kaasalainen MH, Hagström MV, Salonen JJ, Hirvonen JT, Santos HA. Dual-drug delivery by porous silicon nanoparticles for improved cellular uptake, sustained release, and combination therapy. Acta Biomater. 2015;16:206–14.
26. Salonen J, Björkqvist M, Laine E, Niinistö L. Stabilization of porous silicon surface by thermal decomposition of acetylene. Appl Surf Sci. 2004;225(1–4):389–94.
27. Tong WY, Sweetman MJ, Marzouk ER, Fraser C, Kuchel T, Voelcker NH. Towards a subcutaneous optical biosensor based on thermally hydrocarbonised porous silicon. Biomaterials. 2016;74:217–30.
28. Jalkanen T, Torres-Costa V, Mäkilä E, Kaasalainen M, Koda R, Sakka T, Ogata YH, Salonen J. Selective optical response of hydrolytically stable stratified Si rugate mirrors to liquid infiltration. ACS Appl Mater Interfaces. 2014;6(4):2884–92.
29. Tokatlian T, Segura T. siRNA applications in nanomedicine. Wiley Interdiscip Rev Nanomed Nanobiotechnol. 2010;2(3):305–15.
30. Belot N, Rorive S, Doyen I, Lefranc F, Bruyneel E, Dedecker R, Micik S, Brotchi J, Decaestecker C, Salmon I, Kiss R, Camby I. Molecular characterization of cell substratum attachments in human glial tumors relates to prognostic features. Glia. 2001;36(3):375–90.
31. Molinas A, Sicard G, Jakob I. Functional evidence of multidrug resistance transporters (MDR) in rodent olfactory epithelium. PLoS ONE. 2012;7(5):e36167.
32. Hasanzadeh Kafshgari M, Alnakhli M, Delalat B, Apostolou S, Harding FJ, Makila E, Salonen JJ, Kuss BJ, Voelcker NH. Small interfering RNA delivery by polyethylenimine-functionalised porous silicon nanoparticles. Biomater Sci. 2015;3(12):1555–65.
33. Boukherroub R, Wojtyk JTC, Wayner DDM, Lockwood DJ. Thermal hydrosilylation of undecylenic acid with porous silicon. J Electrochem Soc. 2002;149(2):H59–63.
34. Blanco E, Shen H, Ferrari M. Principles of nanoparticle design for overcoming biological barriers to drug delivery. Nat Biotechnol. 2015;33(9):941–51.
35. Hansen KM, Ji HF, Wu G, Datar R, Cote R, Majumdar A, Thundat T. Cantilever-based optical deflection assay for discrimination of DNA single-nucleotide mismatches. Anal Chem. 2001;73(7):1567–71.
36. Smith SB, Cui Y, Bustamante C. Overstretching B-DNA: the elastic response of individual double-stranded and single-stranded DNA molecules. Science. 1996;271(5250):795–9.
37. Hunter RJ. Chapter 6—applications of the zeta potential, zeta potential in colloid science. Cambridge: Academic Press; 1981. p. 219–57.
38. Zeta-Meter I. Everything you want to know about coagulation and flocculation. Staunton: Zeta-Meter Inc.; 1990.
39. Gao S, Dagnaes-Hansen F, Nielsen EJ, Wengel J, Besenbacher F, Howard KA, Kjems J. The effect of chemical modification and nanoparticle formulation on stability and biodistribution of siRNA in mice. Mol Ther. 2009;17(7):1225–33.
40. Legrand O, Simonin G, Perrot J-Y, Zittoun R, Marie J-P. Pgp and MRP activities using calcein-AM are prognostic factors in adult acute myeloid leukemia patients. Blood. 1998;91(12):4480.
41. Cuylen S, Blaukopf C, Politi AZ, Müller-Reichert T, Neumann B, Poser I, Ellenberg J, Hyman AA, Gerlich DW. Ki-67 acts as a biological surfactant to disperse mitotic chromosomes. Nature. 2016;535(7611):308–12.
42. Gu Y, Rosenblatt J, Morgan DO. Cell cycle regulation of CDK2 activity by phosphorylation of Thr160 and Tyr15. EMBO J. 1992;11(11):3995–4005.
43. Hans F, Dimitrov S. Histone H3 phosphorylation and cell division. Oncogene. 2001;20(24):3021–7.
44. Evers R, Zaman GJ, van Deemter L, Jansen H, Calafat J, Oomen LC, Oude Elferink RP, Borst P, Schinkel AH. Basolateral localization and export activity of the human multidrug resistance-associated protein in polarized pig kidney cells. J Clin Invest. 1996;97(5):1211–8.
45. Tyden E, Bjornstrom H, Tjalve H, Larsson P. Expression and localization of BCRP, MRP1 and MRP2 in intestines, liver and kidney in horse. J Vet Pharmacol Ther. 2010;33(4):332–40.
46. Abdelhalim MA, Jarrar BM. The appearance of renal cells cytoplasmic degeneration and nuclear destruction might be an indication of GNPs toxicity. Lipids Health Dis. 2011;10:147.
47. Frazier KS, Seely JC, Hard GC, Betton G, Burnett R, Nakatsuji S, Nishikawa A, Durchfeld-Meyer B, Bube A. Proliferative and nonproliferative lesions of the rat and mouse urinary system. Toxicol Pathol. 2012;40(4 Suppl):14S–86S.
48. Serra S, Jani PA. An approach to duodenal biopsies. J Clin Pathol. 2006;59(11):1133–50.
49. Meng H, Mai WX, Zhang H, Xue M, Xia T, Lin S, Wang X, Zhao Y, Ji Z, Zink JI, Nel AE. Codelivery of an optimal drug/siRNA combination using mesoporous silica nanoparticles to overcome drug resistance in breast cancer in vitro and in vivo. ACS Nano. 2013;7(2):994–1005.
50. O'Connor R, O'Leary M, Ballot J, Collins CD, Kinsella P, Mager DE, Arnold RD, O'Driscoll L, Larkin A, Kennedy S, Fennelly D, Clynes M, Crown J. A phase I clinical and pharmacokinetic study of the multi-drug resistance protein-1 (MRP-1) inhibitor sulindac, in combination with epirubicin in patients with advanced cancer. Cancer Chemother Pharmacol. 2007;59(1):79–87.
51. Saad M, Garbuzenko OB, Minko T. Co-delivery of siRNA and an anticancer drug for treatment of multidrug-resistant cancer. Nanomedicine. 2008;3(6):761–76.
52. Xu H, Nie X, Wu L, Zhu X, Yi W, Huang S. Down-regulation of MRP1 expression in C6/VP16 cells by chitosan-MRP1-siRNA nanoparticles. Cell Biochem Biophys. 2015;72(1):227–33.
53. Sullivan GF, Yang JM, Vassil A, Yang J, Bash-Babula J, Hait WN. Regulation of expression of the multidrug resistance protein MRP1 by p53 in human prostate cancer cells. J Clin Invest. 2000;105(9):1261–7.
54. Hobbs SK, Monsky WL, Yuan F, Roberts WG, Griffith L, Torchilin VP, Jain RK. Regulation of transport pathways in tumor vessels: role of tumor type and microenvironment. Proc Natl Acad Sci USA. 1998;95(8):4607–12.
55. Abdul M, Raja GH, Katas T, Jing W. Stability, intracellular delivery, and release of sirna from chitosan nanoparticles using different cross-linkers. PLoS ONE. 2015;10(6):e0128963.
56. Chen C, Mei H, Shi W, Deng J, Zhang B, Guo T, Wang H, Hu Y. EGFP-EGF1-conjugated PLGA nanoparticles for targeted delivery of siRNA into injured brain microvascular endothelial cells for efficient RNA interference. PLOS ONE. 2013;8(4):e60860.
57. Navarro G, Pan J, Torchilin VP. Micelle-like nanoparticles as carriers for DNA and siRNA. Mol Pharm. 2015;12(2):301–13.

58. Khansarizadeh M, Mokhtarzadeh A, Rashedinia M, Taghdisi SM, Lari P, Abnous KH, Ramezani M. Identification of possible cytotoxicity mechanism of polyethylenimine by proteomics analysis. Hum Exp Toxicol. 2016;35(4):377–87.
59. Siu YS, Li L, Leung MF, Lee KL, Li P. Polyethylenimine-based amphiphilic core-shell nanoparticles: study of gene delivery and intracellular trafficking. Biointerphases. 2012;7(1–4):16.
60. Kuss BJ, Corbo M, Lau WM, Fennell DA, Dean NM, Cotter FE. In vitro and in vivo downregulation of MRP1 by antisense oligonucleotides: a potential role in neuroblastoma therapy, international journal of cancer. J Int Cancer. 2002;98(1):128–33.
61. Peaston AE, Gardaneh M, Franco AV, Hocker JE, Murphy KM, Farnsworth ML, Catchpoole DR, Haber M, Norris MD, Lock RB, Marshall GM. MRP1 gene expression level regulates the death and differentiation response of neuroblastoma cells. Br J Cancer. 2001;85(10):1564–71.
62. Mahdizadeh S, Karimi G, Behravan J, Arabzadeh S, Lage H, Kalalinia F. Crocin suppresses multidrug resistance in MRP overexpressing ovarian cancer cell line. Daru. 2016;24(1):17.
63. Lehne G, De Angelis P, den Boer M, Rugstad HE. Growth inhibition, cytokinesis failure and apoptosis of multidrug-resistant leukemia cells after treatment with P-glycoprotein inhibitory agents. Leukemia. 1999;13(5):768–78.
64. Teodori E, Dei S, Martelli C, Scapecchi S, Gualtieri F. The functions and structure of ABC transporters: implications for the design of new inhibitors of Pgp and MRP1 to control multidrug resistance (MDR). Curr Drug Targets. 2006;7(7):893–909.
65. Carthew RW, Sontheimer EJ. Origins and mechanisms of miRNAs and siRNAs. Cell. 2009;136(4):642–55.
66. Waite CL, Roth CM. Nanoscale drug delivery systems for enhanced drug penetration into solid tumors: current progress and opportunities. Crit Rev Biomed Eng. 2012;40(1):21–41.
67. Schneider SW, Ludwig T, Tatenhorst L, Braune S, Oberleithner H, Senner V, Paulus W. Glioblastoma cells release factors that disrupt blood–brain barrier features. Acta Neuropathol. 2004;107(3):272–6.
68. Long DM. Capillary ultrastructure and the blood–brain barrier in human malignant brain tumors. J Neurosurg. 1970;32(2):127–44.
69. Leuthardt EC, Duan C, Kim MJ, Campian JL, Kim AH, Miller-Thomas MM, Shimony JS, Tran DD. Hyperthermic laser ablation of recurrent glioblastoma leads to temporary disruption of the peritumoral blood brain barrier. PLoS ONE. 2016;11(2):e0148613.
70. Skjulsvik AJ, Mork JN, Torp MO, Torp SH. Ki-67/MIB-1 immunostaining in a cohort of human gliomas. Int J Clin Exp Pathol. 2014;7(12):8905–10.
71. Knudsen KB, Northeved H, Gjetting T, Permin A, Andresen TL, Wegener KM, Lam HR, Lykkesfeldt J. Biodistribution of rhodamine B fluorescence-labeled cationic nanoparticles in rats. J Nanoparticle Res. 2014;16(2):2221.
72. Broker LE, Rodriguez JA, Giaccone G. Molecular pathways of drug resistance. In: Bronchud MH, editor. Principles of molecular oncology. Berlin: Springer; 2004. p. 463–89.
73. Jungsuwadee P, Nithipongvanitch R, Chen Y, Oberley TD, Butterfield DA, St Clair DK, Vore M. Mrp1 localization and function in cardiac mitochondria after doxorubicin. Mol Pharmacol. 2009;75(5):1117–26.
74. Bartlett DW, Davis ME. Insights into the kinetics of siRNA-mediated gene silencing from live-cell and live-animal bioluminescent imaging. Nucleic Acids Res. 2006;34(1):322–33.

REFERENCES:

ABBOTT, N. J. 2005. Dynamics of CNS barriers: evolution, differentiation, and modulation. *Cellular and Molecular Neurobiology,* 25**,** 5-23.

ABE, T., MORI, T., WAKABAYASHI, Y., NAKAGAWA, M., COLE, S. P., KOIKE, K., KUWANO, M. & HORI, S. 1998. Expression of multidrug resistance protein gene in patients with glioma after chemotherapy. *J Neurooncol,* 40**,** 11-8.

ABEL, T., KOIKEL, K., OHGAL, T., KUBOL, T., WADAL, M., KOHNOL, K., MORI2, T., HIDAKA, K. & KUWANOL, M. 1995. Chemosensitisation of spontaneous multidrug resistance by a 1,4-dihydropyridine analogue and verapamil in human glioma cell lines overexpressing MRP or MDRI. *Brifish Journal of Cancer,* 72**,** 6.

ABRAMYAN, J. 2019. Hedgehog signaling and embryonic craniofacial disorders. *Journal of developmental biology,* 7**,** 9.

AGNIHOTRI, S., BURRELL, K. E., WOLF, A., JALALI, S., HAWKINS, C., RUTKA, J. T. & ZADEH, G. 2013. Glioblastoma, a brief review of history, molecular genetics, animal models and novel therapeutic strategies. *Arch Immunol Ther Exp (Warsz),* 61**,** 25-41.

AIHW 2017. Cancer in Australia 2017. *In:* AIHW (ed.) *Cancer series.* Canberra: AIHW.: Australian Institute of Health and Welfare and Australasian.

AKINC, A., THOMAS, M., KLIBANOV, A. M. & LANGER, R. 2005. Exploring polyethylenimine-mediated DNA transfection and the proton sponge hypothesis. *J Gene Med,* 7**,** 657-63.

ALBERTS, B., WILSON, J. H. & HUNT, T. 2008. *Molecular biology of the cell,* New York, Garland Science.

ALDEA, M., FLORIAN, I. A., KACSO, G., CRACIUN, L., BOCA, S., SORITAU, O. & FLORIAN, I. S. 2016. Nanoparticles for Targeting Intratumoral Hypoxia: Exploiting a Potential Weakness of Glioblastoma. *Pharm Res,* 33**,** 2059-77.

ALEXIS, F., PRIDGEN, E. M., LANGER, R. & FAROKHZAD, O. C. 2010. Nanoparticle technologies for cancer therapy. *Drug delivery.* Springer.

ALIABADI, H. M., LANDRY, B., SUN, C., TANG, T. & ULUDAG, H. 2012. Supramolecular assemblies in functional siRNA delivery: where do we stand? *Biomaterials,* 33**,** 2546-69.

ALIABADI, H. M. & ULUDAĞ, H. 2016. Nanoparticle Carriers to Overcome Biological Barriers to siRNA Delivery. *Nanomedicines.*

ALMQUIST, K. C., LOE, D. W., HIPFNER, D. R., MACKIE, J. E., COLE, S. P. & DEELEY, R. G. 1995. Characterization of the Mr 190,000 multidrug resistance protein (MRP) in drug-selected and transfected human tumor cells. *Cancer Research,* 55**,** 102-110.

ALVES, T. R., LIMA, F. R., KAHN, S. A., LOBO, D., DUBOIS, L. G., SOLETTI, R., BORGES, H. & NETO, V. M. 2011. Glioblastoma cells: a heterogeneous and fatal tumor interacting with the parenchyma. *Life Sci,* 89**,** 532-9.

ANGLIN, E. J., CHENG, L., FREEMAN, W. R. & SAILOR, M. J. 2008. Porous silicon in drug delivery devices and materials. *Adv Drug Deliv Rev,* 60**,** 1266-77.

APPIN, C. L. & BRAT, D. J. 2015. Molecular pathways in gliomagenesis and their relevance to neuropathologic diagnosis. *Advances in anatomic pathology,* 22**,** 50-58.

ASTRIAB-FISHER, A., SERGUEEV, D. S., FISHER, M., RAMSAY SHAW, B. & JULIANO, R. L. 2000. Antisense inhibition of P-glycoprotein expression using peptide–oligonucleotide conjugates. *Biochemical Pharmacology,* 60**,** 83-90.

ATWOOD, S. X., SARIN, K. Y., WHITSON, R. J., LI, J. R., KIM, G., REZAEE, M., ALLY, M. S., KIM, J., YAO, C., CHANG, A. L., ORO, A. E. & TANG, J. Y. 2015. Smoothened variants explain the majority of drug resistance in basal cell carcinoma. *Cancer Cell,* 27**,** 342-53.

Badagnani, I., Monshouwer,M., Fretland, A. J. Are The Commonly Used Drug Transport Inhibitors, Elacridar, MK-571, And Ko143, As Selective As Often Assumed? 2008 Drug Metabolism Reviews. Conference: 10th European Regional International society for the study of xenobiotics Meeting

BÄHR, O., RIEGER, J., DUFFNER, F., MEYERMANN, R., WELLER, M. & WICK, W. 2003. P‐Glycoprotein and Multidrug Resistance‐associated Protein Mediate Specific Patterns of Multidrug Resistance in Malignant Glioma Cell Lines, but not in Primary Glioma Cells. *Brain pathology,* 13**,** 482-494.

BALLARIN-GONZALEZ, B., DAGNAES-HANSEN, F., FENTON, R. A., GAO, S., HEIN, S., DONG, M., KJEMS, J. & HOWARD, K. A. 2013. Protection and Systemic Translocation of siRNA

Following Oral Administration of Chitosan/siRNA Nanoparticles. *Mol Ther Nucleic Acids,* 2**,** e76.

BAR, E. E., CHAUDHRY, A., LIN, A., FAN, X., SCHRECK, K., MATSUI, W., PICCIRILLO, S., VESCOVI, A. L., DIMECO, F., OLIVI, A. & EBERHART, C. G. 2007. Cyclopamine-mediated hedgehog pathway inhibition depletes stem-like cancer cells in glioblastoma. *Stem Cells,* 25**,** 2524-33.

BARRETO, J. A., O'MALLEY, W., KUBEIL, M., GRAHAM, B., STEPHAN, H. & SPICCIA, L. 2011. Nanomaterials: applications in cancer imaging and therapy. *Advanced Materials,* 23.

BAX, D. V., KONDYURIN, A., WATERHOUSE, A., MCKENZIE, D. R., WEISS, A. S. & BILEK, M. M. 2014. Surface plasma modification and tropoelastin coating of a polyurethane co-polymer for enhanced cell attachment and reduced thrombogenicity. *Biomaterials,* 35**,** 6797-809.

BECKER, K. P. & BAEHRING, J. M. 2017. Current Standard Treatment Options for Malignant Glioma. *Malignant Brain Tumors.* Springer.

BENNETT, C. F. & SWAYZE, E. E. 2010. RNA targeting therapeutics: molecular mechanisms of antisense oligonucleotides as a therapeutic platform. *Annual review of pharmacology and toxicology,* 50**,** 259-293.

BERNKOP-SCHNURCH, A. & DUNNHAUPT, S. 2012. Chitosan-based drug delivery systems. *Eur J Pharm Biopharm,* 81**,** 463-9.

BIDET, M., TOMICO, A., MARTIN, P., GUIZOUARN, H., MOLLAT, P. & MUS-VETEAU, I. 2012. The Hedgehog receptor patched functions in multidrug transport and chemotherapy resistance. *Mol Cancer Res,* 10**,** 1496-508.

BLANCO, E., SHEN, H. & FERRARI, M. 2015. Principles of nanoparticle design for overcoming biological barriers to drug delivery. *Nat Biotechnol,* 33**,** 941-51.

BLANQUICETT, C., JOHNSON, M. R., HESLIN, M. & DIASIO, R. B. 2002. Housekeeping gene variability in normal and carcinomatous colorectal and liver tissues: applications in pharmacogenomic gene expression studies. *Anal Biochem,* 303**,** 209-14.

BLECHARZ, K. G., COLLA, R., ROHDE, V. & VAJKOCZY, P. 2015. Control of the blood-brain barrier function in cancer cell metastasis. *Biol Cell,* 107**,** 342-71.

BOBBIN, M. L. & ROSSI, J. J. 2016. RNA Interference (RNAi)-Based Therapeutics: Delivering on the Promise? *Annu Rev Pharmacol Toxicol,* 56**,** 103-22.

BONILLA, X., PARMENTIER, L., KING, B., BEZRUKOV, F., KAYA, G., ZOETE, V., SEPLYARSKIY, V. B., SHARPE, H. J., MCKEE, T. & LETOURNEAU, A. 2015. Genomic analysis identifies new drivers and progression pathways in skin basal cell carcinoma. *Nature genetics,* 47**,** 398.

BOTA, D. A., DESJARDINS, A., QUINN, J. A., AFFRONTI, M. L. & FRIEDMAN, H. S. 2007. Interstitial chemotherapy with biodegradable BCNU (Gliadel(®)) wafers in the treatment of malignant gliomas. *Therapeutics and Clinical Risk Management,* 3**,** 707-715.

BOUMENDJEL, A., BAUBICHON-CORTAY, H., TROMPIER, D., PERROTTON, T. & DI PIETRO, A. 2005. Anticancer multidrug resistance mediated by MRP1: recent advances in the discovery of reversal agents. *Med Res Rev,* 25**,** 453-72.

BRAASCH, D. A., JENSEN, S., LIU, Y., KAUR, K., ARAR, K., WHITE, M. A. & COREY, D. R. 2003. RNA interference in mammalian cells by chemically-modified RNA. *Biochemistry,* 42**,** 7967-75.

BRANTL, S. 2002. Antisense-RNA regulation and RNA interference. *Biochim Biophys Acta,* 1575**,** 15-25.

BRAT, D. J., KAUR, B. & VAN MEIR, E. G. 2003. Genetic modulation of hypoxia induced gene expression and angiogenesis: relevance to brain tumors. *Front Biosci,* 8**,** d100-16.

BRAUN, S., OPPERMANN, H., MUELLER, A., RENNER, C., HOVHANNISYAN, A., BARAN-SCHMIDT, R., GEBHARDT, R., HIPKISS, A., THIERY, J., MEIXENSBERGER, J. & GAUNITZ, F. 2012. Hedgehog signaling in glioblastoma multiforme. *Cancer Biol Ther,* 13**,** 487-95.

BREDEL, M. 2001. Anticancer drug resistance in primary human brain tumors. *Brain Res Brain Res Rev,* 35**,** 161-204.

BREM, H., EWEND, M. G., PIANTADOSI, S., GREENHOOT, J., BURGER, P. C. & SISTI, M. 1995. The safety of interstitial chemotherapy with BCNU-loaded polymer followed by radiation therapy in the treatment of newly diagnosed malignant gliomas: phase I trial. *J Neurooncol,* 26**,** 111-23.

BRENNAN, C., MOMOTA, H., HAMBARDZUMYAN, D., OZAWA, T., TANDON, A., PEDRAZA, A. & HOLLAND, E. 2009. Glioblastoma subclasses can be defined by activity among signal transduction pathways and associated genomic alterations. *PLoS One,* 4**,** e7752.

BRENNAN, C. W., VERHAAK, R. G., MCKENNA, A., CAMPOS, B., NOUSHMEHR, H., SALAMA, S. R., ZHENG, S., CHAKRAVARTY, D., SANBORN, J. Z., BERMAN, S. H., BEROUKHIM, R.,

BERNARD, B., WU, C. J., GENOVESE, G., SHMULEVICH, I., BARNHOLTZ-SLOAN, J., ZOU, L., VEGESNA, R., SHUKLA, S. A., CIRIELLO, G., YUNG, W. K., ZHANG, W., SOUGNEZ, C., MIKKELSEN, T., ALDAPE, K., BIGNER, D. D., VAN MEIR, E. G., PRADOS, M., SLOAN, A., BLACK, K. L., ESCHBACHER, J., FINOCCHIARO, G., FRIEDMAN, W., ANDREWS, D. W., GUHA, A., IACOCCA, M., O'NEILL, B. P., FOLTZ, G., MYERS, J., WEISENBERGER, D. J., PENNY, R., KUCHERLAPATI, R., PEROU, C. M., HAYES, D. N., GIBBS, R., MARRA, M., MILLS, G. B., LANDER, E., SPELLMAN, P., WILSON, R., SANDER, C., WEINSTEIN, J., MEYERSON, M., GABRIEL, S., LAIRD, P. W., HAUSSLER, D., GETZ, G., CHIN, L. & NETWORK, T. R. 2013. The somatic genomic landscape of glioblastoma. *Cell,* 155**,** 462-77.

BRIGUI, I., DJAVANBAKHT-SAMANI, T., JOLLES, B., PIGAGLIO, S. & LAIGLE, A. 2003. Minimally modified phosphodiester antisense oligodeoxyribonucleotide directed against the multidrug resistance gene mdr1. *Biochem Pharmacol,* 65**,** 747-54.

BROKER, L. E., RODRIGUEZ, J. A. & GIACCONE, G. 2004. Molecular Pathways of Drug Resistance. *In:* BRONCHUD, M. H. (ed.) *Principles of Molecular Oncology.* Springer Science.

BRUNO, K. 2011. Using drug-excipient interactions for siRNA delivery. *Advanced Drug Delivery Reviews,* 63**,** 1210-1226.

BUMCROT, D., MANOHARAN, M., KOTELIANSKY, V. & SAH, D. W. 2006. RNAi therapeutics: a potential new class of pharmaceutical drugs. *Nat Chem Biol,* 2**,** 711-9.

BURNETT, J. C. & ROSSI, J. J. 2012. RNA-based therapeutics: current progress and future prospects. *Chem Biol,* 19**,** 60-71.

CALATOZZOLO, C., GELATI, M., CIUSANI, E., SCIACCA, F. L., POLLO, B., CAJOLA, L., MARRAS, C., SILVANI, A., VITELLARO-ZUCCARELLO, L., CROCI, D., BOIARDI, A. & SALMAGGI, A. 2005. Expression of drug resistance proteins Pgp, MRP1, MRP3, MRP5 and GST-pi in human glioma. *J Neurooncol,* 74**,** 113-21.

CANCER GENOME ATLAS RESEARCH, N. 2008. Comprehensive genomic characterization defines human glioblastoma genes and core pathways. *Nature,* 455**,** 1061-8.

CANHAM, L. T. 1995. Bioactive silicon structure fabrication through nanoetching techniques. *Advanced Materials,* 7**,** 1033-1037.

CANHAM, L. T. 1997. *in properties of porous silicon,* London, Institution of Electrical Engineers.

CARPENTER, R. L. & LO, H. W. 2012. Identification, functional characterization, and pathobiological significance of GLI1 isoforms in human cancers. *Vitam Horm,* 88**,** 115-40.

CARTHEW, R. W. & SONTHEIMER, E. J. 2009. Origins and Mechanisms of miRNAs and siRNAs. *Cell,* 136**,** 642-55.

CASTRO, M. G., COWEN, R., WILLIAMSON, I. K., DAVID, A., JIMENEZ-DALMARONI, M. J., YUAN, X., BIGLIARI, A., WILLIAMS, J. C., HU, J. & LOWENSTEIN, P. R. 2003. Current and future strategies for the treatment of malignant brain tumors. *Pharmacol Ther,* 98**,** 71-108.

CECCARELLI, M., BARTHEL, FLORIS P., MALTA, TATHIANE M., SABEDOT, THAIS S., SALAMA, SOFIE R., MURRAY, BRADLEY A., MOROZOVA, O., NEWTON, Y., RADENBAUGH, A., PAGNOTTA, STEFANO M., ANJUM, S., WANG, J., MANYAM, G., ZOPPOLI, P., LING, S.,

RAO, ARJUN A., GRIFFORD, M., CHERNIACK, ANDREW D., ZHANG, H., POISSON, L., CARLOTTI, CARLOS G., TIRAPELLI, DANIELA PRETTI DA C., RAO, A., MIKKELSEN, T., LAU, CHING C., YUNG, W. K. A., RABADAN, R., HUSE, J., BRAT, DANIEL J., LEHMAN, NORMAN L., BARNHOLTZ-SLOAN, JILL S., ZHENG, S., HESS, K., RAO, G., MEYERSON, M., BEROUKHIM, R., COOPER, L., AKBANI, R., WRENSCH, M., HAUSSLER, D., ALDAPE, KENNETH D., LAIRD, PETER W., GUTMANN, DAVID H., NOUSHMEHR, H., IAVARONE, A., VERHAAK, R. G. W., ANJUM, S., ARACHCHI, H., AUMAN, J. T., BALASUNDARAM, M., BALU, S., BARNETT, G., BAYLIN, S., BELL, S., BENZ, C., BIR, N., BLACK, KEITH L., BODENHEIMER, T., BOICE, L., BOOTWALLA, MOIZ S., BOWEN, J., BRISTOW, CHRISTOPHER A., BUTTERFIELD, YARON S. N., CHEN, Q.-R., CHIN, L., CHO, J., CHUAH, E., CHUDAMANI, S., COETZEE, SIMON G., COHEN, MARK L., COLMAN, H., COUCE, M., D'ANGELO, F., DAVIDSEN, T., DAVIS, A., DEMCHOK, JOHN A., DEVINE, K., DING, L., DUELL, R., ELDER, J. B., ESCHBACHER, JENNIFER M., FEHRENBACH, A., FERGUSON, M., FRAZER, S., FULLER, G., FULOP, J., GABRIEL, STACEY B., GAROFANO, L., GASTIER-FOSTER, JULIE M., GEHLENBORG, N., GERKEN, M., GETZ, G., GIANNINI, C., GIBSON, WILLIAM J., HADJIPANAYIS, A., HAYES, D. N., HEIMAN, DAVID I., HERMES, B., HILTY, J., HOADLEY, KATHERINE A., et al. 2016. Molecular Profiling Reveals Biologically Discrete Subsets and Pathways of Progression in Diffuse Glioma. *Cell,* 164**,** 550-563.

CHAN, J. H. P., LIM, S. & WONG, W. S. F. 2006. ANTISENSE OLIGONUCLEOTIDES: FROM DESIGN TO THERAPEUTIC APPLICATION. *Clinical and Experimental Pharmacology and Physiology,* 33**,** 533-540.

CHANG, L., ZHAO, D., LIU, H. B., WANG, Q. S., ZHANG, P., LI, C. L., DU, W. Z., WANG, H. J., LIU, X. & ZHANG, Z. R. 2015. Activation of sonic hedgehog signaling enhances cell

migration and invasion by induction of matrix metalloproteinase-2 and-9 via the phosphoinositide-3 kinase/AKT signaling pathway in glioblastoma. Corrigendum in/mmr/12/5/7815. *Molecular medicine reports,* 12**,** 6702-6710.

CHEARWAE, W., WU, C.-P., CHU, H.-Y., LEE, T. R., AMBUDKAR, S. V. & LIMTRAKUL, P. 2006. Curcuminoids purified from turmeric powder modulate the function of human multidrug resistance protein 1 (ABCC1). *Cancer chemotherapy and pharmacology,* 57**,** 376.

CHEN, M.-H., WILSON, C. W., LI, Y.-J., LAW, K. K. L., LU, C.-S., GACAYAN, R., ZHANG, X., HUI, C.-C. & CHUANG, P.-T. 2009. Cilium-independent regulation of Gli protein function by Sufu in Hedgehog signaling is evolutionarily conserved. *Genes & development,* 23**,** 1910-1928.

CHEN, Y.-J., LIAO, H.-F. & CHAO, C. 2011. Hedgehog Signaling and Cancer Treatment Resistance. 151-161.

CHEN, Y., BIEBER, M. M. & TENG, N. N. 2014. Hedgehog signaling regulates drug sensitivity by targeting ABC transporters ABCB1 and ABCG2 in epithelial ovarian cancer. *Mol Carcinog,* 53**,** 625-34.

CHENG, L., ANGLIN, E., CUNIN, F., KIM, D., SAILOR, M. J., FALKENSTEIN, I., TAMMEWAR, A. & FREEMAN, W. R. 2008. Intravitreal properties of porous silicon photonic crystals: a potential self-reporting intraocular drug-delivery vehicle. *British Journal of Ophthalmology,* 92**,** 705-711.

CHENG, S. Y. & YUE, S. 2008. Chapter 2 Role and Regulation of Human Tumor Suppressor SUFU in Hedgehog Signaling. *Advances in Cancer Research.* Academic Press.

CHENG, X., RAJJOUB, K., SHERMAN, J., CANADY, J., RECEK, N., YAN, D., BIAN, K., MURAD, F. & KEIDAR, M. 2015. Cold plasma accelerates the uptake of gold nanoparticles into glioblastoma cells. *Plasma Processes and Polymers,* 12**,** 1364-1369.

CHEREPANOV, S. A., CHEREPANOVA, K. I., GRINENKO, N. F., ANTONOVA, O. M. & CHEKHONIN, V. P. 2016. Effect of Hedgehog Signaling Pathway Activation on Proliferation of High-Grade Gliomas. *Bulletin of Experimental Biology and Medicine,* 161**,** 674-678.

CHINOT, O. L., WICK, W., MASON, W., HENRIKSSON, R., SARAN, F., NISHIKAWA, R., CARPENTIER, A. F., HOANG-XUAN, K., KAVAN, P., CERNEA, D., BRANDES, A. A., HILTON, M., ABREY, L. & CLOUGHESY, T. 2014. Bevacizumab plus radiotherapy-temozolomide for newly diagnosed glioblastoma. *N Engl J Med,* 370**,** 709-22.

CHIU, Y.-L. & RANA, T. M. 2003. siRNA function in RNAi: a chemical modification analysis. *Rna,* 9**,** 1034-1048.

CHOUNG, S., KIM, Y. J., KIM, S., PARK, H.-O. & CHOI, Y.-C. 2006. Chemical modification of siRNAs to improve serum stability without loss of efficacy. *Biochemical and biophysical research communications,* 342**,** 919-927.

CHRISTOPH, T., GRÜNWELLER, A., MIKA, J., SCHÄFER, M. K.-H., WADE, E. J., WEIHE, E., ERDMANN, V. A., FRANK, R., GILLEN, C. & KURRECK, J. 2006. Silencing of vanilloid receptor TRPV1 by RNAi reduces neuropathic and visceral pain in vivo. *Biochemical and biophysical research communications,* 350**,** 238-243.

CLEMENT, V., SANCHEZ, P., DE TRIBOLET, N., RADOVANOVIC, I. & I ALTABA, A. R. 2007. HEDGEHOG-GLI1 signaling regulates human glioma growth, cancer stem cell self-renewal, and tumorigenicity. *Current biology,* 17**,** 165-172.

COCHRANE, C. R., SZCZEPNY, A., WATKINS, D. N. & CAIN, J. E. 2015. Hedgehog Signaling in the Maintenance of Cancer Stem Cells. *Cancers (Basel),* 7**,** 1554-85.

COELHO, T., ADAMS, D., SILVA, A., LOZERON, P., HAWKINS, P. N., MANT, T., PEREZ, J., CHIESA, J., WARRINGTON, S., TRANTER, E., MUNISAMY, M., FALZONE, R., HARROP, J., CEHELSKY, J., BETTENCOURT, B. R., GEISSLER, M., BUTLER, J. S., SEHGAL, A., MEYERS, R. E., CHEN, Q., BORLAND, T., HUTABARAT, R. M., CLAUSEN, V. A., ALVAREZ, R., FITZGERALD, K., GAMBA-VITALO, C., NOCHUR, S. V., VAISHNAW, A. K., SAH, D. W., GOLLOB, J. A. & SUHR, O. B. 2013. Safety and Efficacy of RNAi Therapy for Transthyretin Amyloidosis. *N. Engl. J. Med.,* 369**,** 819.

COFFER, J. L., WHITEHEAD, M. A., NAGESHA, D. K., MUKHERJEE, P., AKKARAJU, G., TOTOLICI, M., SAFFIE, R. S. & CANHAM, L. T. 2005. Porous silicon-based scaffolds for tissue engineering and other biomedical applications. *physica status solidi (a),* 202**,** 1451-1455.

COGHLAN, M. A., SHIFREN, A., HUANG, H. J., RUSSELL, T. D., MITRA, R. D., ZHANG, Q., WEGNER, D. J., COLE, F. S. & HAMVAS, A. 2014. Sequencing of idiopathic pulmonary fibrosis-related genes reveals independent single gene associations. *BMJ Open Respir Res,* 1**,** e000057.

COLE, S., BHARDWAJ, G., GERLACH, J., MACKIE, J., GRANT, C., ALMQUIST, K., STEWART, A., KURZ, E., DUNCAN, A. & DEELEY, R. 1992. Overexpression of a transporter gene in a

multidrug-resistant human lung cancer cell line. *SCIENCE-NEW YORK THEN WASHINGTON-,* 258**,** 1650-1650.

COLE, S. P. 2014. Multidrug resistance protein 1 (MRP1, ABCC1), a "multitasking" ATP-binding cassette (ABC) transporter. *Journal of Biological Chemistry,* 289**,** 30880-30888.

CONNOLLY, N. P., STOKUM, J. A., SCHNEIDER, C. S., OZAWA, T., XU, S., GALISTEO, R., CASTELLANI, R. J., KIM, A. J., SIMARD, J. M. & WINKLES, J. A. 2017. Genetically engineered rat gliomas: PDGF-driven tumor initiation and progression in tv-a transgenic rats recreate key features of human brain cancer. *PloS one,* 12**,** e0174557.

COOPER, A. F., YU, K. P., BRUECKNER, M., BRAILEY, L. L., JOHNSON, L., MCGRATH, J. M. & BALE, A. E. 2005. Cardiac and CNS defects in a mouse with targeted disruption of suppressor of fused. *Development,* 132**,** 4407-17.

CUI, D., XU, Q., WANG, K. & CHE, X. 2010. Gli1 is a potential target for alleviating multidrug resistance of gliomas. *J Neurol Sci,* 288**,** 156-66.

CZAUDERNA, F., FECHTNER, M., DAMES, S., AYGÜN, H., KLIPPEL, A., PRONK, G. J., GIESE, K. & KAUFMANN, J. 2003. Structural variations and stabilising modifications of synthetic siRNAs in mammalian cells. *Nucleic acids research,* 31**,** 2705-2716.

DAS, S., DEBNATH, N., CUI, Y., UNRINE, J. & PALLI, S. R. 2015. Chitosan, Carbon Quantum Dot, and Silica Nanoparticle Mediated dsRNA Delivery for Gene Silencing in Aedes aegypti: A Comparative Analysis. *ACS Applied Materials & Interfaces,* 7**,** 19530-19535.

DAS, S., SAMANT, R. S. & SHEVDE, L. A. 2013. Nonclassical activation of Hedgehog signaling enhances multidrug resistance and makes cancer cells refractory to Smoothened-targeting Hedgehog inhibition. *J Biol Chem,* 288**,** 11824-33.

DE BONIS, P., ANILE, C., POMPUCCI, A., FIORENTINO, A., BALDUCCI, M., CHIESA, S., LAURIOLA, L., MAIRA, G. & MANGIOLA, A. 2013. The influence of surgery on recurrence pattern of glioblastoma. *Clin Neurol Neurosurg,* 115**,** 37-43.

DE ROBLES, P., FIEST, K. M., FROLKIS, A. D., PRINGSHEIM, T., ATTA, C., ST GERMAINE-SMITH, C., DAY, L., LAM, D. & JETTE, N. 2015. The worldwide incidence and prevalence of primary brain tumors: a systematic review and meta-analysis. *Neuro Oncol,* 17**,** 776-83.

DEEKEN, J. F. & LÖSCHER, W. 2007. The blood-brain barrier and cancer: transporters, treatment, and Trojan horses. *Clinical Cancer Research,* 13**,** 1663-1674.

DEGORTER, M. K., CONSEIL, G., DEELEY, R. G., CAMPBELL, R. L. & COLE, S. P. 2008. Molecular modeling of the human multidrug resistance protein 1 (MRP1/ABCC1). *Biochemical and biophysical research communications,* 365**,** 29-34.

DELI, M. A., ÁBRAHÁM, C. S., KATAOKA, Y. & NIWA, M. 2005. Permeability studies on in vitro blood–brain barrier models: physiology, pathology, and pharmacology. *Cellular and molecular neurobiology,* 25**,** 59-127.

DEVI, G. 2006. siRNA-based approaches in cancer therapy. *Cancer gene therapy,* 13**,** 819-829.

DI PASQUA, A. J., SHARMA, K. K., SHI, Y.-L., TOMS, B. B., OUELLETTE, W., DABROWIAK, J. C. & ASEFA, T. 2008. Cytotoxicity of mesoporous silica nanomaterials. *Journal of inorganic biochemistry,* 102**,** 1416-1423.

DOBIN, A., DAVIS, C. A., SCHLESINGER, F., DRENKOW, J., ZALESKI, C., JHA, S., BATUT, P., CHAISSON, M. & GINGERAS, T. R. 2013. STAR: ultrafast universal RNA-seq aligner. *Bioinformatics,* 29**,** 15-21.

DOGAN, A. L., LEGRAND, O., FAUSSAT, A. M., PERROT, J. Y. & MARIE, J. P. 2004. Evaluation and comparison of MRP1 activity with three fluorescent dyes and three modulators in leukemic cell lines. *Leuk Res,* 28**,** 619-22.

DRENKHAHN, S., JACKSON, G., SLUSARZ, A., STARKEY, N. & LUBAHN, D. 2013. Inhibition of Hedgehog/Gli Signaling by Botanicals: A Review of Compounds with Potential Hedgehog Pathway Inhibitory Activities. *Current Cancer Drug Targets,* 13**,** 580-595.

DU, W. Z., FENG, Y., WANG, X. F., PIAO, X. Y., CUI, Y. Q., CHEN, L. C., LEI, X. H., SUN, X., LIU, X., WANG, H. B., LI, X. F., YANG, D. B., SUN, Y., ZHAO, Z. F., JIANG, T., LI, Y. L. & JIANG, C. L. 2013. Curcumin suppresses malignant glioma cells growth and induces apoptosis by inhibition of SHH/GLI1 signaling pathway in vitro and vivo. *CNS Neurosci Ther,* 19**,** 926-36.

DUNNICK, K. M., BADDING, M. A., SCHWEGLER-BERRY, D., PATETE, J. M., KOENIGSMANN, C., WONG, S. S. & LEONARD, S. S. 2014. The effect of tungstate nanoparticles on reactive oxygen species and cytotoxicity in RAW 264.7 mouse monocyte macrophage cells. *Journal of Toxicology and Environmental Health, Part A,* 77**,** 1251-1268.

EASTOE, J., HOLLAMBY, M. J. & HUDSON, L. 2006. Recent advances in nanoparticle synthesis with reversed micelles. *Advances in colloid and interface science,* 128**,** 5-15.

EBRAHIMI SHAHMABADI, H., MOVAHEDI, F., KOOHI MOFTAKHARI ESFAHANI, M., ALAVI, S. E., ESLAMIFAR, A., MOHAMMADI ANARAKI, G. & AKBARZADEH, A. 2014. Efficacy of Cisplatin-loaded polybutyl cyanoacrylate nanoparticles on the glioblastoma. *Tumour Biol*.

EHTESHAM, M., SARANGI, A., VALADEZ, J. G., CHANTHAPHAYCHITH, S., BECHER, M. W., ABEL, T. W., THOMPSON, R. C. & COOPER, M. K. 2007. Ligand-dependent activation of the hedgehog pathway in glioma progenitor cells. *Oncogene,* 26**,** 5752-61.

EKHORUTOMWEN, S. A., SAWAN, S. P., SMITH, B. F., ROBISON, T. W. & WILSON, K. V. 2004. Solution Behavior of Modified Polyethylenimine (PEI) Polymers by Light Scattering Investigations. University of Massachusetts Lowell, Research Foundation (US).

ELAMIN, M. H., SHINWARI, Z., HENDRAYANI, S. F., AL-HINDI, H., AL-SHAIL, E., KHAFAGA, Y., AL-KOFIDE, A. & ABOUSSEKHRA, A. 2010. Curcumin inhibits the Sonic Hedgehog signaling pathway and triggers apoptosis in medulloblastoma cells. *Mol Carcinog,* 49**,** 302-14.

ERNEST, N. J. & SONTHEIMER, H. 2009. Glioma. *In:* EDITOR IN, C., XA & LARRY, R. S. (eds.) *Encyclopedia of Neuroscience.* Oxford: Academic Press.

ERTAO, Z., JIANHUI, C., CHUANGQI, C., CHANGJIANG, Q., SILE, C., YULONG, H., HUI, W. & SHIRONG, C. 2016. Autocrine Sonic hedgehog signaling promotes gastric cancer proliferation through induction of phospholipase Cgamma1 and the ERK1/2 pathway. *J Exp Clin Cancer Res,* 35**,** 63.

EVANS, M. R. & EVANS, S. B. 2016. Glioblastoma multiforme: a devastating diagnosis. *Practical Neurology,* 16**,** 416-418.

EVERS, R., ZAMAN, G. J., VAN DEEMTER, L., JANSEN, H., CALAFAT, J., OOMEN, L. C., OUDE ELFERINK, R. P., BORST, P. & SCHINKEL, A. H. 1996. Basolateral localization and export activity of the human multidrug resistance-associated protein in polarized pig kidney cells. *J Clin Invest,* 97**,** 1211-8.

EWE, A., PANCHAL, O., PINNAPIREDDY, S. R., BAKOWSKY, U., PRZYBYLSKI, S., TEMME, A. & AIGNER, A. 2017. Liposome-polyethylenimine complexes (DPPC-PEI lipopolyplexes) for therapeutic siRNA delivery in vivo. *Nanomedicine,* 13**,** 209-218.

FANG, C., WANG, K., STEPHEN, Z. R., MU, Q., KIEVIT, F. M., CHIU, D. T., PRESS, O. W. & ZHANG, M. 2015. Temozolomide nanoparticles for targeted glioblastoma therapy. *ACS applied materials & interfaces,* 7**,** 6674-6682.

Feller, N., Kuiper, C M., Lankelma, J., Ruhdal, J K., Scheper, R.J., Pinedo, H.M., Broxterman, H.J. 1995 Functional Detection of MDR1/P170 and MRP/P190-mediated Multidrug Resistance in Tumour Cells by Flow Cytometry Br J Cancer. Sep;72(3):543-9.

FERRUZZI, P., MENNILLO, F., DE ROSA, A., GIORDANO, C., ROSSI, M., BENEDETTI, G., MAGRINI, R., MOHR, G., MIRAGLIOTTA, V. & MAGNONI, L. 2012. In vitro and in vivo characterization of a novel Hedgehog signaling antagonist in human glioblastoma cell lines. *International Journal of Cancer,* 131**,** E33-E44.

FILBIN, M. G., DABRAL, S. K., PAZYRA-MURPHY, M. F., RAMKISSOON, S., KUNG, A. L., PAK, E., CHUNG, J., THEISEN, M. A., SUN, Y. & FRANCHETTI, Y. 2013. Coordinate activation of Shh and PI3K signaling in PTEN-deficient glioblastoma: new therapeutic opportunities. *Nature medicine,* 19**,** 1518-1523.

FIRE, A., XU, S., MONTGOMERY, M. K., KOSTAS, S. A., DRIVER, S. E. & MELLO, C. C. 1998. Potent and specific genetic interference by double-stranded RNA in Caenorhabditis elegans. *Nature,* 391**,** 806-811.

FOWLER, A., THOMSON, D., GILES, K., MALEKI, S., MREICH, E., WHEELER, H., LEEDMAN, P., BIGGS, M., COOK, R., LITTLE, N., ROBINSON, B. & MCDONALD, K. 2011. miR-124a is frequently down-regulated in glioblastoma and is involved in migration and invasion. *European Journal of Cancer,* 47**,** 953-963.

FURUKAWA, H., CORDOVA, K. E., O'KEEFFE, M. & YAGHI, O. M. 2013. The chemistry and applications of metal-organic frameworks. *Science,* 341**,** 1230444.

GABAY, L., LOWELL, S., RUBIN, L. L. & ANDERSON, D. J. 2003. Deregulation of dorsoventral patterning by FGF confers trilineage differentiation capacity on CNS stem cells in vitro. *Neuron,* 40**,** 485-499.

GAITZSCH, J., HUANG, X. & VOIT, B. 2015. Engineering Functional Polymer Capsules toward Smart Nanoreactors. *Chemical reviews,* 116**,** 1053-1093.

GANGA, S. 2008. *Multifunctional nanoemulsion system for combination paclitaxel and curcumin delivery in human glioblastoma cells.* M.S., Northeastern University.

GAO, Y., XIE, J., CHEN, H., GU, S., ZHAO, R., SHAO, J. & JIA, L. 2014. Nanotechnology-based intelligent drug design for cancer metastasis treatment. *Biotechnology advances,* 32**,** 761-777.

GE, S. 2010. RNA interference as a gene knockdown technique. *The International Journal of Biochemistry & Cell Biology,* 42**,** 1243-1251.

GELBMANN, C. B. & KALEJTA, R. F. 2019. The Membrane-Spanning Peptide and Acidic Cluster Dileucine Sorting Motif of UL138 Are Required To Downregulate MRP1 Drug Transporter Function in Human Cytomegalovirus-Infected Cells. *Journal of Virology,* 93**,** e00430-19.

GENNUSO, F., FERNETTI, C., TIROLO, C., TESTA, N., L'EPISCOPO, F., CANIGLIA, S., MORALE, M. C., OSTROW, J. D., PASCOLO, L., TIRIBELLI, C. & MARCHETTI, B. 2004. Bilirubin protects astrocytes from its own toxicity by inducing up-regulation and translocation of multidrug resistance-associated protein 1 (Mrp1). *Proc Natl Acad Sci U S A,* 101**,** 2470-5.

GILLERON, J., QUERBES, W., ZEIGERER, A., BORODOVSKY, A., MARSICO, G., SCHUBERT, U., MANYGOATS, K., SEIFERT, S., ANDREE, C., STOTER, M., EPSTEIN-BARASH, H., ZHANG, L., KOTELIANSKY, V., FITZGERALD, K., FAVA, E., BICKLE, M., KALAIDZIDIS, Y., AKINC, A., MAIER, M. & ZERIAL, M. 2013. Image-based analysis of lipid nanoparticle-mediated siRNA delivery, intracellular trafficking and endosomal escape. *Nat Biotechnol,* 31**,** 638-46.

GOLALIPOUR, M., MAHJOUBI, F. & SANATI, M. H. 2006. RNAi Induced Inhibition of MRP1 Expression and Reversal of Drug Resistance in Human Promyelocytic HL60 Cell Line. *Iranian Journal of Biotechnology,* 4**,** 169-173.

GOLDEN, P. L. & POLLACK, G. M. 2003. Blood–brain barrier efflux transport. *Journal of pharmaceutical sciences,* 92**,** 1739-1753.

GORDON, S., TEICHMANN, E., YOUNG, K., FINNIE, K., RADES, T. & HOOK, S. 2010. In vitro and in vivo investigation of thermosensitive chitosan hydrogels containing silica nanoparticles for vaccine delivery. *Eur J Pharm Sci,* 41**,** 360-8.

GOTTESMAN, M. M., FOJO, T. & BATES, S. E. 2002. Multidrug resistance in cancer: role of ATP-dependent transporters. *Nat Rev Cancer,* 2**,** 48-58.

GUO, W., CHEN, W., YU, W., HUANG, W. & DENG, W. 2013. Small interfering RNA-based molecular therapy of cancers. *Chin J Cancer,* 32**,** 488-493.

GUPTA, S., TAKEBE, N. & LORUSSO, P. 2010. Targeting the Hedgehog pathway in cancer. *Therapeutic Advances in Medical Oncology,* 2**,** 237-50.

GUTKIN, A., COHEN, Z. R. & PEER, D. 2016. Harnessing nanomedicine for therapeutic intervention in glioblastoma. *Expert Opinion on Drug Delivery,* 13**,** 1573-1582.

GYORFFY, B., SUROWIAK, P., KIESSLICH, O., DENKERT, C., SCHAFER, R., DIETEL, M. & LAGE, H. 2006. Gene expression profiling of 30 cancer cell lines predicts resistance towards 11 anticancer drugs at clinically achieved concentrations. *Int J Cancer,* 118**,** 1699-712.

HAHN, H., WICKING, C., ZAPHIROPOULOS, P. G., GAILANI, M. R., SHANLEY, S., CHIDAMBARAM, A., VORECHOVSKY, I., HOLMBERG, E., UNDEN, A. B. & GILLIES, S. 1996. Mutations of the human homolog of Drosophila patched in the nevoid basal cell carcinoma syndrome. *Cell,* 85**,** 841-851.

HARTZ, A. M. & BAUER, B. 2011. ABC transporters in the CNS - an inventory. *Curr Pharm Biotechnol,* 12**,** 656-73.

HASANZADEH KAFSHGARI, M., ALNAKHLI, M., DELALAT, B., APOSTOLOU, S., HARDING, F. J., MAKILA, E., SALONEN, J. J., KUSS, B. J. & VOELCKER, N. H. 2015. Small interfering RNA delivery by polyethylenimine-functionalised porous silicon nanoparticles. *Biomaterials Science*.

HASEGAWA, S., TANIGUCHI, K., YOKOMIZO, A., KUWANO, T., ONO, M., MORI, T., HORI, S., KOHNO, K. & KUWANO, M. 1994. Possible involvement of multidrug‐resistance‐associated protein (MRP) gene expression in spontaneous drug resistance to vincristine, etoposide and adriamycin in human glioma cells. *International journal of cancer,* 58**,** 860-864.

HEBROK, M., KIM, S. K., ST JACQUES, B., MCMAHON, A. P. & MELTON, D. A. 2000. Regulation of pancreas development by hedgehog signaling. *Development,* 127**,** 4905-4913.

HENDERSON, M. J., HABER, M., PORRO, A., MUNOZ, M. A., IRACI, N., XUE, C., MURRAY, J., FLEMMING, C. L., SMITH, J. & FLETCHER, J. I. 2011. ABCC multidrug transporters in childhood neuroblastoma: clinical and biological effects independent of cytotoxic drug efflux. *Journal of the National Cancer Institute,* 103**,** 1236-1251.

HERNANDEZ, M., RECIO, G., SEVILLA, P., TORRES-COSTA, V., GARCIA-RAMOS, J. V., DOMINGO, C. & MARTIN-PALMA, R. J. 2012. Development of drug delivery systems based on nanostructured porous silicon loaded with the anti-tumoral drug emodin adsorbed on silver nanoparticles. *Nanostructured Thin Films V,* 8465.

HOBBS, S. K., MONSKY, W. L., YUAN, F., ROBERTS, W. G., GRIFFITH, L., TORCHILIN, V. P. & JAIN, R. K. 1998. Regulation of transport pathways in tumor vessels: role of tumor type and microenvironment. *Proceedings of the National Academy of Sciences,* 95**,** 4607-4612.

HOELZL, M. A., HEBY-HENRICSON, K., GERLING, M., DIAS, J. M., KUIPER, R. V., TRÜNKLE, C., BERGSTRÖM, Å., ERICSON, J., TOFTGÅRD, R. & TEGLUND, S. 2017. Differential requirement of SUFU in tissue development discovered in a hypomorphic mouse model. *Developmental biology,* 429**,** 132-146.

HOLLAND, E. C. 2001. Gliomagenesis: genetic alterations and mouse models. *Nat Rev Genet,* 2**,** 120-129.

HOLLAND, I. B. 2011. ABC transporters, mechanisms and biology: an overview. *Essays Biochem,* 50**,** 1-17.

HOMBACH-KLONISCH, S., MEHRPOUR, M., SHOJAEI, S., HARLOS, C., PITZ, M., HAMAI, A., SIEMIANOWICZ, K., LIKUS, W., WIECHEC, E., TOYOTA, B. D., HOSHYAR, R., SEYFOORI, A., SEPEHRI, Z., ANDE, S. R., KHADEM, F., AKBARI, M., GORMAN, A. M., SAMALI, A., KLONISCH, T. & GHAVAMI, S. 2018. Glioblastoma and chemoresistance to alkylating agents: Involvement of apoptosis, autophagy, and unfolded protein response. *Pharmacology and Therapeutics,* 184**,** 13-41.

HU, C.-M. J. & ZHANG, L. 2012. Nanoparticle-based combination therapy toward overcoming drug resistance in cancer. *Biochemical Pharmacology,* 83**,** 1104-1111.

HU, D. & MARCUCIO, R. S. 2009. A SHH-responsive signaling center in the forebrain regulates craniofacial morphogenesis via the facial ectoderm. *Development,* 136**,** 107-16.

IM, S., CHOI, H. J., YOO, C., JUNG, J. H., JEON, Y. W., SUH, Y. J. & KANG, C. S. 2013. Hedgehog related protein expression in breast cancer: gli-2 is associated with poor overall survival. *Korean J Pathol,* 47**,** 116-23.

INGHAM, P. W. & MCMAHON, A. P. 2001. Hedgehog signaling in animal development: paradigms and principles. *Genes & development,* 15**,** 3059-3087.

ISHIKAWA, M., SONOBE, M., IMAMURA, N., SOWA, T., SHIKUMA, K. & DATE, H. 2014. Expression of the GLI family genes is associated with tumor progression in advanced lung adenocarcinoma. *World J Surg Oncol,* 12**,** 253.

JAIN, R. K., DI TOMASO, E., DUDA, D. G., LOEFFLER, J. S., SORENSEN, A. G. & BATCHELOR, T. T. 2007. Angiogenesis in brain tumours. *Nature Reviews Neuroscience,* 8**,** 610-622.

JAMBHRUNKAR, S., KARMAKAR, S., POPAT, A., YU, M. & YU, C. 2014. Mesoporous silica nanoparticles enhance the cytotoxicity of curcumin. *RSC Advances,* 4**,** 709-712.

JANE, A., DRONOV, R., HODGES, A. & VOELCKER, N. H. 2009. Porous silicon biosensors on the advance. *Trends in biotechnology,* 27**,** 230-239.

JELSMA, R. & BUCY, P. C. 1967. The treatment of glioblastoma multiforme of the brain. *Journal of neurosurgery,* 27**,** 388-400.

JHA, P., AGRAWAL, R., PATHAK, P., KUMAR, A., PURKAIT, S., MALLIK, S., SURI, V., CHAND SHARMA, M., GUPTA, D., SURI, A., SHARMA, B. S., JULKA, P. K., KULSHRESHTHA, R. & SARKAR, C. 2015. Genome-wide small noncoding RNA profiling of pediatric high-grade gliomas reveals deregulation of several miRNAs, identifies downregulation of snoRNA

cluster HBII-52 and delineates H3F3A and TP53 mutant-specific miRNAs and snoRNAs. *International Journal of Cancer,* 137**,** 2343-2353.

JIA, J., KOLTERUD, Å., ZENG, H., HOOVER, A., TEGLUND, S., TOFTGÅRD, R. & LIU, A. 2009. Suppressor of Fused inhibits mammalian Hedgehog signaling in the absence of cilia. *Developmental biology,* 330**,** 452-460.

JIANG, J. & HUI, C.-C. 2008. Hedgehog Signaling in Development and Cancer. *Developmental Cell,* 15**,** 801-812.

KAFSHGARI, M. H., DELALAT, B., TONG, W. Y., HARDING, F. J., KAASALAINEN, M., SALONEN, J. & VOELCKER, N. H. 2015. Oligonucleotide delivery by chitosan-functionalized porous silicon nanoparticles. *Nano Research,* 8**,** 2033-2046.

KAFSHGARI, M. H., HARDING, F. J. & VOELCKER, N. H. 2015. Insights into Cellular Uptake of Nanoparticles. *Current Drug Delivery,* 12**,** 63-77.

KAMALY, N., XIAO, Z., VALENCIA, P. M., RADOVIC-MORENO, A. F. & FAROKHZAD, O. C. 2012. Targeted polymeric therapeutic nanoparticles: design, development and clinical translation. *Chemical Society Reviews,* 41**,** 2971-3010.

KAMALY, N., YAMEEN, B., WU, J. & FAROKHZAD, O. C. 2016. Degradable Controlled-Release Polymers and Polymeric Nanoparticles: Mechanisms of Controlling Drug Release. *Chemical Reviews,* 116**,** 2602-2663.

KARTAL-YANDIM, M., ADAN-GOKBULUT, A. & BARAN, Y. 2016. Molecular mechanisms of drug resistance and its reversal in cancer. *Critical Reviews in Biotechnology,* 36**,** 716-726.

KARVAR, S. 2014. The role of ABC transporters in anticancer drug transport. *Turkish Journal of Biology,* 38**,** 800-805.

KASHANIAN, S., HARDING, F., IRANI, Y., KLEBE, S., MARSHALL, K., LONI, A., CANHAM, L., FAN, D., WILLIAMS, K. A., VOELCKER, N. H. & COFFER, J. L. 2010. Evaluation of mesoporous silicon/polycaprolactone composites as ophthalmic implants. *Acta Biomaterialia,* 6**,** 7.

KATHAWALA, R. J., GUPTA, P., ASHBY JR, C. R. & CHEN, Z.-S. 2015. The modulation of ABC transporter-mediated multidrug resistance in cancer: A review of the past decade. *Drug Resistance Updates,* 18**,** 1-17.

KAWAHIRA, H., MA, N. H., TZANAKAKIS, E. S., MCMAHON, A. P., CHUANG, P.-T. & HEBROK, M. 2003. Combined activities of hedgehog signaling inhibitors regulate pancreas development. *Development,* 130**,** 4871-4879.

KEEGAN, T. H. M., RIES, L. A. G., BARR, R. D., GEIGER, A. M., DAHLKE, D. V., POLLOCK, B. H., BLEYER, W. A., ADOLESCENT, F. T. N. C. I. N. S. F. & GROUP, Y. A. O. E. W. 2016. Comparison of cancer survival trends in the United States of adolescents and young adults with those in children and older adults. 122**,** 1009-1016.

KEIME-GUIBERT , F., CHINOT , O., TAILLANDIER , L., CARTALAT-CAREL , S., FRENAY , M., KANTOR , G., GUILLAMO , J.-S., JADAUD , E., COLIN , P., BONDIAU , P.-Y., MENEÏ , P., LOISEAU , H., BERNIER , V., HONNORAT , J., BARRIÉ , M., MOKHTARI , K., MAZERON , J.-J., BISSERY , A. & DELATTRE , J.-Y. 2007. Radiotherapy for Glioblastoma in the Elderly. *New England Journal of Medicine,* 356**,** 1527-1535.

KELLEHER, F. C. 2011. Hedgehog signaling and therapeutics in pancreatic cancer. *Carcinogenesis,* 32**,** 445-51.

KEMPER, E. M., BOOGERD, W., THUIS, I., BEIJNEN, J. H. & VAN TELLINGEN, O. 2004. Modulation of the blood–brain barrier in oncology: therapeutic opportunities for the treatment of brain tumours? *Cancer Treatment Reviews,* 30**,** 415-423.

KHUNG, Y.-L., GRANEY, S. D. & VOELCKER, N. H. 2006. Micropatterning of Porous Silicon Films by Direct Laser Writing. *Biotechnology Progress,* 22**,** 1388-1393.

KHUNG, Y. L., BARRITT, G. & VOELCKER, N. H. 2008. Using continuous porous silicon gradients to study the influence of surface topography on the behaviour of neuroblastoma cells. *Experimental Cell Research,* 314**,** 789-800.

KIEVIT, F. M., WANG, F. Y., FANG, C., MOK, H., WANG, K., SILBER, J. R., ELLENBOGEN, R. G. & ZHANG, M. 2011. Doxorubicin loaded iron oxide nanoparticles overcome multidrug resistance in cancer in vitro. *J Control Release,* 152**,** 76-83.

KIM, S., NISHIMOTO, S. K., BUMGARDNER, J. D., HAGGARD, W. O., GABER, M. W. & YANG, Y. 2010. A chitosan/[beta]-glycerophosphate thermo-sensitive gel for the delivery of ellagic acid for the treatment of brain cancer. *Biomaterials,* 31**,** 4157-4166.

KINZLER, K. W., BIGNER, S. H., BIGNER, D. D., TRENT, J. M., LAW, M. L., O'BRIEN, S. J., WONG, A. J. & VOGELSTEIN, B. 1987. Identification of an amplified, highly expressed gene in a human glioma. *Science,* 236**,** 70-74.

KLINGER, N. V. & MITTAL, S. 2016. Therapeutic Potential of Curcumin for the Treatment of Brain Tumors. *Oxidative Medicine and Cellular Longevity,* 2016**,** 14.

KNIPPING, J., WIGGERS, H., RELLINGHAUS, B., ROTH, P., KONJHODZIC, D. & MEIER, C. 2004. Synthesis of high purity silicon nanoparticles in a low pressure microwave reactor. *Journal of nanoscience and nanotechnology,* 4**,** 1039-1044.

KNUDSEN, K. B., NORTHEVED, H., GJETTING, T., PERMIN, A., ANDRESEN, T. L., WEGENER, K. M., LAM, H. R. & LYKKESFELDT, J. 2014. Biodistribution of rhodamine B fluorescence-labeled cationic nanoparticles in rats. *Journal of Nanoparticle Research,* 16**,** 2221.

Koelblinger P, Lang R. New developments in the treatment of basal cell carcinoma: update on current and emerging treatment options with a focus on vismodegib. Onco Targets Ther. 2018;11:8327-8340.

KOK, J. W., KLAPPE, K. & HUMMEL, I. 2014. The Role of the Actin Cytoskeleton and Lipid Rafts in the Localization and Function of the ABCC1 Transporter. *Advances in Biology,* 2014**,** 11.

KOLEY, D. & BARD, A. J. 2012. Inhibition of the MRP1-mediated transport of the menadione-glutathione conjugate (thiodione) in HeLa cells as studied by SECM. *Proceedings of the National Academy of Sciences,* 109**,** 11522-11527.

KOPERMSUB, P., MAYEN, V., MCINNES, S. & VOELCKER, N. H. Fabrication and characterization of porous silicon nanoparticles for siRNA delivery. Nanotechnology (IEEE-NANO), 2011 11th IEEE Conference on, 15-18 Aug. 2011 2011. 830-832.

KOSTARELOS, K. 2007. Cellular uptake of functionalized carbon nanotubes is independent of functional group and cell type. *Nature Nanotechnol.,* 2**,** 108-113.

KOVALAINEN, M., MÖNKÄRE, J., KAASALAINEN, M., RIIKONEN, J., LEHTO, V.-P., SALONEN, J., HERZIG, K.-H. & JÄRVINEN, K. 2012. Development of porous silicon nanocarriers for parenteral peptide delivery. *Molecular pharmaceutics,* 10**,** 353-359.

KUNDU, P., MOHANTY, C. & SAHOO, S. K. 2012. Antiglioma activity of curcumin-loaded lipid nanoparticles and its enhanced bioavailability in brain tissue for effective glioblastoma therapy. *Acta Biomaterialia,* 8**,** 2670-2687.

KURRECK, J. 2008. *Therapeutic oligonucleotides,* Cambridge, UK, RSC Pub.

KUSS, B. J., CORBO, M., LAU, W. M., FENNELL, D. A., DEAN, N. M. & COTTER, F. E. 2002. In vitro and in vivo downregulation of MRP1 by antisense oligonucleotides: a potential role in neuroblastoma therapy. *International journal of cancer,* 98**,** 128-133.

KUSS, S., CORNUT, R., BEAULIEU, I., MEZOUR, M. A., ANNABI, B. & MAUZEROLL, J. 2011. Assessing multidrug resistance protein 1-mediated function in cancer cell multidrug resistance by scanning electrochemical microscopy and flow cytometry. *Bioelectrochemistry,* 82**,** 29-37.

LACROIX, M., ABI-SAID, D., FOURNEY, D. R., GOKASLAN, Z. L., SHI, W., DEMONTE, F., LANG, F. F., MCCUTCHEON, I. E., HASSENBUSCH, S. J. & HOLLAND, E. 2001. A multivariate analysis of 416 patients with glioblastoma multiforme: prognosis, extent of resection, and survival. *Journal of neurosurgery,* 95**,** 190-198.

LANGMEAD, B., TRAPNELL, C., POP, M. & SALZBERG, S. L. 2009. Ultrafast and memory-efficient alignment of short DNA sequences to the human genome. *Genome biology,* 10**,** R25.

LAQUINTANA, V., TRAPANI, A., DENORA, N., WANG, F., GALLO, J. M. & TRAPANI, G. 2009. New strategies to deliver anticancer drugs to brain tumors. *Expert Opinion on Drug Delivery,* 6**,** 1017-1032.

LAWRENCE, Y. R., LI, X. A., EL NAQA, I., HAHN, C. A., MARKS, L. B., MERCHANT, T. E. & DICKER, A. P. 2010. Radiation dose-volume effects in the brain. *Int J Radiat Oncol Biol Phys,* 76**,** S20-7.

LEE, S., KIM, M.-S., LEE, D., KWON, T. K., KHANG, D., YUN, H.-S. & KIM, S.-H. 2013. The comparative immunotoxicity of mesoporous silica nanoparticles and colloidal silica nanoparticles in mice. *International journal of nanomedicine,* 8**,** 147.

LEE, T. J., HAQUE, F., SHU, D., YOO, J. Y., LI, H., YOKEL, R. A., HORBINSKI, C., KIM, T. H., KIM, S.-H., KWON, C.-H., NAKANO, I., KAUR, B., GUO, P. & CROCE, C. M. 2015. *RNA nanoparticle as a vector for targeted siRNA delivery into glioblastoma mouse model*.

LEMMA, S., AVNET, S., SALERNO, M., CHANO, T. & BALDINI, N. 2016. Identification and Validation of Housekeeping Genes for Gene Expression Analysis of Cancer Stem Cells. *PLOS ONE,* 11**,** e0149481.

LESCHZINER, G., ZABANEH, D., PIRMOHAMED, M., OWEN, A., ROGERS, J., COFFEY, A. J., BALDING, D. J., BENTLEY, D. B. & JOHNSON, M. R. 2006. Exon sequencing and high resolution haplotype analysis of ABC transporter genes implicated in drug resistance. *Pharmacogenet Genomics,* 16**,** 439-50.

LESLIE, E. M., DEELEY, R. G. & COLE, S. P. C. 2005. Multidrug resistance proteins: role of P-glycoprotein, MRP1, MRP2, and BCRP (ABCG2) in tissue defense. *Toxicology and Applied Pharmacology,* 204**,** 216-237.

LI, M., DENG, H., PENG, H. & WANG, Q. 2014. Functional Nanoparticles in Targeting Glioma Diagnosis and Therapies. *Journal of Nanoscience and Nanotechnology,* 14**,** 415-432.

LI, W., MIAO, S., MIAO, M., LI, R., CAO, X., ZHANG, K., HUANG, G. & FU, B. 2016. Hedgehog Signaling Activation in Hepatic Stellate Cells Promotes Angiogenesis and Vascular Mimicry in Hepatocellular Carcinoma. *Cancer Invest,* 34**,** 424-430.

LI, X., XIE, Q. R., ZHANG, J., XIA, W. & GU, H. 2011. The packaging of siRNA within the mesoporous structure of silica nanoparticles. *Biomaterials,* 32**,** 9546-9556.

LIAN, N., JIANG, Y., ZHANG, F., JIN, H., LU, C., WU, X., LU, Y. & ZHENG, S. 2015. Curcumin regulates cell fate and metabolism by inhibiting hedgehog signaling in hepatic stellate cells. *Laboratory Investigation,* 95**,** 790-803.

LICCIARDI, M., SCIALABBA, C., CAVALLARO, G., SANGREGORIO, C., FANTECHI, E. & GIAMMONA, G. 2013. Cell uptake enhancement of folate targeted polymer coated magnetic nanoparticles. *Journal of biomedical nanotechnology,* 9**,** 949-964.

LIN, T. L. & MATSUI, W. 2012. Hedgehog pathway as a drug target: Smoothened inhibitors in development. *Onco Targets Ther,* 5**,** 47-58.

LIU, D., BIMBO, L. M., MÄKILÄ, E., VILLANOVA, F., KAASALAINEN, M., HERRANZ-BLANCO, B., CARAMELLA, C. M., LEHTO, V.-P., SALONEN, J. & HERZIG, K.-H. 2013. Co-delivery of a

hydrophobic small molecule and a hydrophilic peptide by porous silicon nanoparticles. *Journal of Controlled Release,* 170**,** 268-278.

LIU, X.-Q., XIONG, M.-H., SHU, X.-T., TANG, R.-Z. & WANG, J. 2012. Therapeutic delivery of siRNA silencing HIF-1 alpha with micellar nanoparticles inhibits hypoxic tumor growth. *Molecular pharmaceutics,* 9**,** 2863-2874.

LIVAK, K. J. & SCHMITTGEN, T. D. 2001. Analysis of relative gene expression data using real-time quantitative PCR and the 2− ΔΔCT method. *methods,* 25**,** 402-408.

LOE, D. W., ALMQUIST, K. C., DEELEY, R. G. & COLE, S. P. 1996. Multidrug resistance protein (MRP)-mediated transport of leukotriene C4 and chemotherapeutic agents in membrane vesicles. Demonstration of glutathione-dependent vincristine transport. *J Biol Chem,* 271**,** 9675-82.

LONG, J. 2015. Hedgehog Signaling in Cancer.

LOUIS, D. N., PERRY, A., REIFENBERGER, G., VON DEIMLING, A., FIGARELLA-BRANGER, D., CAVENEE, W. K., OHGAKI, H., WIESTLER, O. D., KLEIHUES, P. & ELLISON, D. W. 2016. The 2016 World Health Organization Classification of Tumors of the Central Nervous System: a summary. *Acta Neuropathologica,* 131**,** 803-820.

LOW, S. P., VOELCKER, N. H., CANHAM, L. T. & WILLIAMS, K. A. 2009. The biocompatibility of porous silicon in tissues of the eye. *Biomaterials,* 30**,** 2873-2880.

LOW, S. P., WILLIAMS, K. A., CANHAM, L. T. & VOELCKER, N. H. 2006. Evaluation of mammalian cell adhesion on surface-modified porous silicon. *Biomaterials,* 27**,** 4538-4546.

LÜ, J.-M., LIANG, Z., WANG, X., GU, J., YAO, Q. & CHEN, C. 2016. New polymer of lactic-co-glycolic acid-modified polyethylenimine for nucleic acid delivery. *Nanomedicine,* 11**,** 1971-1991.

MA, D. 2014. Enhancing endosomal escape for nanoparticle mediated siRNA delivery. *Nanoscale,* 6**,** 6415-6425.

MALHOTRA, M., TOMARO-DUCHESNEAU, C., SAHA, S. & PRAKASH, S. 2014. Intranasal Delivery of Chitosan–siRNA Nanoparticle Formulation to the Brain. *In:* JAIN, K. K. (ed.) *Drug Delivery System.* New York, NY: Springer New York.

MANJUNATH, N. & DYKXHOORN, D. M. 2010. Advances in synthetic siRNA delivery. *Discovery medicine,* 9**,** 418-430.

MARTI, E. & BOVOLENTA, P. 2002. Sonic hedgehog in CNS development: one signal, multiple outputs. *Trends Neurosci,* 25**,** 89-96.

MATSUMOTO, Y., MIYAKE, K., KUNISHIO, K., TAMIYA, T. & NAGAO, S. 2004. Reduction of expression of the multidrug resistance protein (MRP) 1 in glioma cells by antisense phosphorothioate oligonucleotides. *The Journal of Medical Investigation,* 51**,** 194-201.

MCINNES, S. J. & VOELCKER, N. H. 2009. Silicon-polymer hybrid materials for drug delivery. *Future medicinal chemistry,* 1**,** 1051-74.

MENG, H., MAI, W. X., ZHANG, H. Y., XUE, M., XIA, T., LIN, S. J., WANG, X., ZHAO, Y., JI, Z. X., ZINK, J. I. & NEL, A. E. 2013. Codelivery of an Optimal Drug/siRNA Combination Using Mesoporous Silica Nanoparticles To Overcome Drug Resistance in Breast Cancer in Vitro and in Vivo. *Acs Nano,* 7**,** 994-1005.

MENG, X., CAI, J., LIU, J., HAN, B., GAO, F., GAO, W., ZHANG, Y., ZHANG, J., ZHAO, Z. & JIANG, C. 2017. Curcumin increases efficiency of γ-irradiation in gliomas by inhibiting Hedgehog signaling pathway. *Cell Cycle,* 16**,** 1181-1192.

MILLER, D. S. 2015. Regulation of ABC Transporters at the Blood–Brain Barrier. *Clin Pharmacol Ther,* 97**,** 395.

MING, J. E., ROESSLER, E. & MUENKE, M. 1998. Human developmental disorders and the Sonic hedgehog pathway. *Molecular medicine today,* 4**,** 343-349.

MINNITI, G., MUNI, R., LANZETTA, G., MARCHETTI, P. & ENRICI, R. M. 2009. Chemotherapy for glioblastoma: current treatment and future perspectives for cytotoxic and targeted agents. *Anticancer Research,* 29**,** 5171-84.

MOHRI, M., NITTA, H. & YAMASHITA, J. 2000. Expression of Multidrug Resistance-associated Protein (MRP) in Human Gliomas. *Journal of Neuro-Oncology,* 49**,** 105-115.

MORGAN, L. L., MILLER, A. B. & DAVIS, D. L. 2016. Has the incidence of brain cancer risen in Australia since the introduction of mobile phones 29 years ago? *Cancer Epidemiology,* 44**,** 112.

MOZZETTI, S., MARTINELLI, E., RASPAGLIO, G., PRISLEI, S., DE DONATO, M., FILIPPETTI, F., SHAHABI, S., SCAMBIA, G. & FERLINI, C. 2012. Gli family transcription factors are drivers of patupilone resistance in ovarian cancer. *Biochem Pharmacol,* 84**,** 1409-18.

MRUGALA, M. M. 2013. Advances and challenges in the treatment of glioblastoma: a clinician's perspective. *Discovery medicine,* 15**,** 221-230.

MUENKE, M. & BEACHY, P. A. 2000. Genetics of ventral forebrain development and holoprosencephaly. *Curr Opin Genet Dev,* 10**,** 262-9.

MUNOZ, M., HENDERSON, M., HABER, M. & NORRIS, M. 2007. Role of the MRP1/ABCC1 multidrug transporter protein in cancer. *IUBMB life,* 59**,** 752-757.

NACHMIAS, B., ASHHAB, Y. & BEN-YEHUDA, D. 2004. The inhibitor of apoptosis protein family (IAPs): an emerging therapeutic target in cancer. *Seminars in Cancer Biology,* 14**,** 231-243.

NICHOLS, J. W. & BAE, Y. H. 2014. EPR: evidence and fallacy. *Journal of Controlled Release,* 190**,** 451-464.

NIEWIADOMSKI, P., ZHUJIANG, A., YOUSSEF, M. & WASCHEK, J. A. 2013. Interaction of PACAP with Sonic hedgehog reveals complex regulation of the Hedgehog pathway by PKA. *Cellular Signalling,* 25**,** 2222-2230.

NOBUSAWA, S., WATANABE, T., KLEIHUES, P. & OHGAKI, H. 2009. IDH1 mutations as molecular signature and predictive factor of secondary glioblastomas. *Clin Cancer Res,* 15**,** 6002-7.

NÜSSLEIN-VOLHARD, C. & WIESCHAUS, E. 1980. Mutations affecting segment number and polarity in Drosophila. *Nature,* 287**,** 795-801.

O'KEEFFE, E. & CAMPBELL, M. 2016. Modulating the paracellular pathway at the blood–brain barrier: current and future approaches for drug delivery to the CNS. *Drug Discovery Today: Technologies,* 20**,** 35-39.

OHGAKI, H. & KLEIHUES, P. 2013. The Definition of Primary and Secondary Glioblastoma. *American Association for Cancer Research,* 19**,** 764-772.

OLSON, D. P., TAYLOR, B. J. & IVY, S. P. 2001. Detection of MRP functional activity: Calcein AM but not BCECF AM as a multidrug resistance‐related protein (MRP1) substrate. *Cytometry Part A,* 46**,** 105-113.

OSLOBANU, A. & FLORIAN, S. I. 2015. Anatomic locations in high grade glioma. *Romanian Neurosurgery,* 29**,** 271-277.

OSTROM, Q. T., BAUCHET, L., DAVIS, F. G., DELTOUR, I., FISHER, J. L., LANGER, C. E., PEKMEZCI, M., SCHWARTZBAUM, J. A., TURNER, M. C., WALSH, K. M., WRENSCH, M. R. & BARNHOLTZ-SLOAN, J. S. 2014. The epidemiology of glioma in adults: a "state of the science" review. *Neuro Oncol,* 16**,** 896-913.

OSTROM, Q. T., GITTLEMAN, H., FULOP, J., LIU, M., BLANDA, R., KROMER, C., WOLINSKY, Y., KRUCHKO, C. & BARNHOLTZ-SLOAN, J. S. 2015. CBTRUS Statistical Report: Primary Brain and Central Nervous System Tumors Diagnosed in the United States in 2008-2012. *Neuro-Oncology,* 17**,** iv1-iv62.

OSTROM, Q. T., GITTLEMAN, H., TRUITT, G., BOSCIA, A., KRUCHKO, C. & BARNHOLTZ-SLOAN, J. S. J. N.-O. 2018. CBTRUS statistical report: primary brain and other central nervous system tumors diagnosed in the united states in 2011–2015. 20**,** iv1-iv86.

OZBEN, T. 2006. Mechanisms and strategies to overcome multiple drug resistance in cancer. *FEBS Letters,* 580**,** 2903-2909.

PAK, E. & SEGAL, ROSALIND A. 2016. Hedgehog Signal Transduction: Key Players, Oncogenic Drivers, and Cancer Therapy. *Developmental Cell,* 38**,** 333-344.

PARK, J.-H., GU, L., VON MALTZAHN, G., RUOSLAHTI, E., BHATIA, S. N. & SAILOR, M. J. 2009. Biodegradable luminescent porous silicon nanoparticles for in vivo applications. *Nature materials,* 8**,** 331-336.

PARSONS, D. W., JONES, S., ZHANG, X., LIN, J. C., LEARY, R. J., ANGENENDT, P., MANKOO, P., CARTER, H., SIU, I. M., GALLIA, G. L., OLIVI, A., MCLENDON, R., RASHEED, B. A., KEIR, S., NIKOLSKAYA, T., NIKOLSKY, Y., BUSAM, D. A., TEKLEAB, H., DIAZ, L. A., JR., HARTIGAN, J., SMITH, D. R., STRAUSBERG, R. L., MARIE, S. K., SHINJO, S. M., YAN, H., RIGGINS, G. J., BIGNER, D. D., KARCHIN, R., PAPADOPOULOS, N., PARMIGIANI, G., VOGELSTEIN, B., VELCULESCU, V. E. & KINZLER, K. W. 2008. An integrated genomic analysis of human glioblastoma multiforme. *Science,* 321**,** 1807-12.

PASTORINO, L., DELLACASA, E., DABIRI, M. H., FABIANO, B. & EROKHINA, S. 2016. Towards the Fabrication of Polyelectrolyte-Based Nanocapsules for Bio-Medical Applications. *BioNanoScience,* 6**,** 496-501.

PATEL, S. S., TOMAR, S., SHARMA, D., MAHINDROO, N. & UDAYABANU, M. 2017. Targeting sonic hedgehog signaling in neurological disorders. *Neuroscience & Biobehavioral Reviews,* 74**,** 76-97.

PATHI, S., PAGAN-WESTPHAL, S., BAKER, D. P., GARBER, E. A., RAYHORN, P., BUMCROT, D., TABIN, C. J., PEPINSKY, R. B. & WILLIAMS, K. P. 2001. Comparative biological responses to human Sonic, Indian, and Desert hedgehog. *Mechanisms of development,* 106**,** 107-117.

PAZINATO, J., CRUZ, O. M., NAIDEK, K. P., PIRES, A. R., WESTPHAL, E., GALLARDO, H., BAUBICHON-CORTAY, H., ROCHA, M. E., MARTINEZ, G. R. & WINNISCHOFER, S. M. 2018. Cytotoxicity of η6-areneruthenium-based molecules to glioblastoma cells and their recognition by multidrug ABC transporters. *European journal of medicinal chemistry,* 148**,** 165-177.

PEIGÑAN, L., GARRIDO, W., SEGURA, R., MELO, R., ROJAS, D., CÁRCAMO, J. G., SAN MARTÍN, R. & QUEZADA, C. 2011. Combined Use of Anticancer Drugs and an Inhibitor of Multiple Drug Resistance-Associated Protein-1 Increases Sensitivity and Decreases Survival of Glioblastoma Multiforme Cells In Vitro. *Neurochemical Research,* 36**,** 1397-1406.

PERAZZOLI, G., PRADOS, J., ORTIZ, R., CABA, O., CABEZA, L., BERDASCO, M., GÓNZALEZ, B. & MELGUIZO, C. 2015. Temozolomide resistance in glioblastoma cell lines: implication of MGMT, MMR, P-Glycoprotein and CD133 expression. *PloS one,* 10**,** e0140131.

PETERSON, B. G., TAN, K. W., OSA-ANDREWS, B. & IRAM, S. H. 2017. High-content screening of clinically tested anticancer drugs identifies novel inhibitors of human MRP1 (ABCC1). *Pharmacological Research,* 119**,** 313-326.

PETRYK, A., GRAF, D. & MARCUCIO, R. 2015. Holoprosencephaly: signaling interactions between the brain and the face, the environment and the genes, and the phenotypic variability in animal models and humans. *Wiley Interdisciplinary Reviews: Developmental Biology,* 4**,** 17-32.

QUEIROZ, K., RUELA-DE-SOUSA, R., FUHLER, G., ABERSON, H., FERREIRA, C., PEPPELENBOSCH, M. & SPEK, C. 2010. Hedgehog signaling maintains chemoresistance in myeloid leukemic cells. *Oncogene,* 29**,** 6314.

QUEZADA, C., GARRIDO, W., OYARZÚN, C., FERNÁNDEZ, K., SEGURA, R., MELO, R., CASANELLO, P., SOBREVIA, L. & SAN MARTÍN, R. 2013. 5′ ‐ ectonucleotidase mediates multiple ‐ drug resistance in glioblastoma multiforme cells. *Journal of cellular physiology,* 228**,** 602-608.

RAGELLE, H., VANDERMEULEN, G. & PRÉAT, V. 2013. Chitosan-based siRNA delivery systems. *Journal of Controlled Release,* 172**,** 207-218.

REGINA, A., KOMAN, A., PICIOTTI, M., EL HAFNY, B., CENTER, M. S., BERGMANN, R., COURAUD, P. O. & ROUX, F. 1998. Mrp1 multidrug resistance ‐ associated protein and P ‐ glycoprotein expression in rat brain microvessel endothelial cells. *Journal of neurochemistry,* 71**,** 705-715.

RENES, J., DE VRIES, E. G., NIENHUIS, E. F., JANSEN, P. L. & MULLER, M. 1999. ATP- and glutathione-dependent transport of chemotherapeutic drugs by the multidrug resistance protein MRP1. *Br J Pharmacol,* 126**,** 681-8.

RIMKUS, T. K., CARPENTER, R. L., QASEM, S., CHAN, M. & LO, H. W. 2016. Targeting the Sonic Hedgehog Signaling Pathway: Review of Smoothened and GLI Inhibitors. *Cancers (Basel),* 8.

ROBBIANI, D. F., FINCH, R. A., JÄGER, D., MULLER, W. A., SARTORELLI, A. C. & RANDOLPH, G. J. 2000. The Leukotriene C 4 Transporter MRP1 Regulates CCL19 (MIP-3β, ELC)–Dependent Mobilization of Dendritic Cells to Lymph Nodes. *Cell,* 103**,** 757-768.

ROMER, J. T., KIMURA, H., MAGDALENO, S., SASAI, K., FULLER, C., BAINES, H., CONNELLY, M., STEWART, C. F., GOULD, S. & RUBIN, L. L. 2004. Suppression of the Shh pathway using a small molecule inhibitor eliminates medulloblastoma in Ptc1+/− p53−/− mice. *Cancer cell,* 6**,** 229-240.

ROSSI, M., MAGNONI, L., MIRACCO, C., MORI, E., TOSI, P., PIRTOLI, L., TINI, P., OLIVERI, G., COSCI, E. & BAKKER, A. 2011. β-catenin and Gli1 are prognostic markers in glioblastoma. *Cancer Biology & Therapy,* 11**,** 753-761.

ROSTOMILY, R. C., BERMINGHAM-MCDONOGH, O., BERGER, M. S., TAPSCOTT, S. J., REH, T. A. & OLSON, J. M. 1997. Expression of neurogenic basic helix-loop-helix genes in primitive neuroectodermal tumors. *Cancer Res,* 57**,** 3526-31.

Roundhill E.A., and Burchill S.A. Detection and characterisation of multi-drug resistance protein 1 (MRP-1) in human mitochondria. 2012 British Journal of Cancer. 106, 1224-1233.

RUIZ I ALTABA, A., SANCHEZ, P. & DAHMANE, N. 2002. Gli and hedgehog in cancer: tumours, embryos and stem cells. *Nat Rev Cancer,* 2**,** 361-72.

SAAD, M., GARBUZENKO, O. B. & MINKO, T. 2008. Co-delivery of siRNA and an anticancer drug for treatment of multidrug-resistant cancer.

SADETZKI, S., CHETRIT, A., FREEDMAN, L., STOVALL, M., MODAN, B. & NOVIKOV, I. 2005. Long-Term Follow-up for Brain Tumor Development after Childhood Exposure to Ionizing Radiation for Tinea Capitis. *Radiation Research,* 163**,** 424-432.

SAWYER, A. J., PIEPMEIER, J. M. & SALTZMAN, W. M. 2006. New methods for direct delivery of chemotherapy for treating brain tumors. *Yale J Biol Med,* 79**,** 141-52.

SCALES, S. J. & DE SAUVAGE, F. J. 2009. Mechanisms of Hedgehog pathway activation in cancer and implications for therapy. *Trends in pharmacological sciences,* 30**,** 303-312.

SCHNIDAR, H., EBERL, M., KLINGLER, S., MANGELBERGER, D., KASPER, M., HAUSER-KRONBERGER, C., REGL, G., KROISMAYR, R., MORIGGL, R., SIBILIA, M. & ABERGER, F. 2009. Epidermal growth factor receptor signaling synergizes with Hedgehog/GLI in oncogenic transformation via activation of the MEK/ERK/JUN pathway. *Cancer Res,* 69**,** 1284-92.

SECRET, E., SMITH, K., DUBLJEVIC, V., MOORE, E., MACARDLE, P., DELALAT, B., ROGERS, M. L., JOHNS, T. G., DURAND, J. O., CUNIN, F. & VOELCKER, N. H. 2013. Antibody-functionalized porous silicon nanoparticles for vectorization of hydrophobic drugs. *Adv Healthc Mater,* 2**,** 718-27.

SEKULIC, A. & VON HOFF, D. 2016. Hedgehog pathway inhibition. *Cell,* 164**,** 831.

SELVAM, C., MUTISYA, D., PRAKASH, S., RANGANNA, K. & THILAGAVATHI, R. 2017. Therapeutic potential of chemically modified siRNA: Recent trends. *Chemical Biology & Drug Design***,** n/a-n/a.

SHAHI, M. H., LORENTE, A. & CASTRESANA, J. S. 2008. Hedgehog signalling in medulloblastoma, glioblastoma and neuroblastoma. *Oncol Rep,* 19**,** 681-8.

Shahi, M.H., Farheen, S., Mariyath, M.P.M., Castresana, J.S. Potential Role of Shh-Gli1-BMI1 Signaling Pathway Nexus in Glioma Chemoresistance. 2016. Tumour Biol37(11):15107-15114

SHANMUGAM, M. K., ARFUSO, F., SNG, J. C., BISHAYEE, A., KUMAR, A. P. & SETHI, G. 2019. Epigenetic Effects of Curcumin in Cancer Prevention. *Epigenetics of Cancer Prevention.* Elsevier.

Shanmugam, M., Rane, G., Kanchi, M., Arfuso, F., Chinnathambi, A., Zayed, M., Alharbi, S., Tan, B., Kumar, A. and Sethi, G., 2015. The multifaceted role of curcumin in cancer prevention and treatment. *Molecules*, *20*(2), pp.2728-2769.

SHAROM, F. J. 2008. ABC multidrug transporters: structure, function and role in chemoresistance. *Pharmacogenomics,* 9.

SHEN, J., KIM, H. C., SU, H., WANG, F., WOLFRAM, J., KIRUI, D., MAI, J., MU, C., JI, L. N., MAO, Z. W. & SHEN, H. 2014. Cyclodextrin and polyethylenimine functionalized mesoporous silica nanoparticles for delivery of siRNA cancer therapeutics. *Theranostics,* 4**,** 487-97.

SHEN, J., XU, R., MAI, J., KIM, H.-C., GUO, X., QIN, G., YANG, Y., WOLFRAM, J., MU, C. & XIA, X. 2013. High capacity nanoporous silicon carrier for systemic delivery of gene silencing therapeutics. *ACS nano,* 7**,** 9867-9880.

SHEN, W., LIANG, X.-H., SUN, H. & CROOKE, S. T. 2015. 2′ -Fluoro-modified phosphorothioate oligonucleotide can cause rapid degradation of P54nrb and PSF. *Nucleic acids research,* 43**,** 4569-4578.

SHEVDE, L. A. & SAMANT, R. S. 2014. Nonclassical hedgehog-GLI signaling and its clinical implications. *Int J Cancer,* 135**,** 1-6.

SHI, J., XU, Y., XU, X., ZHU, X., PRIDGEN, E., WU, J., VOTRUBA, A. R., SWAMI, A., ZETTER, B. R. & FAROKHZAD, O. C. 2014. Hybrid lipid–polymer nanoparticles for sustained siRNA delivery and gene silencing. *Nanomedicine: Nanotechnology, Biology and Medicine,* 10**,** e897-e900.

SIEGEL, R. L., MILLER, K. D. & JEMAL, A. 2016. Cancer statistics, 2016. *CA Cancer J Clin,* 66**,** 7-30.

SIEGEL, R. L., MILLER, K. D. & JEMAL, A. 2018. Cancer statistics, 2018. *CA: A Cancer Journal for Clinicians,* 68**,** 7-30.

SIMS-MOURTADA, J., IZZO, J. G., AJANI, J. & CHAO, K. S. 2007. Sonic Hedgehog promotes multiple drug resistance by regulation of drug transport. *Oncogene,* 26**,** 5674-9.

SIU, Y. S., LI, L., LEUNG, M. F., LEE, K. L. D. & LI, P. 2012. Polyethylenimine-based amphiphilic core–shell nanoparticles: study of gene delivery and intracellular trafficking. *Biointerphases,* 7**,** 16.

SŁOMKA, M., SOBALSKA-KWAPIS, M., KORYCKA-MACHAŁA, M., BARTOSZ, G., DZIADEK, J. & STRAPAGIEL, D. 2015. Genetic variation of the ABC transporter gene ABCC1 (Multidrug resistance protein 1 – MRP1) in the Polish population. *BMC Genetics,* 16**,** 114.

SONALI, M. K. V., SINGH, R. P., AGRAWAL, P., MEHATA, A. K., DATTA MAROTI PAWDE, N., SONKAR, R. & MUTHU, M. S. 2018. Nanotheranostics: Emerging Strategies for Early Diagnosis and Therapy of Brain Cancer. *Nanotheranostics,* 2**,** 70.

SPIEGL-KREINECKER, S., BUCHROITHNER, J., ELBLING, L., STEINER, E., WURM, G., BODENTEICH, A., FISCHER, J., MICKSCHE, M. & BERGER, W. 2002. Expression and functional activity of the ABC-transporter proteins P-glycoprotein and multidrug-resistance protein 1 in human brain tumor cells and astrocytes. *J Neurooncol,* 57**,** 27-36.

ST-JACQUES, B., HAMMERSCHMIDT, M. & MCMAHON, A. P. 1999. Indian hedgehog signaling regulates proliferation and differentiation of chondrocytes and is essential for bone formation. *Genes & development,* 13**,** 2072-2086.

ST AREVALO, A., I ERICES, J., A URIBE, D., HOWDEN, J., NIECHI, I., MUNOZ, S., S MARTÍN, R. & AQ MONRAS, C. 2017. Current therapeutic alternatives and new perspectives in glioblastoma multiforme. *Current medicinal chemistry,* 24**,** 2781-2795.

STAVROVSKAYA, A. A. 2000. Cellular mechanisms of multidrug resistance of tumor cells. *Biochemistry (Mosc),* 65**,** 95-106.

STECCA, B., MAS, C., CLEMENT, V., ZBINDEN, M., CORREA, R., PIGUET, V., BEERMANN, F. & RUIZ, I. A. A. 2007. Melanomas require HEDGEHOG-GLI signaling regulated by interactions between GLI1 and the RAS-MEK/AKT pathways. *Proc Natl Acad Sci U S A,* 104**,** 5895-900.

STEIN, G. H. 1979. T98G: an anchorage-independent human tumor cell line that exhibits stationary phase G1 arrest in vitro. *J Cell Physiol,* 99**,** 43-54.

STEIN, U., JURCHOTT, K., SCHLAFKE, M. & HOHENBERGER, P. 2002. Expression of multidrug resistance genes MVP, MDR1, and MRP1 determined sequentially before, during, and after hyperthermic isolated limb perfusion of soft tissue sarcoma and melanoma patients. *J Clin Oncol,* 20**,** 3282-92.

STEINIGER, S. C., KREUTER, J., KHALANSKY, A. S., SKIDAN, I. N., BOBRUSKIN, A. I., SMIRNOVA, Z. S., SEVERIN, S. E., UHL, R., KOCK, M., GEIGER, K. D. & GELPERINA, S. E. 2004. Chemotherapy of glioblastoma in rats using doxorubicin-loaded nanoparticles. *Int J Cancer,* 109**,** 759-67.

STRATTON, M. R., CAMPBELL, P. J. & FUTREAL, P. A. 2009. The cancer genome. *Nature,* 458**,** 719-724.

STUKEL, J. M. & CAPLAN, M. R. 2009. Targeted drug delivery for treatment and imaging of glioblastoma multiforme. *Expert opinion on drug delivery,* 6**,** 705-718.

STUMMER, W., NOVOTNY, A., STEPP, H., GOETZ, C., BISE, K. & REULEN, H. J. 2000. Fluorescence-guided resection of glioblastoma multiforme utilizing 5-ALA-induced porphyrins: a prospective study in 52 consecutive patients. *Journal of neurosurgery,* 93**,** 1003-1013.

STUPP , R., MASON , W. P., VAN DEN BENT , M. J., WELLER , M., FISHER , B., TAPHOORN , M. J. B., BELANGER , K., BRANDES , A. A., MAROSI , C., BOGDAHN , U., CURSCHMANN , J., JANZER , R. C., LUDWIN , S. K., GORLIA , T., ALLGEIER , A., LACOMBE , D., CAIRNCROSS , J. G., EISENHAUER , E. & MIRIMANOFF , R. O. 2005. Radiotherapy plus Concomitant and Adjuvant Temozolomide for Glioblastoma. *New England Journal of Medicine,* 352**,** 987-996.

STYLIANOPOULOS, T. 2013. EPR-effect: utilizing size-dependent nanoparticle delivery to solid tumors. *Therapeutic delivery,* 4**,** 421-423.

SU, L., CHENG, C. Y. & MRUK, D. D. 2009. Drug transporter, P-glycoprotein (MDR1), is an integrated component of the mammalian blood-testis barrier. *The International Journal of Biochemistry & Cell Biology,* 41**,** 2578-2587.

SU, W. & PASTERNAK, G. W. 2013. The role of multidrug resistance‐associated protein in the blood‐brain barrier and opioid analgesia. *Synapse,* 67**,** 609-619.

SUKEGAWA, A., NARITA, T., KAMEDA, T., SAITOH, K., NOHNO, T., IBA, H., YASUGI, S. & FUKUDA, K. 2000. The concentric structure of the developing gut is regulated by Sonic hedgehog derived from endodermal epithelium. *Development,* 127**,** 1971-1980.

SULTAN, M., AMSTISLAVSKIY, V., RISCH, T., SCHUETTE, M., DÖKEL, S., RALSER, M., BALZEREIT, D., LEHRACH, H. & YASPO, M.-L. 2014. Influence of RNA extraction methods and library selection schemes on RNA-seq data. *BMC genomics,* 15**,** 675.

SUN, Q., BAI, J. & LV, R. 2016. Hedgehog/Gli1 signal pathway facilitates proliferation, invasion, and migration of cutaneous SCC through regulating VEGF. *Tumor Biology,* 37**,** 16215-16225.

SWEETMAN, M. J., HARDING, F. J., GRANEY, S. D. & VOELCKER, N. H. 2011. Effect of oligoethylene glycol moieties in porous silicon surface functionalisation on protein adsorption and cell attachment. *Applied Surface Science,* 257**,** 6768-6774.

SWERDLOW, A. J., FEYCHTING, M., GREEN, A. C., KHEIFETS, L., SAVITZ, D. A. & INTERNATIONAL COMMISSION FOR NON-IONIZING RADIATION PROTECTION STANDING

COMMITTEE ON, E. 2011. Mobile Phones, Brain Tumors, and the Interphone Study: Where Are We Now? *Environmental Health Perspectives,* 119**,** 1534-1538.

TAKEMI TANAKA, LINGEGOWDA S. MANGALA, PABLO E. VIVAS-MEJIA, RENÉ NIEVES-ALICEA, AMAN P. MANN, EDNA MORA, HEE-DONG HAN, MIAN M.K. SHAHZAD, XUEWU LIU, ROHAN BHAVANE, JIANHUA GU, JEAN R. FAKHOURY, CIRO CHIAPPINI, CHUNHUA LU, KOJI MATSUO, BIANA GODIN, REBECCA L. STONE, ALPA M. NICK, GABRIEL LOPEZ-BERESTEIN, ANIL K. SOOD & FERRARI, A. M. 2010. Sustained small interfering RNA delivery by mesoporous silicon particles. *Cancer research,* 70**,** 3687-3696.

TANG, R., FAUSSAT, A., MAJDAK, P., PERROT, J., CHAOUI, D., LEGRAND, O. & MARIE, J. 2004. Valproic acid inhibits proliferation and induces apoptosis in acute myeloid leukemia cells expressing P-gp and MRP1. *Leukemia,* 18**,** 1246-1251.

TANG, S. N., FU, J., NALL, D., RODOVA, M., SHANKAR, S. & SRIVASTAVA, R. K. 2012. Inhibition of sonic hedgehog pathway and pluripotency maintaining factors regulate human pancreatic cancer stem cell characteristics. *Int J Cancer,* 131**,** 30-40.

TAYLOR, J. & BEBAWY, M. 2019. Proteins regulating microvesicle biogenesis and multidrug resistance in cancer. *Proteomics,* 19**,** 1800165.

TAYLOR, M. D., LIU, L., RAFFEL, C., HUI, C.-C., MAINPRIZE, T. G., ZHANG, X., AGATEP, R., CHIAPPA, S., GAO, L. & LOWRANCE, A. 2002. Mutations in SUFU predispose to medulloblastoma. *Nature genetics,* 31**,** 306-310.

TEMPÉ, D., CASAS, M., KARAZ, S., BLANCHET-TOURNIER, M.-F. & CONCORDET, J.-P. 2006. Multisite protein kinase A and glycogen synthase kinase 3β phosphorylation leads to Gli3 ubiquitination by SCFβTrCP. *Molecular and cellular biology,* 26**,** 4316-4326.

THAYER, S. P., DI MAGLIANO, M. P., HEISER, P. W., NIELSEN, C. M., ROBERTS, D. J., LAUWERS, G. Y., QI, Y. P., GYSIN, S., FERNÁNDEZ-DEL CASTILLO, C. & YAJNIK, V. 2003. Hedgehog is an early and late mediator of pancreatic cancer tumorigenesis. *Nature,* 425**,** 851-856.

THELLIN, O., ZORZI, W., LAKAYE, B., DE BORMAN, B., COUMANS, B., HENNEN, G., GRISAR, T., IGOUT, A. & HEINEN, E. 1999. Housekeeping genes as internal standards: use and limits. *Journal of biotechnology,* 75**,** 291-295.

TIVNAN, A., ZAKARIA, Z., O'LEARY, C., KÖGEL, D., POKORNY, J. L., SARKARIA, J. N. & PREHN, J. H. M. 2015. Inhibition of multidrug resistance protein 1 (MRP1) improves chemotherapy drug response in primary and recurrent glioblastoma multiforme. *Frontiers in Neuroscience,* 9.

TONG, X.-Z., WANG, F., LIANG, S., ZHANG, X., HE, J.-H., CHEN, X.-G., LIANG, Y.-J., MI, Y.-J., TO, K. K. W. & FU, L.-W. 2012. Apatinib (YN968D1) enhances the efficacy of conventional chemotherapeutical drugs in side population cells and ABCB1-overexpressing leukemia cells. *Biochemical Pharmacology,* 83**,** 586-597.

TORCHILIN, V. 2011. Tumor delivery of macromolecular drugs based on the EPR effect. *Advanced drug delivery reviews,* 63**,** 131-135.

TOSI, G., MUSUMECI, T., RUOZI, B., CARBONE, C., BELLETTI, D., PIGNATELLO, R., VANDELLI, M. A. & PUGLISI, G. 2016. The “fate” of polymeric and lipid nanoparticles for brain delivery and targeting: Strategies and mechanism of blood–brain barrier crossing and trafficking into the central nervous system. *Journal of Drug Delivery Science and Technology,* 32**,** 66-76.

TOSTAR, U., FINTA, C., RAHMAN, M. F.-U., SHIMOKAWA, T. & ZAPHIROPOULOS, P. G. 2012. Novel Mechanism of Action on Hedgehog Signaling by a Suppressor of Fused Carboxy Terminal Variant. *PLOS ONE,* 7**,** e37761.

TOSTAR, U., MALM, C. J., MEIS‐KINDBLOM, J. M., KINDBLOM, L. G., TOFTGÅRD, R. & UNDÉN, A. B. 2006. Deregulation of the hedgehog signalling pathway: a possible role for the PTCH and SUFU genes in human rhabdomyoma and rhabdomyosarcoma development. *The Journal of pathology,* 208**,** 17-25.

TREUEL, L., JIANG, X. & NIENHAUS, G. U. 2013. New views on cellular uptake and trafficking of manufactured nanoparticles. *Journal of The Royal Society Interface,* 10**,** 20120939.

TSO, C. L., FREIJE, W. A., DAY, A., CHEN, Z., MERRIMAN, B., PERLINA, A., LEE, Y., DIA, E. Q., YOSHIMOTO, K., MISCHEL, P. S., LIAU, L. M., CLOUGHESY, T. F. & NELSON, S. F. 2006. Distinct transcription profiles of primary and secondary glioblastoma subgroups. *Cancer Res,* 66**,** 159-67.

TUKACHINSKY, H., LOPEZ, L. V. & SALIC, A. 2010. A mechanism for vertebrate Hedgehog signaling: recruitment to cilia and dissociation of SuFu–Gli protein complexes. *The Journal of Cell Biology,* 191**,** 415-428.

TUSON, M., HE, M. & ANDERSON, K. V. 2011. Protein kinase A acts at the basal body of the primary cilium to prevent Gli2 activation and ventralization of the mouse neural tube. *Development,* 138**,** 4921-4930.

TYDEN, E., BJORNSTROM, H., TJALVE, H. & LARSSON, P. 2010. Expression and localization of BCRP, MRP1 and MRP2 in intestines, liver and kidney in horse. *J Vet Pharmacol Ther,* 33**,** 332-40.

TYLER, B. M., PRADILLA, G., HADELSBERG, U., BOW, H., SUK, I. & BREM, H. 2014. Treatment of Brain Tumors. *Focal Controlled Drug Delivery.* Springer.

van Kuppeveld F J M, van der Logt J T M, Angulo A F, van Zoest M J, Quint W G V, Niesters H G M, Galama J M D, Melchers W J G. Genus- and species-specific identification of mycoplasmas by 16S rRNA amplification. 1992 Appl Environ Microbiol. 58:2606–2615

VAN WOENSEL, M., WAUTHOZ, N., ROSIÈRE, R., MATHIEU, V., KISS, R., LEFRANC, F., STEELANT, B., DILISSEN, E., VAN GOOL, S. W. & MATHIVET, T. 2016. Development of siRNA-loaded chitosan nanoparticles targeting Galectin-1 for the treatment of glioblastoma multiforme via intranasal administration. *Journal of Controlled Release,* 227**,** 71-81.

VARJOSALO, M. & TAIPALE, J. 2008. Hedgehog: functions and mechanisms. *Genes Dev,* 22**,** 2454-72.

VASANI, R. B., MCINNES, S. J., COLE, M. A., JANI, A. M., ELLIS, A. V. & VOELCKER, N. H. 2011. Stimulus-responsiveness and drug release from porous silicon films ATRP-grafted

with poly(N-isopropylacrylamide). *Langmuir : the ACS journal of surfaces and colloids,* 27**,** 7843-53.

VELLENGA, E., TUYT, L., WIERENGA, B. J., MÜLLER, M. & DOKTER, W. 1999. Interleukin‐6 production by activated human monocytic cells is enhanced by MK‐571, a specific inhibitor of the multi‐drug resistance protein‐1. *British journal of pharmacology,* 127**,** 441-448.

VERHAAK, R., HOADLEY, K., PURDOM, E., WANG, V., QI, Y., WILKERSON, M., MILLER, C., DING, L., GOLUB, T. & MESIROV, J. 2010a. Cancer Genome Atlas Research Network Integrated genomic analysis identifies clinically relevant subtypes of glioblastoma characterized by abnormalities in PDGFRA, IDH1, EGFR, and NF1. *Cancer cell,* 17**,** 98-110.

VERHAAK, R. G., HOADLEY, K. A., PURDOM, E., WANG, V., QI, Y., WILKERSON, M. D., MILLER, C. R., DING, L., GOLUB, T., MESIROV, J. P., ALEXE, G., LAWRENCE, M., O'KELLY, M., TAMAYO, P., WEIR, B. A., GABRIEL, S., WINCKLER, W., GUPTA, S., JAKKULA, L., FEILER, H. S., HODGSON, J. G., JAMES, C. D., SARKARIA, J. N., BRENNAN, C., KAHN, A., SPELLMAN, P. T., WILSON, R. K., SPEED, T. P., GRAY, J. W., MEYERSON, M., GETZ, G., PEROU, C. M., HAYES, D. N. & CANCER GENOME ATLAS RESEARCH, N. 2010b. Integrated genomic analysis identifies clinically relevant subtypes of glioblastoma characterized by abnormalities in PDGFRA, IDH1, EGFR, and NF1. *Cancer Cell,* 17**,** 98-110.

VITAL, A. L., TABERNERO, M. D., CASTRILLO, A., REBELO, O., TAO, H., GOMES, F., NIETO, A. B., RESENDE OLIVEIRA, C., LOPES, M. C. & ORFAO, A. 2010. Gene expression profiles of human glioblastomas are associated with both tumor cytogenetics and histopathology. *Neuro Oncol,* 12**,** 991-1003.

VOELCKER, N. H. Nanostructured silicon in nanomedicine. ABSTRACTS OF PAPERS OF THE AMERICAN CHEMICAL SOCIETY, 2014. AMER CHEMICAL SOC 1155 16TH ST, NW, WASHINGTON, DC 20036 USA.

VOS, T. A., HOOIVELD, G. J., KONING, H., CHILDS, S., MEIJER, D. K., MOSHAGE, H., JANSEN, P. L. & MÜLLER, M. 1998. Up‐regulation of the multidrug resistance genes, Mrp1 and Mdr1b, and down‐regulation of the organic anion transporter, Mrp2, and the bile salt transporter, Spgp, in endotoxemic rat liver. *Hepatology,* 28**,** 1637-1644.

WALLNER, K. E., GALICICH, J. H., KROL, G., ARBIT, E. & MALKIN, M. G. 1989. Patterns of failure following treatment for glioblastoma multiforme and anaplastic astrocytoma. *Int J Radiat Oncol Biol Phys,* 16**,** 1405-9.

WAN, Y., APOSTOLOU, S., DRONOV, R., KUSS, B. & VOELCKER, N. H. 2014. Cancer-targeting siRNA delivery from porous silicon nanoparticles. *Nanomedicine***,** 1-13.

WANG, B., FALLON, J. F. & BEACHY, P. A. 2000. Hedgehog-Regulated Processing of Gli3 Produces an Anterior/Posterior Repressor Gradient in the Developing Vertebrate Limb. *Cell,* 100**,** 423-434.

WATANABE, A., ARAI, M., YAMAZAKI, M., KOITABASHI, N., WUYTACK, F. & KURABAYASHI, M. 2004. Phospholamban ablation by RNA interference increases Ca2+ uptake into rat cardiac myocyte sarcoplasmic reticulum. *Journal of molecular and cellular cardiology,* 37**,** 691-698.

WĘGLARZ, L., MOLIN, I., ORCHEL, A., PARFINIEWICZ, B. & DZIERŻEWICZ, Z. 2006. Quantitative analysis of the level of p53 and p21WAF1 mRNA in human colon cancer HT-29 cells treated with inositol hexaphosphate.

WESSELING, P. & CAPPER, D. 2018. WHO 2016 Classification of gliomas. *Neuropathol Appl Neurobiol,* 44**,** 139-150.

WETMORE, C. 2003. Sonic hedgehog in normal and neoplastic proliferation: insight gained from human tumors and animal models. *Current Opinion in Genetics & Development,* 13**,** 34-42.

WINTER, S. S., RICCI, J., LUO, L., LOVATO, D. M., KHAWAJA, H. M., SERNA-GALLEGOS, T., DEBASSIGE, N. & LARSON, R. S. 2013. ATP Binding Cassette C1 (ABCC1/MRP1)-mediated drug efflux contributes to disease progression in T-lineage acute lymphoblastic leukemia. *Health (Irvine Calif),* 5.

Woltsche N, Pichler N, Wolf I, Di Meo N, Zalaudek I. Managing adverse effects by dose reduction during routine treatment of locally advanced basal cell carcinoma with the hedgehog inhibitor vismodegib: a single centre experience. J Eur Acad Dermatol Venereol. 2019 Apr;33(4):e144-e145.

WORSFOLD, O., VOELCKER, N. H. & NISHIYA, T. 2006. Biosensing Using Lipid Bilayers Suspended on Porous Silicon. *Langmuir : the ACS journal of surfaces and colloids,* 22**,** 7078-7083.

WORTELBOER, H. M., USTA, M., VAN DER VELDE, A. E., BOERSMA, M. G., SPENKELINK, B., VAN ZANDEN, J. J., RIETJENS, I. M., VAN BLADEREN, P. J. & CNUBBEN, N. H. 2003. Interplay

between MRP inhibition and metabolism of MRP inhibitors: the case of curcumin. *Chemical research in toxicology,* 16**,** 1642-1651.

WU, F., ZHANG, Y., SUN, B., MCMAHON, A. P. & WANG, Y. 2017a. Hedgehog Signaling: From Basic Biology to Cancer Therapy. *Cell Chemical Biology*.

WU, G., WILSON, G., GEORGE, J., LIDDLE, C., HEBBARD, L. & QIAO, L. 2017b. Overcoming treatment resistance in cancer: Current understanding and tactics. *Cancer Letters,* 387**,** 69-76.

XIE, J., MURONE, M., LUOH, S.-M., RYAN, A., GU, Q., ZHANG, C., BONIFAS, J. M., LAM, C.-W., HYNES, M. & GODDARD, A. 1998. Activating Smoothened mutations in sporadic basal-cell carcinoma. *Nature,* 391**,** 90-92.

XU, H., NIE, X., WU, L., ZHU, X., YI, W. & HUANG, S. 2015. Down-Regulation of MRP1 Expression in C6/VP16 Cells by Chitosan-MRP1-siRNA Nanoparticles. *Cell biochemistry and biophysics,* 72**,** 227-233.

XU, M., LI, L., LIU, Z., JIAO, Z., XU, P., KONG, X., HUANG, H. & ZHANG, Y. 2013. ABCB2 (TAP1) as the downstream target of SHH signaling enhances pancreatic ductal adenocarcinoma drug resistance. *Cancer Lett,* 333**,** 152-8.

YALÇıN, S., ÖZLÜER, Ö. & GÜNDÜZ, U. 2016. Nanoparticle-based drug delivery in cancer: the role of cell membrane structures. *Therapeutic Delivery,* 7**,** 773-781.

YANG, J., REILLY, B., DAVIS, T. & RONALDSON, P. 2018. Modulation of opioid transport at the blood-brain barrier by altered ATP-binding cassette (ABC) transporter expression and activity. *Pharmaceutics,* 10**,** 192.

YANG, Z.-Z., LI, J.-Q., WANG, Z.-Z., DONG, D.-W. & QI, X.-R. 2014. Tumor-targeting dual peptides-modified cationic liposomes for delivery of siRNA and docetaxel to gliomas. *Biomaterials*.

YAO, H. H.-C., WHORISKEY, W. & CAPEL, B. 2002. Desert Hedgehog/Patched 1 signaling specifies fetal Leydig cell fate in testis organogenesis. *Genes & development,* 16**,** 1433-1440.

YILDIRIMER, L., BUANZ, A., GAISFORD, S., MALINS, E. L., REMZI BECER, C., MOIEMEN, N., REYNOLDS, G. M. & SEIFALIAN, A. M. 2015. Controllable degradation kinetics of POSS nanoparticle-integrated poly(ε-caprolactone urea)urethane elastomers for tissue engineering applications. *Scientific Reports,* 5**,** 15040.

YIN, S., DU, W., WANG, F., HAN, B., CUI, Y., YANG, D., CHEN, H., LIU, D., LIU, X. & ZHAI, X. 2018. MicroRNA-326 sensitizes human glioblastoma cells to curcumin via the SHH/GLI1 signaling pathway. *Cancer biology & therapy,* 19**,** 260-270.

YOO, H. & JULIANO, R. L. 2000. Enhanced delivery of antisense oligonucleotides with fluorophore-conjugated PAMAM dendrimers. *Nucleic Acids Research,* 28**,** 4225-4231.

YOON, D. J., KWAN, B. H., CHAO, F. C., NICOLAIDES, T. P., PHILLIPS, J. J., LAM, G. Y., MASON, A. B., WEISS, W. A. & KAMEI, D. T. 2010. Intratumoral therapy of glioblastoma multiforme using genetically engineered transferrin for drug delivery. *Cancer research,* 70**,** 4520-4527.

YU, C., DING, B., ZHANG, X., DENG, X., DENG, K., CHENG, Z., XING, B., JIN, D., MA, P. A. & LIN, J. 2018. Targeted iron nanoparticles with platinum-(IV) prodrugs and anti-EZH2 siRNA

show great synergy in combating drug resistance in vitro and in vivo. *Biomaterials,* 155**,** 112-123.

ZAHREDDINE, H. A., CULJKOVIC-KRALJACIC, B., ASSOULINE, S., GENDRON, P., ROMEO, A. A., MORRIS, S. J., CORMACK, G., JAQUITH, J. B., CERCHIETTI, L. & COCOLAKIS, E. 2014. The sonic hedgehog factor GLI1 imparts drug resistance through inducible glucuronidation. *Nature,* 511**,** 90-93.

ZANOTTO-FILHO, A., BRAGANHOL, E., EDELWEISS, M. I., BEHR, G. A., ZANIN, R., SCHRˆDER, R., SIMıES-PIRES, A., BATTASTINI, A. M. O. & MOREIRA, J. C. U. F. 2011. The curry spice curcumin selectively inhibits cancer cells growth in vitro and in preclinical model of glioblastoma. *The Journal of Nutritional Biochemistry,* In Press, Corrected Proof.

ZANOTTO-FILHO, A., BRAGANHOL, E., KLAFKE, K., FIGUEIRÓ, F., TERRA, S. R., PALUDO, F. J., MORRONE, M., BRISTOT, I. J., BATTASTINI, A. M. & FORCELINI, C. M. 2015. Autophagy inhibition improves the efficacy of curcumin/temozolomide combination therapy in glioblastomas. *Cancer letters,* 358**,** 220-231.

ZENG, X., ZHAO, H., LI, Y., FAN, J., SUN, Y., WANG, S., WANG, Z., SONG, P. & JU, D. 2015. Targeting Hedgehog signaling pathway and autophagy overcomes drug resistance of BCR-ABL-positive chronic myeloid leukemia. *Autophagy,* 11**,** 355-372.

ZENG, Y. & CULLEN, B. R. 2002. RNA interference in human cells is restricted to the cytoplasm. *Rna,* 8**,** 855-860.

ZHANG, J., ALSTON, M. A., HUANG, H. & RABIN, R. L. 2006. Human T cell cytokine responses are dependent on multidrug resistance protein-1. *International immunology,* 18**,** 485-493.

ZHANG, R., SAITO, R., SHIBAHARA, I., SUGIYAMA, S., KANAMORI, M., SONODA, Y. & TOMINAGA, T. 2016. Temozolomide reverses doxorubicin resistance by inhibiting P-glycoprotein in malignant glioma cells. *Journal of Neuro-Oncology,* 126**,** 235-242.

ZHANG, X., TIAN, Y., YANG, Y. & HAO, J. 2017. Development of anticancer agents targeting the Hedgehog signaling. *Cellular and Molecular Life Sciences,* 74**,** 2773-2782.

ZHANG, Y., LATERRA, J. & POMPER, M. G. 2009. Hedgehog Pathway Inhibitor HhAntag691 Is a Potent Inhibitor of ABCG2/BCRP and ABCB1/Pgp. *Neoplasia,* 11**,** 96-101.

ZHANG, Y., SCHUETZ, J. D., ELMQUIST, W. F. & MILLER, D. W. 2004. Plasma membrane localization of multidrug resistance-associated protein homologs in brain capillary endothelial cells. *Journal of Pharmacology and Experimental Therapeutics,* 311**,** 449-455.

ZOU, J., BALDWIN, R. K., PETTIGREW, K. A. & KAUZLARICH, S. M. 2004. Solution synthesis of ultrastable luminescent siloxane-coated silicon nanoparticles. *Nano Letters,* 4**,** 1181-1186.